UC Berkeley
UC Berkeley Electronic Theses and Dissertations

Title
The multifunctional nature of motor cortex

Permalink
https://escholarship.org/uc/item/92857408

Author
Telian, Gregory I

Publication Date
2021

Peer reviewed|Thesis/dissertation

The multifunctional nature of motor cortex

By

Gregory Isaiah Telian

A dissertation submitted in partial satisfaction of the

requirements for the degree of

Doctor of Philosophy

in

Neuroscience

in the

Graduate Division

of the

University of California, Berkeley

Committee in charge:

Professor Hillel Adesnik, Chair
Professor Daniel Feldman
Professor Bruno Olshausen
Professor Frederic Theunissen

Summer 2021

Abstract

The multifunctional nature of motor cortex

by

Gregory Isaiah Telian

Doctor of Philosophy in Neuroscience

University of California, Berkeley

Professor Hillel Adesnik, Chair

The cerebral cortex is responsible for neural functions ranging from basic sensory processing to complex decision making. However, the underlying neural processes and the precise function of some cortical areas are not well understood. For humans the cortex is invaluable, providing us with our most powerful cognitive traits. For some species, the cortex can be removed leaving only minor deficits. Stark contrasts like these blur the overall function and importance of cortex. Recent advancements in recording and analysis technology present us with a unique opportunity to search for neural processes previously impossible to find. Recent work has found cortical regions in mice that do more than their functional name implies, in contrast to the specialized cortical regions in higher order species. In this study we explore the hidden functions of mouse motor cortex and elaborate on its role in the whisker system. The mouse whisker system is traditionally divided into sensory regions and motor regions, with sensory cortex (vS1) and motor cortex (vM1) sitting on the border. The functional divisions between sensory and motor cortex have recently blurred, both regions able to drive movements and encode sensory information. Whisker motor cortex, specifically, exhibits disparate functions, making it an ideal place to study multirole cortex. Here we take advantage of advanced neural recording and analysis techniques and uncover a motor cortex that acts as a sensory and possibly a higher order cortical region as well.

In chapter 1, I provide an overview of how cortical regions were defined and then summarize how modern research is blurring the lines between functionally defined cortical areas. I then introduce sensory processing in the mouse whisker system with a focus on motor cortex, a cortical region where its function is increasingly blurring, and then describe how my research explored non-motor functionality in a motor region. In chapter 2, I present my first first-author publication where we determined if somatosensory cortex integrates sensory information over short or long timescales in order to estimate "mean" variables. In this work I first use neural decoding to quantify how well each neuron represents pieces of sensory information and find that some neurons correlate with choice. Chapter 3 is work that I collaborated on, we determined

how multiple sensors contribute to the receptive field of individual neurons and the broader population. We discovered a map of sensory space distributed across somatosensory cortex and determined the map was dependent on neurons integrating information from multiple sensors in parallel. Chapter 4, we explore whether somatosensory cortex is necessary for a whisker dependent discrimination task and further determine what arrangement of sensors are required for task completion. Finally, in Chapter 5 I present my main project investigating vibrissae motor cortex. Here I study the sensory responses present in motor cortex, quantifying vM1 sensory tuning for the first time, and ultimately determining that vS1 does not drive the activity as previously thought. Incredibly, vM1 is not required for whisker movements in general but is required during demanding whisker dependent contexts, such as a whisker discrimination task, affecting both choice, whisker movements, and onset of lick response. Finally, in Chapter 6, I summarize what this tells us about sensory processing, propose some ideas for future research, and discuss how modern tools can enable us to find hidden functionality.

Table of Contents

Dedication

I am fortunate to have many caring people in my life. They have helped me on my academic journey, either directly or in spirit. I am the first person in my family to receive an advanced degree so much of this process has been flying by the seat of my/our pants.

This dissertation is dedicated to:

My mom, Margaret Medrano
You have fought and overcome so much to ensure that I and my sister had as many opportunities to thrive as possible. I am forever grateful, thank you for everything and more. I love you.

My grandfather, Francisco Medrano
You immigrated to this country to provide your family with better opportunities. You were my champion, supporting my academic ambitions even if it meant I had to move away. I wish you were still here to witness this.

And especially my wife, Beth Baribault
Your support, care, and companionship was invaluable during grad school and continues to be every day. I don't know how I would have finished this dissertation without your support. You are my best friend that I wouldn't want to live without. I love you.

Acknowledgements

Publications related to this work

Leah M. McGuire*, Gregory Telian*, Keven J. Laboy-Juárez*, Toshio Miyashita, Daniel J. Lee, Katherine A. Smith, Daniel E. Feldman (2016). Short time-scale sensory coding in S1 during discrimination of whisker vibrotactile sequences. *PLoS Biology* 2016 Aug 30;14(8):e1002549.
* These authors contributed equally to the study

Pluta, S. R.*, Lyall, E. H.*, Telian, G. I., Ryapolova-Webb, E., & Adesnik, H. (2017). Surround Integration Organizes a Spatial Map during Active Sensation. *Neuron*, *94*(6), 1220–1233.e5. https://doi.org/10.1016/j.neuron.2017.04.026 *Contributed equally

Brown, J., Oldenburg, I.A., Telian, G.I., Griffin, S., Voges, M., Jain, V., Adesnik, H.A. Spatial Integration During Active Tactile Sensation Drives Orientation Perception. Neuron. 2021 May 19;109(10):1707-1720.e7. https://doi.org/10.1016/j.neuron.2021.03.020.

Telian, G.I., Adesnik, H.A. The multifunctional nature of motor cortex. (in preparation)

Chapter 1: Introduction

The cerebral cortex is what makes us human. Rather, the sheer relative quantity of cortex is the key differentiator between humans' and other animals' cognitive capacity. The cortex is the neural system responsible for advanced cognitive processes such as adapting to changing surroundings, processing language, and executing important decisions as well as basic functions such as perceiving light and sound. Our personality and our thoughts are determined by its proper function. It is, with no doubt, a vital part of our lives and the lives of other animals. Its importance is well understood but its processes remain largely a mystery. Understanding the underlying neural processes will shed light on the unique behaviors and cognitive abilities of all species possessing a cortex

The cortex is a thin sheet of neurons that constitutes the outer surface of the brain. It typically has six distinct layers of neurons, arranged horizontally on top of each other, with connections amongst its layers forming columns. The columns repeat throughout the cortex ranging from distinct columns separated by well-defined cell boundaries to columns that blend together in both form and function. All cortical areas share the same basic structure, from low order animals such as rodents to high order animals like primates; the architecture of the cerebral cortex is conserved throughout. Its ubiquitousness highlights its importance and its architecture has proven to be robust and adaptable. This adaptability allows the cortex to make up distinct brain regions, each dedicated to a specific type of neural computation.

The theory of cortical localization is a fundamental cortical concept. Particular regions of cortex make up distinct zones acting as specialized hubs, processing their unique data, refining it, and then communicating it to the next cortical hub (Finger, 2010). This idea was debated in the 1800s, the counterargument proposed that the cortex was a distributed system, able to processes unrelated information in the same cortical space with no specialized areas. In the late 1800s strong evidence emerged in favor of the localization theory. Broca, attributed patients inability to process language to lesions in the frontal lobe and Fritsch and Hitzig, identified a cortical region that could move specific limbs when electrically stimulated. Since then more and more specialized cortical regions have been identified, many of which appear common across species.

Identifying cortical regions and their analogues across species has typically relied on finding similarities in anatomical architectonics, body movements elicited with electrical stimulation, neural activity generated by bodily stimulation, and more recently genomics. Early names were prescribed to regions by gross characteristics, typically related to their function or anatomy. For example, motor cortex was defined as the area where electrical stimulation most easily produced limb movements (Li & Waters, 1991; Miyashita, Keller, & Asanuma, 1994; Neafsey et al., 1986). Granular cortex named because it exhibited a cellular layer that looked like fine granules (Hall, Robert; Lindholm, 1974; Koralek, Jensen, & Killackey, 1988; Mitzdorf, 1985). Brain

regions across species were identified using similar techniques and often given the same name. Analogues are similar in gross function, anatomy, and relative position in the brain. Naming conventions and technological differences may have implied that cortical regions were strictly functional and comparable across species.

As neural recording, stimulation, and tracing technologies have become more precise the strict functional definitions of cortex are becoming blurred. It's tempting to assume all cortical analogues are more similar than they are different but modern experiments suggest otherwise. The motor cortex of a monkey is absolutely necessary for movement but the motor cortex of a mouse can be removed and the mouse would remain mobile, appearing mostly normal, with only minor deficits in gate (Ueno & Yamashita, 2011). Other work has found visual information present in mouse motor cortex and decision information in sensory cortex (McGuire et al., 2016; S. Zhang & Dan, 2011). These experiments required advanced technology to observe these subtle changes in gate and sparse neural representations. The multirole ability of cortex may have been overlooked in the past because detecting anything other than major effects was difficult or impossible with technology at the time.

The past three decades has seen an incredible rise in technological power and an increase in "atypical" cortical functions. Now that scientists can observe tens if not thousands of neurons across large swaths of cortex, manipulate them with genetically encoded actuators, and analyze the massive datasets with modern desktop computers the number of subtle and out of place cortical functions has increased (de Vries et al., 2020; Lanzio et al., 2018; Durstewitz & Balauguer-Ballester, 2010; Elie & Theunissen, 2015; Mackay, 2003; Victor & Purpura, 2007). This presents scientists with a new opportunity to uncover previously hidden cortical functionality. Discovering the variety of cortical functions likely present in lower order species will highlight the differences between more advance species. Leading to questions like why are cortical regions less specialized in lower order species, when does cortex become essential for a particular task, are there any neural computations conserved across all lower and higher order species, and is there any advantage to multirole cortical areas.

I propose that studying how interconnected brain regions communicate, while implementing modern analysis methods can more accurately determine the underlying functions of cortical regions. Studying interconnected brain regions provides us the opportunity to identify how information is encoded, transformed, and transmitted (Helmchen, Gilad, & Chen, 2018; Kajikawa & Schroeder, 2011). Changes in that information will better identify what previous regions contributed, if there is unexpected information then that could point to underlying functionality. My dissertation work focuses on questioning fundamental ideas of cortical function. With a focus on sensorimotor processing in the mouse whisker system I look at integrative sensory processing in somatosensory cortex and the unexpectedly general purpose whisker motor cortex. I will demonstrate how modern methods can identify overlooked cortical

functions. I propose that functionally defined cortical regions are generalized in lower order species, behaving as a multirole brain region. This tradeoff in specialization for generalization must be taken into account when making inferences across species.

In my primary project I use modern methods to study vibrissae motor cortex (vM1). vM1 is believed to play an essential role in generating whisker movements and for refining whisker somatosensory (vS1) information with its feedback projections (Diamond, von Heimendahl, Knutsen, Kleinfeld, & Ahissar, 2008; Kleinfeld, Ahissar, & Diamond, 2006; Kleinfeld & Deschnes, 2011). Motor cortex possesses sensory driven activity but none have explored their tuning properties (Farkas, Kis, Toldi, & Wolff, 1999; Petrof, Viaene, & Sherman, 2015). Many non-motor functions have been attributed to vM1, creating some confusion over its primary role in the sensorimotor system. I focus on the non-motor functions of vM1 in order to better understand the true role of this frontal cortical region.

Introduction to vibrissae motor cortex and its various roles

Rodents are a popular model used in sensorimotor research. Nocturnal by nature they rely heavily on their whiskers to navigate the environment. Their whiskers are neatly arranged in a grid, each whisker is under active control, and each have a principal cortical column in somatosensory cortex (Berg & Kleinfeld, 2003; Brecht, Schneider, Sakmann, & Margrie, 2008). Other whiskered species can control the position of their whiskers but they cannot rapidly sweep them to explore the sensory space surrounding their head. Rats and mice use their whiskers actively, sweeping them around 10Hz to 20Hz respectively. Rodents can finely adjust their whisk frequency, their setpoint (the sector of space swept by their whiskers), as well as the amplitude (distance between protraction start and stop) of their whiskers at rapid timescales (Kleinfeld et al., 2006). The whisking pattern is context dependent (Ni & Chen, 2017). Similar to humans exploring a physical object rodents adjust how they whisk depending on what information they need. Protracting whiskers forward coupled with low amplitude whisk cycles is used to determine distances. Asymmetrical whisking is common during head movements, scanning the space their head will eventually be. Foveal whisking is similar to visually focusing or centering your fovea on a particular stimulus, here rodents extend their whiskers accompanied with low amplitude high frequency whisking.

Whisker contacts drive sensory activity that quickly propagates to the trigeminal nucleus of the brainstem, then the VPM and PoM region of the thalamus, and terminates in sensory cortices primarily vibrissae somatosensory cortex. At the cortical level vS1 processes whisker generated sensory information and is believed to feed this sensory information to vibrissae motor cortex as well as a variety of other brain regions. vM1 is thought to integrate the sensory information from vS1 and use it to update the whisker motor program (Helmchen et al., 2018; Feldmeyer et al., 2013). In theory vS1 and vM1 work as a team to refine sensory information by modulating

whisking to refine sensory information which then updates the motor program in a loop. The sensory side of the sensorimotor loop has received extensive research, vS1 is particularly well studied. However, it is unclear how vibrissae motor cortex contributes to the sensorimotor loop.

Early vM1 experiments focused on mapping its borders and homunculus using anatomical and electrical methods (Donoghue & Wise, 1982; Gioanni & Lamarche, 1985; Hall, Robert; Lindholm, 1974; Li & Waters, 1991; Sanderson, Welker, & Shambes, 1984; K. Zhang et al., 2014). Other experiments examined how vM1 electrical stimulation impacted whisker movements. For decades only anesthetized experiments were possible making it difficult to examine how vM1 contributed to adaptive whisker movements (Shin & Chapin, 1990). In the 1990s awake behaving experiments were becoming more common; natural whisking could be observed and rudimentarily quantified. Kleinfeld proposed that vM1 was responsible for controlling the phase and setpoint of the whisker pad in motion (Curtis & Kleinfeld, 2009; Kleinfeld, Berg, & O'Connor, 1999). Neural recordings verified that vM1 units did indeed encode whisking phase and setpoint in their firing rate. vS1 units also contained phase information, which was presumed to be an efferent copy from vM1. The new hypotheses became vM1 controls the phase and setpoint of the whiskers and sends an efferent copy to vS1 in order to frame incoming sensory activity in the context of whisker position (Hill, Curtis, Moore, & Kleinfeld, 2011; Ni & Chen, 2017).

Further work by Kleinfeld found that vM1 current source density (CSD) measurements locked to whisker generated sensory signals (Ahrens & Kleinfeld, 2004). This was one of the few experiments to explore vM1's sensory activity. Not many sensory studies came from this and research continued focusing on vM1's role controlling whisker motion and updating vS1 with motor signals to refine its sensory representations.

The anatomical connections of the whisker system had become well known at the time, at least on a gross scale. The projection from vS1 to vM1 was known but its function was not. Very few studies explored vS1's influence on vM1. One of the earliest vM1 sensory studies measured neural activity in vM1 while delivering electrical shocks to the mystacial pad. They then ablated vS1 and found that activity in vM1 had decreased (Farkas et al., 1999). Another study, using, intracortical microstimulation (ICMS), found two distinct functional regions in vM1, a rhythmic protraction zone and a new retraction zone. Histological analysis determined that the retraction zone was seated in a region with a high density of terminating vS1 projections (Smith & Alloway, 2013). These studies suggested that vS1 had a strong influence on vM1 but it was still unclear what its role was.

Petersen and collogues later cleared things up with voltage sensitive dye studies. By deflecting individual whiskers they determined that vM1's sensory responses occur immediately after the presence of activity in vS1 (Matyas & Petersen, 2010). They proposed that vM1 was driven by

vS1 but this was not directly tested. In the same study they also found that vS1 was able to elicit whisker retractions completely independent of vM1. This suggests that the retractions observed in the earlier ICMS study must have been caused by antidromic spiking of vS1 axons (Smith & Alloway, 2013). These experiments supported the hypothesis that vS1 drives sensory activity in vM1 and, for the first time, found that a sensory area can drive motor output.

At this point the clear distinction between sensory and motor cortex starts becoming blurred. Sensory activity was present in both cortical regions and they both could drive whisker motion. Perhaps they acted as a push-pull system sharing both the sensory and motor workload. Recent studies have further blurred vM1's role, attributing seemingly contradicting roles in whisker control (Lopes, Nogueira, Paton, & Kampff, 2016). Two separate studies found that silencing vM1 resulted in contralateral whisker protraction and the other found silencing vM1 decreased the probability of whisker protraction (Christian Laut Ebbesen, Doron, Lenschow, & Brecht, 2017; Sreenivasan et al., 2016). Other studies attribute disparate motor and non-motor functionality to vM1 as well (Lopes et al., 2016).

Intrigued by sensory activity present in a motor cortex I set out to explore vM1 sensory activity. I wanted to 1) determine what the sensory activity represented, being the first to measure vM1 sensory tuning, 2) directly test if vS1 was the source of this activity, 3) use a neural decoder to quantify how well each region represented the same stimulus and 4) determine if vM1 or vS1 contributed to whisking. As new vM1 studies came out its role became less clear, suggesting it is a more generalized cortex. This, coupled with my initial silencing results, led to my context dependent hypothesis. I hypothesized that vM1 is necessary for demanding tactile tasks that require adaptive whisking to extract behaviorally relevant information.

Our study revealed that vM1 is much more than a motor cortex. In the experiments described here vM1 performed very little motor control, behaving as a sensory cortex and possibly as a higher order cortical area contributing to response inhibition. Our experiments found that vM1 sensory responses are less driven and less widely distributed compared to vS1. Interestingly, both regions have a similar distribution of tuned units, ranging from moderately broadly tuned and moderately selectively tuned. Decoding did very well with vS1 and moderately well with vM1 data, clearly depicting the relative difference between the two's sensory detail. Silencing vS1 did not abolish sensory activity, instead vS1 modulated vM1's gain, increasing the sensory signal from a units' baseline firing rate in normal conditions. Silencing vM1 did not have a noticeable change on vS1 firing rates, however the decoder found that silencing vM1 did slightly decrease vS1's predictive power. Finally, both regions are not necessary for whisking but are required for a demanding whisker dependent task. vM1 silencing reduced the performance of the mouse, reduced both whisking setpoint and whisk frequency, and increased the onset of licking, making it harder for mice to inhibit behavioral responses.

Our results suggests that functional cortical regions in mice, and possibly other lower order animals, have broader functionality than those in higher species. Here vibrissae motor cortex behaved as a sensory cortex, accurately representing spatial stimuli. It is possible that the disruption to vM1's sensory activity caused mice to perform worse on the task by making it difficult to identify particular sensory cues tied to a stimulus. Motor cortex also impacted response inhibition behaving similar to a higher cortical area. This study finds that vM1 acts as a multirole cortical region, having a much broader role compared to its analogues in higher order species.

Chapter 2: Short time-scale sensory coding in S1 during discrimination of whisker vibrotactile sequences

Foreword

This work was conducted early in graduate school during my last lab rotation with Prof. Dan Feldman. The experiments and early analyses had been completed prior to my arrival but the project as a whole was left unfinished. I was responsible for verifying that all the previous findings were accurate as well as implementing my own analyses to answer the remaining questions. The project was designed to determine how sensory cortex in rats represents relevant sensory information. Specifically, do neurons in whisker somatosensory cortex integrate stimulus information to form a mean parameter estimate or do they rely on the precise timing of sensory inputs. I developed a custom neural decoder, based on multinomial logistic regression, that we used to quantify whether fast timescale or long timescale stimulus representations contained more stimulus information and, if so, determine if it was associated with a particular unit type. The decoder, in conjunction with traditional spike train analyses, found that fast timescale units, those with spike rates that rapidly followed the stimulus, utilized the temporal structure of the stimulus. While slow timescale units, those with spike rates that increased or decreased monotonically, did not encode stimulus identity but did encode the choice of the animal. Using the neural decoder we were able to more easily quantify the effect we observed in the spike trains. I am forever grateful to Dan Feldman for giving me the opportunity to work on this project.

Citation

Summary

Rodent whisker input consists of dense microvibration sequences that are often temporally integrated for perceptual discrimination. Whether primary somatosensory cortex (S1) participates in temporal integration is unknown. We trained rats to discriminate whisker impulse sequences that varied in single-impulse kinematics (5–20-ms time scale) and mean speed (150-ms time scale). Rats appeared to use the integrated feature, mean speed, to guide discrimination in this task, consistent with similar prior studies. Despite this, 52% of S1 units, including 73% of units in L4 and L2/3, encoded sequences at fast time scales (≤20 ms, mostly 5–10 ms), accurately reflecting single impulse kinematics. 17% of units, mostly in L5, showed weaker impulse

responses and a slow firing rate increase during sequences. However, these units did not effectively integrate whisker impulses, but instead combined weak impulse responses with a distinct, slow signal correlated to behavioral choice. A neural decoder could identify sequences from fast unit spike trains and behavioral choice from slow units. Thus, S1 encoded fast time scale whisker input without substantial temporal integration across whisker impulses.

Introduction

Natural sensory input comprises dense temporal series of discrete events, which animals often temporally integrate to guide perceptual decisions. The temporal integration process has been studied in primate somatosensation and vision [1,2], but less in rodents, in which modern tools could reveal the underlying circuit mechanisms. In the whisker tactile system, active whisking generates dense streams of stick-slip events on surfaces (5–10 ms duration, ~60 ms interval) [3,4] and contact events on object edges [5,6]. These temporal series constitute the whisker vibrotactile signal. While animals can perceive individual brief whisker impulses alone or within trains [7–11], behavioral discrimination of vibrotactile sequences is often based on a time-averaged composite feature, mean whisker speed, rather than the kinematics or precise pattern of individual deflections [12,13]. This suggests that the brain generates both short time-scale (individual impulse) and temporally integrated, long time-scale (mean speed or intensity) representations of whisker input. How these time scales are represented in the cortex is unknown.

We tested which time scale(s) of information are represented in S1 in awake behaving rats discriminating rapid whisker sequences. Under anesthesia, most S1 neurons spike phasically to whisker deflections, and responses adapt strongly during stimulus trains. This suggests that S1 does not temporally integrate across impulses (we use "integration" to mean temporal summation or averaging) [14–18]. Most S1 neurons also spike phasically to whisker deflection in basic detection tasks [7,9,10,19] or when rats must detect kinematically distinct impulses within ongoing stimulus trains [8]. However, these tasks do not require stimulus integration for behavioral performance [7–10]. Whether temporal integration occurs in S1 during tasks in which animals behaviorally integrate whisker information is unknown. A subset of S1 neurons exhibit sustained responses to stimulus sequences in awake mice [20], but whether these contribute to perceptual integration is unclear.

We trained rats to discriminate rapid sequences of three brief whisker impulses with an ~60 ms interpulse interval. This interval matches the median interval between stick-slip events during texture palpation [21]. S1 is required for passive vibrotactile discrimination [13,22,23]. Stimuli differed in both rapid temporal structure (kinematics and order of individual impulses) and time-integrated information (mean speed of the entire sequence). Rats could use either for discrimination. Behavioral choice correlated with mean speed, suggesting that rats temporally integrated whisker impulse sequences, as shown explicitly in similar prior studies in which both rapid kinematic and slow intensity cues were available [12,13]. In tetrode recordings during behavior, most S1 units accurately encoded single-impulse kinematics on a rapid (≤20 ms) time scale with modest adaptation. A minority of units responded weakly to individual impulses but exhibited slowly increasing or decreasing spiking during the stimulus period. However, these units did not effectively integrate across impulses and instead combined transient impulse responses with a distinct, slow signal correlated to behavioral choice. Thus, S1 appears to

8

represent only short time-scale information about whisker impulse trains during vibrotactile discrimination. This suggests that temporal integration may occur downstream of S1.

Results

Behavioral Discrimination of FFF, FMS, SMF, and SSS Sequences

We developed a novel whisker vibrotactile discrimination task in which rats initiated trials by entering a nose poke with their right whiskers resting on a wall panel coupled to a hidden piezoelectric actuator (Fig 1). The panel delivered a rapid sequence of three up-down impulses. Each impulse was 16–26 ms long and had Fast (F), Medium (M), or Slow (S) rise/fall velocity. Sequences had FFF, FMS, SMF, or SSS pulse order (34 ms interval from end of a pulse to beginning of next pulse; 120–148 ms sequence duration). Sequences were constructed so that mean speed was greatest for FFF, lowest for SSS, and equal and intermediate for FMS and SMF sequences (Fig 1; Table 1; S1 Fig). One sequence was delivered per trial, beginning 75–100 ms after nose poke entry. Rats had to maintain nose poke for 250 ms to ensure delivery of the entire sequence and then discriminate by selecting a right or left drink port for water reward. FFF and FMS sequences were rewarded right, and SMF and SSS were rewarded left. Training was conducted under infrared light, and sound cues from the piezo were masked. In a subset of trials (43 trials, 4 rats), we verified with high-speed video that whiskers remained on the panel throughout the stimulus period and that rats did not whisk while in the nose poke, as shown previously [22]. Head movement averaged 0.8 mm in right-left position and 1.0 mm in

rostrocaudal position during the stimulus period. Rats initially trained on FFF versus SSS discrimination and then FMS and SMF stimuli were added (see Materials and Methods).

Fig 1. Whisker stimuli and behavioral apparatus. (A) Schematic of training apparatus, showing the rat's right whiskers resting on the moveable stimulus panel. (B) Panel kinematics for fast, medium, and slow impulses. Circles indicate maximum velocity. (C) Panel kinematics for FFF, FMS, SMF, and SSS sequences. Data for this panel are in S1 Data. (D) Mean speed, total duration, and first pulse peak velocity for the four sequences. SMF and FMS sequences had similar mean speed and duration (dashed lines). These sequences differed in both rapid stimulus features, like identity of individual impulses, and slow features, like mean speed of the entire sequence. We designed the task so that fully correct discrimination is only possible if rats attend to fine time-scale information, like precise internal structure of the train (FFF or FMS indicates choose right, SMF or SSS indicates choose left), or identity of the first impulse (F indicates choose right, S indicates choose left). In contrast, if
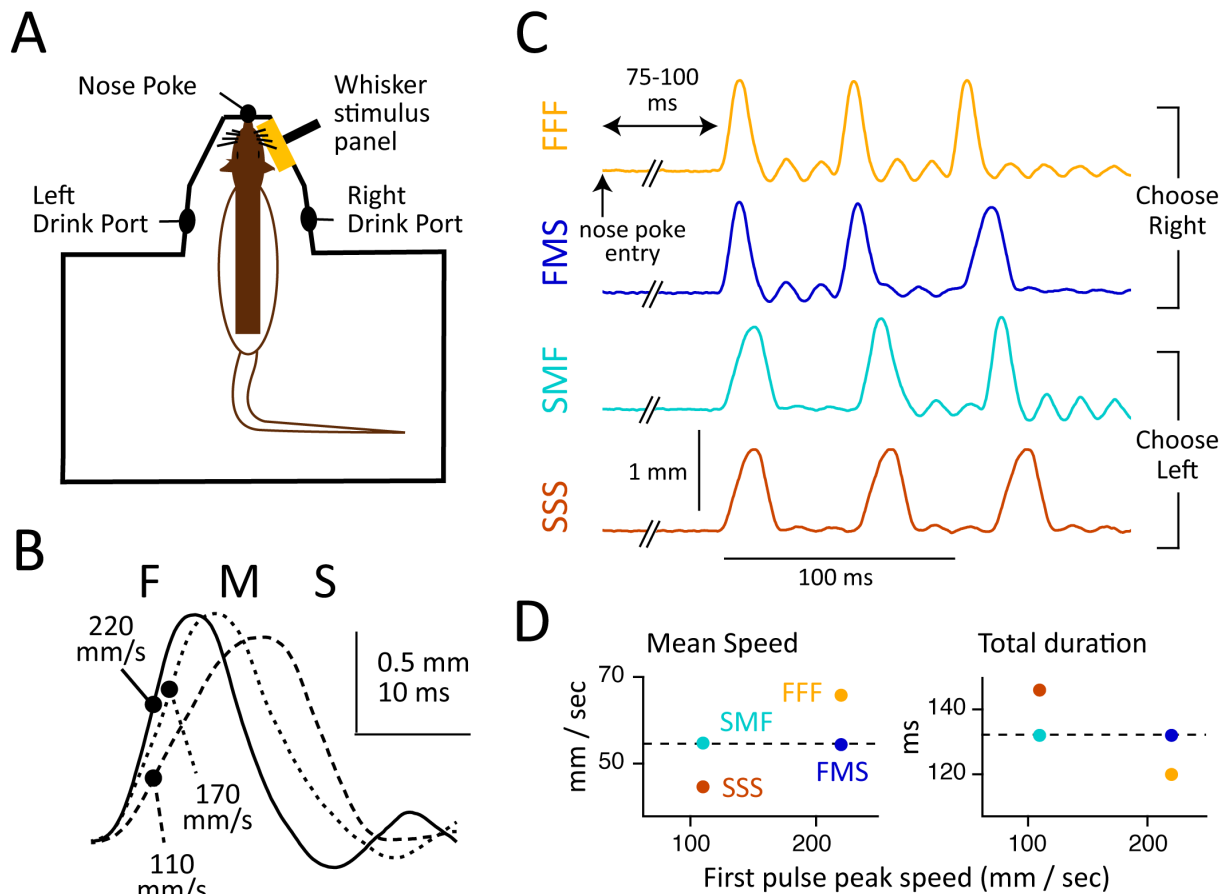
behavior is guided by mean speed (or duration) of the entire sequence, then rats should respond to FFF and SSS correctly but make mistakes in which they treat SMF and FMS identically and intermediate to FFF or SSS. Using a similar task design in which both rapid and slow, integrated cues were available, two prior studies found that rats choose to guide vibrotactile discrimination by the integrated variable, mean speed or intensity [12,13].

After 14.2 ± 4.4 (standard deviation [s.d.]) (range: 8–22) d of training on FFF-FMS-SMF-SSS discrimination, all eight rats successfully discriminated FFF from SSS stimuli, but failed to respond appropriately to FMS and SMF stimuli, instead treating them as equivalent and intermediate between FFF and SSS (Fig 2A and 2B). Seven out of eight rats failed to differentiate at all between FMS from SMF stimuli (proportion test, Bonferroni-adjusted p-value >0.00625). One rat (62SC) showed modest but significant discrimination, with more right-side choices to FMS than SMF stimuli ($p = 0.0039$). Behavior was stable, on average, across the training period (S2 Fig). Thus, seven out of eight rats showed behavior consistent with guiding decisions by time-integrated whisker information. To examine this further, we plotted the mean behavioral performance of each rat versus the mean speed of panel movement across the entire sequence (150 ms). Behavioral performance was computed as (fraction of right drink port choices for each stimulus) – (mean fraction of right drink port choices for all stimuli), to account

for right-left choice bias by some rats (Fig 2B). Right drink port choice was strongly related to mean sequence speed for all rats (Fig 2C).
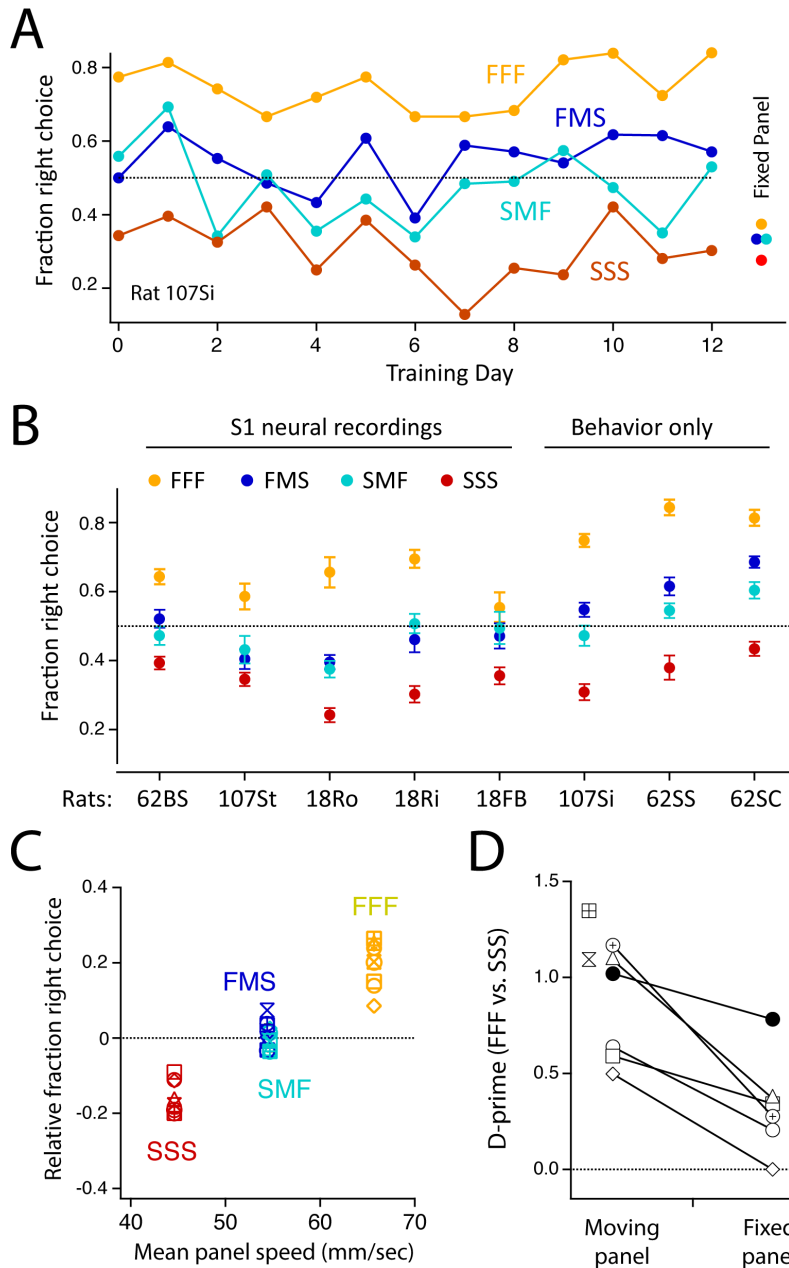
Fig 2. Behavioral performance on FFF-FMS-SMF-SSS discrimination task. (A) Discrimination performance for one example rat, across 13 d of training (44–50 trials for each stimulus per day). FMS and SMF stimuli were first introduced on Day 0. The rat reliably discriminated FFF from SSS stimuli but treated FMS and SMF stimuli identically and at chance. The rat responded similarly to all stimuli when the panel was fixed, and thus was not discriminating based on piezo auditory cues. (B) Mean performance (± SEM) for all rats across all behavior sessions. (C) Relative right drink port choice as a function of mean panel speed over the entire 150-ms sequence. Each symbol is a different rat ($n = 8$). (D) D-prime analysis of FFF versus SSS discrimination in fixed-panel control experiments versus normal sessions. Solitary points show rats not tested on the fixed-panel control. Data for this figure are in S1 Data.

To confirm that rats guided behavior by panel movement, we ran a "fixed panel" control in six rats, immediately after the final normal training session. The panel was fixed in place, while the piezo behind it moved normally. Panel fixation strongly impaired behavioral discrimination in all but one rat (example rat, Fig 2A; population data using d-prime analysis, Fig 2D; population data using a simpler non-parametric analysis, S2B Fig). Some residual discrimination did persist and may have been mediated by inadequately masked piezo sound cues. Further analysis showed that three rats treated the average fixed-panel stimulus similarly to SSS stimuli; one rat responded by choosing right or left randomly; and one rat stopped completing trials in the fixed-panel condition (S2C Fig). Thus, different rats had different strategies for handling the unfamiliar fixed panel trials.

These results suggests that, as in prior studies [12,13], rats used slow, integrated information (mean speed or intensity) to guide discrimination, rather than rapid information (first or last impulse identity or impulse order). This may reflect either a predisposition for intensity cues, or task factors such as our use of strong intensity cues in initial training or the nose poke time requirement, which may have promoted an integration-based strategy. Rats are known to sense fast kinematic cues during ongoing sequences [7–11], and they can utilize these cues for discrimination in some cases [8]. We did not apply additional stimuli to further dissociate slow from rapid information (as was done in [12,13]), and thus we cannot independently rule out the possibility that rats guided behavior from a hidden fast cue (e.g., second impulse identity) that correlated with mean speed.

Discrimination of FSFS versus SFFS Sequences

To test whether failure to discriminate FMS versus SMF reflected insufficient training on these sequences or the presence of easier FFF and SSS stimuli on 50% of trials, we trained two rats on a modified task. This used a very simple task structure with only two stimuli: an FSFS sequence (rewarded at the right drink port) and an SFFS sequence (rewarded at the left drink port). F and S impulses had 216 and 120 mm/s peak velocity and 1.2 and 0.7 mm amplitude, respectively. Both trains had 34 ms interpulse interval and 188 ms total duration (Fig 3A). We constructed two sets of stimuli: a "same-intensity" version in which FSFS and SFFS trains had nearly identical mean speed (25.7 and 26.4 mm/s, calculated across the full sequence), and a "different-intensity"

version in which FSFS and SFFS stimuli were scaled in amplitude so that mean speed was 27.8 and 8.7 mm/s, respectively.
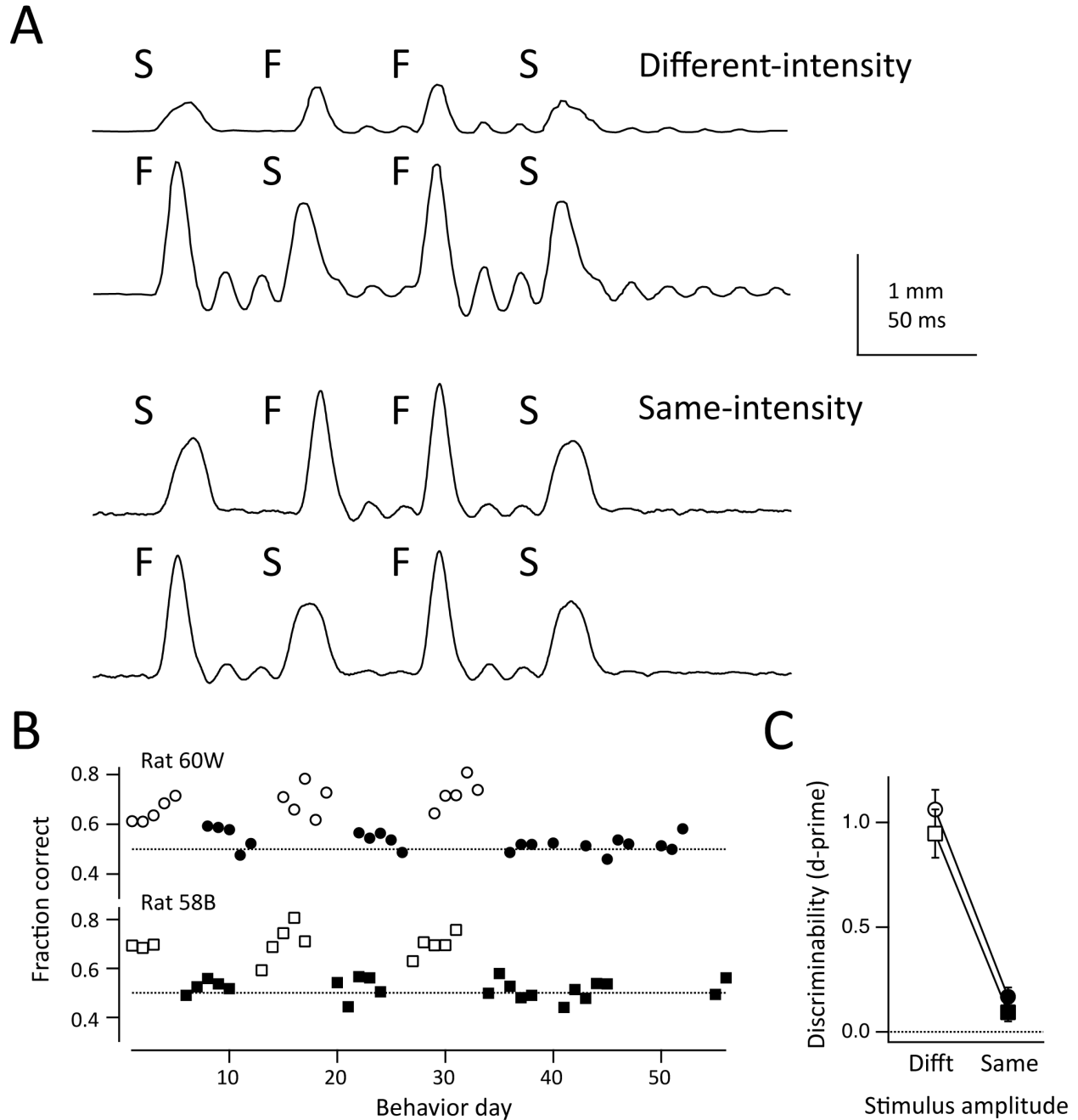
Fig 3. Behavioral performance on FSFS-SFFS discrimination task. (A) Panel kinematics for SFFS and FSFS sequences, showing both different-intensity and same-intensity versions. (B) Behavioral performance across all behavioral sessions, for the two rats trained on this task. Open symbols: sessions using the different-intensity version of the stimuli. Filled symbols: the same-intensity version. Both rats could discriminate the different-intensity version but not the same-intensity version. (C) D-prime analysis of discrimination performance for the same two rats (circles: 60W, squares: 58B), across all behavioral sessions. Symbols are mean ± SEM across sessions. Data for this figure are in S1 Data.

14

Two rats (58B and 60W) were initially trained to discriminate the different-intensity sequences (>65% correct over 3 d). Then, we replaced these stimuli with the same-intensity FSFS and SFFS sequences, so that discrimination could only occur by detecting differences in fine temporal structure, not mean speed. Performance dropped to chance and did not improve over 5 d of training (Fig 3B). We then alternated weekly training on different- and same-intensity sequences. Both rats consistently discriminated FSFS from SFFS when they had different mean speed (58B: 70 ± 1.5% correct, 60W: 69.2 ± 1.6%), but not when they had the same mean speed, even after >20 cumulative days of training (58B: 52 ± 0.8% correct; 60W: 53 ± 0.8% correct). This was evident in the d-prime measure of discrimination between FSFS and SFSF stimuli, which was 1.02 for different-intensity stimuli and 0.12 for same-intensity stimuli (Fig 3C). Thus, behavior correlated with the presence of a slow, integrated cue.

S1 Recordings during Behavioral Discrimination

To study S1 coding of whisker sequences during vibrotactile discrimination, we recorded S1 spiking during the FFF-FMS-SMF-SSS behavioral task using chronic multi-tetrode microdrives. Four tetrodes (~350 um lateral spacing) were driven as a group, enabling simultaneous recording of many neurons in several whisker-related columns (Fig 4A). Tetrodes were initially implanted into mid-L2/3 and advanced by ~140 μm every one to two recording sessions, sampling neurons from L3 to L6 over 12–22 d of recording. Spike sorting yielded 3.8 (range: 0–11) well-separated single units per recording session (Fig 4B). Additional units showed clear separation from noise but failed the interspike interval criterion for single units and were classified as multi-units. We obtained 306 single units and 167 multi-unit clusters (total: 473 units) across 80 recording sessions in five rats (18FB, 18Ri, 18Ro, 62BS, 107St), spanning across L3 to L6 (Fig 4C). Fast-spike (FS) and regular-spike (RS) units were well separated by spike width. Recordings were localized to C1-4, D2-4, and E3 columns based on receptive field mapping under light isoflurane anesthesia and recovery of marking lesions. These whiskers were visually confirmed to contact the panel, as in a prior study using this behavioral apparatus [22].
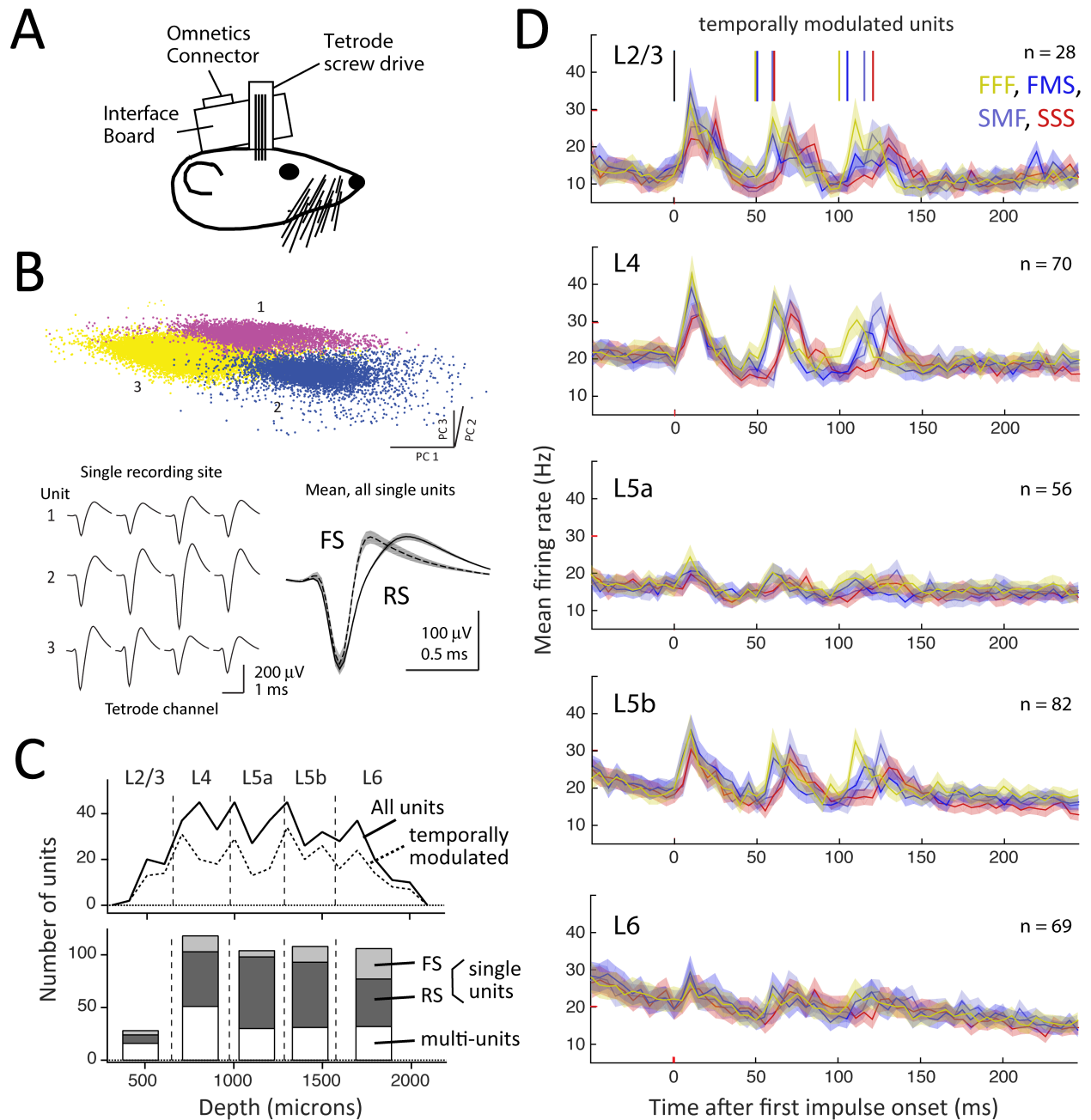
Fig 4. S1 recordings during discrimination behavior. (A) Schematic of multi-tetrode chronic microdrive. (B) Cluster separation for one recording site (top) with mean spike waveforms for three simultaneously recorded single units (bottom left). Bottom right, mean spike waveform for all fast-spike (FS) and regular-spike (RS) single units. (C) Laminar distribution of recorded units. (D) Population peri-stimulus time histogram (PSTH) for all temporally modulated units by layer and stimulus type. Different sequences have different onset times for impulses 2 and 3 (colored ticks). Data for this figure are at crcns.org repository (accession ssc-4).

Mean firing rate during a 25-ms prestimulus baseline period in the nose poke was 6–10 Hz across layers for RS units, 8–32 Hz for FS units, and higher for multi-unit clusters (Table S1). Lowest firing rates were observed in L2/3, L4, and L6. Firing rate distributions were positively skewed (S3A Fig). Firing rates for RS units were higher than in prior studies using cell-attached or whole-cell recording in rodents whisking mostly in air [6,24,25]. This likely reflects recording bias for more active units and the fact that whiskers contacted the stimulus panel through the entire nose poke duration, including the baseline period.

We first identified units whose average firing rate was significantly temporally modulated with any dynamics during the nose poke period ($p < 0.05$, temporal modulation permutation test, see Materials and Methods). Three hundred five out of 473 units (63.5%) showed significant temporal modulation. Temporally modulated units were distributed uniformly across whisker columns and layers (Fig 4C) and had higher baseline firing rates than non-modulated units (S3B Fig). Subsequent analysis focused only on these temporally modulated (i.e., task-involved) units. Single- and multi-units showed similar response properties and were combined for analysis unless indicated.

The average population response, compiled across all temporally responsive units in each layer, was dominated by a brief, phasic increase in firing rate following each panel impulse (Fig 4D). This was greatest in L2/3, L4, and L5b, and weakest in L5a and L6. The mean impulse-evoked firing rate modulation (in Hz above pre-impulse baseline) was 14.2 ± 2.3 in L2/3, 15.2 ± 1.9 in L4, 6.3 ± 1.2 in L5a, 14.4 ± 2.3 in L5b, and 7.0 ± 1.5 in L6 ($n = 28$–82 units per layer). Among units with significant impulse responses, peak response latency was shortest in L4, L5a, and L5b (9.8, 10.3, and 12.0 ms) and longest in L2/3 and L6 (13.8 and 16.1 ms). Superimposed on these phasic responses to individual impulses was a gradual decrease in average firing rate during the nose poke period, observed in all layers except L5a (Fig 4D).

Individual units most commonly showed phasic responses to individual impulses (examples, Fig 5A and 5B). However, some units instead showed cumulatively increasing firing rate during the stimulus period (Fig 5C and 5D) or decreasing firing rate (not shown). These were intermixed in the same columns and recording sites.
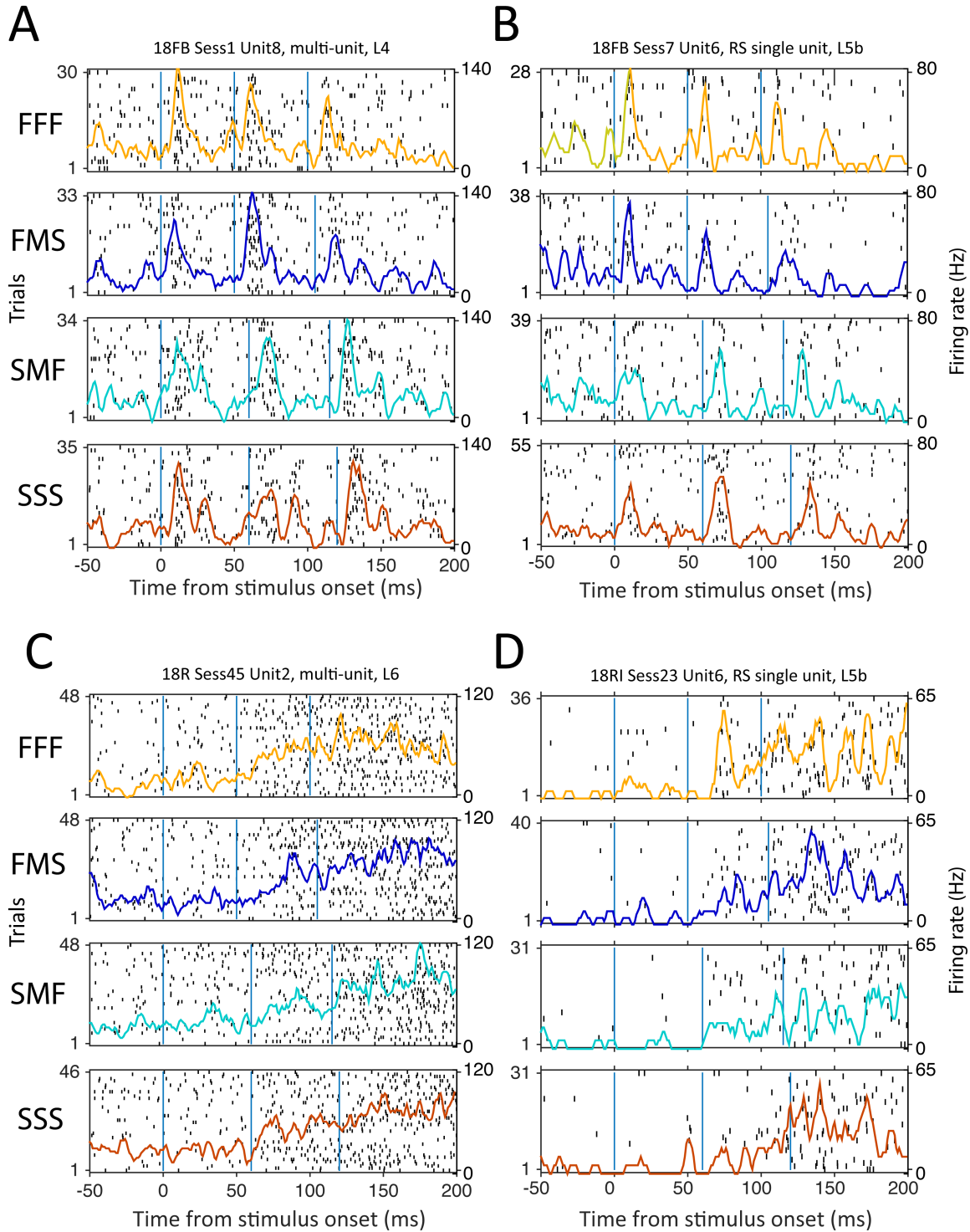
Fig 5. Sequence responses for example units. (A and B) L4 multi-unit and L5b RS single unit with phasic response to each impulse. (C and D) L6 multi-unit and L5b RS single unit with increasing firing rate during the stimulus period. Each panel shows the spike raster and PSTH across trials, for one stimulus sequence. Vertical lines: onset of each impulse. Data for this figure are at crcns.org repository (accession ssc-4).

Regression Analysis to Identify Fast- and Slow-Time Scale Units

To quantify the time scales of stimulus representation in S1, we performed a multiple regression analysis for each temporally modulated unit (n = 305), whose goal was to identify the time window of stimulus integration that best predicted the neuron's firing rate (Fig 6). The dependent variable was firing rate, in 5 ms bins, calculated over all trials for each stimulus sequence. The regressors were integrated speed of panel movement over a variety of temporal integration windows (5, 10, 15, … 180 ms, for a total of 36 regressions). Firing rate in each 5 ms bin was predicted from the integrated panel speed in the preceding bin. Two hundred four units showed a significant regression for at least one stimulus integration window (α = 0.05/36 = 0.0014, using Bonferroni correction for the multiple regressions). For each unit, we defined the best fit integration window as the stimulus integration window with the highest R^2 value.
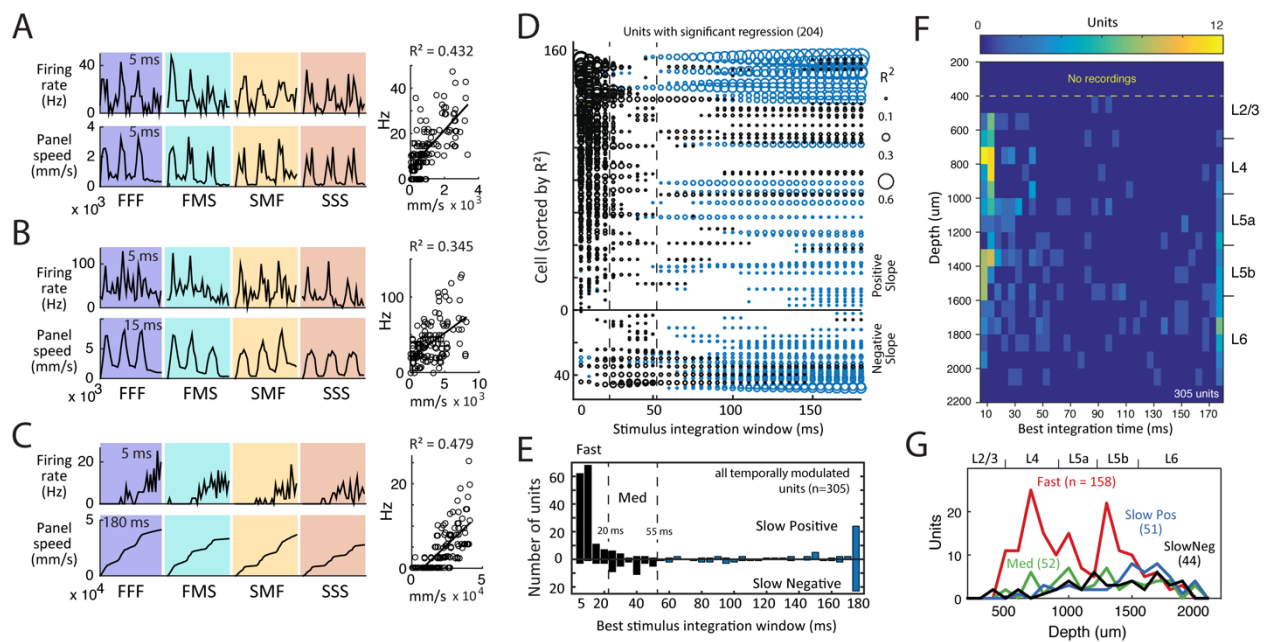
Fig 6. Classification of S1 units by stimulus regression. (A–C) Stimulus regression for three example units. Top, PSTH in 5 ms time bins. Bottom, stimulus panel speed integrated over 5, 15, or 180 ms, which was the best fit stimulus integration window for each unit. Right, regression of firing rate on integrated stimulus speed. (D) Coefficient of determination (R^2) for all stimulus integration windows with a significant regression, for each unit with a significant regression to at least one window. Black: Fast and Medium time scale units (best integration window <55 ms). Blue: Slow units. Cells are sorted by peak R^2 and by sign of the regression slope for the best integration window. (E) Number of units with each best integration window and positive or negative regression slope. (F,G) Laminar distribution of units by best integration window. Data for this figure are in S1 Data.

Most units had a short best fit integration window (5–20 ms), indicating that firing rate was best predicted by stimulus speed on a short time scale (examples, Fig 6A and 6B). However, some units exhibited slowly increasing or decreasing firing that was correlated with integrated speed over long timescales, most often the whole stimulus period (example, Fig 6C). Individual cells had high R^2 values for either short or long integration windows but rarely both (Fig 6D). Most units showed a positive regression slope for the best integration window, indicating that firing rate increased with integrated stimulus speed, while ~20% showed a negative slope (Fig 6D and 6E). Empirically, units with 5–20 ms best integration windows (Fast units; $n = 158$) had positive slopes. Units with 25–55 ms integration windows were rarer (Medium units; $n = 52$) and had largely negative slopes. Units with slow (55–180 ms) integration windows had either positive regression slope (Slow Positive units; $n = 51$) or negative regression slope (Slow Negative units; $n = 44$).

Fast units were 73% of temporally modulated units in L2/3 and L4, 50% in L5, and 23% in L6. Overall, 52% of temporally modulated units were Fast units. Both Fast and Medium units were most prevalent in L2/3, L4, and L5b. In contrast, both Slow Positive and Slow Negative units were located primarily in L5 and L6 (Fig 6F and 6G). Overall, slow units were 13% of temporally responsive units in L2/3 and L4, 31% in L5 and 56% in L6. Fast, Medium, Slow Positive, and Slow Negative categories each contained both single- and multi-units and both RS and FS units.

Fast and Medium Time Scale Units

Fast time scale units showed temporally precise coding of individual panel impulses and sequences (Fig 7A–7C). Population PSTHs for the fastest units (5 ms best integration window) showed responses to F impulses (16 ms duration) that lasted just ~20 ms and responses to S impulses that tracked impulse onset and offset separately. Units with 10 ms and 15–20 ms best integration windows had somewhat slower responses, as expected, but still tracked individual impulses. Adaptation within each train was quantified as mean firing rate to pulse N/pulse 1 and was modest in FFF trains (2/1: 0.80 ± 0.11, 3/1: 0.70 ± 0.14, $p < 0.05$ by t test, $n = 61$ single RS units with significant response to F impulses) and statistically absent in SSS trains (2/1: 1.09 ± 0.26, 3/1: 0.86 ± 0.35, all mean $\pm$ SEM) (Figs 7A and S4). This is less adaptation than reported for non-whisking, non-task-engaged rats [16,26] and is similar to passive whisker detection [10].
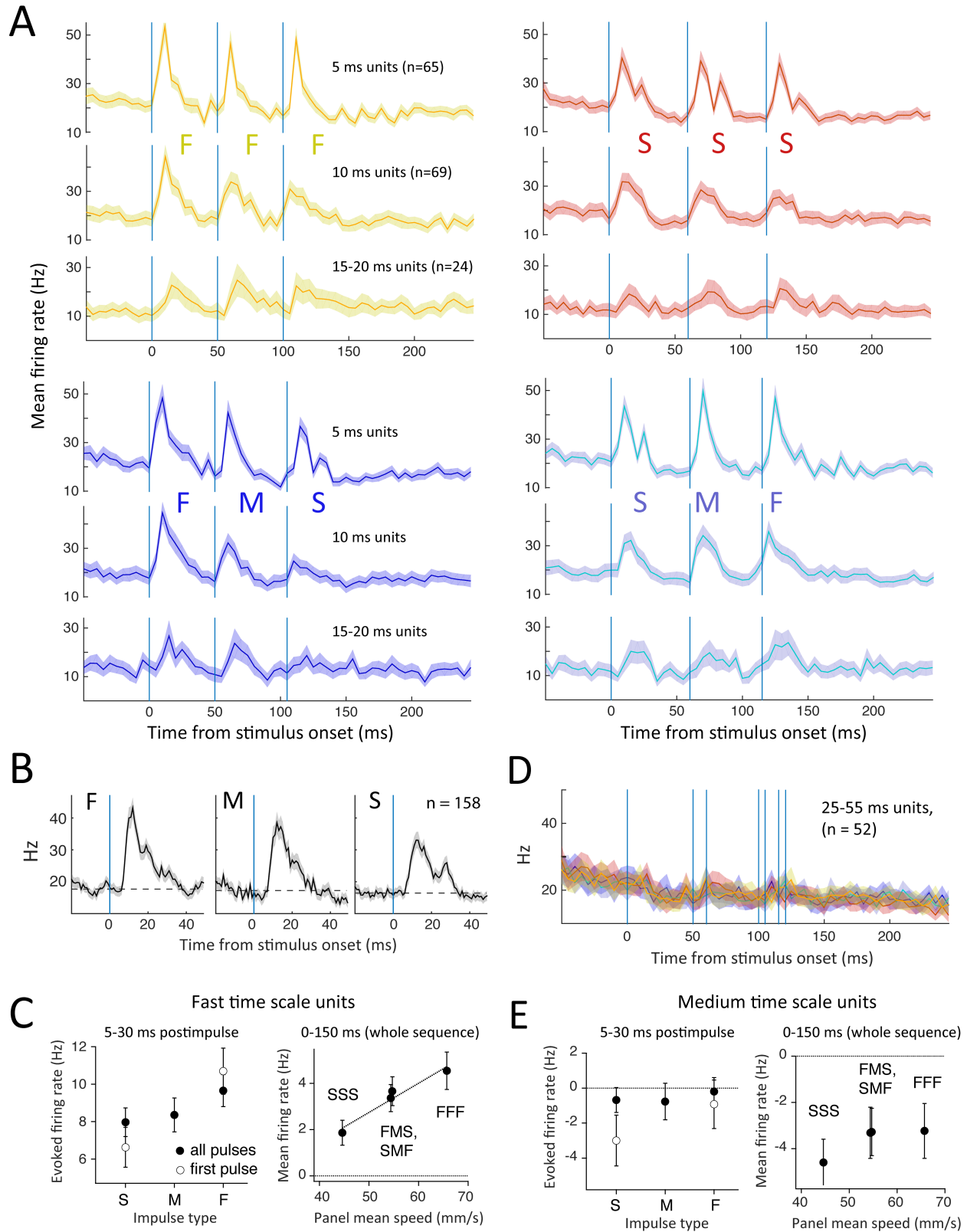
21

Fig 7. Stimulus coding by fast time scale units. (A) Population PSTH (mean ± SEM) for Fast units with 5, 10, and 15–20 ms best integration windows. (B) Population PSTH for all individual F, M, or S impulses, irrespective of sequence membership, for all Fast units. Dashed line: pre-impulse firing rate. (C) Left: net evoked rate for individual impulses, calculated as post-impulse rate – pre-impulse rate. Right: mean rate across the entire sequence above pre-stimulus baseline, as a function of mean panel speed. Symbols show mean ± SEM across units. Line: regression. (D) Population PSTH for Medium units for FFF, FMS, SMF, and SSS sequences. (E) Net evoked rate for individual impulses and mean rate across the sequence for Medium units. Conventions as in C. Firing rate was suppressed by all impulses and sequences. Data for this figure are at crcns.org repository (accession ssc-4).

To determine whether Fast units accurately discriminate impulse velocity, we calculated the average response to all individual F, M, or S impulses (compiled across all sequences). The firing rate of Fast units ($n = 158$) in a brief window after each impulse was greater for F versus S impulses, and intermediate for M impulses (Fig 7C, left). Mean firing rate measured over the entire duration of a sequence (0–150 ms after sequence onset) varied closely with mean speed of the sequence, being highest for FFF, lowest for SSS, and intermediate and equal for FMS and SMF (Fig 7C, right). Thus, population average firing rate of Fast units over the entire sequence closely matched the mean behavioral performance of the animals (Fig 2C).

In addition to coding pulse velocity, Fast unit coding was also influenced by pulse order because of adaptation. Fast RS single units ($n = 61$) showed greater adaptation during FFF than SSS sequences. Consistent with this, the middle M pulse in FMS sequences appeared weaker than in SMF sequences, though this did not achieve statistical significance ($p = 0.08$, paired t test, $n = 61$ units) (S4A Fig). Thus, Fast units represent impulse velocity, but with some history dependence due to adaptation, and no sign of positive temporal integration across impulses.

In contrast, medium time scale units responded to impulses with a modest decrease in firing rate, rather than an increase, consistent with the negative regression slope for most of these cells (Figs 6E and 7D). In firing rate analysis, these cells were inhibited by F, M, and S impulses and did not distinguish either individual impulse identity or whole sequence identity (Fig 7D and 7E). Thus, medium time scale units do not represent stimulus information useful for this discrimination task.

Slow Positive and Slow Negative Units

Slow positive units ($n = 51$) also showed a time-locked increase in firing rate after panel impulses, on average, but mostly to the second and third impulses in the sequence. Responses were small and sustained (unlike the large, transient responses by Fast units) and were evident for F and M impulses but not S impulses (Fig 8A). However, mean firing was not different for FFF, FMS, SMF, or SSS trains, suggesting that these neurons do not appreciably integrate impulse information for sequence discrimination (Fig 8A). Slow negative units did not respond

to impulses at all, and firing rate steadily declined over time, not locked to panel impulses (Fig 8B).
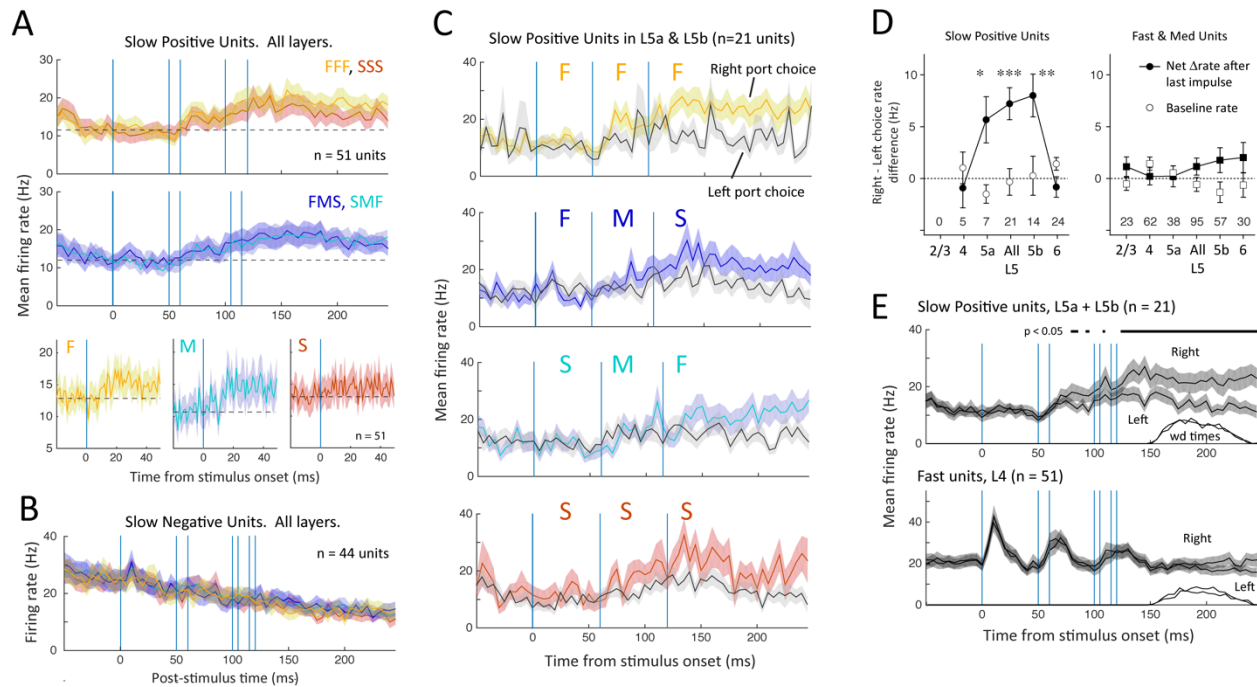
Fig 8. Choice coding by slow time scale units. (A) Top: population PSTH (mean ± SEM) for Slow Positive units across all layers. Responses were indistinguishable between FFF, FMS, SMF and SSS trains. Bottom: population PSTH for individual F, M, and S impulses, irrespective of sequence membership. (B) Population PSTH for slow negative units, showing lack of any impulse-evoked firing rate modulation. (C) Population PSTH for slow positive units in L5a and L5b, separated by stimulus type and drink port choice. Slow Positive units fired more on right-choice trials for all stimuli. (D) Difference in evoked rate between right- and left-choice trials, measured 5–50 ms after start of the final impulse, for all Slow Positive units (left) or Fast and Medium units (right). Number of units in each layer is shown at bottom. Open symbols, baseline rate before sequence onset for the same trials. * $p = 0.022$; ** $p = 9.5^{e-4}$; *** $p = 7.5^{e-5}$, paired t test comparing rate on right versus left choice trials. (E) Population PSTH averaged across all four sequences, for right- versus left-choice trials, for Slow Positive units in L5 (top), and for Fast units in L4 (bottom). Bar shows times when rate is significantly different between right- and left-choice trials by sliding t test ($p < 0.05$). The distribution of nose poke withdrawal times is shown for the same trials. Data for this figure are at crcns.org repository (accession ssc-4).

Unexpectedly, firing of Slow Positive units correlated with the animal's behavioral choice on each trial. Fig 8C shows population PSTHs for Slow Positive units in L5a and L5b, divided into trials in which the rat chose the right- or left-side drink port. Slow Positive units fired more on trials when the rat chose right (contralateral to the S1 recording). This was true for both FFF and FMS stimuli, for which right was the correct response, and SMF and SSS stimuli, for which right

23

was the incorrect response. We quantified right-choice bias as the firing rate difference on right versus left trials, measured 5–50 ms after the start of the final impulse. Right-choice bias was significant for Slow Positive units in L5a and L5b, but not other layers (Fig 8D). Firing rate began to diverge on right versus left choice trials after the second impulse and was consistently significant by 125 ms, which is during the third impulse ($p < 0.05$, sliding paired t test) (Fig 8E). This preceded the earliest withdrawals (150 ms) and mean withdrawal time (190 ms). Choice-related activity was absent in fast time scale units in L4 (Fig 8E).

Thus, L5 Slow Positive units exhibited weak impulse-evoked spiking and strong choice-related spiking (Fig 8). We tested for stimulus integration in these units by comparing firing rate during each impulse of FFF, FMS, SMF, and SSS sequences on right- and left-choice trials separately, which removes choice as a factor (S5 Fig). Evoked firing was minimal for pulses 1 and 2 and was not correlated with pulse velocity. Pulse 3 firing rate was higher but was essentially identical for FFF, FMS, SMF, and SSS sequences and did not correlate with mean speed of the entire sequence or of the last two impulses. Thus, these units did not effectively summate stimulus information across impulses.

We asked whether choice-related firing could reflect a feed-forward sensory reafferent signal generated by decision-related movements in the nose poke. Reafference from fast whisker deflections is unlikely, because L4 Fast units did not exhibit choice-related firing (Fig 8). However, a distinct slow reafferent signal is possible. We tested for choice-related postural movements by analyzing high-speed videos in 43 trials (22 left choice, 21 right choice) from four rats. In each trial, we tracked head position, head angle, and whisker tip position with ~100 μm precision at 8.4-ms intervals from 0 to 150 ms after stimulus onset. Head angle and whisker tip trajectories were invariant between right- and left-choice trials. Head position differed modestly between right- and left-choice trials beginning at 100 ms, with a 0.6 mm difference at 125 ms (S6 Fig). Thus, slow head movements are a potential reafferent driver of choice-related firing in L5.

RS and FS Single Units

Fast, Medium, Slow Positive, and Slow Negative response classes all included RS, FS, and multi-unit clusters, although few FS cells were found in the Slow classes (S7 Fig). Among Fast units, all three unit types had similar sequence-related PSTHs. Among L5 Slow Positive units, both RS units and multi-unit clusters had similar choice-related firing, and no FS units existed in this category (S7 Fig). Thus, all response classes involved RS units.

Neural Decoding of Stimulus Identity and Behavioral Choice

S1 neurons spike sparsely, with individual whisker deflections eliciting mostly zero spikes, occasionally one spike, and, very infrequently, two spikes on a single trial [21,27,28]. We also observed this highly variable, sparse single-trial spiking behavior (Fig 5). To test whether S1

24

accurately encodes whisker sequences on single trials, we constructed a neural population decoder that predicted stimulus identity from single-trial spike trains. In the model, each recorded neuron was represented by a separate, independent one-vs-all (OVA) classifier that predicted the probability of each sequence (FFF, FMS, SMF, or SSS) given one spike train, chosen randomly from that neuron's recorded spike trains in vivo, and binned in discrete time bins. Each OVA classifier was trained by logistic regression from a randomly chosen subset of spike trains for that unit. The output of each classifier was the probability of each stimulus type versus all others, based on the presented spike train. To create a population prediction, stimulus probabilities were summed across units, and the sequence with highest summed probability was taken as the population stimulus prediction (Fig 9A). This model assumes independence between neurons and allows stimulus prediction by both firing rate and temporal information within spike trains.
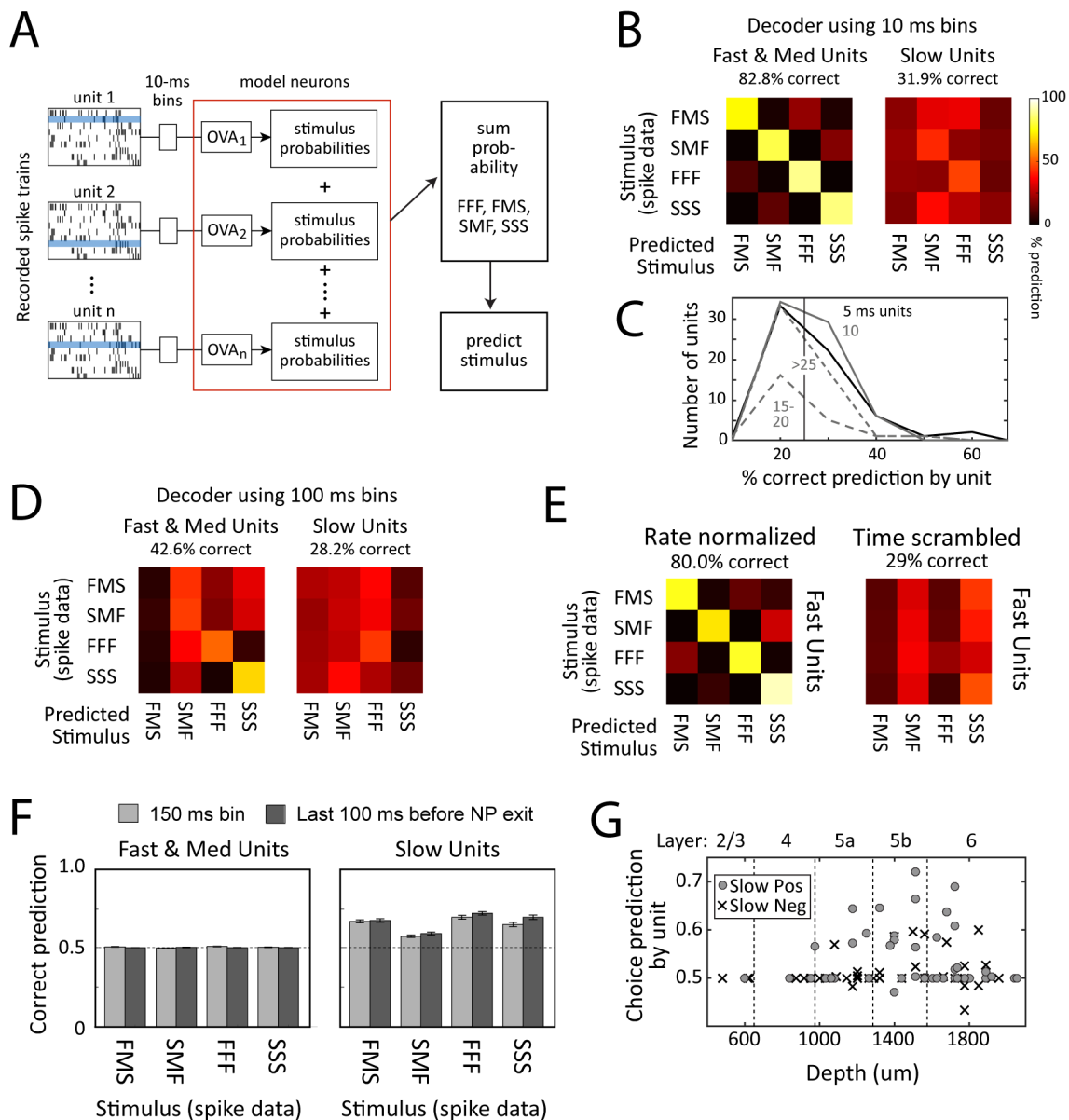

25

Fig 9. Population decoding of sequence identity and behavioral choice. (A) Decoder architecture for stimulus decoding. Each neuron was represented by a one-versus-all (OVA) classifier, trained by logistic regression to calculate the probability of each stimulus given a single-trial spike train (blue trial). The stimulus with the highest summed probability across neurons was taken as the population prediction. (B) Average performance of stimulus decoder with 10 ms time bins, constructed from all Fast and Medium units or all Slow units. The title reports average percent correct classification across all four stimuli. Entries along the diagonal are percent correct, and rows sum to 1.0. (C) Percent correct performance for each unit in the Fast/Medium model in (B), separated by best integration window. Vertical line, chance prediction of 25%. (D) Average performance of stimulus decoder with a single 150 ms time bin. (E) Average performance of a Fast/Medium stimulus decoder with 10-ms bins, using rate-normalized or time-scrambled spike trains. (F) Performance of behavioral choice decoders, built from Fast and Medium units or Slow units, using two different bin sizes. Chance performance is 50%. (G) Choice prediction for each unit in the Slow model, using a single 100-ms bin prior to nose poke withdrawal. Units are separated by depth and response type. Best choice prediction was by Slow Positive units in L5b. Data for B–E are in S1 Data.

We first constructed a decoder from all Fast and Medium units, using 10 ms time bins. This model predicted sequence identity, using one single-trial spike train per model unit, with 83% overall accuracy (range: 74% for FMS to 88% for FFF spike trains). Chance performance is 25% (Fig 9B). The individual neurons with best stimulus prediction were those with 5–10 ms best integration windows (Fig 9C). Remarkably, this model identified SMF and FMS sequences with 78% accuracy, even though rats could not. A second decoder constructed of all Slow units, also using 10 ms bins, predicted sequence identity at near chance levels (32% correct, not significantly different from chance, $p = 0.47$) (Fig 9B). Decoding from mean firing rate in a single 150-ms bin substantially reduced Fast/Medium decoder accuracy (43% correct) and did not improve Slow decoder accuracy (Fig 9D).

To test whether the Fast/Medium model recognized sequences by mean firing rate or temporal spike pattern, we rate-normalized the spike train data (preserving temporal information across the 10-ms bins) or time-scrambled spike trains within trials (preserving firing rate information). Fast/Medium decoders trained on rate-normalized data performed well (80% correct), but time-scrambling spikes abolished performance (Fig 9E). Thus, the Fast/Medium decoder primarily identified stimuli by temporal spike patterns, which varied between FFF, FMS, SMF, and SSS sequences (Fig 7). Thus, sequence identity was primarily encoded in short time-scale spiking information, carried by Fast units.

We constructed a similar decoder to predict behavioral choice. This was trained on spike data from all four sequences and was tested for prediction of right versus left drink port choice separately for FFF, FMS, SMF, and SSS trials. A choice decoder based on Fast/Medium units was unable to predict drink port choice, either using 10 ms bins (not shown), mean firing rate in a single 150-ms bin, or mean firing rate in the last 100 ms prior to nose poke withdrawal (Fig

9F). A choice decoder based on Slow units successfully predicted drink port choice using a single 150-ms bin, or mean firing rate in the last 100 ms before nose poke withdrawal (65% correct for both models) (Fig 9F). Post-hoc analysis showed that units with best choice prediction were Slow Positive units located primarily in L5b (Fig 9G). Thus, spiking of Slow Positive units was sufficient to decode behavioral choice but not sequence identity.

Discussion

Behavioral Integration of Stimulus Sequences

Cortical sensory systems temporally integrate sensory signals for many types of perceptual decision-making [2]. Where and how integration is performed is unclear. In fingertip vibrotactile discrimination by primates, S1 neurons spike to each rapid skin deflection, and this information is temporally integrated downstream of S1 to guide behavioral discrimination [1,29]. In the rodent whisker system, passive vibrotactile discrimination is often based on slow, time-integrated input [12,13], although rats are also capable of discrimination based on rapid kinematics [8]. Integration is also implicated in discrimination of surface texture (roughness), in which surface whisking generates temporally dense sequences of stick-slip whisker micromotions, whose mean statistics, including mean whisker speed, correlate with roughness [3,4,21,30–33]. S1 neurons spike phasically to stick/slip events and other features such as dynamic changes in whisker bend [3,21,34], and behavioral judgments of surface roughness correlate with mean firing rate and rate of synchronous spiking across S1 neurons [21,35,36]. Thus, roughness discrimination likely involves temporal integration of stick/slip events and S1 spike trains. Integration is useful because it reduces the complexity of the vibrotactile signal to a single scalar quantity of stimulus intensity. Intensity-based discrimination is common across modalities and is a defining feature of texture discrimination in people and non-human primates [37]. Integration is also evident in whisker-based object localization, in which S1 spikes are time-locked to object contact, but mice judge object location by behaviorally integrating spike counts over ~50 ms, rather than using precise timing [19].

In our task, rats were able to distinguish FFF versus SSS sequences that differed in mean speed, but not FMS versus SMF sequences that had the same mean speed, and choice behavior was strongly related to mean speed across the sequence (Fig 2). Similar performance was observed in the SFSF versus FSSF task (Fig 3). Task performance was relatively low (d-prime for FFF versus SSS: 0.5–1.5), as in a prior study [13], indicating the difficulty of these tasks. The results suggest that rats utilized slow, time-integrated information for task performance, even though simple, short time-scale cues (e.g., identity of the first impulse) would have led to more rewards. This hypothesis is consistent with two prior vibrotactile discrimination studies using a similar

27

design, in which rapid kinematics and slow intensity cues were manipulated separately to prove that rats guided discrimination by slow, time-integrated cues [12,13]. We did not test this causally in our study, so we cannot rule out that rats may have solved our task using a hidden short time scale cue.

Integration is not required for simpler detection tasks [7,9,10] or detection-of-change tasks [8], and rodents can perceive single brief whisker impulses within ongoing deflection trains [7–11,38]. This suggests that rats generate neural codes for both rapid and integrated features that guide different aspects of sensory-guided behavior. Rats may differentially use these codes depending on task demands and training strategies. In our task, initial training involved strong intensity cues, which may have promoted adoption of an integration-based strategy. An intensity-like feature of vibrotactile stimuli is encoded in primate dorsolateral prefrontal cortex during a working memory task [39], but no explicit intensity representation is known yet in the rodent whisker system.

Stimulus Encoding in S1 Occurs at Fast (5–20 ms) Time Scales

We tested for stimulus integration in S1 during task performance but found that S1 encoded whisker sequences almost exclusively at very rapid time scales. Forty-four percent and 52% of temporally responsive units showed very fast (5–10 ms) and fast (5–20 ms) stimulus integration, respectively (Fig 6E). These units spiked to individual whisker impulses, with firing rate encoding impulse velocity, and mean firing rate correlated with mean whisker speed across the sequence (Fig 7A–7C). Seventeen percent of units showed firing rate modulations on medium (25–55 ms) time scales, but these were inhibited by whisker impulses and did not discriminate different impulses or sequences (Fig 7D and 7E). Sequence identity could be decoded accurately from Fast units but not Medium units, and stimulus information was abolished by scrambling spike times across 10-ms bins. Thus, Fast units encode sequence identity by representing the velocity and timing of individual impulses. Fast units accurately distinguished FMS from SMF sequences, even though rats could not (Fig 9B). Thus, accurate short time-scale representation of vibrotactile sequences exists in S1 but does not appear to be used efficiently to guide behavior in our task. This is identical to primate S1, in which precise spike timing discriminates vibrotactile flutter more accurately than the animal [40].

Fast units had phasic whisker responses similar to classic anesthetized studies [14,41] and S1 units recorded during detection tasks [7,8,11]. Responses were weak in L5a and L6 (Fig 4), which may reflect involvement of this layer in active whisking, which was absent in our task [42]. Adaptation was minimal: ~25% for FFF trains and absent for SSS trains (Fig 7A–7C). This level of adaptation is less than occurs under anesthesia [15,18] or in quiescent, non-task engaged rats [16,26] and is similar to that during active exploration [16,26] or in a whisker detection task [10]. While adaptation generates history dependence and thus carries information about prior impulses [43,44], Fast units showed no evidence of positive integration across impulses.

Slow Units Do Not Integrate Stimuli but Reflect Behavioral Choice

Seventeen percent of units, primarily in deep layers, were Slow Positive units with small, sustained responses to individual whisker impulses and progressively increasing firing rate during the stimulus period. However, these units did not accurately encode or integrate whisker impulses. Responses were generally absent to the first impulse of sequences, and firing rate did not differ between FFF, FMS, SMF, and SSS sequences or correlate with mean speed (Figs 8A and S5). Thus, Slow Positive units do not appear to carry integrated stimulus information for sequence discrimination. Slow Negative units had slowly decreasing firing rate and no stimulus-related firing modulation at all (Fig 8). Consistent with these observations, sequence identity could not be decoded from Slow unit spike trains (Fig 9B). Slow whisker-evoked spiking occurs in some L2/3 units in mice [20] but was not evident in our dataset in rats.

Instead, firing of Slow Positive units in L5 was strongly related to drink port choice. Choice-related spiking [45] occurs in many cortical areas, including primary visual cortex [46], S1 of primates and rodents [11,47–49], and even subcortically [49,50]. In rodent S1, many L2/3 neurons exhibit choice-related spiking in near-threshold detection tasks [11,49]. Choice-related firing emerged significantly after the second impulse of the sequence and was consistent during the third impulse, 65 ms before the average nose poke withdrawal (Fig 8E). A neural decoder built from Slow unit spike trains predicted behavioral choice from mean firing rate in the stimulus period and in the 100 ms prior to nose poke withdrawal (Fig 9). Choice-related firing was absent in L4 Fast units, suggesting it did not represent reafference from fast whisker sensory signals (Fig 8E). Choice-related spiking could reflect reafference from slow head movements prior to nose poke withdrawal, potentially mediated by POm afferents to L5 [51] or an internal decision or motor preparatory signal. Its onset after the second impulse could reflect an early behavioral decision based on first and second impulse stimulus information or an early stimulus-independent ""guess" that biased subsequent stimulus-dependent drink port choice. Thus, Slow Positive units do not appear to integrate across whisker impulses but combine weak impulse responses with a distinct, slow signal related to behavioral choice.

Where in the Brain Does Temporal Integration Occur?

We found that during vibrotactile discrimination, most S1 neurons represent the velocity and timing of individual whisker impulses at rapid, 5–20 ms time scales. While there was some history dependence of whisker responses due to modest adaptation, we did not observe evidence of positive integration across whisker impulses in S1 firing rates. Thus, temporal integration for discrimination is likely to occur downstream of S1, in higher sensory or premotor regions. These may include S2, prefrontal cortex, and premotor cortex, as in primate vibrotactile discrimination [1]. We cannot rule out that S1 could learn to temporally integrate under conditions in which rats were more reliant on slow cues for behavioral discrimination. For whisker texture perception, our finding of short time scale coding in S1 suggests that S1 primarily encodes low-

level kinematics of individual stick/slips and bends [6,21], which are integrated downstream to represent texture or other surface features.

Materials and Methods

Female Long-Evans rats were >3 mo of age. All procedures were approved by the UC Berkeley Animal Care and Use Committee (protocol R309-0516BC) and comply with NIH guidelines.

FFF-SMF-FMS-SSS Discrimination Task

The computer-automated chamber contained a nose poke, flanked by a wall-mounted whisker stimulus panel (2 x 2 cm) that was carried on a hidden piezoelectric actuator (Piezo Systems PSI-5H4E). Whiskers were trimmed to 15 mm in length. The right-side C, D, and E row whisker tips rested against the panel while the rat was in the nose poke (Fig 1A). Nearby right and left drink ports contained infrared-LED beam sensors to detect nose entry and delivered calibrated water rewards. Trials were monitored by infrared video.

Each trial was self-initiated by entry into the nose poke. After a variable delay (75–100 ms), a sequence of three rapid whisker deflections was delivered via the panel. The rat was required to remain in the nose poke for 250 ms to ensure full sequence delivery. The rat then withdrew from the nose poke and was rewarded (0.05–0.1 mL water) for choosing the drink port that was associated with the presented stimulus. Incorrect drink port choice or premature nose poke withdrawal triggered a time-out tone (4–6 s) and no reward. In a subset of sessions, high-speed video (119 Hz) was recorded.

Whisker sequences. Each whisker deflection sequence consisted of three up-down ramp-return deflections (pulses). Each pulse had either slow (S), medium (M), or fast (F) rise-fall velocity. These pulses differed in rise-fall time and therefore had different pulse durations but similar amplitude (Fig 1B and 1C; Table 1). Sequences had either FFF, FMS, SMF, or SSS pulse order, with 34 ms between the end of one pulse and the beginning of the next, yielding 50–62 ms interval between pulse onsets. Total train duration (from beginning of the first pulse to end of the last pulse) was 120–146 ms. Mean speed, calculated over the entire train, was highest for FFF, intermediate and equal for FMS and SMF, and lowest for SSS sequences (Fig 1D; Table 1; S1 Fig). One sequence was presented per trial, with random order across trials. Training was in the dark, and acoustic cues were obscured using masking noise composed of white noise densely intermixed with sampled piezo sounds. To further mask any unintended auditory cues, an

additional "dummy" piezo was hidden behind the stimulus panel and actuated on each trial in a manner uncorrelated with panel movement.

Table 1. Kinematics of FFF-FMS-SMF-SSS whisker sequences.

Impulse	Rise/Fall Time (ms)	Peak Velocity (mm/s)	Duration* (ms)	Peak Amplitude (mm)
Fast (F)	8	220	16	1.03
Medium (M)	11	170	22	1.15
Slow (S)	14	110	28	1.14

Sequence	Interpulse Interval (ms)	Peak Velocity (mm/s)	Duration* (ms)	Peak amplitude (mm)
FFF	34	120	65.7	Right
FMS	34	132	54.4	Right
SMF	34	132	54.7	Left
SSS	34	148	44.6	Left

* Duration measured as time from initial deflection to return to baseline position.

Training stages and reward contingency. First, rats were trained to nose poke for >150 ms and to drink from the drink ports. Next, rats were presented in the nose poke with exaggerated amplitude and velocity versions of FFF and SSS stimuli and were trained to choose the right drink port for FFF stimuli and the left drink port for SSS. When each rat achieved >60% correct, stimulus amplitude was stepped closer to the final amplitude, and the nose poke time requirement was incrementally increased. This was iterated until the final stimulus amplitude and 250 ms nose poke time requirement were reached. Rats then performed FFF versus SSS discrimination using final-amplitude stimuli for 1–4 wk. At this point, the chronic recording drive was implanted, rats rested for 1 week of recovery, and then training was re-initiated until performance regained pre-surgical levels, usually about a week. Finally, FMS and SMF stimuli were added (rewarded right and left, respectively). All behavioral and neural data reported in the study were collected during this final stage.

FSFS-SFFS Discrimination Task

In this task, each whisker sequence consisted of four pulses. Two pulses were low-amplitude, slow pulses (S) that were 0.7 mm amplitude, 120 mm/sec peak velocity, 12.5 ms rise and fall time, and 25 ms total duration. Two were higher-amplitude, fast pulses (F) that were 1.2 mm amplitude, 216 mm/sec peak velocity, 9 ms rise and fall time, and 18 ms total duration. Trains of F-S-F-S or F-S-S-F pulses were presented (34 ms inter-pulse interval, total train duration 188

ms). In the "same-intensity" stimulus set, both FSFS and SFFS trains had identical pulse amplitude and, therefore, mean speed (mean speed 25.7 mm/sec for FSFS, and 26.4 mm/sec for SFFS). In the "different intensity" stimulus set, FSFS stimulus amplitude (and velocity) was increased to achieve a mean speed of 27.8 mm/sec, and SFFS stimulus amplitude (and velocity) was decreased to achieve a mean speed of 8.7 mm/sec. Training was performed in identical steps as above, using the "different-intensity" stimuli at the second training stage. No recordings were performed.

Neural Recordings

Recordings were made with an array of four tetrodes carried in a custom 3D-printed chronic microdrive. Tetrodes (12.5 μm nichrome wire, gold plated to 0.2–0.3 MΩ impedance) were spaced 0.35 mm apart in a square configuration and moved together as a single bundle along a radial penetration. The tetrode drive was mounted in a surgical procedure under initial ketamine-xylazine anesthesia (90 mg/kg and 10 mg/kg), maintained by transition to 0.5%–3% isoflurane. A 4-mm craniotomy was opened over S1 (5.5 mm lateral, 2.5 mm caudal to bregma), the dura was removed, and the microdrive was positioned over the durotomy. The tetrodes were lowered into L2 of S1 and the microdrive was mounted with dental cement, sealing the craniotomy. Reference and ground electrodes were mounted in the skull. Postoperative analgesia was provided with Buprenorphine (0.05 mg/kg every 8 h) for 1–2 d post-surgery. Animals recovered 5–10 d prior to behavioral and recording sessions.

Recordings were made during one to two behavioral sessions per day for each rat. Tetrode signals were amplified and filtered (Plexon, 100x gain, 0.3–8 kHz bandpass filter) and digitized at 32 kHz, using methods as in [21]. Neural data was acquired continuously. Tetrodes were advanced a half-turn (140 μm) every one to two recording sessions, at least 30 min before recording started. A new set of units was sampled in every session. If new units appeared spontaneously overnight, the tetrode was not advanced. Recording ended when the tetrode entered the white matter, as judged by absence of spiking activity when advancing the drive. Twelve to 22 d of recording were performed per animal.

Recordings were made in C1–4, D2–4, and E3 whisker columns, as determined by hand mapping under isoflurane anesthesia prior to the recording sessions. An electrolytic lesion was made at the final recording location to determine recording depth. Lesions were recovered in cytochrome oxidase-stained histological sections (100 μm thick) cut in the "across-row" plane, 45° coronal to the midsagittal plane [52,53]. This allowed the whisker row identity (A–E) of the recorded column and laminar identity of recording sites to be confirmed. Laminar boundaries were determined by aligning lesions with layer-specific CO staining boundaries, and were as follows: L2/3: 200–650 μm, L4: 650–975 μm; L5A: 975–1285 μm; L5B: 1285–1575 μm; L6: 1575–2200 μm.

Single units were isolated offline using Wave_clust in Matlab [54]. After an initial automated clustering step, manual evaluation of all clusters was performed and manual changes to the clustering were carried out as needed. Single units were required to meet an interspike interval criterion (<0.5% of intervals less than 1.5 ms) and a signal-to-noise (STN) criterion for spike height (STN>2, with STN defined as the difference from trough to peak in the mean waveform divided by the average standard deviation across all samples in the waveform). Fast-spiking and regular-spiking units were classified by spike width, which was bimodally distributed. Fast spiking units had width <0.375 ms trough-peak delay.

Neural Data Analysis

Neural data were analyzed for five rats, including one rat for whom the fixed-panel control task showed substantial task performance in the absence of panel movement (filled circles in Fig 2D). This rat's data were included because panel-evoked responses, stimulus decoding, and choice decoding did not differ from other rats (not shown).

Temporal response modulation. We identified units whose firing rate was significantly temporally modulated during the stimulus presentation period (0–180 ms after NP entry) using a permutation test [55]. Measured firing rate was compared in 10-ms bins with randomly time-permuted spikes (10,000 permutations). Units with significant difference from permuted data ($p < 0.05$) were considered temporally modulated and were included in further analysis.

Stimulus-evoked responses. PSTHs were calculated with 1 ms time bins, aligned to onset of the first impulse. Unit PSTHs were smoothed (10 ms boxcar) for display only (Fig 4). Stimulus-evoked firing modulation quantifies the peak evoked response in a 40-ms window post-stimulus. It was calculated as the difference between mean baseline firing rate (0–10 ms prior to pulse onset) and maximum or minimum firing rate anywhere in a 40 ms window after stimulus onset (with 10 ms smoothing). Peak response latency was defined as the time of this maximum response. Mean impulse-evoked firing rate was quantified in a 5–35 ms window after impulse onset. Impulse-responsive units were defined as those neurons whose mean impulse-evoked firing rate was significantly greater than baseline firing rate (0–10 ms before impulse onset) by t test.

Stimulus regression. We performed a multiple regression to determine the optimal stimulus integration window for each unit. The neural responses from 0 to 180 ms relative to stimulus onset were binned into 5 ms windows and used as the dependent variable in this regression. The independent variables (regressors) were the integrated speed of the panel over a series of fixed integration windows, from 5 to 180 ms in 5-ms steps. Each speed bin (e.g., from -20 to 0 ms in the 20 ms integration window regression) was used to predict firing rate in the subsequent 5-ms bin (from 0 to 5 ms in this example). For cells that had significant regressions in at least one stimulus integration window ($p < 0.05/36 = 0.0014$, Bonferroni correction for 36 integration windows tested), the best fit integration window was taken as the stimulus integration window

with the highest R^2 value. Regression was performed in Matlab. Integration window is not independent from latency in this analysis; however, inspection of PSTHs shows that units identified by the regression as having progressively longer best integration windows exhibited progressively slower whisker-evoked responses, not just longer latencies (Figs 7A, 7B, 8A, and 8B).

Neural Decoders

A neural decoder was constructed to predict stimulus identity (FFF, FMS, SMF, SSS) from single-trial spike trains of the recorded units. Each unit was represented by a one-versus-all (OVA) classifier that was trained by logistic regression to report the probability of each stimulus given a single-trial spike train (0–150 ms after stimulus onset, binned using either 10 ms bins or a single fixed time bin), selected randomly from recorded spike trains for that unit. Each classifier comprised four logistic functions, one for each stimulus. Logistic functions were fit using logistic regression and k-fold cross-validation and were specified by coefficients (one for each time bin, plus a bias term) that relate spike rate in each time bin to the probability of stimulus *s* being delivered. Model fitting was performed using a randomly chosen subset of the recorded trials (70%), and decoder performance was assessed on the remaining trials. The output of each unit classifier was normalized so that each unit had the same weight in population decoding. The population stimulus prediction s_p was calculated by summing the probabilities of each stimulus over all units and selecting the stimulus with the maximal summed probability. Model fitting and population decoding were repeated 300 times, and average performance is reported. This framework is equivalent to determining s_p as the stimulus that maximizes the conditional probability of the four stimuli given the neural population response, assuming that all single units are independent and the prior distribution of *s* is uniform. Rate-normalized and time-scrambled spike trains were generated by dividing each spike train by its -Euclidean norm and shuffling spike times within trials, respectively.

A separate behavioral choice decoder was constructed similarly and was used for predicting right or left drink port choice on a given trial. Since this is a binary decision, a single logistic function was fit for each unit. The model was fit using spike train and behavioral choice data from all four stimuli. Decoder performance was assessed separately for FFF, FMS, SMF, or SSS stimulus trials in order to dissociate stimulus identity from the rat's behavioral choice. The population choice prediction c_p was selected as the choice with maximal summed probability across all units, given single-trial spike trains from trials with the chosen stimulus type. Model fitting and decoding procedures were the same as above.   All decoding analysis was performed using Python and the scikit-learn machine learning toolbox [56].

Acknowledgments

We are grateful to Sei Ahn for video analysis of behavior.

References

1. Romo R, Salinas E. Flutter discrimination: neural codes, perception, memory and decision making. Nat Rev Neurosci. 2003;4: 203–218. doi:10.1038/nrn1058

2. Gold JI, Shadlen MN. The neural basis of decision making. Annu Rev Neurosci. 2007;30: 535–574. doi:10.1146/annurev.neuro.29.051605.113038

3. Arabzadeh E, Zorzin E, Diamond ME. Neuronal encoding of texture in the whisker sensory pathway. PLoS Biol. 2005;3: e17. doi:10.1371/journal.pbio.0030017

4. Wolfe J, Hill DN, Pahlavan S, Drew PJ, Kleinfeld D, Feldman DE. Texture coding in the rat whisker system: slip-stick versus differential resonance. PLoS Biol. 2008;6: e215. doi:10.1371/journal.pbio.0060215

5. O'Connor DH, Clack NG, Huber D, Komiyama T, Myers EW, Svoboda K. Vibrissa-based object localization in head-fixed mice. The Journal of Neuroscience. 2010;30: 1947–1967. doi:10.1523/JNEUROSCI.3762-09.2010

6. Andrew Hires S, Gutnisky DA, Yu J, O'Connor DH, Svoboda K. Low-noise encoding of active touch by layer 4 in the somatosensory cortex. Elife. 2015;4. doi:10.7554/eLife.06619

7. Stüttgen MC, Schwarz C. Psychophysical and neurometric detection performance under stimulus uncertainty. Nature Neuroscience. 2008;11: 1091–1099. doi:10.1038/nn.2162

8. Waiblinger C, Brugger D, Schwarz C. Vibrotactile discrimination in the rat whisker system is based on neuronal coding of instantaneous kinematic cues. Cereb Cortex. 2015;25: 1093–1106. doi:10.1093/cercor/bht305

9. Ollerenshaw DR, Bari BA, Millard DC, Orr LE, Wang Q, Stanley GB. Detection of tactile inputs in the rat vibrissa pathway. J Neurophysiol. 2012;108: 479–490. doi:10.1152/jn.00004.2012

10. Stüttgen MC, Schwarz C. Integration of vibrotactile signals for whisker-related perception in rats is governed by short time constants: comparison of neurometric and psychometric detection performance. The Journal of Neuroscience. 2010;30: 2060–2069. doi:10.1523/JNEUROSCI.3943-09.2010

11. Sachidhanandam S, Sreenivasan V, Kyriakatos A, Kremer Y, Petersen CCH. Membrane potential correlates of sensory perception in mouse barrel cortex. Nature Neuroscience. 2013;16: 1671–1677. doi:10.1038/nn.3532

12. Gerdjikov TV, Bergner CG, Stüttgen MC, Waiblinger C, Schwarz C. Discrimination of vibrotactile stimuli in the rat whisker system: behavior and neurometrics. Neuron. 2010;65: 530–540. doi:10.1016/j.neuron.2010.02.007

13. Adibi M, Diamond ME, Arabzadeh E. Behavioral study of whisker-mediated vibration sensation in rats. Proc Natl Acad Sci USA. 2012;109: 971–976. doi:10.1073/pnas.1116726109

14. Simons DJ. Response properties of vibrissa units in rat SI somatosensory neocortex. J

Neurophysiol. 1978;41: 798–820.

15. Khatri V, Hartings JA, Simons DJ. Adaptation in thalamic barreloid and cortical barrel neurons to periodic whisker deflections varying in frequency and velocity. J Neurophysiol. 2004;92: 3244–3254. doi:10.1152/jn.00257.2004

16. Castro-Alamancos MA. Absence of rapid sensory adaptation in neocortex during information processing states. Neuron. 2004;41: 455–464.

17. Chung S, Li X, Nelson SB. Short-term depression at thalamocortical synapses contributes to rapid adaptation of cortical sensory responses in vivo. Neuron. 2002;34: 437–446.

18. Hirata A, Castro-Alamancos MA. Effects of cortical activation on sensory responses in barrel cortex. J Neurophysiol. 2011;105: 1495–1505. doi:10.1152/jn.01085.2010

19. O'Connor DH, Hires SA, Guo ZV, Li N, Yu J, Sun Q-Q, et al. Neural coding during active somatosensation revealed using illusory touch. Nature Neuroscience. 2013;16: 958–965. doi:10.1038/nn.3419

20. Yamashita T, Pala A, Pedrido L, Kremer Y, Welker E, Petersen CCH. Membrane potential dynamics of neocortical projection neurons driving target-specific signals. Neuron. 2013;80: 1477–1490. doi:10.1016/j.neuron.2013.10.059

21. Jadhav SP, Wolfe J, Feldman DE. Sparse temporal coding of elementary tactile features during active whisker sensation. Nature Neuroscience. 2009;12: 792–800. doi:10.1038/nn.2328

22. Miyashita T, Feldman DE. Behavioral Detection of Passive Whisker Stimuli Requires Somatosensory Cortex. Cereb Cortex. 2012. doi:10.1093/cercor/bhs155

23. Adibi M, Arabzadeh E. A comparison of neuronal and behavioral detection and discrimination performances in rat whisker system. J Neurophysiol. 2011;105: 356–365. doi:10.1152/jn.00794.2010

24. de Kock CPJ, Sakmann B. High frequency action potential bursts (>or= 100 Hz) in L2/3 and L5B thick tufted neurons in anaesthetized and awake rat primary somatosensory cortex. J Physiol (Lond). 2008;586: 3353–3364. doi:10.1113/jphysiol.2008.155580

25. Crochet S, Poulet JFA, Kremer Y, Petersen CCH. Synaptic mechanisms underlying sparse coding of active touch. Neuron. 2011;69: 1160–1175. doi:10.1016/j.neuron.2011.02.022

26. Fanselow EE, Nicolelis MA. Behavioral modulation of tactile responses in the rat somatosensory system. The Journal of Neuroscience. 1999;19: 7603–7616.

27. Barth AL, Poulet JFA. Experimental evidence for sparse firing in the neocortex. Trends Neurosci. 2012;35: 345–355. doi:10.1016/j.tins.2012.03.008

28. de Kock CPJ, Bruno RM, Spors H, Sakmann B. Layer- and cell-type-specific suprathreshold stimulus representation in rat primary somatosensory cortex. J Physiol (Lond). 2007;581: 139–154. doi:10.1113/jphysiol.2006.124321

29. Luna R, Hernandez A, Brody CD, Romo R. Neural codes for perceptual discrimination in primary somatosensory cortex. Nature Neuroscience. 2005;8: 1210–1219. doi:10.1038/nn1513

30. Diamond ME. Texture sensation through the fingertips and the whiskers. Curr Opin

Neurobiol. 2010;20: 319–327. doi:10.1016/j.conb.2010.03.004

31. Jadhav SP, Feldman DE. Texture coding in the whisker system. Curr Opin Neurobiol. 2010;20: 313–318. doi:10.1016/j.conb.2010.02.014

32. Ritt JT, Andermann ML, Moore CI. Embodied information processing: vibrissa mechanics and texture features shape micromotions in actively sensing rats. Neuron. 2008;57: 599–613. doi:10.1016/j.neuron.2007.12.024

33. Zuo Y, Perkon I, Diamond ME. Whisking and whisker kinematics during a texture classification task. Philos Trans R Soc Lond, B, Biol Sci. 2011;366: 3058–3069. doi:10.1098/rstb.2011.0161

34. Pammer L, O'Connor DH, Hires SA, Clack NG, Huber D, Myers EW, et al. The mechanical variables underlying object localization along the axis of the whisker. The Journal of Neuroscience. 2013;33: 6726–6741. doi:10.1523/JNEUROSCI.4316-12.2013

35. Heimendahl von M, Itskov PM, Arabzadeh E, Diamond ME. Neuronal activity in rat barrel cortex underlying texture discrimination. PLoS Biol. 2007;5: e305. doi:10.1371/journal.pbio.0050305

36. Zuo Y, Safaai H, Notaro G, Mazzoni A, Panzeri S, Diamond ME. Complementary contributions of spike timing and spike rate to perceptual decisions in rat S1 and S2 cortex. Curr Biol. 2015;25: 357–363. doi:10.1016/j.cub.2014.11.065

37. Johnson KO, Hsiao SS, Yoshioka T. Neural coding and the basic law of psychophysics. Neuroscientist. 2002;8: 111–121.

38. Waiblinger C, Brugger D, Whitmire CJ, Stanley GB, Schwarz C. Support for the slip hypothesis from whisker-related tactile perception of rats in a noisy environment. Front Integr Neurosci. 2015;9: 53. doi:10.3389/fnint.2015.00053

39. Romo R, Brody CD, Hernandez A, Lemus L. Neuronal correlates of parametric working memory in the prefrontal cortex. Nature. 1999;399: 470–473. doi:10.1038/20939

40. Hernandez A, Zainos A, Romo R. Neuronal correlates of sensory discrimination in the somatosensory cortex. Proc Natl Acad Sci USA. 2000;97: 6191–6196.

41. Armstrong-James M, Fox K. Spatiotemporal convergence and divergence in the rat S1 "barrel" cortex. J Comp Neurol. 1987;263: 265–281. doi:10.1002/cne.902630209

42. Oberlaender M, Boudewijns ZSRM, Kleele T, Mansvelder HD, Sakmann B, de Kock CPJ. Three-dimensional axon morphologies of individual layer 5 neurons indicate cell type-specific intracortical pathways for whisker motion and touch. Proc Natl Acad Sci USA. 2011;108: 4188–4193. doi:10.1073/pnas.1100647108

43. Pitas A, Albarracin AL, Molano-Mazon M, Maravall M. Variable Temporal Integration of Stimulus Patterns in the Mouse Barrel Cortex. Cereb Cortex. 2016. doi:10.1093/cercor/bhw006

44. Webber RM, Stanley GB. Nonlinear encoding of tactile patterns in the barrel cortex. J Neurophysiol. 2004;91: 2010–2022.

45. Britten KH, Newsome WT, Shadlen MN, Celebrini S, Movshon JA. A relationship between behavioral choice and the visual responses of neurons in macaque MT. Vis

Neurosci. 1996;13: 87–100.

46. Nienborg H, Cohen MR, Cumming BG. Decision-related activity in sensory neurons: correlations among neurons and with behavior. Annu Rev Neurosci. 2012;35: 463–483. doi:10.1146/annurev-neuro-062111-150403

47. Romo R, Hernandez A, Zainos A, Lemus L, Brody CD. Neuronal correlates of decision-making in secondary somatosensory cortex. Nature Neuroscience. 2002;5: 1217–1225.

48. de Lafuente V, Romo R. Neural correlate of subjective sensory experience gradually builds up across cortical areas. Proc Natl Acad Sci USA. 2006;103: 14266–14271. doi:10.1073/pnas.0605826103

49. Yang H, Kwon SE, Severson KS, O'Connor DH. Origins of choice-related activity in mouse somatosensory cortex. Nature Neuroscience. 2016;19: 127–134. doi:10.1038/nn.4183

50. Liu S, Gu Y, DeAngelis GC, Angelaki DE. Choice-related activity and correlated noise in subcortical vestibular neurons. Nature Neuroscience. 2013;16: 89–97. doi:10.1038/nn.3267

51. Bureau I, Saint Paul von F, Svoboda K. Interdigitated paralemniscal and lemniscal pathways in the mouse barrel cortex. PLoS Biol. 2006;4: e382. doi:10.1371/journal.pbio.0040382

52. Finnerty GT, Roberts LS, Connors BW. Sensory experience modifies the short-term dynamics of neocortical synapses. Nature. 1999;400: 367–371. doi:10.1038/22553

53. Allen CB, Celikel T, Feldman DE. Long-term depression induced by sensory deprivation during cortical map plasticity in vivo. Nature Neuroscience. 2003;6: 291–299. doi:10.1038/nn1012

54. Quiroga RQ, Nadasdy Z, Ben-Shaul Y. Unsupervised spike detection and sorting with wavelets and superparamagnetic clustering. Neural Comput. 2004;16: 1661–1687. doi:10.1162/089976604774201631

55. Good P. Permutation Tests. 2nd ed. Heidelberg: Springer; 2000.

56. Pedregosa F, Varoquaux G, Gramfort A, Michel V, Thirion B, Grisel O, et al. Scikit-learn: Machine Learning in Python. Journal of Machine Learning Research. 2011;12: 2825–2803.

Supplementary Table & Figures

Leah M. McGuire, Gregory Telian, Keven J. Laboy-Juárez, Toshio Miyashita, Daniel J. Lee, Katherine A. Smith, Daniel E. Feldman (2016). Short time-scale sensory coding in S1 during discrimination of whisker vibrotactile sequences. *PLoS Biology* 2016 Aug 30;14(8):e1002549.

| | | Baseline Firing Rate (Hz) | | Average Firing Rate (Hz) | | |
Layer	Type	Mean ± SEM	Median	Mean ± SEM	Median	N units
L23	RS	6.0 ± 1.5	4.9	7.6 ± 1.2	8.1	9
L23	FS	7.9 ± 2.4	5.7	9.0 ± 1.6	10.4	5
L23	MU	15.9 ± 3.1	14.5	17.8 ± 3.3	17.3	23
L4	RS	7.8 ± 0.8	5.7	7.4 ± 0.8	5.1	52
L4	FS	9.8 ± 2.7	3.9	10.9 ± 2.8	6.9	15
L4	MU	25.3 ± 2.9	20.9	25.8 ± 2.8	18.8	51
L5a	RS	10.8 ± 0.9	9.6	11.0 ± 1.0	9.0	68
L5a	FS	10.7 ± 4.8	10.9	12.6 ± 5.6	7.6	6
L5a	MU	26.6 ± 3.1	25.8	25.6 ± 2.9	23.9	30
L5b	RS	9.0 ± 1.0	7.0	10.0 ± 1.1	8.4	62
L5b	FS	31.6 ± 9.1	15.2	34.0 ± 8.9	15.8	15
L5b	MU	23.3 ± 2.9	20.7	23.1 ± 2.3	20.2	31
L6	RS	7.7 ± 2.1	2.4	7.2 ± 1.6	3.3	45
L6	FS	21.6 ± 4.1	13.8	22.0 ± 4.3	14.8	29
L6	MU	25.2 ± 4.4	15.5	22.9 ± 3.7	14.9	32

S1 Table. Firing rates by layer and unit type. These data include both temporally modulated and non-modulated units.

S1 Data. Data for Figures 1, 2, 3, 6 and 9 available online.

S2 Data. Data for S1, S2, and S6 Figures available online.
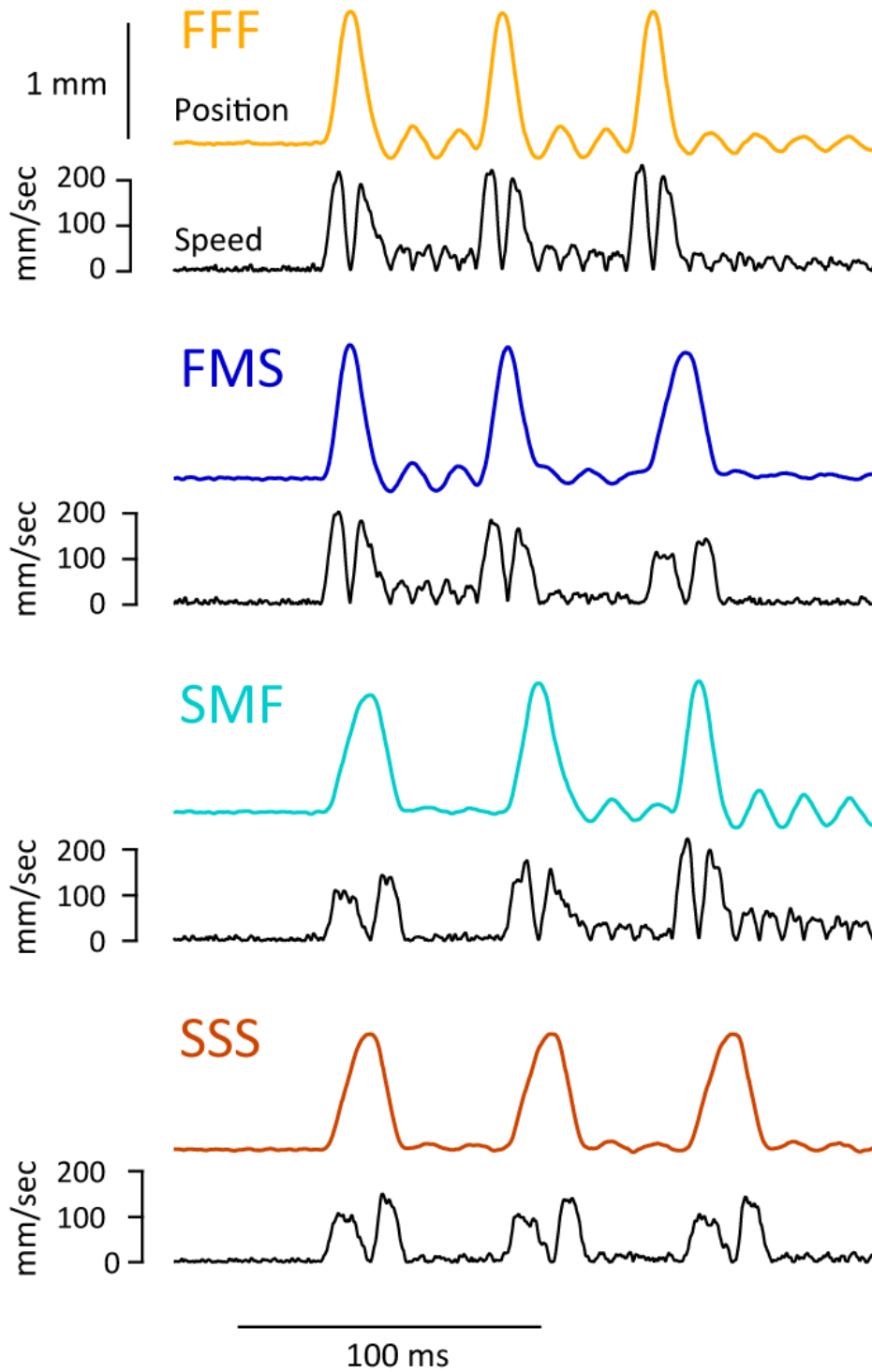
S1 Fig. Speed profile of each stimulus. Position and speed profiles for FFF, FMS, SMF, and SSS stimuli. Data are in S2 Data.
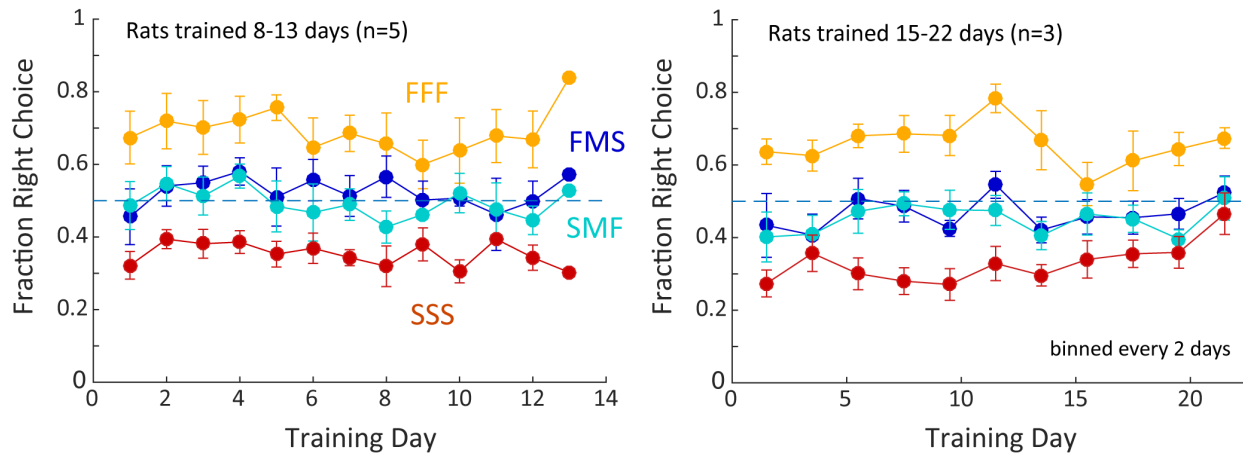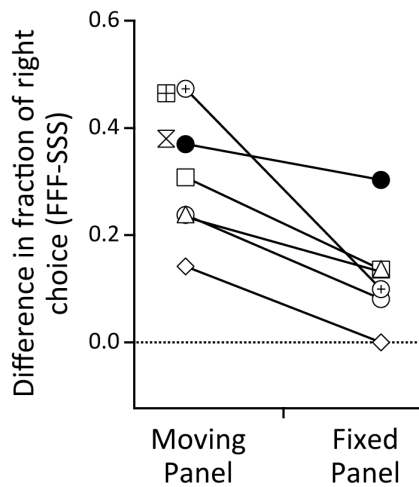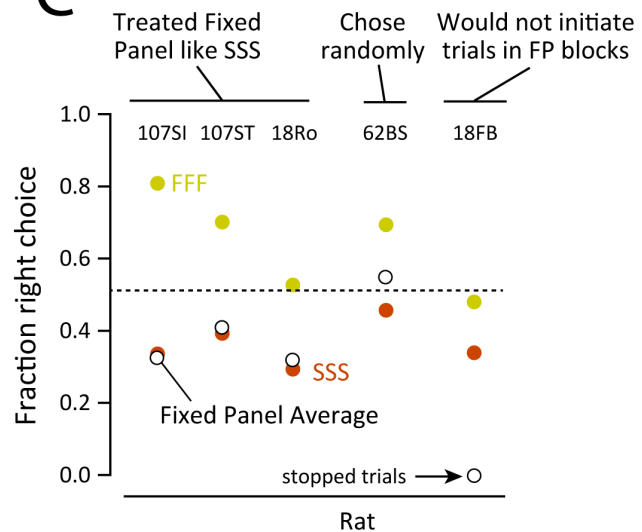
S2 Fig. Additional analysis of FFF-FMS-SMF-SSS behavior. A, Behavior performance was stable over 8–22 d of training. Left, average performance for five rats that had 8–13 d of training. Right, three rats that had 15–22 d of training (2-day bins were used because of low number of animals). Points are mean ± SEM. B, Behavioral effect of fixed panel trials, assessed using a simple alternative to d-prime. FFF versus SSS discrimination was quantified as (fraction of right choices to FFF stimuli – fraction of right choices to SSS stimuli). Discrimination was reduced on fixed panel trials ($p = 0.012$, two-sided paired t test). One rat (filled) was not significantly impaired, suggesting that he based discrimination on inadequately masked auditory cues. C, Varied responses to fixed-panel trials across rats. The plot shows fraction of right-side choice for FFF and SSS moving panel stimuli, and for the average of all fixed-panel stimuli. Only the five rats who showed behavioral impairment in the fixed panel session are included. Three rats treated fixed panel stimuli like SSS; one rat chose right or left nearly at random (50% right-side choice); and one rat did not complete trials during fixed-panel blocks. Data are in S2 Data.
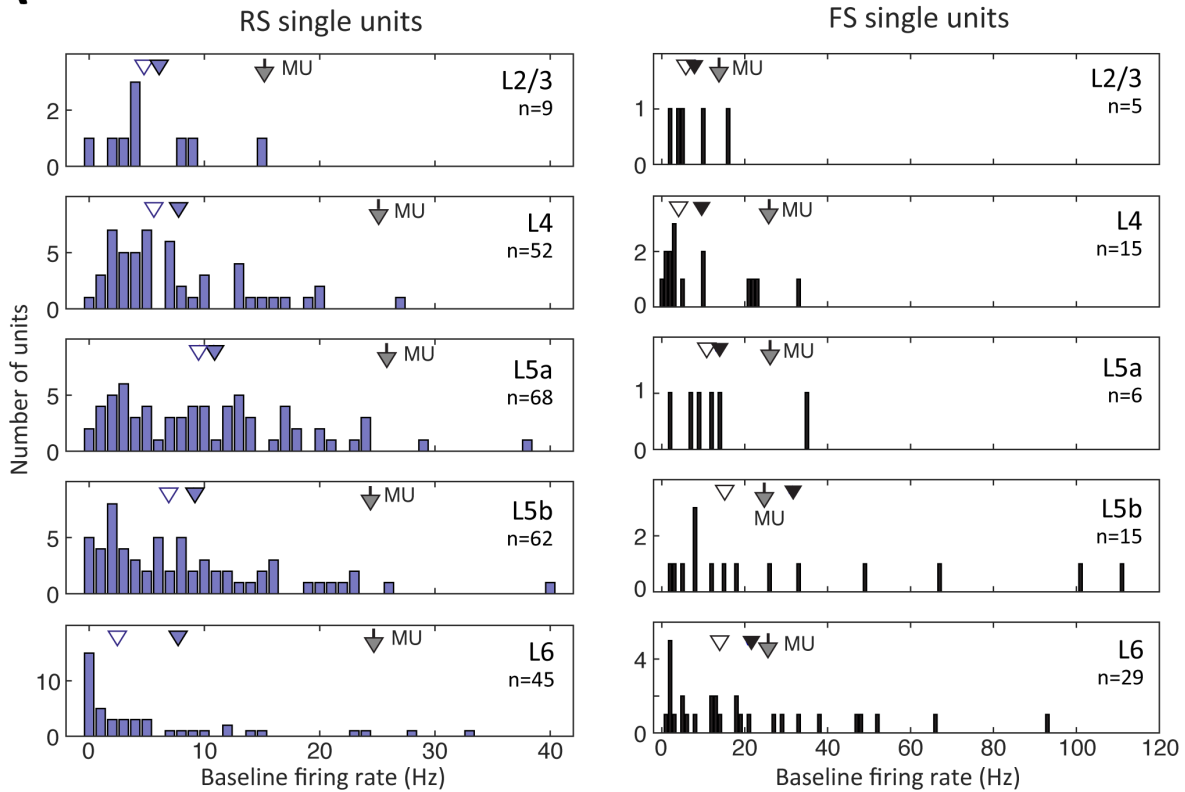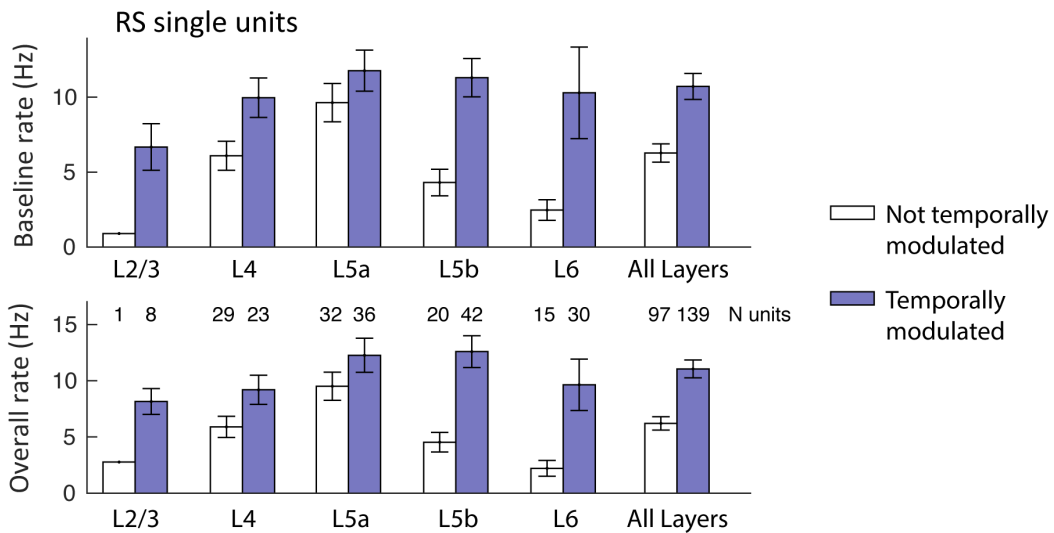
S3 Fig. Firing rate for single units by layer. A, Firing rate distributions for RS single units (left) and FS single units (right). Both temporally modulated and non-modulated units are included. Open triangles, median. Filled triangle, mean. Arrowhead, mean for multi-unit clusters, shown for comparison. Note different firing rate scales for RS and FS units. B, Firing rate (mean ± SEM) for temporally modulated and non-modulated RS single units. Temporally modulated units generally had higher firing rates, even during the baseline period.
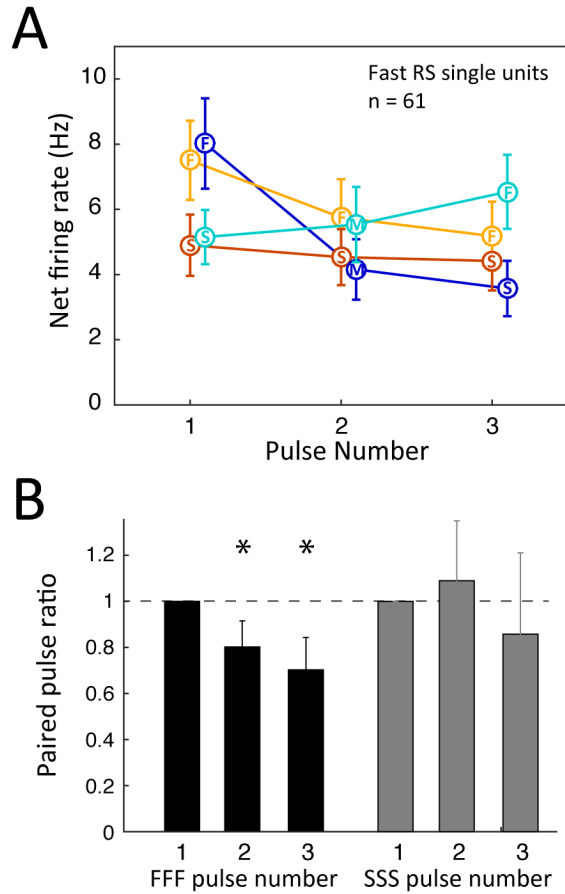
S4 Fig. Adaptation for Fast units. A, Panel-evoked responses to each individual impulse within FFF, FMS, SMF, and SSS trains, measured as firing rate 5–35 ms after impulse onset, above pre-sequence baseline. Points are mean ± SEM across all Fast RS units. Adaptation is evident in FFF but not SSS trains. B, Adaptation quantified by paired pulse ratio during FFF and SSS trains. For the same units as in (A). Paired pulse ratio is defined as panel-evoked firing rate during Pulse N/Pulse 1. Error bars, SEM.
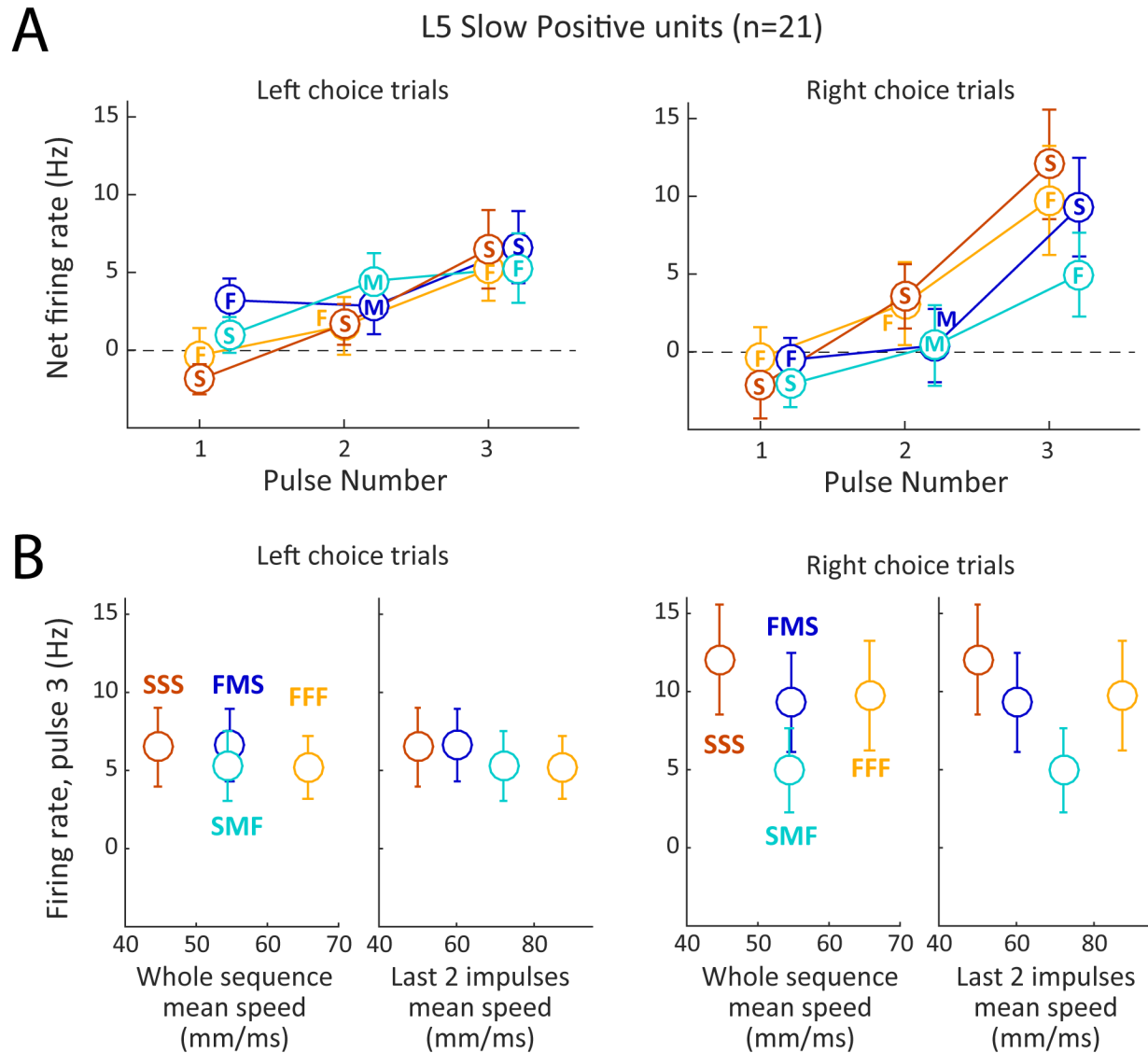
S5 Fig. Responses to panel impulses by L5 Slow Positive units. A, Mean evoked firing during each impulse (defined as in S4 Fig), for all Slow Positive units in L5a and L5b. Left- and right-choice trials were analyzed separately. Error bars are SEM. Right-choice trials had higher firing rate than left-choice trials, consistent with Fig 8. Firing during pulse 3 did not differ between FFF, FMS, SMF, and SSS stimuli, for either left- or right-choice trials. B, Firing during pulse 3 did not correlate with overall mean sequence speed or with mean speed of the preceding two pulses.
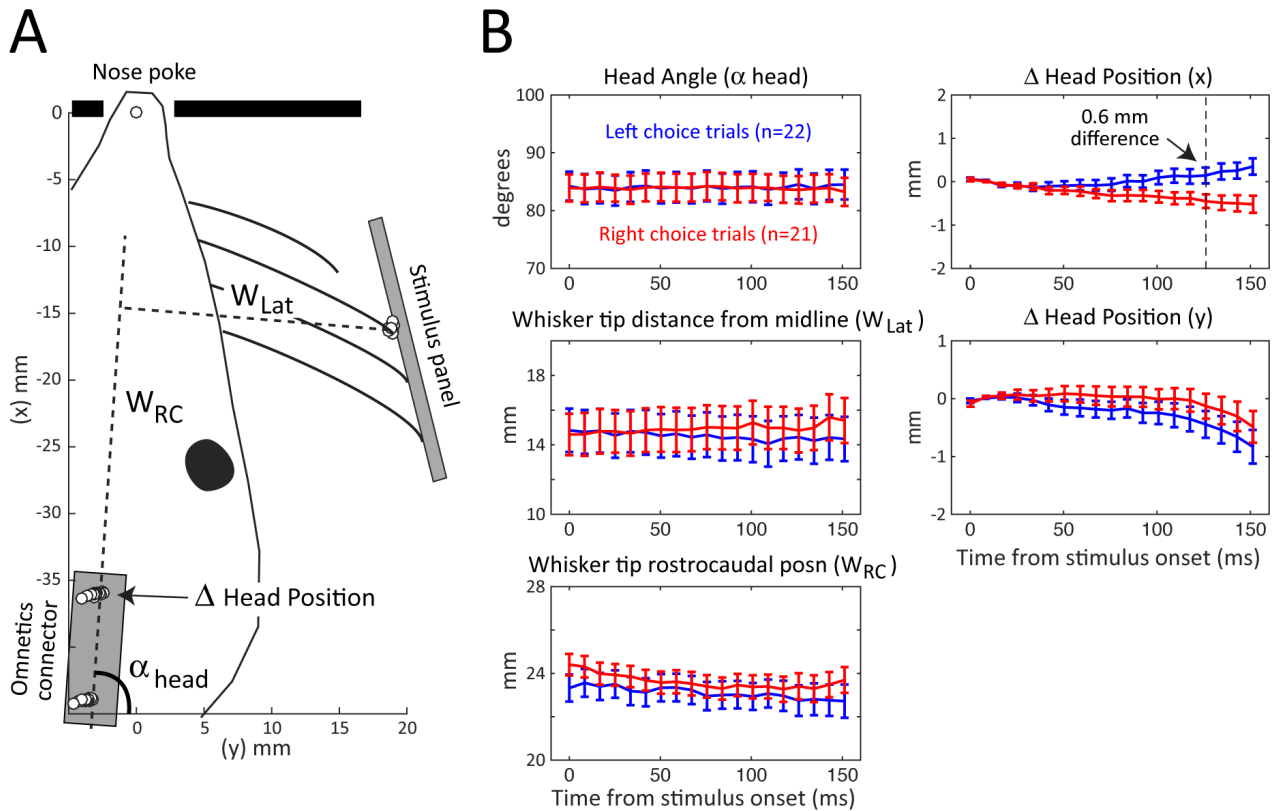
S6 Fig. High-speed video analysis of head and whisker movements during the stimulus presentation period. A, Schematic of a rat in the nose poke with head and whisker position measured during each 8.4-ms frame of a single trial, from 0 to 150 ms after stimulus onset. Nose poke entry occurred 50–75 ms prior to stimulus onset. Circles show measured positions of two points on the head (which were pins on a skull-mounted Omnetics connector) and one whisker tip. Nose poke center position is shown at top. We calculated head angle, head position relative to its starting position, and whisker tip position relative to the head. B, Mean trajectories of each variable across 22 left-choice and 21 right-choice trials (n = 4 rats). Bars are SEM. Significant right-choice versus left-choice differences were found for the x position (right-left position) of the head, but for no other variable. Data are in S2 Data.
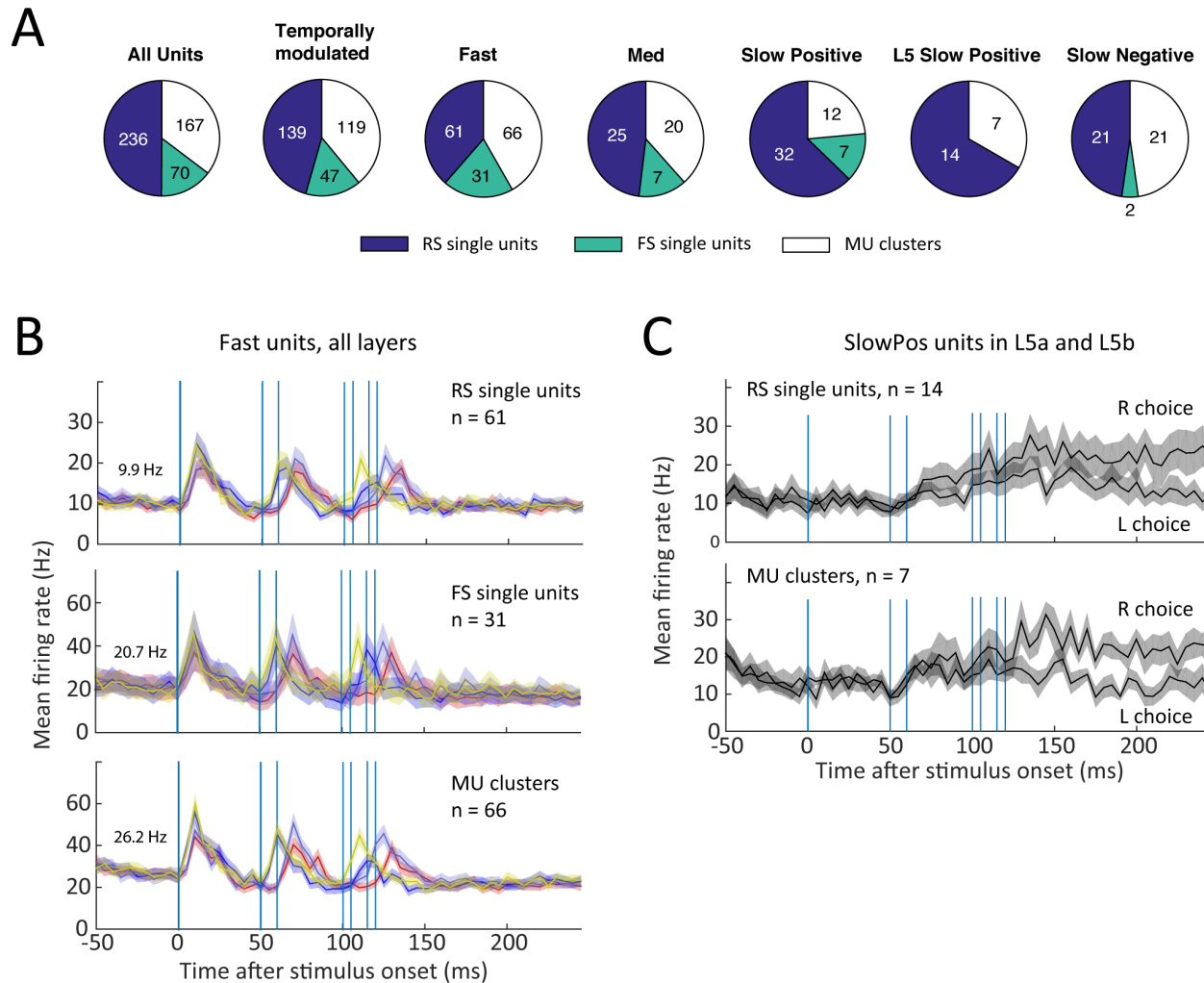
S7 Fig. Contribution of RS and FS units to response classes. A, Prevalence of RS single units, FS single units, and multi-unit clusters within each response class. B, Population PSTHs for Fast units that were RS single units, FS single units, or multi-unit clusters. Each color trace is a different sequence (FFF, FMS, SMF, SSS). Conventions as in Fig 4D. Bars show onset of individual impulses. C, Population PSTH for Slow Positive units in L5 that were RS single units or multi-unit clusters. There were no FS units in this response class. Traces are mean for all four sequences, shown separately for right- and left-choice trials.

Corrected Table 1.

The published version has incorrect titles for section 2 of the table. Our table in the accepted manuscript was correct; the incorrect titles somehow were introduced during copy editing, and we failed to notice them at the proof stage.

Please replace Table 1 in the online and PDF versions with this table.

Table 1. Kinematics of FFF-FMS-SMF-SSS whisker sequences.

Impulse	Rise/Fall Time (ms)	Peak Velocity (mm/s)	Duration* (ms)	Peak Amplitude (mm)
Fast (F)	8	220	16	1.03
Medium (M)	11	170	22	1.15
Slow (S)	14	110	28	1.14

Sequence	Interpulse Interval (ms)	Total Sequence Duration (ms)	Mean Speed (mm/s)	Target Drink Port
FFF	34	120	65.7	Right
FMS	34	132	54.4	Right
SMF	34	132	54.7	Left
SSS	34	148	44.6	Left

* Duration measured as time from initial deflection to return to baseline position.

S1 Table. Firing rates by layer and unit type. These data include both temporally modulated and non-modulated units.

Chapter 3: Surround integration organizes a spatial map during active sensation

Foreword

In order to get a complete picture of the environment the brain must integrate sensory information across multiple sensors from different modalities. Understanding how the brain integrates sensory information at the systems level is not well known. In this project I was fortunate to work with my collogues and good friends. It was here that I developed a custom whisker tracking system and associated data processing and analysis pipeline to quantify whisking kinematics and detect any changes in whisking. I used this setup to determine that the whiskers were contacting the stimulus in the same way before and after whisker trimming. This verified that all neural responses where due to neural processes rather than changes in kinematics. I also developed a custom tuning metric called spatial selectivity. It is a nonparametric measurement of a neurons tuning specificity. Developed to assess how sharply or broadly tuned a neuron is when its tuning curve is not Gaussian and cannot be accurately measured by traditional full width at half max measurements. Here Dr. Scott Pluta and Evan Lyall use extracellular recordings and calcium imaging to probe how somatosensory cortex encodes information either after integrating across multiple sensors or from a single sensor. To do this they present a vertical pole positioned at different linear locations to the whiskers of a headfixed mouse. Recording from somatosensory cortex they found that single neurons often saw their preferred stimulus position change after trimming all whiskers but the principal whisker, showing that integrating across multiple sensors was critical to shaping individual neurons' receptive fields. Additionally, integrating across multiple sensors produced a map of the sensory space swept out by the whiskers which was distributed across a large swath of sensory cortex. Removing all but one whisker destroyed the map of sensory space. This study demonstrated the importance of sensory integration, which not only contributes to individual neurons' receptive fields but is also essential for creating broad representations of the environment distributed across a cortical region.

Citation

Summary

During active sensation, sensors scan space in order to generate a representation of the outside world. However, since spatial coding in sensory systems is typically addressed by measuring receptive fields in a fixed, sensor-based coordinate frame, the cortical representation of scanned

space is poorly understood. To address this question, we probed spatial coding in the rodent whisker system using a combination of two photon imaging and electrophysiology during active touch. We found that surround whiskers powerfully transform the cortical representation of scanned space. On the single neuron level, surround input profoundly alters response amplitude and modulates spatial preference in the cortex. On the population level, surround input organizes the spatial preference of neurons into a continuous map of the space swept out by the whiskers. These data demonstrate how spatial summation over a moving sensor array is critical to generating population codes of sensory space.

Introduction

Cortical neurons represent sensory space through topographic projections of the peripheral sense organs, creating maps of the physical world in the brain. Sensory coding through maps is thought to make both the structure and function of neural circuits more efficient (Knudsen et al., 1987). In passive systems, maps can be probed by systematically stimulating different parts of the sensor array and measuring the receptive fields of individual neurons. In many sensory systems, such as the retina, integration over the sensor array is critical for receptive field formation (Hartline et al., 1956; Kuffler, 1953). During active sensation, however, the sensors themselves move – scanning space to provide greater coverage of the outside world (Kleinfeld et al., 2006). How neurons in the cortex encode scanned space, and whether integration across the sensor array is involved, is not known. Furthermore, sensor scanning has the potential to create its own spatial map in the cortex, not of the sensor array itself, but of the space swept out by the sensors. Such a map of scanned space could provide a basis for fine object localization and identification needed for behaviors such as prey capture, predator avoidance, and navigation.

The rodent whisker system is an advantageous system to address this question (Brecht, 2007; Feldmeyer et al., 2013; Petersen, 2007). On one hand, the topographic and discretized representation of the rodent's whiskers along the sensory hierarchy facilitates detailed analysis for how sensory neurons perform multi-whisker integration (Woolsey and Van der Loos, 1970). On the other, the stereotyped pattern of whisking during spatial exploration facilitates investigation into the sensorimotor processes underlying active sensation (Diamond et al., 2008; Hartmann, 2011). Decades of physiological analysis have quantified how spatial summation across the whisker array influences the cortical representation of touch (Armstrongjames et al., 1992; Boloori and Stanley, 2006; Brecht et al., 2003; Brecht and Sakmann, 2002; Brumberg et al., 1996, 1999; Chen-Bee et al., 2012; Ego-Stengel et al., 2005; Estebanez et al., 2012; Ghazanfar and Nicolelis, 1999; Goldreich et al., 1999; Higley and Contreras, 2003; Hirata and Castro-Alamancos, 2008; Kwegyir-Afful et al., 2005; Mirabella et al., 2001; Moore and Nelson, 1998; Moore et al., 1999; Petersen et al., 2001; Ramirez et al., 2014; Shimegi et al., 2000a; Zhu and Connors, 1999). Yet nearly all these investigations have utilized passive whisker stimulation, which can only probe receptive fields in discretized whisker space, and not in the continuous space scanned by the whiskers. An artificial whisking paradigm in anesthetized animals has

allowed investigators to probe spatial coding during active touch, albeit in a reduced brain state (Brown and Waite, 1974; Castro-Alamancos and Bezdudnaya, 2015; Szwed et al., 2003; Wallach et al., 2016; Yu et al., 2015). These studies have revealed how spatial summation and the vibrissotopic map evolve across the sensory hierarchy or change dynamically with experience (Feldman and Brecht, 2005; Fox, 2002; Oberlaender et al., 2012).

Surprisingly, despite the well-ordered anatomical topography of the barrels in L4 (Woolsey and Van der Loos, 1970), two-photon imaging in layer 2/3 (L2/3) has revealed that on the cellular scale, the whisker map breaks down, exhibiting a salt and pepper tuning for whisker preference (Clancy et al., 2015) with some spatial correlation on the more global level (Sato et al., 2007). Similar receptive field studies in other rodent cortical areas, such as the auditory and visual cortices, have also found local breakdowns in maps of sensory space (Bandyopadhyay et al., 2010; Rothschild et al., 2010; Smith and Hausser, 2010), despite some evidence of an underlying organization (Ringach et al., 2016). Nonetheless, these works analyzed maps of a fixed sensor array and not of scanned space. It remains uncertain whether an orderly map of scanned space exists in the barrel cortex or elsewhere.

During active touch, barrel cortex neurons are often well tuned to the horizontal location of an object (Pluta et al., 2015; Yu et al., 2015). Multiple mechanisms potentially contribute to their tuning. These include selectivity for the phase (Curtis and Kleinfeld, 2009), deflection angle (Knutsen et al., 2008), inter-contact interval (Crochet et al., 2011), or contact forces (Bagdasarian et al., 2013; Yang and Hartmann, 2016) at the moment of touch. These schemes can all operate at the single whisker level, and do not require multi-whisker integration, which is likely to occur in most natural contexts. Several studies have found that rodents perform better on whisker-guided behaviors when using multiple whiskers, suggesting that multi-whisker integration is critical for perceptual acuity (Knutsen et al., 2006; Krupa et al., 2001; O'Connor et al., 2010a). Although spatial summation is not required for spatial tuning *per se*, multi-whisker integration could powerfully transform the cortical representation of space. This might be particularly true during active sensing, where neighboring sensors probe overlapping regions of space. This raises the possibility that multi-whisker integration during active sensing might transform a discretized vibrissotopic map into a continuous map of scanned space that could be highly advantageous for object localization and discrimination.

Whether such a map exists in the barrel cortex, and, more specifically, how multi-whisker integration could shape its organization, is unknown. Most prior studies of the barrel cortex during active sensation have either been done in unrestrained animals, when controlling the stimulus is challenging, or in head-fixed mice where only a single whisker is left intact. One study in unrestrained animals quantified tactile responses before and after removing select whiskers surrounding the principal whisker (PW) column and found opposing effects in the cortex and the thalamus (Kelly et al., 1999). Yet in these freely behaving conditions, precise measurements of neuronal receptive fields could not be obtained.

We used two photon imaging and multi-electrode array physiology to address spatial summation and map organization in the somatosensory thalamocortical system. First, we tracked how spatial summation evolves across four stages of the sensory hierarchy, from the thalamus through three cortical layers. We found that neurons in the cortex, but not in the thalamus, exhibited an asymmetric, rostro-caudal gradient of summation over surround whiskers. Surround modulation not only had dramatic impacts on firing rates, but also generated a heterogeneous and substantial shift in the spatial preference of most neurons. On the population level, our data reveal a highly ordered and continuous map of scanned space in L2/3 of the barrel cortex. This map was nearly absent when only a single whisker was intact, indicating that summation over surrounding whiskers is critical to map organization. These data demonstrate that multi-whisker integration in the cortex organizes the spatial preference of neurons to create a continuous map of scanned space. Maps of scanned space may contribute to high fidelity encoding of the location and shape of objects during natural exploration.

Results

Quantifying spatial coding and summation during active sensation

To address how barrel cortex neurons encode scanned space and summate over whiskers in naturally whisking mice, we employed a head-fixed preparation in which mice ran on a free-spinning circular treadmill while we presented a vertical bar to the whiskers at fixed locations for 1.5 seconds (Fig. 1A). Mice were habituated to run for extended periods, a condition in which they move their whiskers in a highly rhythmic fashion (Pluta et al., 2015; Sofroniew et al., 2014) (Fig 1G). Under these conditions we could measure and quantify spatial representations with high precision. Neural activity was recorded with two-photon calcium imaging in the upper cortical layers or multi-electrode arrays in the lower cortical layers and the ventro-posterior medial nucleus of the thalamus (VPM). Neural data was analyzed in the final 500 ms of stimulus presentation, during which neural activity and whisking kinematics had returned to a stable state after abrupt positioning of the stimulus bar (Fig. S1). Experimental trials were selected based on the velocity and consistency of treadmill running to minimize variation in whisking behavior (Fig. S1E, and see Methods). This strict sampling of running behavior ensured consistent, repetitive touches with the stimulus throughout the object presentation period (Fig. S1F). Prior to each experiment, we first identified the location of the C2 whisker's representation in each mouse using intrinsic optical imaging. In both imaging and electrophysiology experiments, we found neurons across all layers of the barrel cortex whose tactile-evoked responses were tuned to the horizontal location of the vertical pole (Fig 1B-D). By labeling a single 'principal whisker' (PW) in a subset of mice with reflective paint we could track this whisker reliably in the presence of all other whiskers (Fig. 1E-H, Fig. S1). Using high-speed whisker tracking we found that across the full 'whisking field' the PW made rhythmic contact with the stimulus bar

throughout the stimulus period at central but not lateral locations, where only adjacent whiskers (AWs) contacted the bar, defining a principal whisker contact zone (PWCZ) and an adjacent whisker contact zone (AWCZ, Fig. 1E,F).

To explore spatial summation during active sensation, we sought to quantify the contribution of the PW and the AWs to each neuron's spatial representation. We reasoned that we could measure this by comparing a neuron's spatial tuning function before and after acutely trimming off all the surround whiskers. The difference in these two measurements would reveal the parallel contributions of the AWs and PW to each neuron's spatial receptive field. Towards this aim, we collected spatial tuning curves both before and after trimming all but the principal whisker in a single experimental session (< 1 hour), so that after trimming, only the PW could contact the stimulus bar. Importantly, whisker trimming on such an acute time-scale is much shorter than required for the induction of sensory-deprivation induced plasticity (Bender et al., 2006; Glazewski and Fox, 1996; Wen et al., 2013). The dataset consisted of 1016 neurons in L4 (340±120 ROIs/mouse; 3 mice), 2572 neurons in L2/3 (640±120 ROIs/mouse; 4 mice), 172 regular spiking (RS) units in L5 (10±2 units/mouse; 16 mice), and 90 units in VPM (11±2/mouse; 8 mice). Since acute whisker trimming might alter an animal's pattern of whisking during active sensation, in a subset of mice we tracked the PW both before and after surround whisker trimming and found that trimming did not significantly alter the kinematics of the animals' whisking patterns, except for a minute difference in amplitude (Fig. S1, mean ± s.e.m: 0.90 ± 0.20 degrees, far smaller than the 10–15 degrees between presented stimuli). This indicates that any changes we observed in neuronal response functions were due to changes in neural computation and not to changes in whisking behavior.

Spatial summation in L4

First we addressed spatial coding and summation in excitatory neurons in L4 of the barrel cortex. To record from a large population of L4 excitatory neurons across the spatial map in S1 we expressed GCaMP6s (Chen et al., 2013) in excitatory neurons in L4 using a Cre-dependent AAV and a L4-specific Cre line (Madisen et al., 2010; Pluta et al., 2015) (Fig. 2A). Prior to whisker trimming we observed contact-evoked responses across the entire imaging field. Following removal of the surround whiskers, sensory evoked responses were essentially abolished outside of the PW 'column' (68 ± 9% decrease in number of significantly driven units, n = 3 mice, for column identification see Methods and Fig. S2), demonstrating that the PW preferentially drives touch responses within its anatomically aligned column, consistent with prior observations under both passive and active conditions (Goldreich et al., 1999; Hires et al., 2015). Strikingly, in the rostral position of the PWCZ the majority (56 ± 8%, n = 3 mice) of L4 neurons within the PW column exhibited significant enhancements in their contact-evoked activity following surround whisker trimming (4.0 ± 1.3 fold increase in population mean, n = 231, Wilcoxon sign rank, p <

0.001, Fig. 2B-E). We computed a 'trimming index' as a metric for how surround whiskers influenced the evoked firing rate of each given neuron, defined as the difference over the sum of evoked activity between pre and post-trimming conditions. In the rostral PWCZ position, nearly all neurons had a positive trimming index, indicating pronounced disinhibition following surround whisker trimming (trimming index = 0.33 ± 0.03, n = 231, $p < 0.001$, Wilcoxon sign rank, Fig. 2F). In contrast, in the caudal PWCZ position, most neurons showed a reduction in tactile evoked response (0.8 ± 0.1 fold decrease in population mean, trimming index = -0.30 ± 0.03, n = 231, $p < 0.001$, Wilcoxon sign rank, Fig. 2F). These data indicate that surround input from more caudal whiskers provides facilitation, whereas input from the more rostral whiskers primarily provides suppression. To address how surround whisker input influences spatial coding, we computed an index of spatial preference (the center of mass of the spatial tuning curve in the PWCZ). We found that for nearly all L4 neurons that exhibited spatial tuning (1-way ANOVA), spatial preference shifted forwards (1.77 ± 0.09 mm mean shift, n = 139, $p < 0.001$, t-test, Fig. 2G).

Spatial summation in cortical projection layers

Next we addressed spatial coding and summation in L2/3 and L5, the two major output layers of the barrel cortex. In L2/3 we used two-photon imaging (110-195 microns deep) to sample a large number of L2/3 neurons across the spatial map in S1. In L5 we employed laminar multi-channel electrodes that spanned the complete depth of L5. The laminar position of the electrode in each experiment was confirmed with a combination of depth readings off a precise micromanipulator, current source density analysis of the touch-induced local field potential (LFP), and post-hoc histology of the electrode track (Fig. S2). Prior to any trimming, we observed that L2/3 and L5 neurons in the PW column very often exhibited substantial evoked activity in the AWCZ, the region where the PW makes no contact (Fig S2), consistent with prior imaging studies showing that a single whisker could evoke broad activity across multiple barrel columns in L2/3 (Clancy et al., 2015; Peron et al., 2015). This is in contrast to neurons in L4 and in VPM which responded more specifically (but not exclusively) to stimuli within the PWCZ (see Fig. S2). This suggests that surround whisker input in L2/3 and L5 might be particularly important for spatial representations in these cortical projection layers.

To address this hypothesis, we recorded tactile evoked responses in both layers prior and subsequent to trimming all but a single whisker, as above. L2/3 exhibited suppression in the anterior PWCZ, but nearly exclusive facilitation in the caudal PWCZ (rostral position trimming index = 0.14 ± 0.02, n = 631, $p < 0.001$, Wilcoxon sign rank; caudal position trimming index = -0.37 ± 0.02, n = 631, $p < 0.001$, Wilcoxon sign rank, Fig. 3B-F). As a consequence, surround input altered the spatial preference of L2/3 neurons, but did so somewhat more heterogeneously than L4, with most neurons shifting rostrally, but some shifting caudally in their preference (1.42

± 0.07 mm mean shift, n = 413, p < 0.001, Wilcoxon sign rank, Fig. 3G). In L5, similar to L2/3, the predominant impact of surround input was to facilitate responses at the caudal PWCZ position (37 ± 7% mean decrease in spike rate, mean trimming index = -0.29 ± 0.06, n = 48, p < 0.001, Wilcoxon sign rank, Fig. 4A-D), which likewise had the net effect of altering spatial preference in most neurons (0.6 ± 0.2 mm mean shift forward, n = 39, p = 0.001, Wilcoxon sign rank, Fig. 4E).

As a control for these changes, we performed a separate set of experiments where we sham trimmed the whiskers (total experimental time equal to trimming experiments), and observed no significant effects on the population, demonstrating that the neural responses were stable over the recording session (Fig. S3). In addition, to assess the stability of spatial preference in each neuron in the trimming datasets, we analyzed the first and second halves of the control and trimmed whisker trials separately. We found that the spatial preference of neurons within each condition were stationary over time (Fig. S3), further indicating that slow changes in neuronal response properties independent of surround whisker trimming cannot explain our results. To determine how spatial preference evolves over the time course of object presentation, we analyzed each neuron's activity during eleven different time windows during object presentation. We found that the trimming-induced forward shift in spatial preference plateaued for analysis periods starting more than 600 ms after object presentation (Fig. S4). This result agrees with our behavioral analysis of whisking set-point, which stabilized approximately 600 ms after object presentation (Fig. S1C), also emphasizing the importance of analyzing the neural data in a time window of high behavioral consistency. It should also be noted that the temporal resolution of GCaMP6s as a reporter of neural activity is substantially lower than that of electrophysiology. Nevertheless, GCaMP6s activity during our analysis period displayed temporal dynamics not too dissimilar from electrophysiology (Fig. S4 E&F).

Spatial summation in the somatosensory thalamus

The data described above demonstrate that surround whisker input powerfully influences how cortical neurons represent scanned space. Which of these surround effects emerge in the cortex, and which are inherited upstream via the thalamus? Whisker pathways converge even at the brainstem level, and can contribute to multi-whisker receptive fields in the thalamus (Timofeeva et al., 2004). To answer this question, we recorded from thalamic neurons in the ventro-posterior medial nucleus (VPM, dorsomedial portion) and compared the impact of surround whisker input on VPM neurons to our observations in cortical neurons. We found that thalamic neurons showed robust spatial tuning like their cortical counterparts (fraction of neurons tuned, VPM: 83%, L4: 86%, L2/3: 89%, L5: 67%, 1-way ANOVA), demonstrating that tuning, *per se*, is likely to be generated sub-cortically, perhaps as early as the primary mechanoreceptors, according to previous reports (Szwed et al., 2003; Yu et al., 2015) (Fig. 5A-C). Nevertheless,

trimming the surround whiskers demonstrated that surround input modified thalamic responses, but weakly compared to L4 (Fig. 5D-E). A minority of VPM neurons exhibited a significant change in their evoked activity across the center of their spatial receptive field (within the 'PWCZ', Fig. 5D). As a population, VPM neurons displayed a reduction in their evoked firing rate at the rostral PWCZ position (trimming index = -0.13 ± 0.06, p = 0.047, n = 54, paired t-test, Fig. 5E). This distinctly contrasts to the robust enhancement we observed in L4 neurons at the rostral PWCZ position. Furthermore, unlike for cortical neurons, surround input did not change the spatial preference of VPM neurons (0.16 ± 0.14mm mean shift, n = 51, p = 0.23, t-test, Fig. 5F). These results imply that surround modulation of the spatial preference of cortical neurons emerges primarily in the cortex.

As a whole, the data above demonstrate that surround input uniquely transforms the cortical representation of space. Conversely, we sought to determine the importance of principal whisker (PW) input to spatial tuning in an output layer of the cortex, L5. Towards this end, in a separate set of mice, we measured spatial tuning functions before and after trimming off only the PW, leaving all the surround whiskers intact (Fig. S5). Following removal of the PW, we observed a pronounced reduction in the evoked firing rates of neurons that were facilitated by touch, consistent with the expected function of the principal whisker (-28 ± 5% change, trimming index: -0.20 ± 0.03, Fig. S5a, n = 36, p < 0.001, paired t-test). Even though almost all (95%) L5 units retained significant touch-evoked firing after removal of their PW, they exhibited no change in spatial preference (Fig. S5C, n = 20, p = 0.53, Wilcoxon sign rank), in notable contrast to the effect of removing surround whiskers. However, the spatial selectivity of the population was significantly reduced, typified by flatter tuning curves (n = 50, p = 0.003, Wilcoxon sign rank, Fig. S5D). These data indicate that the PW is the primary, but not sole, contributor to the amplitude of a given neuron's tactile response, while surround whiskers potently influence its spatial preference.

Surround input organizes a map of scanned space in the barrel cortex

The data above indicate that surround whisker input powerfully influences how individual neurons in the barrel cortex encode scanned space. How might spatial coding be organized on the more global level? On one hand, the spatial preference of nearby neurons might show little correlation, similar to the salt and pepper distribution of orientation tuning in rodent visual cortex (Ohki et al., 2005). Alternatively, the spatial preference of neurons might gradually shift across the rostro-caudal axis of cortex, constituting a continuous map of scanned space. To address this question in L2/3, we plotted spatial preference for each neuron across the entire field of view ($1.06 ± 0.30$ mm^2), encompassing the region above several adjacent barrels (Fig. S6). Strikingly, we observed a topographic representation in the positional preference of neurons across the rostro-caudal axis of stimulus space, arranged approximately across the row axis of the barrel

cortex (Fig. 6A, see Methods and Fig. S6 for a description of how the map axis was determined). The spatial resolution of the aggregated maps was 6.7 μm of physical space per micron of cortical tissue, as quantified by the slope of the linear regression of spatial preferences across all mice (Fig. 6D).

Since we did not observe clear discretization in any of the individual maps (see Fig. S7), it is possible that summation over surround whiskers help generate this continuous map. To test this idea, we asked how the spatial map changed following removal of all but one whisker. While many neurons across the entire field of view retained significantly evoked responses and spatial tuning, the spatial map all but disappeared (Fig. 6B, Fig. S7). We quantified this change in several ways. First we compared the correlation of neurons' spatial preference across the axis of best fit before and after trimming (see Methods). Before trimming, the spatial preference of the imaged neurons exhibited a clear correlation along the rostro-caudal axis (Pearson's R = 0.70, p < 0.001), implying the presence of a map; however, after trimming, this correlation disappeared (Pearson's R = 0.00, p = 0.9, Fig. 6D-E). This relationship held true both across the entire field of view and within a restricted zone that retained strong activity following trimming (Pearson's R pre-trim = 0.48, p < 0.001, vs. Pearson's R post-trim = 0.08, p = 0.063), most likely corresponding to the region directly above the spared L4 barrel (486 ± 70 microns along axis of best fit, n = 4 mice). Second, we computed correlations between the spatial preferences of all pairs of neurons within a given map as a function of cortical distance along the axis of best fit. For a map to exist, nearby neurons should display similar spatial preferences, while distant neurons should diverge. Consistent with this notion, before trimming, an analysis of pairwise correlations show that nearby neurons have much greater similarity in spatial preference than distant neurons (Fig. 6F). However, after trimming to a single whisker, the relationship between pair-wise cortical distance and spatial preference similarity dramatically decreased (Fig. 6F). As a third means to quantify this map, we constructed cumulative distribution functions of spatial preference along the axis of best fit before and after trimming. With surround input intact, there was a gradual and systematic tiling of spatial preference along the entire axis of cortical space (p < 0.001, ANOVA, n = 1486, Fig. 6G). Following trimming to the C2 whisker, these spatial preference distributions coalesced (Fig. 6H), due to an increasingly greater forward shift in caudal neurons (Fig. 6I), demonstrating that multi-whisker integration is critical for an organized map of the scanned region. The apparent disorganization of the map was not simply due to noisier responses in the cortex after trimming, since our analysis is restricted to neurons significantly tuned for space and significantly driven by the stimuli. Nor is it due to analyzing different total numbers of responsive and tuned neurons between the two conditions, since the results held true even when we restricted our analysis to the population of neurons that were significantly tuned both before and after trimming (Fig. S8). Lastly, we addressed whether behavioral variation, such as minute trial-to-trial differences in whisker set-point, could have affected the smoothness (Pearson's R) of the sensory map in L2/3. However, in our L2/3 dataset, the faster the mouse ran on the treadmill (the narrower the range of whisker set-points,

57

Fig. S1), the smoother the map became (Fig. S8). Therefore, behavioral variation is in fact detrimental to map smoothness.

Finally, we probed this spatial map electrophysiologically using multi-shank laminar electrodes (Fig. 7A, B). We inserted three 8-electrode shanks across the C-row axis of the barrel cortex (identified with intrinsic optical imaging and electrophysiologically verified, Fig. S2) and measured spatial tuning functions of cortical units across 3 barrel columns both before and after trimming to the C2 whisker (Fig. 7C, D). Across the electrode shanks, the rostro-caudal distributions of spatial preference could be quantified by plotting cumulative distribution functions. Before trimming, neurons in different cortical columns had significantly different spatial preferences that corresponded to their relative location in the cortex ($p < 0.001$, ANOVA, $n = 70$, Fig. 7C, E). After trimming, the spatial preference of the neurons that retained significant tuning coalesced onto a narrow region of space ($p = 0.32$, ANOVA, $n = 45$, Fig. 7D, F). Furthermore, the magnitude of the change in spatial preference varied with cortical location; neurons in the caudal cortical column shifted further forward than neurons in the rostral column ($p = 0.03$, ANOVA, $n = 31$). These results are not simply due to inferior measurements of spatial preference caused by a uniform reduction in response strength, because the spatial selectivity of neurons outside of the spared column did not systematically decrease after trimming ($p = 0.73$, $n = 24$, Wilcoxon sign rank). Although these electrophysiological recordings cannot reveal the same degree of continuity we observed with two photon imaging, they nevertheless further support the notion that surround whisker input distributes the spatial preference of neurons to generate a map of scanned space in the barrel cortex. Lastly, we asked if the map was centered on the head, rather than on the set point of the whisking envelope. If so, the spatial preference of neurons should stay the same, despite a shift in whisker set-point. However, we observed that spatial preference follows the set-point of whisking, implying that the map is not head-centered (Fig. S9).

Discussion

This study examines how neurons across four sequential stages of the thalamocortical system integrate across a sensor array during active sensation to encode the space scanned by the sensors, in this case, the rodent's whiskers. While many previous studies have addressed spatial summation in anesthetized, paralyzed, or fixating animals, how summation influences sensory coding when the sensors are actively and volitionally moving has remained largely unexplored. Several previous studies have compared neural responses between active and passive conditions and reported significant differences, including reduced response amplitudes and more restricted spatial or temporal spread of activity (Fanselow and Nicolelis, 1999; Ferezou et al., 2007; Hentschke et al., 2006; Lee et al., 2008). Yet spatial summation, *per se*, has not been rigorously characterized in awake, volitionally whisking mice. In this study, we found that surround

whisker input potently transformed barrel cortex neurons' spatial tuning, strongly impacting firing rates, and shifting their spatial preference. In L2/3, these shifts acted to organize a sensory map of scanned space. Such a map – referenced not to the sensors, but instead to the space probed by the moving sensor array, has not been previously demonstrated in any sensory system to our knowledge. Although the whisker system bears many unique qualities that distinguish it from other sensory systems, this spatial map of scanned space in the barrel cortex raises the possibility that similar maps might exist in other cortical areas in rodents, and in other mammalian species. Primates move their hands across surfaces to localize and identify objects (Chapman and Ageranioti-Belanger, 1991), similar to how rodents use their whiskers, and a continuous map of scanned space in the primate somatosensory cortex might also exist.

The map we observed was not an ego-centric map – i.e., a head-centered map – but rather a map centered on the set-point of the scanned region (Fig. S9). Nonetheless, a map of scanned space, as was observed here, may contribute to the generation of an egocentric (head-centered) map of space downstream that is independent of the scanned region (or 'field of view'). Based on prior evidence in non-human primates, the posterior parietal cortex is a brain area that may be involved in this transformation (Andersen et al., 1985), but likely builds on cues present even at the mechanoreceptors themselves (Yang and Hartmann, 2016).

How might a map of scanned space be generated? First, it is important to note that while the map depends on summation over multiple whiskers, spatial tuning for individual cortical neurons persists even with only a single whisker intact. This is largely consistent with prior reports that horizontal location can be computed by cortical neurons even with information from a single whisker (Curtis and Kleinfeld, 2009; O'Connor et al., 2010b), or even by neurons at very early stages of the somatosensory system (Szwed et al., 2003; Yu et al., 2015), a fact consistent with the strong tuning we observed in thalamic neurons. Thus horizontal tuning *per se* does not appear to depend on cortical computation. Instead, we propose that summation over the underlying whisker map, specifically in the cortex, is what helps create the map of scanned space. This computation might be analogous to local smoothing, and could be implemented by the broad dendritic trees and horizontal projections of L2/3 pyramidal neurons that cross cortical column boundaries, as well as the divergence of ascending L4 axons (Bender et al., 2003). Nevertheless, many other possibilities exist, including computations involving efferent or re-afferent signals of whisker motion. While future experiments can address the underlying mechanisms that generate the map of scanned space in L2/3, we propose that the role of surround input in the cortex is not to generate spatial coding *de novo*, but rather to act on the global level to organize spatial preference across the horizontal axis of the cortex in such a way so as to generate a continuous map of space. Whether other maps that exist in the barrel cortex, such as for contact angle or for correlation selectivity, contribute to the generation of this spatial map, remains to be seen (Andermann and Moore, 2006; Estebanez et al., 2016; Kremer et al., 2011; Peron et al., 2015).

In this study, owing to the highly stereotyped pattern of whisking that mice exhibit during head-fixed locomotion, we were also able to reliably quantify single neuron's spatial tuning curves during active sensation. Although this preparation resembles in some respects anesthetized conditions where the whiskers are made to move artificially by electrical stimulation of the facial motor nerves (Brown and Waite, 1974; Castro-Alamancos and Bezdudnaya, 2015; Szwed et al., 2003), all of our data were collected in the awake, alert state. Since several studies have highlighted how brain state and the level of alertness can dramatically influence sensory processing and the firing of specific cortical subtypes (Adesnik et al., 2012; Castro-Alamancos, 2004a, b; Castro-Alamancos and Oldford, 2002; Greenberg et al., 2008; Lee et al., 2013; Niell and Stryker, 2010; Poulet and Petersen, 2008; Reimer et al., 2014; Vinck et al., 2015), we consider it essential that we performed all of our experiments in the awake state while mice ran and whisked of their own volition.

The second key finding of this study with respect to spatial summation is the presence of an asymmetric rostro-caudal gradient of response modulation that emerges in the cortex. This modulation is most pronounced in L4, where contact with anterior whiskers powerfully suppresses responses to the PW, while contact with more posterior whiskers generate substantial facilitation. This effect is very likely to be related to the well-known impact of the temporal sequence of whisker-object contacts revealed in anesthetized recordings (Civillico and Contreras, 2006; Drew and Feldman, 2007; Higley and Contreras, 2003; Shimegi et al., 2000a, b). What is the utility of such across-whisker modulation? One possibility is that the combined action of anterior suppression and posterior facilitation strongly enhances spatiotemporal contrast in the population response in L4 during whisker contact. In other words, as an animal sweeps its whiskers forwards into an object, the largest neural responses will be in the barrel representing the first whisker to contact the stimulus, both because it gets no suppression from any anterior whisker and because it gets facilitation from the more posterior whisker that contacts the object second. However, at the same time, the L4 barrel representing the second whisker to touch will be suppressed by touch with the first whisker. The net effect of this scheme is to generate a high spatial gradient of evoked responses in L4 barrels that could sharpen the population representation of touch in the barrel cortex (Brumberg et al., 1996; Drew and Feldman, 2007). This contrast-enhancing, asymmetric integration appears to be involved in generating the continuous map of scanned space we observed in L2/3, although it could be important on its own for other spatial computations. Additional factors unrelated to timing, such as asymmetry in forces on the PW across different object positions, likely shape the properties of surround integration.

Taken together, the results of this study reveal fundamental modes of cortical computation during active sensation, and shed light on key underlying neural mechanisms. Previous studies, primarily in anesthetized or sedated animals, have highlighted how summation across whiskers depends critically on the timing and spatial patterns of surround whisker

stimulation (Brumberg et al., 1996; Shimegi et al., 2000a). In at least two studies, coordinated waves of surround input, mimicking that which occurs naturally, can profoundly alter the response properties of cortical neurons (Drew and Feldman, 2007; Jacob et al., 2008). In this study, since the animals whisked freely, the timing and pattern were not under experimental control, but our results are nevertheless consistent with prior experiments under anesthesia. A previous study, in anesthetized animals, demonstrated that the degree of correlated whisker movement across the array could profoundly influence single unit responses – with some units enhanced and other suppressed by global correlations (Estebanez et al., 2012). Furthermore, recent work showed that the enhanced neurons in L2/3 are clustered above the edges of the L4 barrels (Estebanez et al., 2016). In our study, since the mice naturally whisked in a coherent fashion at a vertical bar, the stimulus we used is likely to be more similar to the global correlation condition. In any condition, the precise spatiotemporal pattern of multi-whisker touch likely has a profound influence on sensory integration. Similar to previous studies that investigated active sensation with a single whisker (Ferezou et al., 2007; Hentschke et al., 2006; Lee et al., 2008), our results have the advantage that they are drawn from volitionally whisking mice, and thus within the ethologically relevant range of multi-whisker contact patterns. However, this naturalistic approach prevented us from identifying the precise moments of multi-whisker touch, thereby obscuring the effects of multi-whisker integration on the fine temporal structure of spiking. Future studies, using technological advances that permit the imaging and quantification of multi-whisker contacts during exploration of objects with complex surface geometry (Hobbs et al., 2016), in combination with the physiological approaches here, could address how a spatial map in S1 facilitates the encoding of higher order stimulus features. Furthermore, processing stages downstream of S1 could integrate topographic information of scanned space with sensorimotor signals conveying whisking set point to construct an egocentric map of space.

Author Contributions

Conceptualization, S.R.P. and H.A.; Methodology, S.R.P., E.H.L., and H.A.; Investigation, S.R.P., E.H.L., G.I.T., and E.R.; Formal Analysis, S.R.P., E.H.L., and G.I.T.; Writing, S.R.P., E.H.L., and H.A.; Supervision, H.A.

References

Adesnik, H., Bruns, W., Taniguchi, H., Huang, Z.J., and Scanziani, M. (2012). A neural circuit for spatial summation in visual cortex. Nature *490*, 226-231.

Andermann, M.L., and Moore, C.I. (2006). A somatotopic map of vibrissa motion direction within a barrel column. Nature neuroscience *9*, 543-551.

Andersen, R.A., Essick, G.K., and Siegel, R.M. (1985). Encoding of spatial location by posterior parietal neurons. Science *230*, 456-458.

Armstrongjames, M., Fox, K., and Dasgupta, A. (1992). Flow of Excitation within Rat Barrel Cortex on Striking a Single Vibrissa. J Neurophysiol *68*, 1345-1358.

Bagdasarian, K., Szwed, M., Knutsen, P.M., Deutsch, D., Derdikman, D., Pietr, M., Simony, E., and Ahissar, E. (2013). Pre-neuronal morphological processing of object location by individual whiskers. Nature neuroscience *16*, 622-+.

Bandyopadhyay, S., Shamma, S.A., and Kanold, P.O. (2010). Dichotomy of functional organization in the mouse auditory cortex. Nature neuroscience *13*, 361-368.

Bender, K.J., Allen, C.B., Bender, V.A., and Feldman, D.E. (2006). Synaptic basis for whisker deprivation- induced synaptic depression in rat somatosensory cortex. Journal of Neuroscience *26*, 4155-4165.

Bender, K.J., Rangel, J., and Feldman, D.E. (2003). Development of columnar topography in the excitatory layer 4 to layer 2/3 projection in rat barrel cortex. Journal of Neuroscience *23*, 8759-8770.

Boloori, A.R., and Stanley, G.B. (2006). The dynamics of spatiotemporal response integration in the somatosensory cortex of the vibrissa system. Journal of Neuroscience *26*, 3767-3782.

Brecht, M. (2007). Barrel cortex and whisker-mediated behaviors. Curr Opin Neurobiol *17*, 408-416.

Brecht, M., Roth, A., and Sakmann, B. (2003). Dynamic receptive fields of reconstructed pyramidal cells in layers 3 and 2 of rat somatosensory barrel cortex. J Physiol-London *553*, 243-265.

Brecht, M., and Sakmann, B. (2002). Dynamic representation of whisker deflection by synaptic potentials in spiny stellate and pyramidal cells in the barrels and septa of layer 4 rat somatosensory cortex. J Physiol-London *543*, 49-70.

Brown, A.W., and Waite, P.M. (1974). Responses in the rat thalamus to whisker movements produced by motor nerve stimulation. The Journal of physiology *238*, 387-401.

Brumberg, J.C., Pinto, D.J., and Simons, D.J. (1996). Spatial gradients and inhibitory summation in the rat whisker barrel system. J Neurophysiol *76*, 130-140.

Brumberg, J.C., Pinto, D.J., and Simons, D.J. (1999). Cortical columnar processing in the rat whisker-to-barrel system. J Neurophysiol *82*, 1808-1817.

Castro-Alamancos, M.A. (2004a). Absence of rapid sensory adaptation in neocortex during information processing states. Neuron *41*, 455-464.

Castro-Alamancos, M.A. (2004b). Dynamics of sensory thalamocortical synaptic networks during information processing states. Progress in neurobiology *74*, 213-247.

Castro-Alamancos, M.A., and Bezdudnaya, T. (2015). Modulation of artificial whisking related signals in barrel cortex. J Neurophysiol *113*, 1287-1301.

Castro-Alamancos, M.A., and Oldford, E. (2002). Cortical sensory suppression during arousal is due to the activity-dependent depression of thalamocortical synapses. J Physiol-London *541*, 319-331.

Chapman, C.E., and Ageranioti-Belanger, S.A. (1991). Discharge properties of neurones in the hand area of primary somatosensory cortex in monkeys in relation to the performance of an active tactile discrimination task. I. Areas 3b and 1. Exp Brain Res *87*, 319-339.

Chen-Bee, C.H., Zhou, Y., Jacobs, N.S., Lim, B., and Frostig, R.D. (2012). Whisker array functional representation in rat barrel cortex: transcendence of one-to-one topography and its underlying mechanism. Front Neural Circuits *6*, 93.

Chen, T.W., Wardill, T.J., Sun, Y., Pulver, S.R., Renninger, S.L., Baohan, A., Schreiter, E.R., Kerr, R.A., Orger, M.B., Jayaraman, V*., et al.* (2013). Ultrasensitive fluorescent proteins for imaging neuronal activity. Nature *499*, 295-300.

Civillico, E.F., and Contreras, D. (2006). Integration of evoked responses in supragranular cortex studied with optical recordings in vivo. J Neurophysiol *96*, 336-351.

Clancy, K.B., Schnepel, P., Rao, A.T., and Feldman, D.E. (2015). Structure of a single whisker representation in layer 2 of mouse somatosensory cortex. The Journal of neuroscience : the official journal of the Society for Neuroscience *35*, 3946-3958.

Crochet, S., Poulet, J.F., Kremer, Y., and Petersen, C.C. (2011). Synaptic mechanisms underlying sparse coding of active touch. Neuron *69*, 1160-1175.

Curtis, J.C., and Kleinfeld, D. (2009). Phase-to-rate transformations encode touch in cortical neurons of a scanning sensorimotor system. Nature neuroscience *12*, 492-501.

Diamond, M.E., von Heimendahl, M., Knutsen, P.M., Kleinfeld, D., and Ahissar, E. (2008). 'Where' and 'what' in the whisker sensorimotor system (vol 9, pg 601, 2008). Nat Rev Neurosci *9*, I-I.

Drew, P.J., and Feldman, D.E. (2007). Representation of moving wavefronts of whisker deflection in rat somatosensory cortex. J Neurophysiol *98*, 1566-1580.

Ego-Stengel, V., Mello e Souza, T., Jacob, V., and Shulz, D.E. (2005). Spatiotemporal characteristics of neuronal sensory integration in the barrel cortex of the rat. J Neurophysiol *93*, 1450-1467.

Estebanez, L., Bertherat, J., Shulz, D.E., Bourdieu, L., and Leger, J.F. (2016). A radial map of multi-whisker correlation selectivity in the rat barrel cortex. Nat Commun *7*.

Estebanez, L., El Boustani, S., Destexhe, A., and Shulz, D.E. (2012). Correlated input reveals coexisting coding schemes in a sensory cortex. Nature neuroscience *15*, 1691-+.

Fanselow, E.E., and Nicolelis, M.A.L. (1999). Behavioral modulation of tactile responses in the rat somatosensory system. Journal of Neuroscience *19*, 7603-7616.

Feldman, D.E., and Brecht, M. (2005). Map plasticity in somatosensory cortex. Science *310*, 810-815.

Feldmeyer, D., Brecht, M., Helmchen, F., Petersen, C.C., Poulet, J.F., Staiger, J.F., Luhmann, H.J., and Schwarz, C. (2013). Barrel cortex function. Progress in neurobiology *103*, 3-27.

Ferezou, I., Haiss, F., Gentet, L.J., Aronoff, R., Weber, B., and Petersen, C.C.H. (2007). Spatiotemporal dynamics of cortical sensorimotor integration in behaving mice. Neuron *56*, 907-923.

Fox, K. (2002). Anatomical pathways and molecular mechanisms for plasticity in the barrel cortex. Neuroscience *111*, 799-814.

Ghazanfar, A.A., and Nicolelis, M.A. (1999). Spatiotemporal properties of layer V neurons of the rat primary somatosensory cortex. Cereb Cortex *9*, 348-361.

Glazewski, S., and Fox, K. (1996). Time course of experience-dependent synaptic potentiation and depression in barrel cortex of adolescent rats. J Neurophysiol *75*, 1714-1729.

Goldreich, D., Kyriazi, H.T., and Simons, D.J. (1999). Functional independence of layer IV barrels in rodent somatosensory cortex. J Neurophysiol *82*, 1311-1316.

Greenberg, D.S., Houweling, A.R., and Kerr, J.N.D. (2008). Population imaging of ongoing neuronal activity in the visual cortex of awake rats. Nature neuroscience *11*, 749-751.

Hartline, H.K., Wagner, H.G., and Ratliff, F. (1956). Inhibition in the Eye of Limulus. J Gen Physiol *39*, 651-673.

Hartmann, M.J. (2011). A night in the life of a rat: vibrissal mechanics and tactile exploration. Annals of the New York Academy of Sciences *1225*, 110-118.

Hentschke, H., Haiss, F., and Schwarz, C. (2006). Central signals rapidly switch tactile processing in rat barrel cortex during whisker movements. Cerebral Cortex *16*, 1142-1156.

Higley, M.J., and Contreras, D. (2003). Nonlinear integration of sensory responses in the rat barrel cortex: an intracellular study in vivo. The Journal of neuroscience : the official journal of the Society for Neuroscience *23*, 10190-10200.

Hill, D.N., Mehta, S.B., and Kleinfeld, D. (2011). Quality Metrics to Accompany Spike Sorting of Extracellular Signals. Journal of Neuroscience *31*, 8699-8705.

Hirata, A., and Castro-Alamancos, M.A. (2008). Cortical transformation of wide-field (multiwhisker) sensory responses. J Neurophysiol *100*, 358-370.

Hires, S.A., Gutnisky, D.A., Yu, J.N., O'Connor, D.H., and Svoboda, K. (2015). Low-noise encoding of active touch by layer 4 in the somatosensory cortex. Elife *4*.

Hobbs, J.A., Towal, R.B., and Hartmann, M.J.Z. (2016). Spatiotemporal Patterns of Contact Across the Rat Vibrissal Array During Exploratory Behavior. Front Behav Neurosci *9*.

Jacob, V., Le Cam, J., Ego-Stengel, V., and Shulz, D.E. (2008). Emergent Properties of Tactile Scenes Selectively Activate Barrel Cortex Neurons. Neuron *60*, 1112-1125.

Kelly, M.K., Carvell, G.E., Kodger, J.M., and Simons, D.J. (1999). Sensory loss by selected whisker removal produces immediate disinhibition in the somatosensory cortex of behaving rats. The Journal of neuroscience : the official journal of the Society for Neuroscience *19*, 9117-9125.

Kleinfeld, D., Ahissar, E., and Diamond, M.E. (2006). Active sensation: insights from the rodent vibrissa sensorimotor system. Curr Opin Neurobiol *16*, 435-444.

Knudsen, E.I., du Lac, S., and Esterly, S.D. (1987). Computational maps in the brain. Annual review of neuroscience *10*, 41-65.

Knutsen, P.M., Biess, A., and Ahissar, E. (2008). Vibrissal kinematics in 3D: tight coupling of azimuth, elevation, and torsion across different whisking modes. Neuron *59*, 35-42.

Knutsen, P.M., Pietr, M., and Ahissar, E. (2006). Haptic object localization in the vibrissal system: behavior and performance. The Journal of neuroscience : the official journal of the Society for Neuroscience *26*, 8451-8464.

Kremer, Y., Leger, J.F., Goodman, D., Brette, R., and Bourdieu, L. (2011). Late Emergence of the Vibrissa Direction Selectivity Map in the Rat Barrel Cortex. Journal of Neuroscience *31*, 10689-10700.

Krupa, D.J., Matell, M.S., Brisben, A.J., Oliveira, L.M., and Nicolelis, M.A. (2001). Behavioral properties of the trigeminal somatosensory system in rats performing whisker-dependent tactile discriminations. The Journal of neuroscience : the official journal of the Society for Neuroscience *21*, 5752-5763.

Kuffler, S.W. (1953). Discharge Patterns and Functional Organization of Mammalian Retina. J Neurophysiol *16*, 37-68.

Kwegyir-Afful, E.E., Bruno, R.M., Simons, D.J., and Keller, A. (2005). The role of thalamic inputs in surround receptive fields of barrel neurons. The Journal of neuroscience : the official journal of the Society for Neuroscience *25*, 5926-5934.

Lee, S., Carvell, G.E., and Simons, D.J. (2008). Motor modulation of afferent somatosensory circuits. Nature neuroscience *11*, 1430-1438.

Lee, S., Kruglikov, I., Huang, Z.J., Fishell, G., and Rudy, B. (2013). A disinhibitory circuit mediates motor integration in the somatosensory cortex. Nature neuroscience *16*, 1662-1670.

Madisen, L., Zwingman, T.A., Sunkin, S.M., Oh, S.W., Zariwala, H.A., Gu, H., Ng, L.L., Palmiter, R.D., Hawrylycz, M.J., Jones, A.R.*, et al.* (2010). A robust and high-throughput Cre reporting and characterization system for the whole mouse brain. Nature neuroscience *13*, 133-U311.

Mirabella, G., Battiston, S., and Diamond, M.E. (2001). Integration of multiple-whisker inputs in rat somatosensory cortex. Cereb Cortex *11*, 164-170.

Moore, C.I., and Nelson, S.B. (1998). Spatio-temporal subthreshold receptive fields in the vibrissa representation of rat primary somatosensory cortex. J Neurophysiol *80*, 2882-2892.

Moore, C.I., Nelson, S.B., and Sur, M. (1999). Dynamics of neuronal processing in rat somatosensory cortex. Trends Neurosci *22*, 513-520.

Niell, C.M., and Stryker, M.P. (2010). Modulation of Visual Responses by Behavioral State in Mouse Visual Cortex. Neuron *65*, 472-479.

O'Connor, D.H., Clack, N.G., Huber, D., Komiyama, T., Myers, E.W., and Svoboda, K. (2010a). Vibrissa-based object localization in head-fixed mice. The Journal of neuroscience : the official journal of the Society for Neuroscience *30*, 1947-1967.

O'Connor, D.H., Peron, S.P., Huber, D., and Svoboda, K. (2010b). Neural Activity in Barrel Cortex Underlying Vibrissa-Based Object Localization in Mice. Neuron *67*, 1048-1061.

Oberlaender, M., Ramirez, A., and Bruno, R.M. (2012). Sensory experience restructures thalamocortical axons during adulthood. Neuron *74*, 648-655.

Ohki, K., Chung, S., Ch'ng, Y.H., Kara, P., and Reid, R.C. (2005). Functional imaging with cellular resolution reveals precise micro-architecture in visual cortex. Nature *433*, 597-603.

Peron, S.P., Freeman, J., Iyer, V., Guo, C., and Svoboda, K. (2015). A Cellular Resolution Map of Barrel Cortex Activity during Tactile Behavior. Neuron *86*, 783-799.

Petersen, C.C.H. (2007). The functional organization of the barrel cortex. Neuron *56*, 339-355.

Petersen, R.S., Panzeri, S., and Diamond, M.E. (2001). Population coding of stimulus location in rat somatosensory cortex. Neuron *32*, 503-514.

Pluta, S., Naka, A., Veit, J., Telian, G., Yao, L., Hakim, R., Taylor, D., and Adesnik, H. (2015). A direct translaminar inhibitory circuit tunes cortical output. Nature neuroscience *18*, 1631-1640.

Poulet, J.F., and Petersen, C.C. (2008). Internal brain state regulates membrane potential synchrony in barrel cortex of behaving mice. Nature *454*, 881-885.

Ramirez, A., Pnevmatikakis, E.A., Merel, J., Paninski, L., Miller, K.D., and Bruno, R.M. (2014). Spatiotemporal receptive fields of barrel cortex revealed by reverse correlation of synaptic input. Nature neuroscience *17*, 866-875.

Reimer, J., Froudarakis, E., Cadwell, C.R., Yatsenko, D., Denfield, G.H., and Tolias, A.S. (2014). Pupil fluctuations track fast switching of cortical states during quiet wakefulness. Neuron *84*, 355-362.

Ringach, D.L., Mineault, P.J., Tring, E., Olivas, N.D., Garcia-Junco-Clemente, P., and Trachtenberg, J.T. (2016). Spatial clustering of tuning in mouse primary visual cortex. Nat Commun *7*.

Rothschild, G., Nelken, I., and Mizrahi, A. (2010). Functional organization and population dynamics in the mouse primary auditory cortex. Nature neuroscience *13*, 353-360.

Sato, T.R., Gray, N.W., Mainen, Z.F., and Svoboda, K. (2007). The functional microarchitecture of the mouse barrel cortex. Plos Biol *5*, 1440-1452.

Shimegi, S., Akasaki, T., Ichikawa, T., and Sato, H. (2000a). Physiological and anatomical organization of multiwhisker response interactions in the barrel cortex of rats. The Journal of neuroscience : the official journal of the Society for Neuroscience *20*, 6241-6248.

Shimegi, S., Akasaki, T., Ichikawa, T., and Sato, H. (2000b). Physiological and anatomical organization of multiwhisker response interactions in the barrel cortex of rats. Journal of Neuroscience *20*, 6241-6248.

Smith, S.L., and Hausser, M. (2010). Parallel processing of visual space by neighboring neurons in mouse visual cortex. Nature neuroscience *13*, 1144-1149.

Sofroniew, N.J., Cohen, J.D., Lee, A.K., and Svoboda, K. (2014). Natural whisker-guided behavior by head-fixed mice in tactile virtual reality. The Journal of neuroscience : the official journal of the Society for Neuroscience *34*, 9537-9550.

Szwed, M., Bagdasarian, K., and Ahissar, E. (2003). Encoding of vibrissal active touch. Neuron *40*, 621-630.

Timofeeva, E., Lavallee, P., Arsenault, D., and Deschenes, M. (2004). Synthesis of multiwhisker-receptive fields in subcortical stations of the vibrissa system. J Neurophysiol *91*, 1510-1515.

Vinck, M., Batista-Brito, R., Knoblich, U., and Cardin, J.A. (2015). Arousal and Locomotion Make Distinct Contributions to Cortical Activity Patterns and Visual Encoding. Neuron *86*, 740-754.

Wallach, A., Bagdasarian, K., and Ahissar, E. (2016). On-going computation of whisking phase by mechanoreceptors. Nature neuroscience *19*, 487-+.

Wen, J.A., DeBlois, M.C., and Barth, A.L. (2013). Initiation, Labile, and Stabilization Phases of Experience-Dependent Plasticity at Neocortical Synapses. Journal of Neuroscience *33*, 8483-8493.

Woolsey, T.A., and Van der Loos, H. (1970). The structural organization of layer IV in the somatosensory region (SI) of mouse cerebral cortex. The description of a cortical field composed of discrete cytoarchitectonic units. Brain research *17*, 205-242.

Yang, A.E.T., and Hartmann, M.J.Z. (2016). Whisking Kinematics Enables Object Localization in Head-Centered Coordinates Based on Tactile Information from a Single Vibrissa. Front Behav Neurosci *10*.

Yu, C.X., Horev, G., Rubin, N., Derdikman, D., Haidarliu, S., and Ahissar, E. (2015). Coding of Object Location in the Vibrissal Thalamocortical System. Cerebral Cortex *25*, 563-577.

Zhu, J.J., and Connors, B.W. (1999). Intrinsic firing patterns and whisker-evoked synaptic responses of neurons in the rat barrel cortex. J Neurophysiol *81*, 1171-1183.
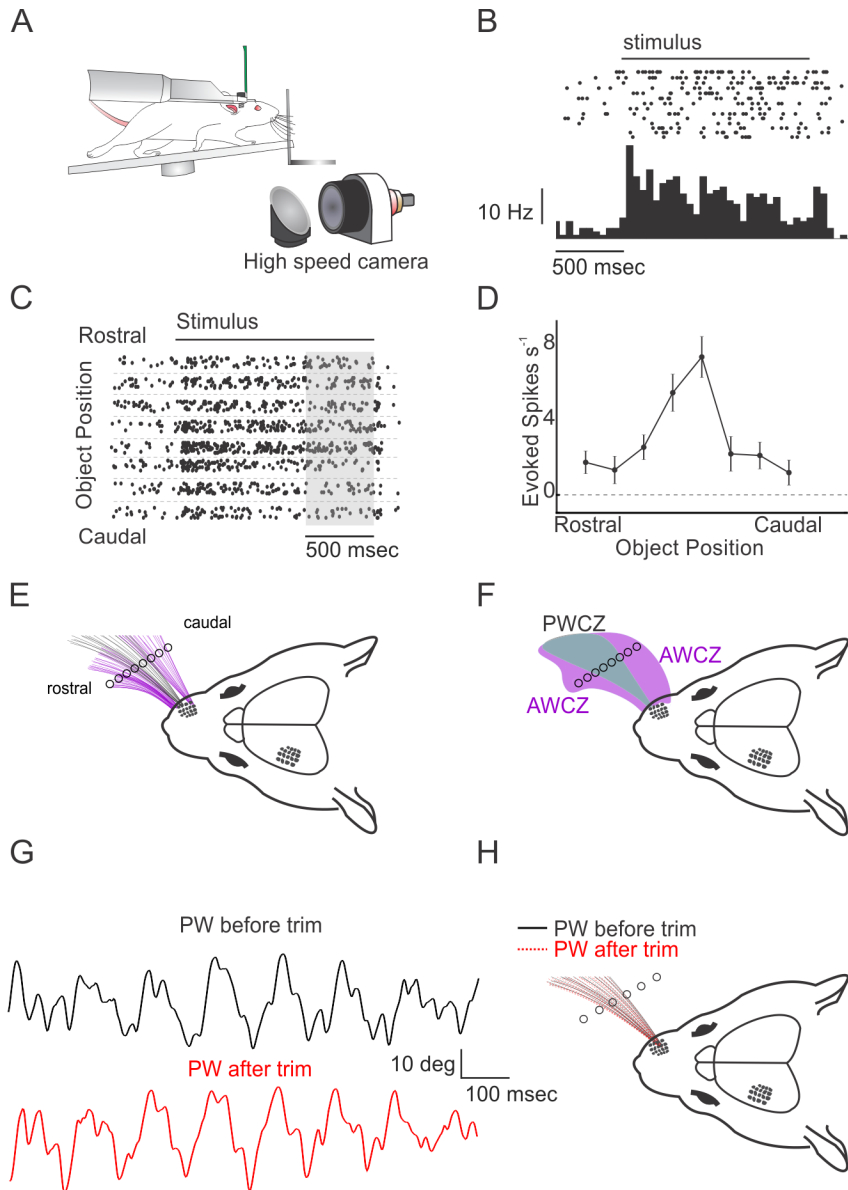
Figure 1: Probing the cortical representation of scanned space in the whisker system.
A) Experimental schematic: a head-fixed mouse runs on a circular treadmill, while a vertical bar is moved to different locations along the horizontal whisking axis. A high speed camera captures movements of the whiskers. B) An example raster plot (top) and PSTH (bottom) of a cortical L5 unit in response to touch with the stimulus bar at its preferred location. C) Raster plot for the same unit for several trials across each of the 8 positions probed. The grey rectangle indicates the time window for analysis of neural data. D) Tuning curve (mean ± s.e.m.) for this example unit. E) Plot of the whisker positions across the full range of protraction for four tracked whiskers (during free whisking) overlaid on a schematic of the animal's head. Grey: the selected principal whisker (C2). Purple: the adjacent whiskers of the C row. F) Diagram of the zone swept out by the principal whisker (PWCZ, red) and the adjacent whiskers of the same row (AWCZ, purple). G) Example traces of the principal whisker's (C2) movement along the horizontal axis before (black) and after (red) trimming all but the C2 whisker. H) Example plot of the PW's movement before (black) and after (red) trimming all but the C2 whisker. Red and black traced whisker positions are overlaid.

71
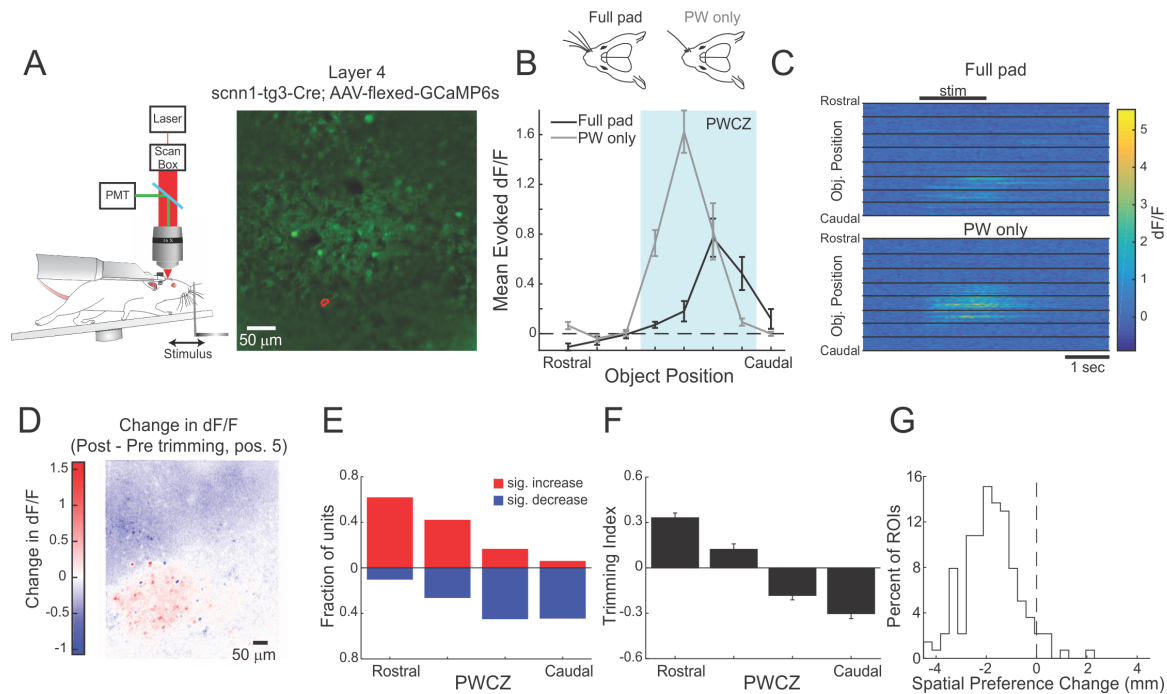
Figure 2: Surround whisker input powerfully modulates spatial representations in L4 excitatory neurons. A) Left: experimental schematic of a head-fixed mouse under a two photon microscope. Right: Example image of GCaMP6s-expressing L4 excitatory neurons. The C2 barrel is at center. The red outline indicates the position of the example neuron in B,C. B) Top: schematic of the pre- and post-surround whisker trimming conditions. Bottom: Example tuning curve (mean ± s.e.m.) of a single L4 neuron before (black) and after (grey) trimming all but the C2 whisker. C) Example 'raster' plot of calcium responses of the neuron from B). Top: before trimming. Bottom: after trimming. Responses from all eight stimulus positions are presented in both cases. D) Example image of the mean change in dF/F for each neuron in the field of view in L4 between post and pre trimming conditions for stimulus position five. Red indicates an increase in mean evoked responses, blue indicates a decrease. A Gaussian blur was applied. E) Plot of the fraction of cells in the C2 barrel that show significant increases (red) or decreases (blue) across each of the four stimulus positions within the PWCZ (n = 231 cells in 3 mice). F) Plot of the average trimming index for the same cells across the same stimulus conditions. G) Histogram of the change in spatial preference for all imaged neurons in the C2 barrel that exhibited significant spatial tuning both before and after surround whisker trimming (n = 139 cells across 3 mice, p < 0.001, t-test).
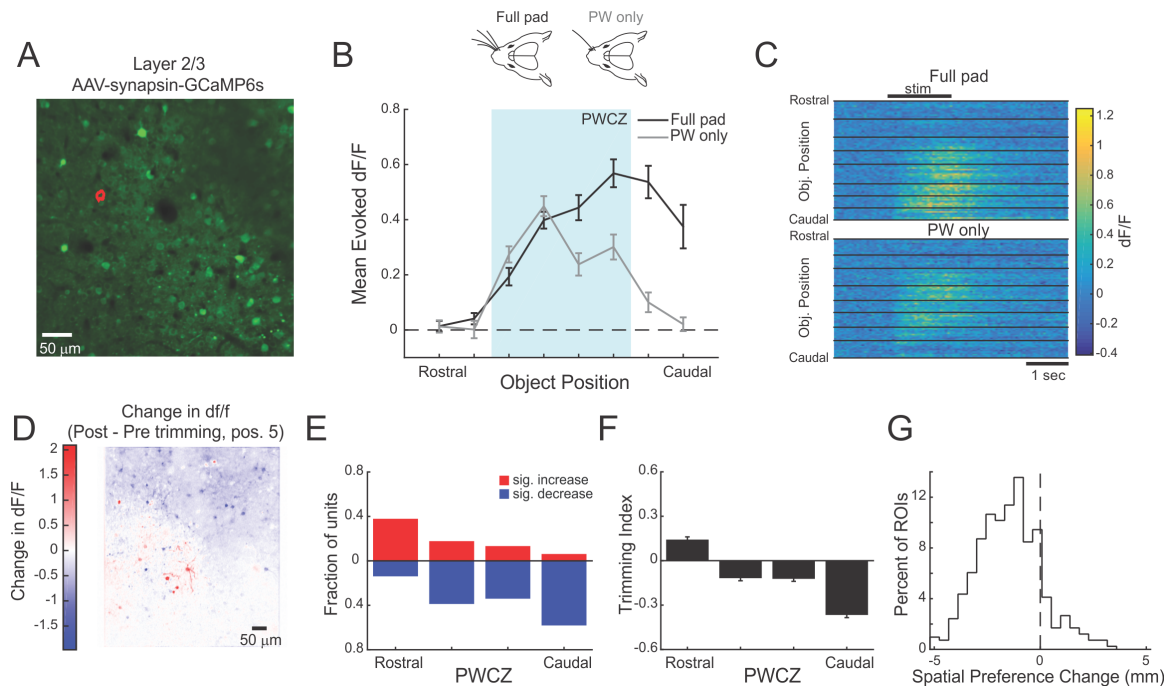
Figure 3: Spatial summation in L2/3 neurons. A) Example image of GCaMP6s-expressing L2/3 neurons. The anatomic aligned C2 column is at center. The red outline indicates the position of the example neuron in B, C. B) Top: schematic of the pre- and post-surround whisker trimming conditions. Bottom: Example tuning curve (mean ± s.e.m.) of a single L2/3 neuron before (black) and after (grey) trimming all but the C2 whisker. C) Example 'raster' plot of calcium responses of the cell from B). Top: before trimming. Bottom: after trimming. Responses from all 8 stimulus positions are presented in both cases. D) Example image of the mean change in dF/F for each neuron in the field of view in L2/3 between post and pre trimming conditions for stimulus position 5. Red indicates an increase in mean evoked responses, blue indicates a decrease. A Gaussian blur was applied. E) Plot of the fraction of cells in the C2 barrel that show significant increases (red) or decreases (blue) across each of the four stimulus positions within the PWCZ (n = 631 cells in 4 mice). F) Plot of the average trimming index for the same cells across the same stimulus conditions. G) Histogram of the change in spatial preference for all imaged neurons in the C2 column that exhibited significant spatial tuning both before and after surround whisker trimming (n = 413 cells across 4 mice, p < 0.001, Wilcoxon sign rank).
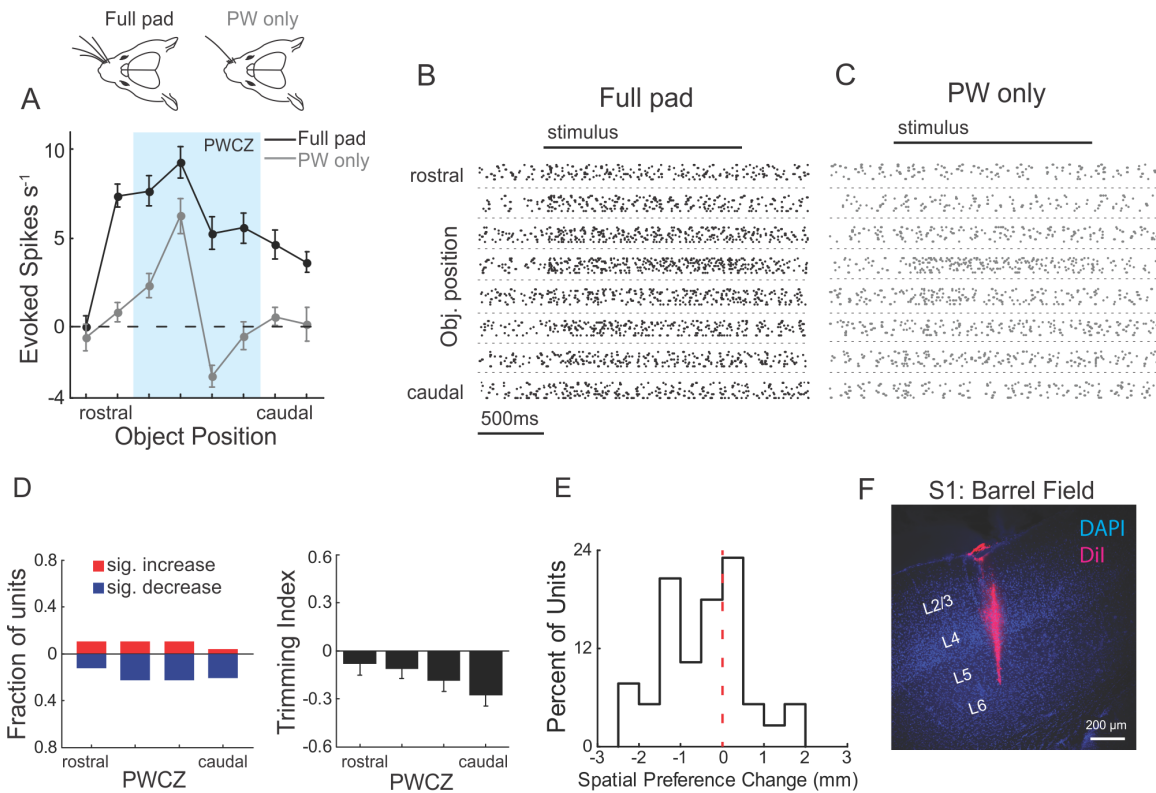
Figure 4: Spatial summation in touch responsive regular spiking units of L5. A) Top: schematic of the pre- and post-surround whisker trimming conditions. Bottom: Example tuning curve (mean ± s.e.m.) of a single L5 RS unit before (black) and after (grey) trimming all but the principal whisker. B) Example raster of the unit from A) before trimming to the principal whisker. C) As in B) but for after trimming. Responses from all 8 stimulus positions are presented in both cases. D) Left: Plot of the fraction of L5 RS units in the spared whisker column that show significant increases (red) or decreases (blue) across each of the four stimulus positions within the PWCZ. Right: Plot of the average trimming index for the same cells across the same stimulus conditions (n = 48 units in 8 mice). E) Histogram of the change in spatial preference for all recorded L5 RS units in the spared column with significant spatial tuning both before and after surround whisker trimming (n = 39 units across 8 mice, p = 0.001, Wilcoxon). F) Example image from a recorded animal showing the DiI track (red) of the multi-electrode array extending into L5.
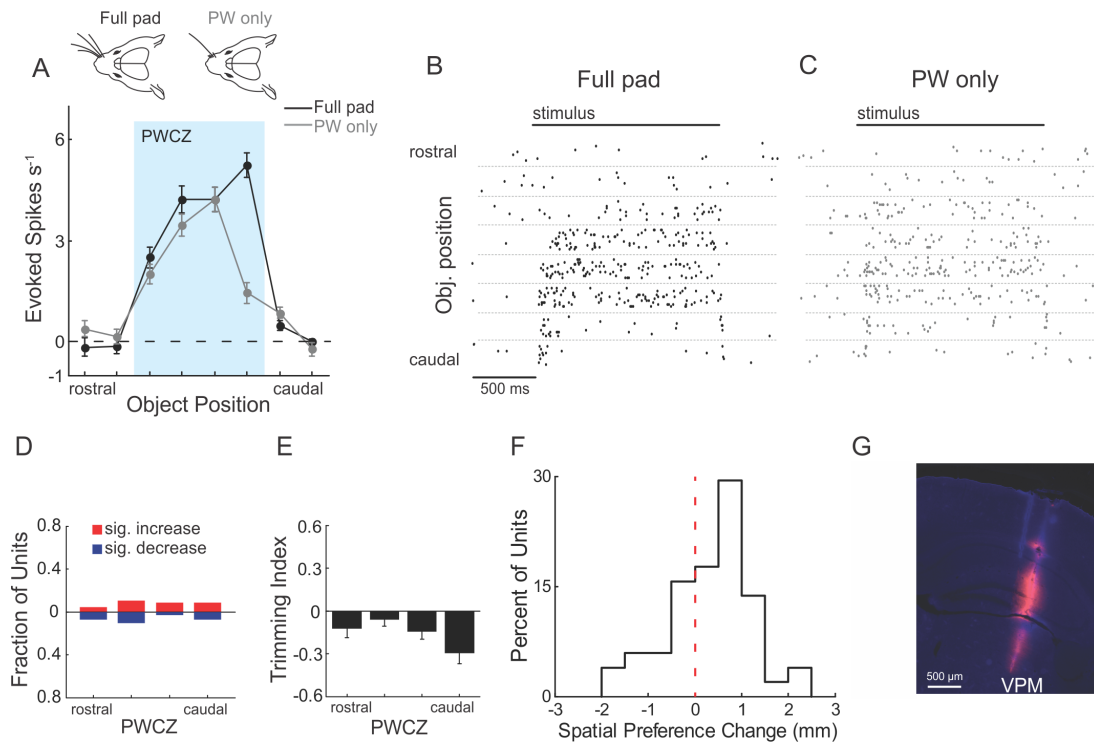
Figure 5: Weak surround modulation in thalamic neurons in VPM. A) Top: schematic of the pre- and post-surround whisker trimming conditions. Bottom: Example tuning curve (mean ± s.e.m.) of a single VPM unit before (black) and after (grey) trimming all but the C2 whisker. B) Example raster of the unit from A) before trimming to the C2 whisker. C) As in B) but for after trimming. Responses from all 8 stimulus positions are presented in both cases. D) Plot of the fraction of units in the C2 barreloid that show significant increases (blue) or decreases (red) across each of the four stimulus positions within the PWCZ (n = 54 units across 8 mice). E) Plot of the average trimming index for the same cells across the same stimulus conditions. F) Histogram of the change in spatial preference for all recorded units in the C2 barreloid with significant spatial tuning both before and after surround whisker trimming (n = 51 units across 8 mice, p = 0.23, paired t-test). G) Example image form a recorded animal showing the DiI track (red) of the multi-electrode array extending into VPM.
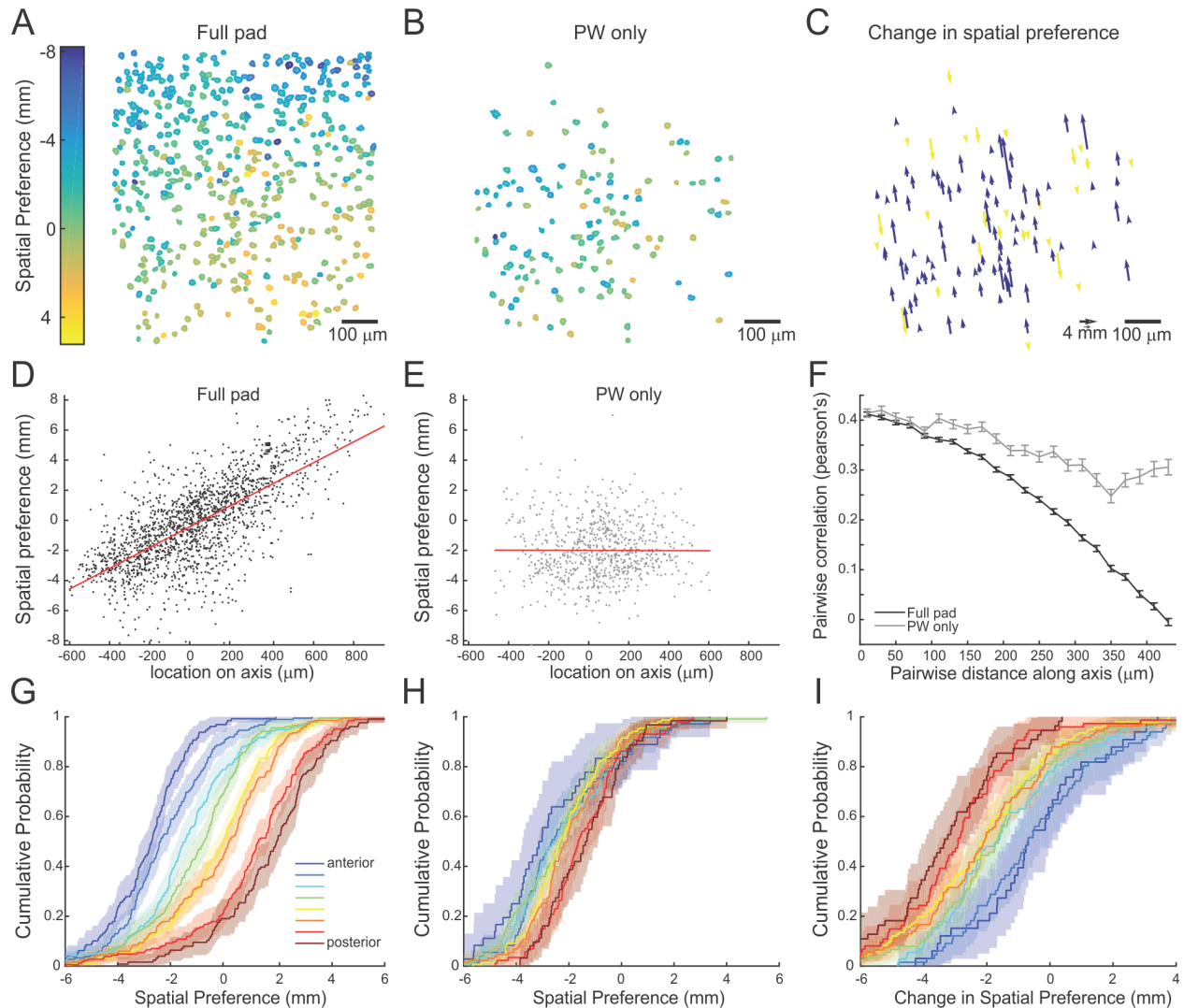
Figure 6: Surround whiskers organize a spatial map in L2/3 of the barrel cortex. A) Example spatial preference map in a mouse with all the whiskers intact of a field of view in L2/3 imaged with two photon microscopy. The color indicates the spatial preference of the stimulus bar's position. Only neurons that exhibited significant activity and spatial tuning are shown. B) Same field of view as in A) but collected immediately after removing all but the C2 whisker. Again, only neurons that exhibited significant activity and spatial tuning are shown. C) Plot of the magnitude and direction of change in spatial preference for all imaged neurons within A) and B) that exhibited significant spatial tuning both before and after surround whisker trimming. Yellow: rostral shift, purples: caudal shift. The length of each arrow corresponds to the magnitude of change in spatial preference, and its direction indicates the sign of the change. The arrows are all aligned to the axis of best fit for preferred position calculated prior to trimming. D) Plot of the spatial preference of all significantly tuned L2/3 cells versus their position along the axis of best fit (1789 neurons, 4 mice). The red line is a linear regression to the data. E) As in

76

D) but for after trimming to the C2 whisker (796 neurons, 4 mice). F) Binned plot of the pairwise correlation of spatial tuning curves for all pairs of significantly tuned L2/3 neurons within each mouse as a function of distance in cortical space. G) Cumulative distribution plots of spatial preference of significantly driven and tuned neurons before trimming as a function of cortical position along the axis of best fit. H) As in G) but for after trimming to the C2 whisker. I) Cumulative distribution plot of the change in spatial preference for all the recorded neurons.
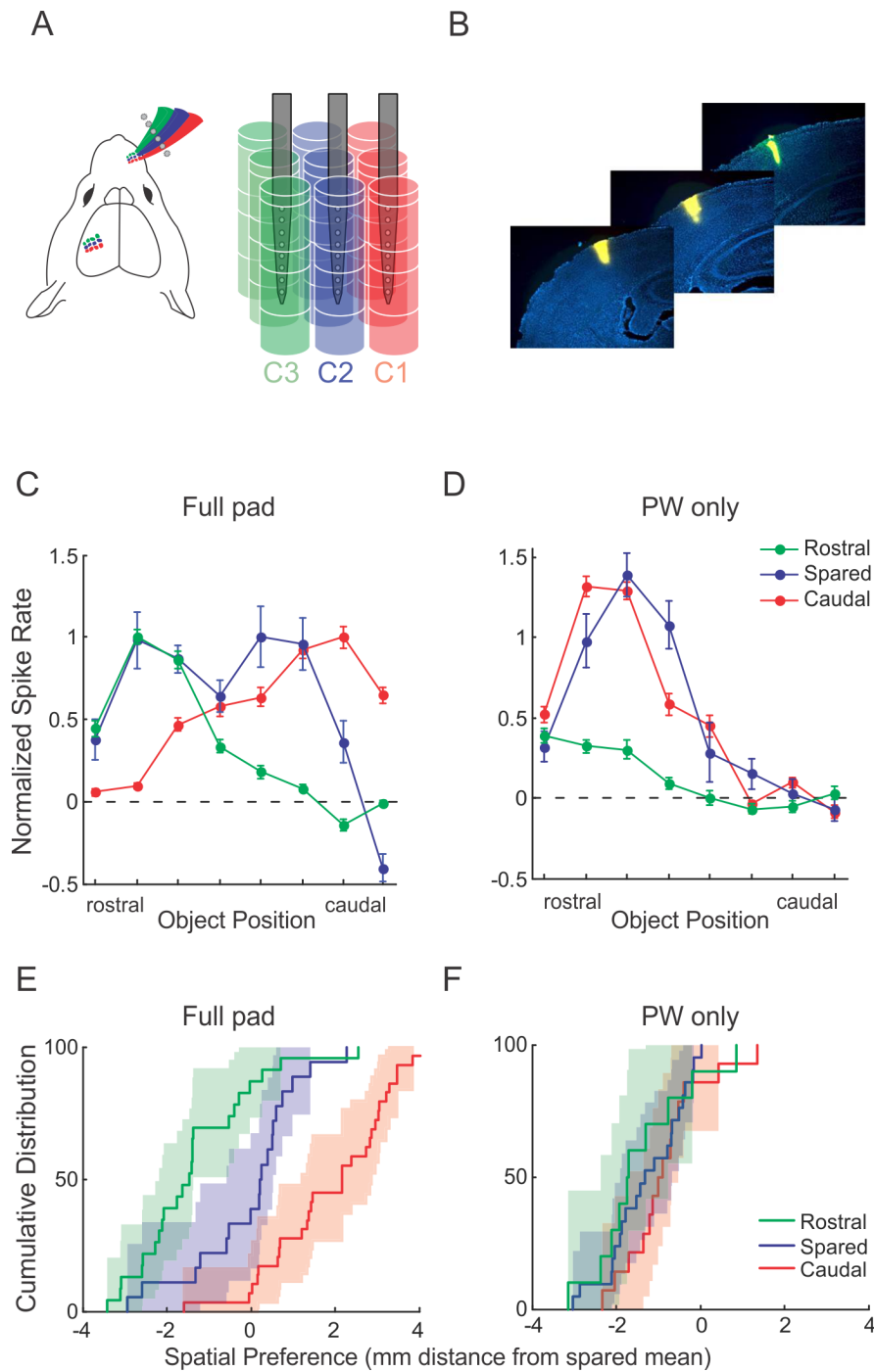
Figure 7: Surround whiskers distribute spatial representations in L5. A) Schematic of multi-shank laminar recordings in L5. B) Example histological images of the electrode of three adjacent shanks in S1. C) Example spatial tuning curves from three units on three adjacent electrode shanks. D) As in C) but following trimming off the surround whiskers. E) Cumulative distribution plots of spatial preference of significantly tuned units on each electrode shank before trimming. F) As in E) but following trimming off the surround whiskers.

STAR Methods

Contact for Reagent and Resource Sharing

Further information and requests for resources and reagents should be directed to and will be fulfilled by the Lead Contact, Hillel Adesnik (hadesnik@berkeley.edu).

Experimental Model and Subject Details

Wild-type adult ICR white (Charles River) mice between 6 and 10 weeks of age and of either gender were used for all experiments, except for those involving imaging cortical layer 4, for which the scnn1-tg3-Cre line (JAX), outcrossed to the ICR line for several generations, was used. All procedures were approved by the Animal Care and Use Committee of UC Berkeley. Both female and male animals were used and maintained on a 12:12 reversed light:dark cycle. For supplemental figure 6, we used a Thy1-GCaMP6s (4.3) mouse.

Methods Details

Preparation for *in vivo* electrophysiology

Anesthesia was induced with 5% isoflurane and then maintained at 1 – 3% during surgery. Respiratory rate and response to toe/tail pinching was monitored throughout surgery to ensure adequate anesthetic depth. 0.05 mg/kg of buprenorphine was administered for post-operative analgesia. After disinfecting the scalp with 70% alcohol and 5% iodine, the skin and fascia above the sensory cortices were removed with surgical instruments. Following application of Vetbond (3M) to the skull surface and wound margins, a custom stainless steel headplate was fixed to the skull with dental cement (Metabond). Two days after surgery, mice were habituated over increasing durations for 4 – 8 days to head-fixation on a free-spinning circular treadmill, until they freely ran at a fast and steady pace (>35 cm/s). Intrinsic optical imaging was performed to localize one or two barrel columns of interest (C1 – C3). In preparation for electrophysiology, mice were briefly (10 – 15 minutes) anesthetized with isoflurane, the skull over S1 was thinned with a dental drill (Foredom), and a small (<200 μm for a single shank) craniotomy was made with a 27 gauge needle. For mutli-shank experiments a long, thin craniotomy was opened over S1 in a similar fashion. The small size of the craniotomy minimized motion of the brain during electrode penetration and animal movement. For recordings from the cortex, a 16 or 32-channel linear silicon probe (NeuroNexus) was guided into the brain using a micromanipulator (Sutter Instruments) and a stereomicroscope (Leica) to the desired barrel column (C1 – C3) by aligning

the intrinsic optical signal (Fig. S2) with superficial blood vessels. For multi-shank experiments, a Neuronexus Buzsak32 probe was used. The principal whisker was verified electrophysiologically by deflecting individual whiskers and listening to multiunit activity (MUA). There was an audibly clear difference in MUA between principal and surround whisker contact. For recordings of the thalamus, a 16-channel linear silicon probe (NeuroNexus) was guided into the brain at 1600 μm posterior and 2000 μm lateral from bregma. The electrode was lowered until strong whisker responses were detected, usually around 2700-2800 μm, indicating the border of the ventro-posterior medial nucleus. The electrode was lowered further until it reached a barreloid corresponding to C2 or B2, where that whisker caused the strongest response from deflection. In all cases, electrical contacts on the probe spanned the C1 – C3 or B1 – B3 barreloids, as verified by electrophysiology.

Preparation for *in vivo* two photon imaging

The surgery was as described above, but with the following modifications for transcranial imaging through a glass window. 2 mg/kg of dexamethasone were administered as an anti-inflammatory. A 3 mm diameter craniotomy over the left primary somatosensory cortex was drilled, and a Nanoinject II nanoliter injector was used to inject 18.4 nL of AAV-GCaMP6s at ten to twenty sites within the craniotomy at an overall rate of 0.5 nL/s. AAV9-synapsin-GCaMP6s (UPenn Vector Core) was injected into wildtype ICR mice (Charles River) for L2/3 datasets, and AAV9-flexed-CAG-GCaMP6s (UPenn Vector Core) was injected into scnn1-tg3-Cre mice (JAX) for L4 datasets. After viral injection a window plug consisting of two 3mm diameter coverslips glued to the bottom of a single 5mm diameter coverslip using Norland Optial Adhesive #71 was placed over the craniotomy and sealed permanently using Orthojet. Mice were head-fixed on a freely spinning running wheel under a Nixon 16x-magnification water immersion objective and imaged with a Neurolabware two-photon resonant scanning microscope within a light tight box. Image acquisition was at 15.45 Hz with fields of view (FoVs) ranging from 600 μm by 650 μm to 1.25 mm by 1.15 mm. To obtain large fields of view in all cases, in some experiments four adjacent FoVs were imaged sequentially. Wide-field reflectance imaging with a white LED was used to illuminate the vasculature and center the FoV on the region the intrinsic signal identified as corresponding to the C2 barrel. For L2/3 imaging, imaging depth was 100 – 300 μm, and for L4 imaging, depth was 400 – 500 μm deep.

Tactile Stimulus presentation

During continuous two-photon imaging or electrophysiological recording, a modified 0.7mm Hex key (McMaster-Carr) was presented vertically at 8 locations along an axis perpendicular to whisking motion and ~1 cm away from the mouse's face. The pole was presented to the whiskers

for 1.5 seconds during each trial using a stepper motor (Oriental Motor) to quickly move the pole in, hold the pole stationary for the entire stimulus period, and then move it back out. There was an interval of 3 - 4.5 seconds between trials for imaging to allow the evoked calcium response to return to baseline. At the beginning of each inter-trial interval the stepper motor and pole were translated to the next trial's horizontal position using a motorized linear stage (Zaber). Stimuli were randomized in batches such that no stimulus was presented more than twice in a row. After >15 repetitions of the stimulus batches, data collection was paused and all but the principal whisker (always C2 for imaging experiments) were trimmed such that only the remaining whisker could contact the vertical pole stimulus at any position. Data collection immediately recommenced and at least 16 new batches of stimuli were presented. After conclusion of the experiment, the vertical pole was presented at each of the stimulus positions, and the PWCZ positions were identified by high speed camera acquisition or by visual inspection using stereomicroscope. This was verified post-hoc by determining which stimulus positions evoked significant activity throughout the object presentation period after trimming the surround whiskers.

Two photon imaging analysis

Raw two photon movies were first corrected for brain motion using Scanbox's fourier transform-based sbxalign script, written in MATLAB, to correct for the 2D translation of individual frames. The mean of each motion-corrected video was used to translate and register the before and after trimming datasets to within a single pixel of each other. Regions of interest (ROIs) encompassing neurons were identified in a semi-automated manner using Scanbox's sbxsegmentflood (MATLAB, Mathworks) which computes and thresholds the pixel-wise cross-correlation for all pixels within a 60 by 60 pixel window. If an ROI only appeared in one of the datasets via the semi-automated method, then the ROI was copied over to its relative location in the dataset in which it was not identified. The ROI's signal (R_i) was taken as the mean value across all pixels within and unique to that ROI (Fig. S2). This signal is assumed to be a mixture of the cell's actual fluorescence signal and a contaminating neuropil signal resulting from scattering producing off-target excitation, high illumination powers producing out of focus fluorescence, or unresolvable neurites passing through the microscope's point spread function. The neuropil signal (N_i) for each ROI was computed by averaging over an annulus of pixels surrounding the ROI but excluded pixels assigned to other ROIs as well as a smaller annulus of pixels that acted as a buffer in case any motion artifact was not perfectly accounted for (Fig. S2). This buffer annulus existed for all ROIs and was excluded from any neuropil calculation. As a result the max diameter of the neuropil annulus varied per ROI in order to ensure a similar number of usable pixels to average over. Each neuron's true fluorescence signal (F_i) was computed per ROI by the following equation:

$$F_i(t) = R_i(t) - k_i * N_i(t)$$

The amount of contamination (k_i) was assumed to be constant per ROI, but vary between ROIs as a result of local differences in expression and scattering. Each k_i was defined by assuming that the neuron's true fluorescence signal (F_i) can never be negative (i.e. $k_i * N_i(t) \leq R_i(t)$), and that there must be a maximal bound for contamination. The contamination coefficient per neuron was defined as follows:

$$k_i = \min\left(\frac{R_i(t)}{N_i(t)}\right); if\ k_i > .65, k_i = .65$$

The true signal was then converted into a trial-wise change in fluorescence ($\frac{f(t)-f_0}{f_0}$ or df/f) to capture the stimulus-evoked changes in neural activity while compensating for any fluctuations in baseline fluorescence. The baseline fluorescence (f_0) for a trial was taken to be the mean fluorescence over the one second prior to stimulation.

High-Speed Whisker Tracking

In a subset of experiments the whiskers were tracked at high speed (~500 frames per second). Previous data, confirmed here (Fig. S1), indicate a tight correlation between run-speed of the mouse and whisker set-point, which plateaus above 35 cm/s (Sofroniew et al., 2014). A high-speed camera (Basler, acA2000-340kc) was placed below the running wheel; the principal whisker was imaged from below using a mirror angled at 45 degrees. The base of the PW was painted with a thin layer of Titanium White (Liquitex) paint and illuminated from below using a bright red LED, providing contrast from the other whiskers. High-speed videos were acquired at 500 fps with a 100 μs exposure and were synchronized with neural data acquisition via external triggers. Videos were processed in MATLAB using custom tracking software. An ROI was placed over the sector that the painted whisker swept out, cropping out other reflective surfaces (e.g. mouse's nose) that would otherwise interfere with tracking. All frames were luminance-thresholded to create a binary image, and the center of the painted region was calculated; the angle between the center of the painted region and a user defined position on the face was calculated for all frames. Angle traces were created from these measurements to calculate the whisker kinematic features in Figure S1: set-point (median angle of envelope), amplitude (half-width of envelope), speed (distance/time), and frequency (cycles/second). The image of the PWCZ and the AWCZ in Figure 1 was created from tracking a mouse with a single row of whiskers illuminated from the top. The whisker traces were manually traced for display purposes only. It was not possible to detect contacts between the painted whisker and the stimulus bar, since only the base of the whisker was painted to avoid adding substantial weight to this whisker or altering its curvature.

Spike Sorting

16-32 channels of electrodes were amplified (AM Systems), filtered (0.1-5 kHz) and digitized at 30 kHz (National Instruments) using custom acquisition software (MATLAB, Mathworks). Spike detection was performed using the UltraMegaSort2000 package in MATLAB (Hill et al., 2011) (Mathworks). After detection, spikes were automatically sorted into clusters of units. Units were then further sorted manually to meet inclusion criteria and prevent pseudo-replication. Quality metrics included analysis of spike amplitude, spike rate, auto- and cross-correlation, inter-spike interval, outlier removal, distance from threshold, and cortical depth of largest waveform. With the exception of a small subset of fast-spiking or bursting units, included units had no more 1% of their individual waveforms violating a refractory period of 2.5 ms. The surround whisker trimming data was collected from 8 mice for the L5 RS population and 8 mice for the thalamus population. The principal whisker trimming data was collected from 8 separate mice.

Spike Waveform classification

Fast-spiking units were separated from regular spiking units using a k-means cluster analysis of two waveform components. One component was the normalized difference between the two positive-going peaks. The other component was the trough-to-peak latency of the large negative-going deflection. Fast-spiking units were categorized by a larger 2nd positive-going peak (positive difference), and a short (less than 0.33ms) trough-to-peak latency, following previously established approaches. Units on the border between the classification as FS or RS was excluded from analysis. FS neurons were excluded from the paper.

Trial inclusion criteria and layer boundaries

In sorted units, firing rates were computed by counting spikes in the final 500 ms of stimulus presentation. This window was chosen because within 1000 ms of the bar entering the whisker field, neuronal firing rates and behavior reached steady-state. Trials containing stimulation periods where the animal's mean run speed during the stimulus period dropped below 1.3 standard deviations of it population mean were excluded, to ensure consistency in whisking behavior across trials. In addition, trials where the standard deviation of an animal's run speed was more than 0.8 standard deviations from the population mean were excluded. Trials where the animal was not moving, thresholded by the animal's run speed being below 3 cm/s, were completely excluded from analysis. The depth of each unit was assigned based on the calculated depth of the electrode on the linear array that exhibited its largest waveform. Layer

boundaries were confirmed post-hoc using current source density analysis (CSD, Fig. S2) and labeling of the electrode track with a dye. CSDs were calculated from the trial-averaged local field potential (0.5 – 300 Hz) measured at each electrode contact, as previously published. We estimated the layer 4/5 boundary as the base of the current sink corresponding to layer 4.

Analytical Metrics

A *Trimming Index* for each condition was computed as the difference between the mean evoked firing rates during post-trimming (T) and control (C) conditions, divided by the sum of their mean evoked firing rates:

$$Trimming\ Index = \frac{T - C}{T + C}$$

The *Spatial Preference* of a neuron was determined by calculating the center of mass (CM) on the absolute value of its spatial tuning curves. FR, the mean evoked firing rate (or delta F) at position, P, at stimulus locations 1 through n:

$$Spatial\ Preference\ (CM) = \frac{FR_1 * P_1 + FR_2 * P_2 + \ldots + FR_n * P_n}{FR_1 + FR_2 + \ldots + FR_n}$$

Statistically significant changes in spatial preference at the level of single units was computed using a standard permutation test. For each unit, a null distribution of change in spatial preference was created by randomly sampling values among both conditions 5000 times. Significance ($p < 0.05$) was observed if the experimental effect was beyond the 97.5 percentile or below the 2.5 percentile of the null (two-tailed) distribution.

The relationship between the center and surround of the horizontal receptive fields of neurons was calculated as the difference between the max evoked firing rate (or delta F) in the PWCZ and the max evoked firing rate in the AWCZ divided by their sum.

$$Cent{:}Surr\ Index = \frac{\max(abs(PWCZ)) - \max(abs(AWCZ))}{\max(abs(PWCZ)) + \max(abs(AWCZ))}$$

The spatial selectivity of neurons was calculated from the normed (Euclidean) vector of the peak normalized spatial tuning curves. This value was then divided by square root of n dimensions – 1 to restrict its range from 0 to 1. Larger values signify higher spatial selectivity (lower broadness). Raw spike rates were used.

$$Spatial\ Selectivity\ =\ 1 - \left(\frac{\frac{||x||}{max(x)} - 1}{\sqrt{n} - 1} \right)$$

Map analysis

Within each dataset, the centroids of all significantly driven and tuned ROIs were whitened and projected onto 1800 axes spanning from 0 to pi. The centroids of the ROIs were whitened to minimize spurious correlations derived from the structure of the ROIs sampled. A linear regression was computed between the projected location of the ROIs and their preferred positions (calculated over the entire tuning curve) for each axis. The axis of best fit was determined to be the axis whose linear regression had the largest r^2 value. This axis of best fit was then transformed into cortical space via the inverse of the whitening transform. The center of the axis was located to the center of the spared whisker column (as identified above) allowing for data across mice to be aggregated.

A Pearson's correlation was computed for the significantly driven and tuned neurons between their projected locations on the axis of best fit and their preferred positions, both before and after trimming. A linear regression was performed to compute the slope of that correlation. The mean pairwise correlation in tuning over the PWCZ (Pearson's R) was computed as a function of their pairwise difference of their projections along the axis of best fit and binned within 20 μm bins. Cumulative distribution functions were created by binning the location of the neurons along the projection into 18 equally sized bins. Only the central 8 bins, which had more than 145 neurons each (the expected value if the distribution of ROIs along the axis were uniform), are shown.

Quantification and Statistical Analysis

Statistically significant differences between conditions were determined using standard parametric or nonparametric tests in MATLAB, including a 1-way ANOVA, student's t-test, rank sum, and a Wilcoxon sign-rank test. Tests for normality were performed with a Lilliefors test. Units were defined as tuned for space if their evoked spike rate changed as a function of object position, determined by a 1-way ANOVA. Analysis of spatial preference changes was restricted to neurons that were significantly tuned for the stimulus both before and after trimming. The number of neurons that significantly changed their response per position was

defined as neurons whose pre- and post-trimming response distributions were significantly different via a rank sum test. All "n" values are referring to the number of cells present in an analysis except when explicitly stated that the n is referring to the number of mice used.

Electrophysiology

Unless stated otherwise, analyses were performed from evoked spike rates. The spontaneous firing rate of a neuron in the 500 ms window preceding stimulation was subtracted from its firing rate of the last 500 ms of active touch, on a trial by trial basis. Neurons in L5 and the thalamus were classified as touch-facilitated or touch-suppressed. Touch facilitated neurons had a positive mean evoked spike rate in the principal whisker contact zone (PWCZ), while touch-suppressed neurons had a negative mean evoked rate in the PWCZ.

Two-photon calcium imaging

Analyses were performed on trial-wise dF/F. Analysis was limited to ROIs that met several criteria: they must be significantly driven by at least one stimulus, be larger than 50 μm^2, and for Figs. 2 and 3 have been within the principle whisker column. A significant response for a position had to meet two criteria: have a mean df/f greater than .2, and pass a t-test between the evoked responses at that position and the measured df/f values during control trials. The Benjamini & Hochberg false discovery rate correction was used to correct for the multiple comparisons taken across the multiple stimuli. Outlier responses per stimulus position were identified by the median rule, where values further than 2.3 times the inter-quartile range from the median are determined to be outliers, and were removed prior to any analysis. Neurons were identified to be within the spared principle whisker column or to be in a surrounding column by using a custom MATLAB (Mathworks) algorithm to segment the pixels that exhibited a significant response post-trimming (t-test between control trials and the mean of PWCZ stimulus trials) which is putatively localized to the spared column (Fig. S2). The neural response for a single trial was calculated as the average df/f during the last 500 ms of stimulation.

Chapter 4: Spatial integration during active tactile sensation drives orientation perception

Foreword

In this project we set out to determine what aspects of sensory integration are necessary for object discrimination. I was responsible for the high speed whisker tracking and some of the initial extracellular electrophysiology experiments. Unlike the previous study where we could isolate and track a single whisker out of a small subset, either by trimming whiskers for a clear view or using reflective paint, we could not do that here. In this experiment mice required a full pad of whiskers. I adapted and programmed the custom whisker tracking apparatus to work with a full whisker pad and the new behavior system as well as analyzed the data generated. Jenny Brown created a novel whisker dependent discrimination task where mice had to determine if a stimulus bar was in one of four GO angles or in one of four NOGO angles. Mice were able to do the task with as few as two to three whiskers, however if the remaining whiskers were positioned in a row the mouse could no longer complete the task. Optogenetic silencing of somatosensory cortex prevented mice from performing well on the task, even with all whiskers intact. This made it clear that vS1 stimulus integration was critical for the task. Calcium imaging verified that vS1 neurons encoded the behavioral stimuli. High speed whisker tracking and a novel whisker contact detector found that expert mice contacted the stimulus bar differently with the whiskers than naïve mice. It also showed that the whiskers contacted the stimulus properly even on trials during silencing or when the mouse made a mistake. Poor performance on the task was not due to changes in whisking but due to vS1 computations integrating across whisker arcs.

Citation

Brown, J., Oldenburg, I.A., Telian, G.I., Griffin, S., Voges, M., Jain, V., Adesnik, H.A. Spatial Integration During Active Tactile Sensation Drives Orientation Perception. Neuron. 2021 May 19;109(10):1707-1720.e7. https://doi.org/10.1016/j.neuron.2021.03.020.

Summary

Active haptic sensation is critical for object identification, but its neural circuit basis is poorly understood. We combined optogenetics, two-photon imaging, and high-speed behavioral tracking in mice solving a whisker-based object orientation discrimination task. We found that orientation discrimination required animals to summate input from multiple whiskers specifically along the whisker arc. Animals discriminated the orientation of the stimulus *per se*, as their performance was invariant to the location of the presented stimulus. Populations of barrel cortex neurons summated across whiskers to encode each orientation. Finally, acute optogenetic inactivation of the barrel cortex and cell-type specific optogenetic suppression of layer 4 excitatory neurons degraded performance, implying that infragranular layers alone are not

sufficient to solve the task. These data suggest that spatial summation over an active haptic array generates representations of an object's orientations, which may facilitate the encoding of complex three-dimensional objects during active exploration.

Introduction

To judge the shape, size and location of objects, cortical circuits must integrate information arriving from different parts of the sensor array, whether this be from different parts of the retina, the body surface, or the cochlea. Many animals, including humans, move their sensors to optimize information gathering, a process termed 'active sensation'(Gibson, 1962). Humans use active sensation to investigate and manipulate objects by executing various stereotyped hand motions(Lederman and Klatzky, 1987). Tactile input from adjacent fingers conveys multi-dimensional information about the orientation and structural relationship of the object's surfaces to give rise to a coherent object percept. In the primate somatosensory cortex, individual neurons can encode the orientation and curvature of a stimulus(Hsiao et al., 2002, DiCarlo and Johnson, 2000). Sensing the shape of an object, however, depends on dynamic integration of tactile input (i.e., skin indentation) with proprioceptive information about hand and joint position(Hsiao, 2008). How cortical circuits extract shape information during active sensation is poorly understood.

The rodent vibrissal system is a powerful model for active sensation and tactile perception, and the mouse offers the genetic tools that make dissecting the cellular and circuit basis of tactile perception possible(Petersen, 2019). Rodents sweep their whiskers across objects to localize and identify them(Ahissar and Knutsen, 2008, Diamond et al., 2008, Brecht et al., 1997). Judging object location and shape uses sensory circuits to integrate ex-afferent signals due to whisker contact and re-afferent signals due to self-generated whisker motion, conceptually analogous to proprioceptive input from the hand(Kleinfeld and Deschênes, 2011). Subsets of neurons in the barrel cortex integrate these two afferent streams to accurately localize stimuli in a head-centered coordinate frame(Diamond et al., 2008, Curtis and Kleinfeld, 2009). Rodents can readily identify and discriminate objects with their whiskers purely based on shape(Brecht et al., 1997, Anjum et al., 2006, Polley et al., 2005, Kim et al., 2020), and barrel cortex neurons are sensitive to the location(O'Connor et al., 2010, Sofroniew et al., 2015, Curtis and Kleinfeld, 2009), texture(Arabzadeh et al., 2003, Isett et al., 2018, Chen et al., 2013), shape(Anjum et al., 2006), deflection angle of individual whiskers(Kim et al., 2020, Bruno et al., 2003, Andermann and Moore, 2006, Lavzin et al., 2012, Simons, 1985, Kwon et al., 2018), and correlated motion of multiple whiskers across the whisker pad(Vilarchao et al., 2018, Jacob et al., 2008, Drew and Feldman, 2007). Discriminating some, but not all of these tactile features utilizes spatial summation over the whisker array (Pluta et al., 2017, Brumberg et al., 1996, Krupa et al., 2004, Kathleen Kelly et al., 1999). However, despite this work, the neural basis for orientation

perception during active sensation, which may contribute to shape identification, is not understood.

To investigate the neural circuit basis of object orientation we developed an active whisker dependent orientation discrimination task for head-fixed mice, explored the behavioral and sensory basis of task performance, and measured neural activity in the barrel cortex as the mice solved the task. Object orientation discrimination required integration over vertically stacked whiskers, mice discriminated the object orientation *per se*, and calcium imaging revealed that neurons in the barrel cortex encoded all presented orientations of the stimulus, which required summation across whiskers. Inactivating the barrel cortex optogenetically, strongly impaired performance, and even much more selective optogenetic inactivation of layer 4 (L4) excitatory neurons reduced task performance. These data help define the circuits and computations that are required for the discrimination of object orientations during active sensation.

Results

Mice can use active touch to discriminate object orientations with high acuity

To probe the neural circuit basis of orientation perception, we developed a whisker dependent task that required mice to discriminate the orientation of tactile stimuli (Figure 1A,B). A stimulus bar was presented unilaterally to the mouse's right intact whisker field in one of eight possible orientations. Mice were trained to discriminate positive orientations (GO) and negative orientations (NOGO), licking for rewarded GO stimuli, but withholding licking to unrewarded NOGO stimuli (Figure 1C, S1). Mice routinely reached high levels of performance (d': 2.3±1.2 std, Figure 1E-H), performed high numbers of trials (301±89 std) and reached performance criterion (d'>1.5) after roughly one to two weeks of training (8.3±2.2 std days, Figure 1I). Mice readily discriminated orientations as small as 7° (Figure 1E-G), though further training may reveal even finer acuity. Even well-trained mice exhibited some licking for unrewarded NOGO trials. To test if this is an intrinsic perceptual bias towards such orientations or simply a bias towards licking, we trained a separate cohort of mice on the reverse orientation contingency. In these mice we also observed licking for NOGO orientations, strongly implying that the bias was a product of the operant training and not an asymmetry in perception (Figure S1F).

We developed a photo-interrupt touch detector to estimate the timing and the number of whisker contacts made with the stimulus bar before its decision (Figure 1C,D, S2). The mean latency from first touch to lick was around 400ms (full pad; 0.44±0.08s, 2 whiskers; 0.48±0.15s, std, Figure 1D, S2I). Mice made ~8 whisker contacts with the stimulus bar prior to licking (full pad; 8.5±1.4, 2 whiskers; 7.1±1.9, std, Figure S2J,K). We observed a tight coordination between whisking, running and licking behavior in trained mice during success trials: upon presentation of the stimulus all trained mice decelerated (most strongly to GO stimuli), adjusted their whisker set point caudally, and reduced their whisking amplitude in a stimulus dependent manner (Figure

S3D,E). Naive mice showed modest, largely stimulus independent, changes in running and whisking, and no licking behavior (Figure S3B,C). These data indicate that multiple motor systems (running, whisking, and licking) were highly coordinated as a consequence of learning and successful performance in the task, implying a closed-loop process(Ahissar and Assa, 2016, Saig et al., 2012).

Orientation discrimination requires spatial summation across multiple whiskers

To probe how mice discriminate the orientation of the stimulus, we first confirmed the role of whiskers in task performance. Once mice had reached threshold and stable performance on the task, all whiskers were trimmed (~2mm length) preventing any contact with the stimulus bar. Trimming whiskers significantly reduced performance to chance levels (Figure 2B; p<0.001), confirming that mice solved the task through whisker touch and not through other sensory cues such as motor sounds.

We hypothesized that orientation perception may depend on integration over the whisker pad. Therefore, we asked whether contacts from multiple whiskers were required to solve the task. To address this directly, we measured performance as we acutely trimmed the whisker array to different combinations of whiskers (Figure 2A). We hypothesized that mice would require at least two whiskers, presumably in different rows (i.e., along an arc), to obtain relevant information on object orientation. Whiskers in different rows could discriminate positive from negative orientations by computing the relative horizontal position of object contact; in contrast, whiskers in the same row would only access the object at nearly the same elevation, and therefore have less information on object orientation.

 Trimming the whiskers to a row of four or fewer significantly impaired task performance with discriminability dropping to chance levels (Figure 2C,E,F; p <0.01). In contrast, trimming to an arc of whiskers did not affect performance (Figure 2D-F; p=0.74). In fact, even just two whiskers in an arc was sufficient to perform the task (Figure 2D-F). Importantly, however, trimming to one whisker abolished performance (Figure 2D-F). These results demonstrate that mice solved the orientation discrimination task specifically by integrating multiple whiskers in an arc; contact information from a single whisker was insufficient. A similar study showed that mice with only one whisker can discriminate object orientation(Kim et al., 2020), perhaps by adopting alternative whisking strategies or by relying on the differing deflections of the remaining whisker. However, our data indicate that when trained with multiple whiskers in this task, the default strategy the mice use is to summate sensory information over at least two whiskers along an arc.

Mice can use the orientation of the stimulus *per se* to solve the task

Orientation perception should be invariant to the vantage point or absolute location of the object. Therefore, we next asked whether trained mice use the orientation of the stimulus bar *per se* to

91

solve the task, rather than a more specific code that relies on contacting the stimulus bar with a specific set of whiskers in a specific location. Using high-speed whisker tracking data, we found that mice with intact whiskers contacted the stimulus bar primarily with their frontmost whisker arcs, and rarely made contact with the middle or back arcs prior to making their decision (Figure 3A). When these mice were acutely trimmed to a single middle arc of whiskers (Arc 2) they showed no significant drop in performance even though they had not been previously employing this arc to solve the task (Figure 3A). Thus, mice could immediately use these alternate whiskers to solve the task, indicating that they were employing a more general orientation-perception based strategy.

Next, we designed an experiment in a new group of mice that would not require whisker trimming. We hypothesized that if mice were using an orientation-based rather than a specific whisker/location-based strategy to solve the task, behavioral performance should be unaffected by acutely presenting the oriented stimulus bar in random horizontal locations within the whisking field. Thus, mice should discriminate the bar's orientation with different sets of whiskers on different trials. Therefore, we jittered the absolute horizontal location of the oriented bar, trial by trial, and monitored the effect on each mouse's performance. For these experiments, the stimulus bar was moved in from the side ('lateral presentation') rather than from the front to prevent the mice from solving the task while the stimulus bar was still moving towards its final position (Figure 3B). Although these mice were initially trained with the stimulus moving in from the front ('rostral presentation'), all mice quickly acclimatized to lateral presentation (1-3 days). Once they regained their original performance level, we began presenting the stimulus to one of three positions, each engaging different sets of whiskers. All three positions were randomly interleaved in the test session. Three out of five of the test mice maintained high levels of performance (d'>1.5) across all of the positions, strongly suggesting that these mice solved the task by sensing the stimulus orientation *per se* (Figure 3C,D). The other two mice showed a drop in performance only for the more distant position (pos2), which returned to baseline proficiency in 1-4 days. The transient drop in performance for these two mice might be due to the difficulty in acclimatizing to altered task conditions (multiple final locations of the stimulus), or to the need to re-learn new spatial rules for the two additional stimulus positions. The latter explanation would require them to solve the task by remembering three unique spatial coding rules, as opposed to a single orientation-based rule. These data show that mice can solve the task with multiple strategies, but that a majority of tested mice learn a more generalizable orientation-based rule.

To control for a strategy where mice adaptively adjust their whisking to different stimulus positions and thus are still able to solve the task with a spatial rule (in coordinates invariant to the whisking field), we tracked the motion of the whiskers with high-speed imaging. Whisker tracking showed that whisking properties were largely invariant across the different jitter positions (Figure 3E). Furthermore, high-speed video analysis showed that different whiskers

primarily contacted the stimulus bar at each of the different jitter positions (Figure 3F). These results suggest that mice that showed no acute drop in performance when the stimulus bar was presented to different horizontal locations are using different sets of whiskers to determine the orientation of the stimulus bar and solve the task.

Barrel cortex neurons encode object orientation through spatial integration over the sensory array

Next, we sought to address the neural basis for object orientation discrimination. As we show that mice integrate over multiple whiskers to solve the task, we began by recording neural activity in the barrel cortex whose neurons integrate over the whisker array(Brumberg et al., 1996, Pluta et al., 2017, Krupa et al., 2004, Ramirez et al., 2014). We trained transgenic mice expressing GCaMP6s in excitatory neurons of the cortex on the task with a full whisker pad (camk2-tTa; tetO-GCaMP6s mice, Wekselblatt et al., 2016). Following training we imaged activity in the barrel cortex with volumetric calcium imaging, collecting neural data from approximately 1,000 neurons per recording in 3 planes of ~800 x 800μm field of view (Figure S4A,B), encompassing several columns of the barrel cortex. We relied on 'Suite2P' for source extraction and neuropil subtraction (see Methods; Figure S4C-H, Pachitariu et al., 2016).

To explore the stimulus-evoked activity we analyzed calcium activity (both ΔF/F and deconvolved calcium (see Methods)) beginning at the estimated time of first whisker contact and extending to the end of the behavioral response window, 0.5 seconds prior to reward delivery (Figure 4A; see Methods and see Figure S5 where expanded and restricted time windows are considered). Across the imaged population of neurons, about 45% of identified neurons showed significant responses during presentation of the stimulus bar (see classification in Methods), and about one third showed significant tuning across the stimuli (Movie 1; Figure 4B-D). Importantly, we identified neurons in each mouse that responded best to each of the eight presented stimuli (Figure 4D, S6). This distribution of neuronal tuning across the discriminated orientations was robust as it was observable after cross-validation (Figure 4D, S7A) and visible across a wide range of analysis conditions (Figure S5A,B, S7B,C,D). We validated that the imaging resolution of our optical system was sufficient to resolve individual cells without cross-contamination (Figure S4C-J, and see Methods).

To quantify the selectivity of neural responses we computed a selectivity index (see Methods). Across all cells the selectivity index was much higher than shuffled controls or randomly generated data (Figure S7E; $p<1e-99$, rank sum test). Across the population of imaged neurons we observed a bias towards neurons encoding NOGO orientations, which may be due to earlier contact times with NOGO stimuli (Figure S2E,F,H), more contacts on NOGO trials (Figure S2G), different whisker kinematics following contact with the angled bar, other asymmetries in the stimulation or recording setup (Figure S3), or a physiological bias towards representing these orientations(Vilarchao et al., 2018). This overrepresentation was not dependent on task training

since we also observed it in naive, untrained mice (Figure S5D). Despite this overrepresentation of cells selective for NOGO orientations, dimensionality reduction (see Methods) revealed that the population of imaged neurons smoothly represented and could discriminate all stimulus orientations (Figure 4E). In each recording, the population responses for each stimulus orientation diverged shortly after the estimated first whisker contact, indicating a high level of discriminability within the earliest touches (Figure S7F).

Although the barrel cortex exhibits topographic maps of whisker input(Woolsey and Van der Loos, 1970) and spatial input in the whisking field(Pluta et al., 2017), we did not observe any obvious organization of orientation selectivity, though we cannot rule out finer structure as further investigation is required. In all recorded mice, neurons with distinct tuning preferences appeared to be intermingled with each other (Figure 4F, S6), this observation was robust to the analysis window (Figure S5C).

We next asked how the animal's behavior and trial type modulated neural activity in the barrel cortex. While the stimulus bar's orientation was the strongest predictor of most neurons' responses in the task, trial type (GO vs NOGO), as well as motor decision (lick vs no lick) also modulated the activity of many neurons, consistent with prior results(Yang et al., 2015) (Figure S8A). Furthermore, at their preferred stimulus orientation neuronal responses were slightly larger on trials where the animal responded correctly (Figure S8B; success trials: 0.28±0.004 vs failure trials 0.25±0.005 z-scored deconv. Ca^{2+} $p<10^{-34}$ rank sum test). However, this performance-based difference was much smaller than the difference between the presence and absence of a stimulus (Figure S8B). To compare the relative importance of different features of the task we employed a measure of absolute discriminability (see Methods). As this metric can be susceptible to low trial counts, we focused only on the middle four angles (±15°, ±7°) where there was a more even distribution of success and failure trials (mean: 11±2 failure trials, 23±2 success trials per condition, per mouse). We found cells that discriminated each tested features of the task (GO vs NOGO, lick vs no lick, success vs failure, or any orientation vs catch) at rates higher than in a shuffled control. However, cells were far more discriminative of the stimulus bar orientation (preferred orientation vs catch or vs least preferred) than any other comparison (Figure S8C,D, when computing scores that require a preferred orientation only cell's whose preferred orientation is one of the middle angles are included). This indicates that while the animal's behavior and task features modulate many neurons' responses, the stimulus orientation had the strongest influence on their physiological responses.

To determine if spatial summation(Simons, 1985, Kleinfeld and Delaney, 1996) across the whisker array was necessary for the orientation selectivity in the barrel cortex, in a subset of mice we acutely trimmed the mouse's whiskers from an arc of three to one whisker, a condition in which the mice fail to perform the task (see Figure 2). As a control, orientation tuned neurons were observed at similar rates and distributions in mice with three whiskers in an arc compared to mice with all whiskers intact (Figure 4G; S9; 37% tuned). However, when trimmed, we

observed roughly half as many tuned cells, with some previously tuned cells becoming unresponsive (Figure 4G; top) and others losing their tuning (Figure 4G; below), leading to an increase in the proportion of responsive but untuned cells (Figure 4G; S9A-B; 20% remained tuned after trimming). Among the neurons that were both responsive in the three-whisker condition and after trimming, most tuned cells showed a decrease in orientation selectivity (p <1e-41, rank sum test), whereas untuned cells remained untuned (Figure 4H; S9C; p>0.32, rank sum test). Further trimming to remove the last remaining whisker reduced task evoked activity to chance levels (Figure S9A,B). This implies that integrating across two or more whiskers is required for much of the object orientation coding in the barrel cortex in this task. This across-whisker summation might arise in the barrel cortex, or upstream, such as in the thalamus, where neurons show multi-whisker receptive fields(Timofeeva et al., 2004). Although barrel cortex neurons are well-known to encode angular deflections of single whiskers(Simons and Carvell, 1989, Bruno et al., 2003, Kim et al., 2020), here angular tuning alone appears insufficient for orientation coding and behavioral performance. Instead, these data imply that the mice used more global computations across the whisker array.

Orientation discrimination depends on neural activity in the barrel cortex

The data above show that mice learn to solve the orientation discrimination task by integrating touch information from multiple whiskers. Although neurons in the whisker system as early as the trigeminal nucleus show sensitivity to multiple whiskers(Minnery and Simons, 2003), prior work(Brecht et al., 2003, Brumberg et al., 1996, Pluta et al., 2017) and our imaging data show that spatial integration is pronounced at the level of S1. Therefore, we tested whether neural activity in S1 would be required for task performance. Since studies have shown that the barrel cortex can be dispensable for tactile tasks(Hutson and Masterton, 1986, Hong et al., 2018), we inactivated S1 neural activity in several ways.

First, we suppressed excitatory neurons in the barrel cortex by virally expressing the potent inhibitory opsin eGtACR1 in emx1-Cre mice(Govorunova et al., 2015, Mardinly et al., 2018). An optic fiber coupled to a 470nm LED was positioned over S1 to illuminate all or nearly all of the barrel cortex. We randomly switched the LED on during one third of trials. To ensure silencing occurred before the first whisker contact, the LED was turned on one second before and remained on throughout the sampling and response window. Optogenetically suppressing excitatory neurons strongly reduced performance on the task (Figure 5A,E). Second, we photo-stimulated parvalbumin-positive (PV) GABAergic interneurons to silence nearly all barrel cortex activity by driving cortical inhibition(Sachidhanandam et al., 2013). This silencing likewise significantly reduced performance (Figure 5B,E). As a control, illumination in mice not expressing any opsin (WT) or targeted inactivation of the primary visual cortex (V1) had no impact on behavioral performance (Figure 5C-E). These results imply that barrel cortex activity is required for object orientation discrimination.

We observed that performance degradation was largely due to an increase in FA rates (Figure 5A,B). Perhaps because mice had a strong bias to lick across all stimuli from how they were trained (Figure S1), or because suppression of the barrel cortex directly induced licking. To address this issue, we first analyzed the impact of cortical suppression on catch trials, where the stimulus was not within reach of the whiskers. On these trials, barrel cortex suppression strongly increased the probability that mice would lick even though there was no contact between the whiskers and the stimulus bar (Figure 5A,B,F). Perhaps more importantly, the increase in the FA rate on catch trials predicted a corresponding increase in FAs for NOGO stimuli during optogenetic suppression but not in control mice (Figure 5A-D). This suggests that eliminating barrel cortex activity may have reduced the ability of mice not only to discriminate stimulus orientation but also to determine whether they were touching a stimulus at all. Next, we silenced the barrel cortex during inter-trial intervals (ITI) when there was no audible cue that a trial had been initiated (unlike catch trials when the stimulus did move but did not reach the whisking field). In contrast to catch trials, illumination of the barrel cortex during the ITI did not increase the probability of licking (Figure 5F). This shows that suppressing the barrel cortex did not directly induce the mice to lick in the absence of a contextual cues indicating the initiation of a trial. These data suggest that the GO/NOGO training paradigm we employed may have generated a strong bias to lick on trials when mice either could not discriminate stimulus orientation or could not determine whether a stimulus was present.

Although these results imply that barrel cortex activity is required for task performance, they provide no information on which sub-classes of cortical neurons might be important. Next, we specifically suppressed activity in a subset of layer 4 (L4) excitatory neurons with the neuronal silencer eNpHR3.0 in scnn1a-Cre mice targeted to the barrel cortex (Figure 6A). Suppressing L4 excitatory neurons is a more subtle perturbation than cortex-wide inactivation; as we have previously shown, L4 suppression significantly degrades spatial representations in S1, but does not abolish sensory-evoked activity in any cortical layer(Pluta et al., 2015). We found that optogenetic suppression of a subset of L4 neurons significantly impaired performance, albeit more modestly than for total cortical inactivation (Figure 6A,C). In contrast, illumination of control mice not expressing any opsin had no effect on behavior (Figure 6B,C; WT). This demonstrates that L4 activity is required for normal behavioral performance, most likely either by driving sensory input to L2/3, or by sculpting activity in L5 through translaminar inhibition(Pluta et al., 2015). Together, these results imply that barrel cortex activity, *per se*, is necessary for object orientation discrimination.

Discussion

Using a tactile discrimination task we addressed how animals use active touch to discriminate object orientation. We propose that during natural object exploration, when many whiskers contact adjacent or overlapping surfaces, spatially distributed orientation-selective activity across

many columns of the barrel cortex may give rise downstream to shape-specific neurons, akin to those found in the primate inferotemporal cortex(Perrett et al., 1982) that might be closely linked to object identification.

Since haptic perception in our task involves active whisker scanning, mice may have solved the discrimination task in a number of ways. Mice could use either 'open loop' or 'closed-loop'(Ahissar and Assa, 2016, Saig et al., 2012) strategies to identify the object orientation. In an open-loop scheme, mice would not (or at least not need to) adaptively modify their whisking strategy to optimize orientation discrimination. One intuitive open-loop solution would be for neurons to compute the relative contact time with the oriented stimulus for each whisker. Contact time is known to be encoded both at peripheral levels(Jones et al., 2004, Leiser and Moxon, 2007) and in the cortex(Curtis and Kleinfeld, 2009, Waiblinger et al., 2015). Positive and negative lags of the relative contact time would thus indicate either positive or negative orientations, which in our paradigm indicate either GO or NOGO behavioral choices. Conversely, mice could adopt a 'closed-loop' strategy adapting their whisking kinematics across successive touches during a trial to optimize their stimulus orientation estimate(Saig et al., 2012, Ahissar and Assa, 2016). Whisker tracking revealed significant orientation-dependent changes in whisking kinematics including the whisker set point and amplitude following first contact with the stimulus. These changes were largely learned as they did not appear to the same magnitude or have the same orientation specificity in naive mice (Figure S2, S3).

Although it seems probable that different mice adopt different strategies, a significant fraction of mice seemed to perceive the orientation of the stimulus bar *per* se as acutely challenging them with the stimulus bar at different horizontal positions resulted in little to no drop in performance (Figure 3). Since mice could not perform the task with just one whisker, it also seems unlikely that mice simply computed the orientation of deflection of each whisker. Although with sufficient training they may adopt this strategy. Indeed, a recent study trained mice with one whisker to discriminate the angle of a stimulus bar and found angular tuning maps in the barrel cortex(Kim et al., 2020). Thus, mice can determine the orientation of a contacted object with multiple strategies. Understanding the computations that mediate orientation discrimination should be a fruitful subject of additional work.

It is possible that some mice could have reduced the discrimination task to a detection task by adjusting their whisking strategy so that they only contact the stimulus bar for either the GO or NOGO stimuli. Our whisker and contact tracking do not support this scenario (Figure S2, S3). However, mice could adopt a whisking strategy where one whisker would only contact either GO or NOGO stimuli and only attend to whether this specific whisker made contact – reducing it to a touch-detection task. Since location coding is robustly encoded in the whisker system this is plausible(Knutsen et al., 2006, Knutsen et al., 2008, Ahissar and Knutsen, 2008). However, this seems to be unlikely since acutely trimming mice from a full whisker pad to an arc (trimming all but four whiskers) only slightly reduces performance (Figure 2) and jittering the azimuthal

position of the stimulus did not reduce performance in most tested mice (Figure 3), which should have negated such a strategy. Therefore, the results more likely support the conclusion that the mice discriminate the different orientation *per se*, although a detection strategy cannot be ruled out.

Mice may discriminate the orientation of stimuli using the multipoint location of an object in space. Rodent whiskers move in a three-dimensional fashion that may facilitate precise location coding(Knutsen et al., 2008), and rodents can perform fine location discrimination with specific sets of whiskers(Knutsen et al., 2006). Different aspects of location representation are encoded in independent pathways(Knutsen and Ahissar, 2009) that likely converge in the barrel cortex, enabling barrel cortex neurons to faithfully encode this higher order feature. It is highly likely that the extraction of stimulus location must be essential to shape discrimination(Diamond et al., 2008). Our study supports the idea that the organization of whiskers involved in such extraction is critical, with an arc of whiskers carrying the richest information upon stimulus orientation or location when presented with a vertically orientated stimulus(Knutsen et al., 2006). If we had presented more horizontally oriented stimuli, contacts from different rows of whiskers might instead be most informative.

Importantly, with multiple approaches, we showed that normal activity in S1 is required for animals to discriminate object orientation in our task (Figure 5,6). S1 inactivation could impair performance because S1 activity encodes the surface orientation and passes this information downstream to generate the orientation-selective percept. Alternatively, S1 inactivation might simply disrupt activity in another region, such as the superior colliculus, that is more directly responsible for computing object orientation and passing this onto decision and motor execution circuits. Previously, focal inactivation or ablation of a specific sensory or motor area can lead to spontaneous recovery. This recovery could be explained by homeostatic rebalancing of activity in another brain region whose activity was disrupted by the lesion, or by the animals relearning the task with auxiliary circuits(Hong et al., 2018, Otchy et al., 2015). Although these are both difficult to rule out in our experiments, a more parsimonious explanation is that S1 activity and sensory computation in S1 *per se* are likely to be required, as S1 neurons encode the object orientations explicitly (Figure 4, S7). Finally, we found that degrading spatial representations in S1 via a much more subtle and partial L4-inactivation also impaired performance on the task (Figure 6), demonstrating that normal L4 activity is required, or at least that activity in other layers is not sufficient. This lends additional support to the notion that S1 computation – putatively via L4 neurons - is necessary for object orientation discrimination.

Imaging S1 revealed that populations of neurons in S1 encoded all stimulus orientations in the task, and that much of this selective encoding depended on summation over multiple whiskers, as it largely disappeared in mice trimmed to a single whisker. We observed a large overrepresentation of neurons tuned to NOGO (-45°) orientations in expert (Figure 4; Figure S5) and naive (Figure S5) mice implying it was not a product of training but instead either related to

kinematic differences in how the whiskers interact with the NOGO stimuli, or a biased representation of these stimuli in the cortex. During active whisking rodents palpate their whiskers against objects in a forward motion to induce whisker bending, vibrations and stick-slips(Isett et al., 2018, Hires et al., 2013, Arabzadeh et al., 2003, Jadhav et al., 2009). One explanation for the overrepresentation of NOGO stimuli could be that whiskers made a greater number of contacts and/or with higher force than with the GO (+45°) stimuli. To support this, we have shown that mice contact the -45° stimulus sooner than the other orientations resulting in a higher number of contacts during the initial decision period of the task. Furthermore, in a recent study, detailed kinematic analysis of whisker motion following contact with an oriented bar shows greatest vertical bending and displacement of the whisker following contact with more rostrally oriented bars compared to bars oriented more caudally(Kim et al., 2020). Interestingly, when we trimmed the whiskers down to a single C2 whisker, aligned with the fulcrum of the stimulus bar, we found a more even overrepresentation of -45° and 45° angles and an underrepresentation of intermediate angles. This is consistent with Kim *et al* in which detailed single whisker tracking showed that whisker contact with an +45° and -45° angled stimuli generates the greatest slide distances of the whisker compared to the intermediate angles, which may contribute towards such overrepresentations in S1(Kim et al., 2020).

Understanding how animals employ active sensorimotor strategies to optimize sensation and generate coherent percepts of the external world is critical for analyzing brain function and behavior. The head-fixed training paradigm we developed is simple but powerful – learning is quick and robust and can be probed by high-speed whisker tracking, and neural activity measurement and perturbation. Future experiments aimed at identifying the downstream circuits in the somatosensory system responsible for integrating multiple object orientations into a specific percept of a 3D object, will yield key insights into high level perceptual processes. Mice offer the most powerful genetic toolkit of any mammalian species, and like other rodents, presumably use high-resolution touch input to discriminate and identify small objects near their head. Therefore, mice trained on this and similar tactile tasks might yield fundamental insights into the neural mechanisms of higher order shape perception.

Acknowledgements

Author contributions

J.B. and H.A. conceived the study. J.B. conducted all the behavioral experiments. J.B. and I.A.O. conducted the imaging experiments. G.I.T. provided software for whisker tracking. S.G., V.J., and M.V. assisted in behavioral training and experiments. V.J. built the whisker contact detector. H.A., J.B., and I.A.O. wrote the paper.

Inclusion and Diversity

One or more of the authors of this paper self-identifies as an underrepresented ethnic minority in science. One or more of the authors of this paper self-identifies as a member of the LGBTQ+ community. One or more of the authors of this paper self-identifies as living with a disability. One or more of the authors of this paper received support from a program designed to increase minority representation in science. While citing references scientifically relevant for this work, we also actively worked to promote gender balance in our reference list.

Declaration of interests

The authors declare no competing interests.

A
Eye patch
Air puffer
Stimulus bar
Lick detector/
Reward spout
Free-spinning circular
treadmill

B
GO   0°   NOGO
+45°   -45°

C
· Whisker Contact   ▬ HIT
· Licks   ▬ FA
· Water   ▬ MISS/CR

GO   NOGO

Trial Count

Time (s)   Time (s)

D
GO
Norm. Values

NOGO
Norm. Values
— Whisker Contacts
— Licks
— Running

Time (s)

E
Lick Probability

Stim. Orientation (°)

F
d'

Stim. Orientation (°)

G
Hit Rate

FA Rate
○ ± 45°
○ ± 29°
○ ± 15°
○ ± 7°
× C

H
Session Count

d'

I
Cum. Frac. of Mice

Sessions To Criterion

Figure 1. An orientation discrimination task for mice during active haptic sensation

A. Schematic of experimental setup. An orientated stimulus bar is presented unilaterally to the right whisker field of a head-fixed, freely running mouse.

B. Stimulus bar is either positively oriented (GO trials; blue shades) or negatively oriented (NOGO trials; red shades).

C. Raster plot of behavioral during a single example session separated into GO (*left*) and NOGO trials (*right*). The whiskers contact the stimulus bar (black tick marks) as it moves into the whisker field. Time points 0 represents when the bar stops and the start of the 1 second response window (shaded gray). Licks (magenta ticks), reward delivery (blue ticks). Bars to the right of raster plots show performance on each trial (green; Hit, red; FA, gray; CR or Miss).

D. Average normalized running velocity (blue), whisker contacts (black) and lick frequency (magenta) separated into GO trials (*top*) and NOGO trials (*bottom*) for a subset of mice where whisker contact data was collected (n=3 mice, 6 sessions).

E. Psychometric performance curve (n=25 mice, averages from individual mice (gray); group mean ± SEM and fit (black)). Dashed lines represent midpoints for 0° stimulus orientation and 0.5 lick probability. C= catch trial.

F. d' for corresponding orientation pairs (n=25 mice, averages from individual mice (gray); group mean ± SEM (black)). Dashed line represents performance criterion (d'>1.5).

G. Hit and FA rates for all sessions over performance criterion separated into orientation pairs and catch trials (n=25 mice).

H. Distribution of d' values during learning. Dashed line represents performance criterion.

I. Cumulative histogram of the number of sessions to reach performance criterion across mice.
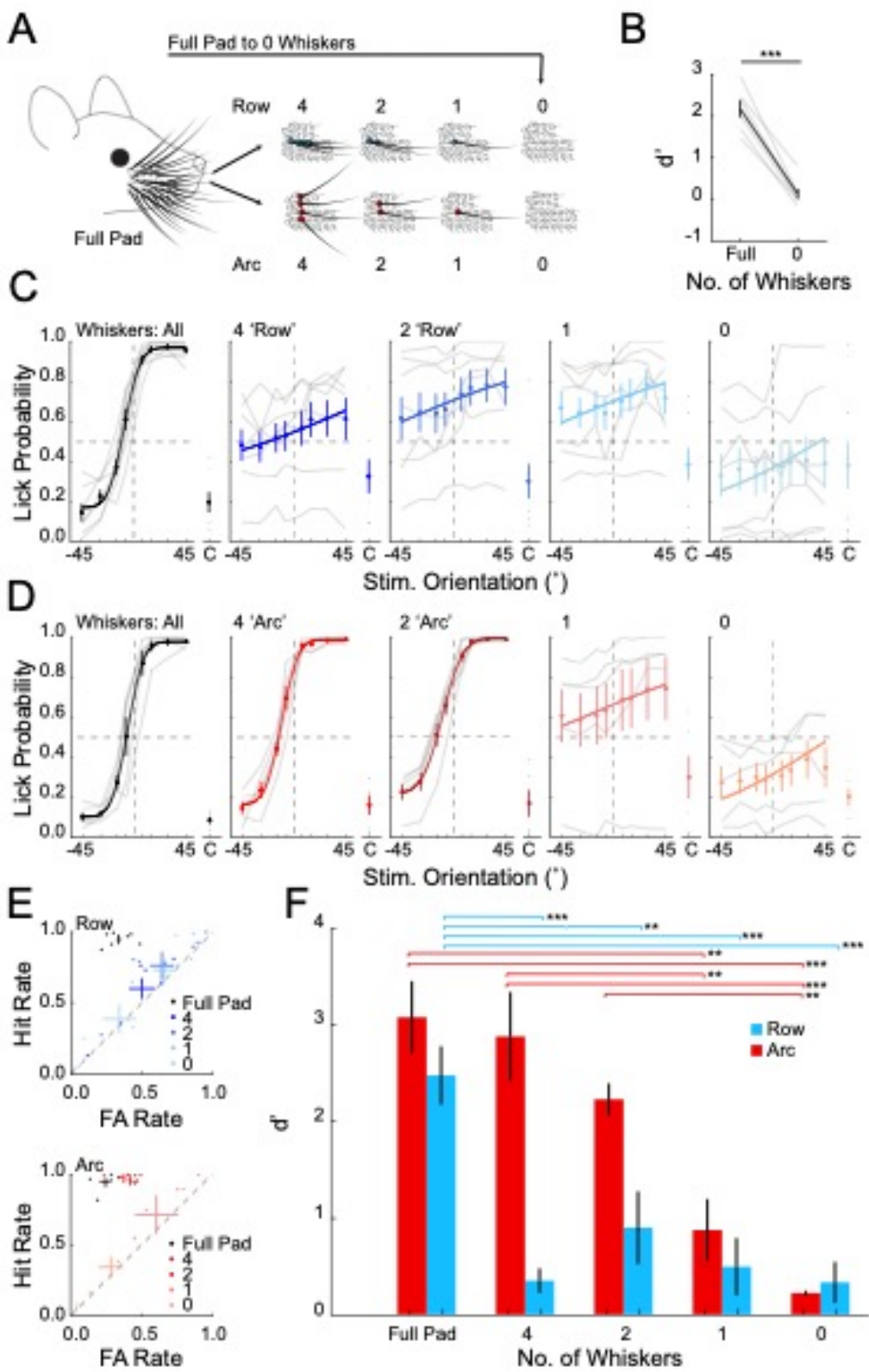
Figure 2. Mice must integrate sensory input from at least two vertically stacked whiskers to discriminate orientations

A. Schematic of the progressive whisker trimming experiment.

B. Performance of mice that was abruptly trimmed from full whisker pad to 0 whiskers (***p<0.001, n=6 mice, rank sum test).

C. Task performance in mice progressively trimmed to a row of whiskers (n=7 mice; averages from individual mice (gray); mean ± SEM and fit (solid colors).

D. As in C) but for mice trimmed to an arc of whiskers (n=5 mice).

E. Hit and FA rates for mice trimmed to a row (*top*) or an arc (*bottom*) of whiskers. Color shade indicates the number of remaining whiskers in each condition. Individual mice (points) and means ± SEM (solid colors).

Summary plot of average performance of each group during the progressive trimming paradigm (**p<0.01, ***p<0.001, ANOVA).

A

Rostral presentation

Full Pad

Trim

Rostral presentation

Arc 2

Full Pad

Arc 2

10mm

Whisker Arcs
1 2 1 G
3 4
5
6
Back
Middle
Front

Frac. of Contacts
1.0
0.5
0.0
Front Middle Back
Whisker Arc

d'
4
3
2
1
0
Full Pad   Arc 2

B

pos2
pos1
pos0

Lateral presentation

Full Pad

pos0

pos1

pos2

10mm

C

pos0
d'
3
2
1
0

pos1
3
2
1
0

pos2
3
2
1
0
0 1 2 3 4
Session No.

D

Lick Probability
1.0
0.8
0.6
0.4
0.2
0.0
-45 -29 -15 -7 7 15 29 45
Stim. Orientation (°)

pos0
pos1
pos2

E

Analysis Window
1 2 3 4   5

pos0
Whisker Set point
20

pos1
20

+45°   -45°

pos2
20

-1   0   1
Time (s)

Analysis Window
1   2   3   4   5

Amp.
5

Set point
10

Run
50

-45 45 -45 45 -45 45 -45 45 -45 45
Stim. Orientation (°)

pos0
pos1
pos2

F

pos 0
Frac. of Contacts
1.0
0.5
0.0
-45   45
Stim. Orientation (°)

pos 1
-45   45

pos 2
-45   45

Front
Middle
Back

Frac. of Contacts
1.0
0.5
0.0
Front Middle Back
Whisker Arcs

Frac. of Contacts
1.0
0.5
0.0
0   1   2
Jitter Position

Front
Middle
Back

105

Figure 3. Mice can generalize the orientation discrimination rules to multiple stimulus positions

A. Schematic of mouse using full whisker pad (*top; left*) or an arc of whiskers (*bottom; left*) to perform task, corresponding example frame from high-speed imaging (*middle; top*) and schematic of mouse whisker pad (*middle; bottom*). Distribution of whiskers (front, middle or back) contacting stimulus bar during the decision period with full pad (Right; top, n=3 mice, 3 sessions). Performance with full and arc of whiskers intact (right; *bottom,* n=5 mice replotted from Figure 2F).

B. Schematic of positional jitter experiment (*left*). The stimulus bar was presented laterally to one of three final stationary positions (pos 0, pos 1, pos 2; targeting front, middle and back whiskers respectively). *Right*; example frames of whiskers contacting stimulus bar at each position.

C. d' for each mouse one day before lateral jitter is introduced (session number 0; stimulus bar presented laterally to one position, pos0) and four days (session number 1-4) separated by each position. Dashed line represents performance criterion.

D. Average psychometric curves from days 3-4 (n=5 mice), averages from individual mice (light colors according to position); group mean ± SEM and fit (solid colors). Dashed lines are 0° stimulus orientation and 0.5 lick probability.

E. *Left*; example average whisker set point separated by stimulus orientation (colored lines) and jitter position (top to bottom; pos0, pos1 and pos2) for a single session. Gray bars represent each analysis window (see Methods and Figure S3). *Right*: mean value during each analysis window for whisker amplitude (amp. (degrees)), whisker set point (degrees) and run velocity (cm/s^2; n=5 mice, ANOVA).

F. *Left*: fraction of contacts with each whisker group for each lateral jitter positions and for each stimulus orientation. *Middle*: average fraction of contacts each whisker group made to the stimulus bar across jitter positions. *Right*: Re-plotted to show fraction of contacts each jitter position received from each whisker group (n=5 mice, *P<0.05, ANOVA).

Figure with panels A–H. Panel A: schematic of imaging setup and traces (Running, Decon. Ca²⁺ Activity, Licks), 1s scale bar. Panel B: Z Decon. Ca²⁺ tuning curves numbered 1–8 across Stim. Orientation (°), ΔF/F and Decon. Ca²⁺ traces, Cell Mask images. Panel C: donut chart with legend (-45°, -29°, -15°, -7°, 7°, 15°, 29°, 45°, Unresponsive, Untuned, Suppressed). Panel D: heatmap Cell Number vs Stim. Orientation, Norm. Decon. Ca²⁺. Panel E: PC1, PC2, PC3 trajectory plot (Run Change, Lick Start, Time). Panel F: spatial map, 100µm scale. Panel G: 3 Whiskers vs 1 Whisker, Z-Scored Decon. Ca²⁺ vs Stim. Orientation (Sel. = 0.88, Sel. = 0.76). Panel H: Tuned Cells and Untuned Cells scatter plots of Orientation Selectivity 1 Whisker vs 3 Whiskers (***).
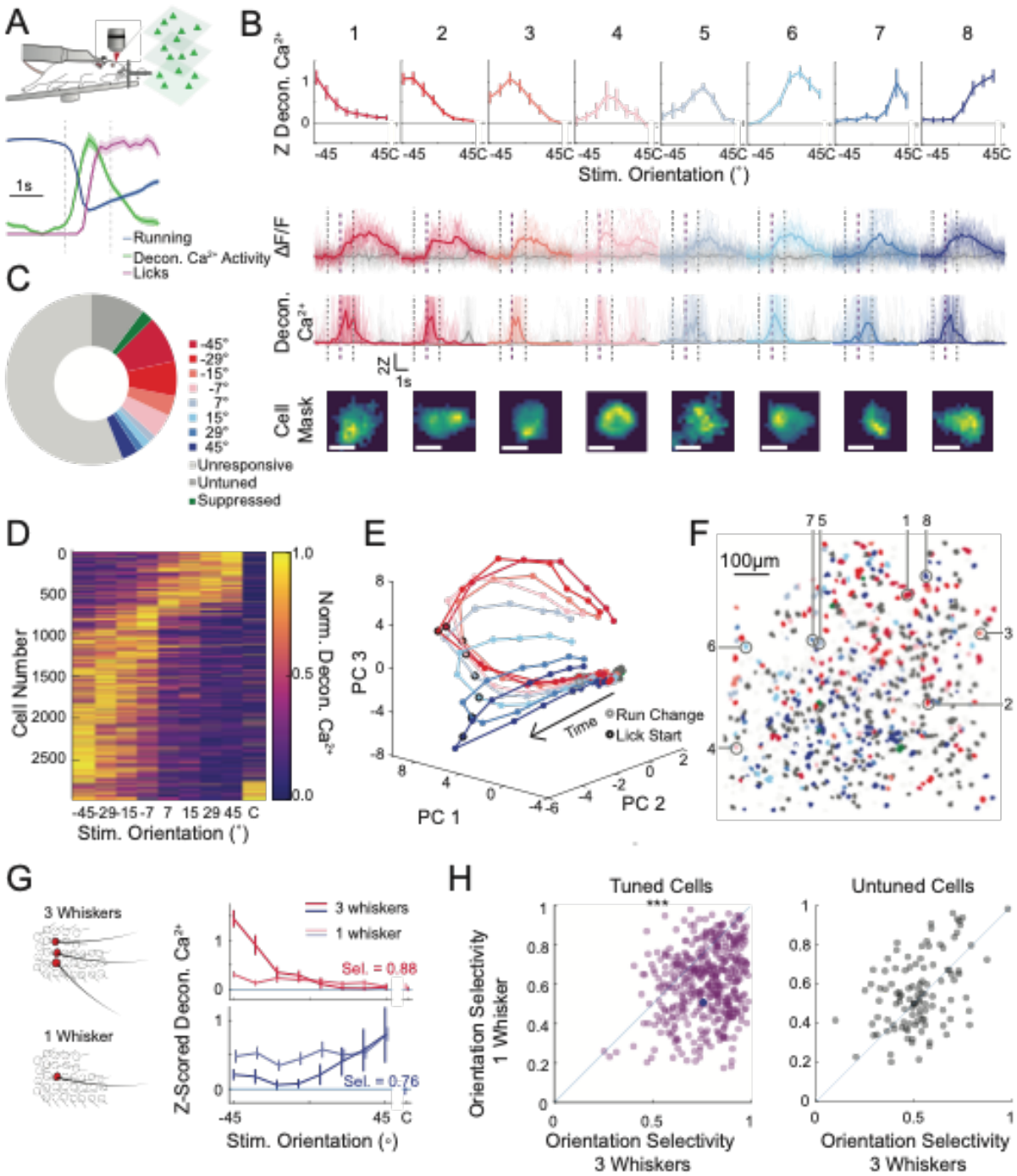
Figure 4. Somatosensory cortical neurons encode each stimulus orientation

A. Schematic of Ca^{2+} imaging experiment. Normalized mean ± SEM for run speed (blue), lick rate (magenta), and deconvolved Ca^{2+} response (all neurons, green). Standard analysis window (vertical dashed lines).

B. *Top:* Mean z-scored deconvolved Ca^{2+} responses of 8 representative neurons from the same field of view, tuned to each of the presented stimuli (color coded to preferred stimulus, mean ±95% confidence interval). *Middle:* Fluorescence response for each neuron during presentation of preferred stimulus (color) or catch trial (gray). Presented as ΔF/F (*above*) or deconvolved Ca^{2+} activity (*below*) (individual trial responses (faint lines), mean response (solid line)). *Bottom:* Weighted pixel mask from raw images. Scalebar 10μm. Standard analysis window (vertical dashed lines). Lick onset (in GO trials; vertical dashed purple line).

C. Pie chart showing the relative fractions of all imaged neurons that prefer each stimulus orientation (n=10,140 cells, 9 recordings, 4 mice).

D. Cross-validated tuning curves for all significantly tuned cells detected across all mice normalized and sorted by preferred stimulus (determined by half the data that is not shown).

E. Population activity from a representative recording reduced in dimensionality through principal component analysis (PCA). The mean trajectory through PCA space for each oriented stimulus is presented. Each dot is an imaging frame, the time of run deviation (gray circle) and lick onset (black circle) are noted.

F. Stimulus preference map of all neurons recorded in a single recording session; 3 imaging planes are superimposed. Significantly tuned cells are color coded by their preferred orientation (red to blue), untuned but touch-responsive cells (dark gray), unresponsive cells (light gray). The 8 example cells from B are identified.

G. *Left*: Schematic of the trimming experiment. *Right:* Orientation tuning curves for two representative neurons during presentation of stimuli with three intact whiskers in an arc (solid line), and a single remaining whisker (lighter dotted line). Inset: orientation selectivity (Sel.) in the three-whisker condition.

H. Scatter plot of orientation selectivity of neurons before (three whiskers) or after trimming to one whisker. Magenta (*left*), cells that were tuned in the three-whisker condition and responsive in the one whisker condition (n=446 cells, p<3e-41, signed rank test) and gray (*right*), cells that were untuned (aka touch responsive but not tuned) before trimming and responsive (with any tuning) in the one whisker condition (n=110 cells p=0.32). Cells that were unresponsive before or after trimming are not displayed (n=2 mice; 2138 cells). The b*ottom* example neuron from (I) is marked by a solid blue circle.

Also see Figure S4-9 and Movie 1.
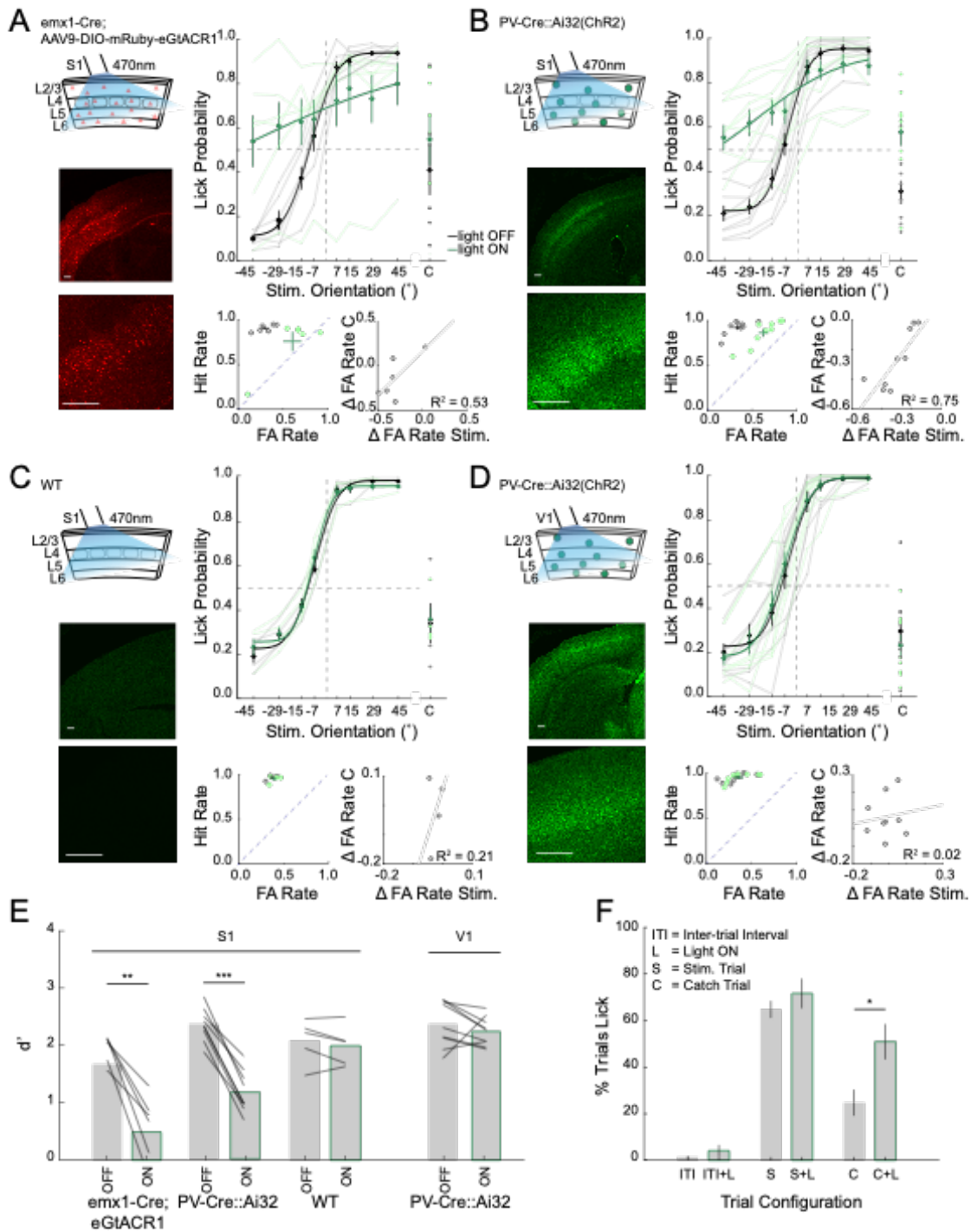
Figure 5. Acute inactivation of the barrel cortex impairs performance in the orientation discrimination task

A. *Left top*: Schematic of optogenetic suppression of S1 via emx1-Cre mice virally expressing GtACR1. *Left bottom*: Confocal image of coronal section through S1 (Scalebar 200μm). *Right top*: Task performance during light off (gray) and light on (green) trials (n=6 mice, average from individual mice (thin lines) and group mean ± SEM and fit (solid lines)). *Right bottom; left*: FA versus Hit rate for each mouse, dashed line represents unity line (light off (gray), light on (green)). *Right bottom; right*: change in FA rate (light on – light off) for stimulus (Stim.) versus catch (C) trials (fit line - linear regression).

B. As in A but for PV-Cre::Ai32(ChR2) in S1 (n=9 mice).

C. As in A, B but for wild type (WT) mice in S1 (n=4 mice).

D. As in A-C but for PV-Cre::Ai32(ChR2) mice where the optogenetic illumination was targeted to the primary visual cortex (V1, n=9 mice).

E. Average d' for each cohort (black lines: individual mice, mean ± SEM, **p<0.01, ***p<0.001, rank sum test).

Quantification of licking of PV-Cre::Ai32 mice with optogenetic silencing over S1 during the inter-trial interval (ITI), stimulus trial (S) or catch trial (C) with (L) and without light on (For S and C conditions; n=11 mice, 22 sessions, for ITI conditions 3 mice, 5 sessions, *p<0.05, rank sum test).
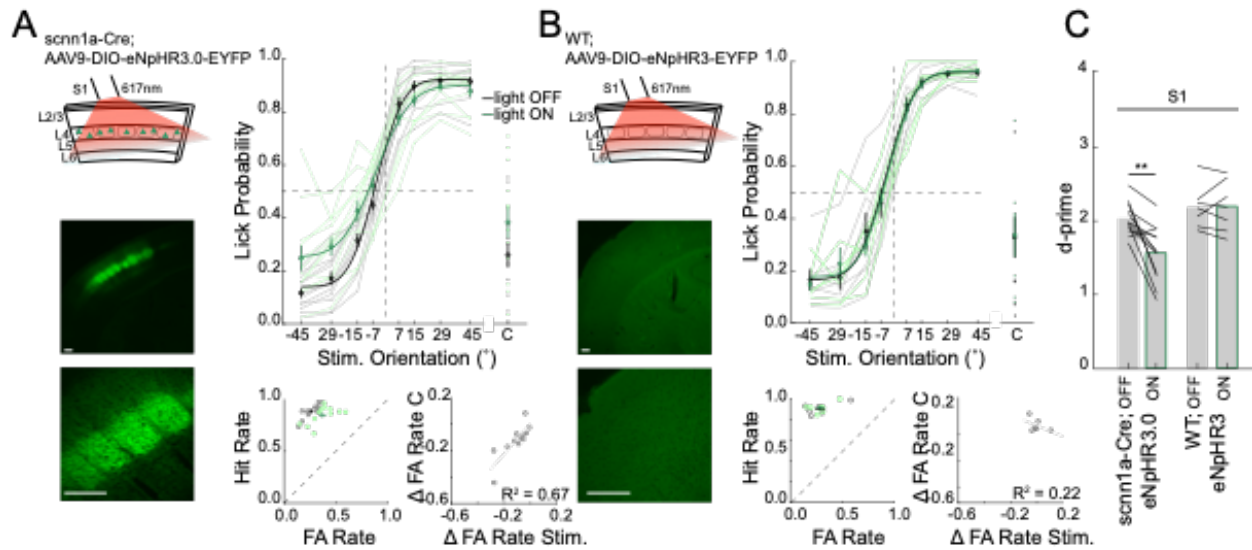
Figure 6. Selective optogenetic suppression of layer 4 excitatory neurons decrease performance in the object discrimination task

A. *Left top*: Schematic of optogenetic suppression of S1 layer 4 excitatory neurons via scnn1a-Cre mice virally expressing eNpHR3. *Left bottom*: Confocal image of coronal section through S1 (Scalebar 200µm). *Right top*: Task performance during light off (gray) and light on (green) trials (n=12 mice, average from individual mice (thin lines) and group mean ± SEM and fit (solid lines)). *Right bottom; left*: FA versus Hit rate for each mouse, dashed line represents unity line (light off (gray) light on (green)). *Right bottom; right*: change in FA rate (light on – light off) for stimulus (Stim.) versus catch (C) trials (fit line - linear regression).

B. As in A but for Cre-negative (WT) control mice virally injected with eNpHR3.0 in S1 (n=5 mice).

Average d' for light off and light on conditions (black lines; individual mice, mean ± SEM **p<0.01, rank sum test).

STAR Methods

RESOURCE AVAILABILITY

Lead contact: Further information and requests for resources should be directed to the Lead Contact, Hillel Adesnik (hadesnik@berkeley.edu).

Materials availability: All animal strains used in this study are available from Jackson Laboratories. All viral vectors are available from Addgene. All design files for custom fabricated parts are available upon request. No new strains or viral vectors were produced for this study.

Data and Code and Availability: All data and analysis software are available on request.

EXPERIMENTAL MODEL AND SUBJECT DETAILS

Animals

Mice used for experiments in this study were either wild type (WT (n=29 males); CD-1 (ICR) white strain, Charles River), PV-IRES-Cre (Jax stock# 008069) crossed with Rosa-LSL-ChR2 (n=9 males; PV-Cre::Ai32) (Jax stock# 012569), emx1-IRES-Cre (n=3 females, 3 males; JAX stock# 005628), scnn1a-tg3-Cre (n=8 females, 4 males; Jax stock# 009613), or tetO-GCaMP6s (Jax stock # 024742) crossed to Camk2a-tTA (n=4 females, 3 males; Jax stock# 003010). For Scnn1a-Cre;eNPHR3.0 (n=8 females, 4 males) and emx1-Cre;eGtACR1 (n=3 females, 4 males) there was no significant difference of the effect of light between males and females (P>0.05, t-test). Mice were housed in cohorts of five or fewer in a reverse light:dark cycle of 12:12 hours, with experiments occurring during the dark phase.

METHOD DETAILS

Headpost surgery

All experiments were performed in accordance with the guidelines and regulations of the Animal Care and Use Committee of the University of California, Berkeley.

For head fixation during behavioral and physiological experiments, a small custom

stainless-steel headplate was surgically implanted. Briefly, adult mice (P35-P50) were anesthetized with 2-3% isoflurane and mounted in a stereotaxic apparatus. Body temperature was monitored and maintained at 37°C. The scalp was removed, the fascia retracted, and the skull lightly scored with a drill bit. Vetbond was applied to the skull surface, and the headplate was fixed to the skull with dental cement (Metabond). A fine-point marker was used to note the approximate location of bregma and the left primary somatosensory barrel field (S1; 3.5mm lateral, 1.5mm posterior to bregma) and/or left primary visual cortex (V1; 2.7mm lateral, 0mm posterior to lambda), to guide the placement of optical fibers above the skull during optogenetic manipulations. Mice received buprenorphine and meloxicam for pain management and could recover for at least three days before being placed on water restriction.

Cranial window surgery

For imaging experiments, a second similar surgery was performed to implant a cranial window over S1. Briefly, mice were anesthetized as above, a 3-3.5mm region of skull located by stereotaxic coordinates (3.5mm lateral, 1.5mm posterior to bregma) was removed using a dental drill (Foredom) with a 0.24mm drill bit (George Tiemann & Co.) and/or a biopsy punch (Robbins Instruments). The window was replaced with three glass coverslips (two 3mm and one 5mm) and cemented into place with dental cement. Mice were given additional saline during surgery (0.3ml 0.9% NaCl). Mice were not water deprived at the time of surgery and were given several days to recover before water deprivation resumed. Mice received buprenorphine and meloxicam for pain management and dexamethasone to reduce brain swelling.

Viral infection

Neonatal emx1-IRES-Cre (P3-4) or scnn1a-tg3-Cre mice (P4-5) were injected intracranially with ~150-200nl of AAV9-CAG-DIO-nls-mRuby3-IRES-ST-eGtACR1 (eGtACR1) or AAV9-EF1a-DIO-eNPHR3.0-EYFP (eNPHR3.0) respectively. With respect to the lamba suture coordinates were: 1.8-2mm anterior, 2.5-3mm lateral, 0.3mm ventral. Neonates were briefly cryo-anesthetized and placed in a head mold. Viruses were acquired from or custom produced at the University of Pennsylvania Vector Core.

Water restriction

Initial animal weight was recorded for 3 days before water restriction to establish baseline weight. Mice were then placed on controlled water and received 1.0ml/day of water. On training days, mice received most water during the task. Mice were weighed after training and given additional water if their weight dropped below 80% initial weight. Food was available *ad libitum*. The weight and health (quality of the fur and nails, gait, posture) of the mice were monitored daily.

Behavioral apparatus

The behavioral apparatus was controlled in real time by an Arduino Mega 2560 or Due, which interfaced with custom written software in Java. Mouse running velocity was measured via an incremental encoder (US Digital). Mouse licking was detected with a custom 2-transistor circuit between the 0.05-inch diameter steel tube lickport and a stainless steel headpost of the mouse(Slotnick, 2009). Whisker contacts were detected using a custom designed sensor attached to a 3D printed stimulus bar emitting an infrared (IR) beam that when broken by a whisker was recorded by the IR photodiode as a voltage deflection (see below). Water was delivered by gravity through a lickport under solenoid valve control (Neptube Research Inc.). A linear bar (25 x 3 x 1mm) was coupled to a stepper motor (NEMA 8; 'stimulus motor') via a custom cylindrical arm. The stimulus motor was mounted at 90° to a larger stepper motor (NEMA 17; 'position motor'). The entire apparatus was mounted on an 8.0 x 8.0 x 0.5 inch (Thorlabs) anodized aluminum breadboard and enclosed in a light isolation box (80/20). Negative reinforcement was delivered via a single puff of compressed air, gated by a solenoid valve, to the contralateral eye from the whisker stimulus bar through a 0.05-inch-diameter steel tube positioned ~2mm from the eye. Air puff pressure was increased until it produced a blink response by the mouse. An optical fiber coupled to an LED (M470F3 or M617F2, Thorlabs) was placed on a separate manipulator above the mouse's head and attached to a driver (LEDD1B, Thorlabs). On sessions with photo-stimulation, the fiber was positioned over the approximate locations of S1 or V1, as close to the thinned skull as possible. A masking LED light to minimize behavioral detection of the optogenetic light was also used on every trial during photo-stimulation sessions. The masking light was positioned directly in front of the mouse's eyes and would turn on each trial for 1 second preceding and 1 second during the response window.

Behavioral task design

The orientation discrimination task followed the classical GO/NOGO paradigm (Figures 1 and S1). Head-fixed mice were trained to lick when they detected a GO stimulus and withhold licking when they detected a NOGO stimulus. Mice were presented with stimuli in one of eight possible orientations, defined by their angular position in the vertical plane. The eight stimulus orientations were ±45°, ±29°, ±15°, or ±7° from the dorsal-ventral axis. Except for the reversal contingency experiment (Figure S1), GO stimuli were oriented in the posterior direction and arbitrarily defined as positive orientations. NOGO stimuli were oriented in the anterior direction and defined as negative orientations. On each trial, stimulus orientations were chosen at random subject to the constraint that all eight stimulus orientations be presented once in each block of eight trials, and not in a sequence of more than three GOs or three NOGOs in a row. On a subset of trials (10%), catch trials were randomly presented whereby the stimulus stopped just anterior to the mouse and outside of the whisker field.

The sequence for each trial was as follows (Figure S1). Each trial began with the stimulus in the home position for a 3-5 second waiting period. During this period, the stimulus motor rotated the stimulus bar to one of the possible pseudo-randomly selected orientations. After the waiting

period, mice initiated the start of each trial by exceeding a ~50cm running requirement. This triggered the positioning motor to move the stimulus to the target position, within reach of the whiskers, except for catch trials whereby it was held just outside of the whisker field. The trajectory of the stimulus was aligned in roughly the same horizontal plane as the C row whiskers of the mouse's right whisker field, and centered around whisker C2. The distance between the stimulus and the whisker pad was 10.5 ± 0.3mm from follicle pad, n=10. For jitter experiments, the stimulus bar was attached to a linear stage and moved in laterally from the mouse whisker pad. The stimulus bar was jittered $20.6 \pm 1.2°$ for first contact and $39.1 \pm 0.9°$ at its final resting position relative to the mouse's whisker pad. Because the target position was in the approximate midpoint of the whisker field, mice typically made their first whisker contact with the stimulus before it reached the target position (Figure 1C,D, S2). Once stationary in the target position, mice were trained to either lick or withhold licking during a 1 second response window. The reinforcement schedule was as follows (Figure S1): correctly licking for a GO orientation (Hit) was rewarded with a drop of water (~5μl) 0.5 seconds after the response window ended. Incorrectly licking for a NOGO orientation during the response window (false alarm; FA) immediately triggered an air puff and a 5-second time-out period was added to the waiting period at the end of the trial. Correctly withholding licking to NOGO orientation (correct rejection; CR) were not rewarded and incorrectly not licking for GO responses (Miss) was not punished. All licks were recorded but licks outside of the response window had no consequences. At the end of the response window, the positioning motor moved the stimulus in reverse out of the whisker field and back to the home position. The exact location of the home position randomly jittered each trial by ±2cm radially so that the mouse could not predict catch trials based on the time in which the motor was moving. Once in the home position a random time-out period was given if the last trial was a false alarm.

Behavioral training

Training began after headplate application, recovery (~3days), and 5-10 days of water restriction. We did not find it necessary to handle the mice extensively before training or anesthetize them before head-fixation. Prior to training with the behavioral apparatus, mice were habituated to head-fixation on a free-spinning circular treadmill (diameter, 6 inches) for 4 daily sessions lasting ~60 minutes each (these run training days were not included when calculating number of sessions mice took to reach criterion (Figure 1I)). The training schedule was as follows (Figure S1): in the first stage of behavioral training ('1Ori $_{auto}$'), mice were classically conditioned to lick in response to the stimulus. The stimulus was only presented in the most extreme GO +45° orientation (or -45° on the subset of experiments conducted with the reverse GO/NOGO contingency). On each trial, stimulus presentation was paired with a drop of water delivered 0.5 seconds into the response window. Once mice were reliably licking before the water was delivered (i.e. showing anticipatory licking on >70% of the trials), they were moved onto the operant conditioning phase of training.

In the second stage of training ('1Ori'), mice were operantly conditioned to lick in response to the stimulus bar and withhold licking during the no stimulus, catch trials (10% of trials). The stimulus bar was only presented in the GO +45° (or -45° for reverse contingency experiments) orientation. A water reward was delivered only if mice licked during the response window to the GO stimulus. Once mice reliably licked upon detection of the stimulus and withheld licking to catch (>70% correct), they moved onto the simplest stage of the discrimination task ('2Ori'). For both '1Ori $_{auto}$' and '1Ori' training mice could be moved onto the next stage of training within a training session if they performed above 70% correct for >100 trials to not over train the mice on this preparatory detection task.

During '2Ori' discrimination training, mice were conditioned to lick only for GO trials (+45° or -45° for reverse contingency experiments) and withhold licking to NOGO (-45° or +45° for reverse contingency experiments) stimuli. GO and NOGO trials were randomly interleaved and catch trials were still presented on 10% of trials. A water reward was delivered on GO trials only if mice licked during the response window. In contrast, an air puff and time-out period were delivered if mice licked to the NOGO stimulus. When mice performed >70% for two consecutive days they were advanced to the final stage of the discrimination task ('8Ori'). During '8Ori', 4 GO and 4 NOGO stimuli were randomly presented to the mouse: ±45°, ±29°, ±15° and ±7°, and catch. Mice had to achieve >1.5 d' (performance criterion) during '8Ori' training to be used in subsequent experiments.

Mice were trained 5-7 days per week. All mice had a full pad of whiskers during training and for experiments unless otherwise stated. All sessions on '2Ori' and '8Ori' were preceded with ~10-20 trials on '1Ori$_{auto}$' to ensure the lickport was positioned correctly and to prime mice for training.

Whisker tracking

A high-speed camera (Basler acA2000-340km) was placed below the running wheel; whiskers were imaged from below using a telecentric lens (Edmund Optics NT58-257) and a mirror oriented at approximately 45°. Some mice and experimental setups required slight adjustments to the mirror orientation to properly view the whiskers and object interaction. Whiskers were backlit from above using high-powered diffused infrared LEDs (CMVision-IR200). High-speed videos were acquired with a frame grabber (Silicon Software) at 500 frames per second with a 100µs exposure and were synchronized with behavioral data via external triggers. Whisker tracking was performed offline using Whisk (Janelia Research Campus, Howard Hughes Medical Institute), which returned whisker angles and positions for every frame. The whisker angle is in reference to the longitudinal axis of the mouse where 0° is fully retracted pointed towards the rear of the mouse, 90° is orthogonal to this axis, and 180° is fully protracted pointing directly forward. Typical whisker angles range from 70° at rest and 160° during a typical full protraction. Tracking data was further processed and analyzed using custom MATLAB scripts

written to extract set point and amplitude. Briefly, set point was calculated as the average of the upper and lower peak envelope of the orientation signal and amplitude was the difference between the upper and lower peak envelope. To define the sample analysis window for all except the Calcium imaging experiments (see later), we estimated first contact time as the period following a 2 standard deviation change in average baseline run velocity or set point (whichever occurred first) and estimated the end of the sample window as the start of average licking response (30% rise in lick rate from baseline). We then broke the trial into five 200ms analysis windows; baseline (#1: 500ms before first contact (#2)), the start (#2; corresponding to the estimated time of first contact), middle (#3; midpoint between first contact (#1) and first lick (#4)), end (#4; corresponding to the estimated time of first lick for expert mice, or the deviation in running velocity back to baseline for naive mice) and response time (#5; 500ms after first lick (#4)).

For jitter experiments, a subset of high-speed whisker tracking videos were manually annotated to identify which whiskers (front (arcs 4-6), middle (arcs 2-3) or back (arcs 1&G)) primarily contacted the stimulus bar. Each visually identified contact before the stimulus bar stopped moving into position (to estimate the 'decision period') was annotated. Only contacts where the mouse was actively whisking at the bar were included. Whiskers passively contacting the bar or being bent as the bar moved into position were not included in analysis. The most frequent (mode) whiskers making contact with the bar was calculated for each trial.

Whisk contact annotation validation

For manual whisker contact validation, two experimenters blind to experimental conditions annotated the same 10% of the data; if the interrater reliability (IRR) was less than 90%, experimenters discussed annotation approach and criteria. A new test data set was then selected, and the procedure repeated until >90% IRR was achieved. The remaining data was then annotated by either one or both experimenters.

Whisker contact detector

Whisker contacts were quantified in a subset of sessions using a custom designed sensor. The sensor was attached to a 3D printed stimulus bar emitting an infrared (IR) beam that when broken by a whisker or multiple whiskers was recorded by the IR photodiode as a voltage deflection (Figure S2). The raw voltage signal from the photodiode was baseline subtracted and smoothed. A contact was detected when a whisker or multiple whiskers occluded the sensor causing a voltage change in the photodiode that exceeded a given threshold. A threshold was calculated for each session as 3 standard deviations from the mean of the baseline period (-1 to -0.6 seconds before response period). Each contact in theory would generate two threshold crossings (one during protraction when the whisker or whiskers contact the stimulus bar and a second during retraction when the whisker or whiskers retract away from the stimulus bar),

therefore putative contacts were calculated as the mid-point between sequential threshold crossings. For multi whisker data, whiskers frequently moved in synch and therefore would generate just one contact for multiple whiskers, therefore we used multi whisker data to describe multi whisker contacts, or 'whisks', as opposed to individual whisker contacts. To this end, threshold crossings spaced less than 20ms apart were averaged together to generate a single contact. Trials that started below threshold or crossed threshold but did not return to baseline (largely caused by whiskers maintaining contact with the stimulus bar rather than actively pulsing at the bar) were excluded.

We validated the accuracy of the contact detector via two methods: piezo validation and high-speed video validation. For piezo validation, a single mouse whisker was plucked and tethered via glue onto a computer controlled piezo bender (Noliac Systems, NDR6110-100). Whisker deflections were controlled by custom written scripts in MATLAB that varied the frequency of deflections, and the whisker was positioned at different horizontal locations along the stimulus shaft to vary the distance of whisker deflection from the IR beam. The detected contacts were compared to the piezo output pulses. A true hit occurred when there was a contact detected within ±5ms from a piezo pulse. We found the detector was 100% accurate in detecting contacts for all the frequencies and positions tested. A second validation was conducted with an awake mouse performing the orientation discrimination task with two whiskers while simultaneously imaging the whiskers using high-speed video. *Post hoc* two human observers manually annotated a subset of trials and marked each frame whereby they observed a whisker or multiple whiskers contacting the stimulus bar. A threshold crossing within ±20ms of an annotated whisker contact was identified as a Hit. No threshold crossings within ±20ms of an annotated whisker contact was a Miss, while more than 1 threshold crossing within ±20ms of an annotated whiskers contact was identified as a False Alarm. Agreement between human observers was 98.3%. Hit rate comparing video annotations and contacts was 96%. We further annotated first contacts, defined by the first contact observed of a whisker or whiskers with the stimulus bar, and compared this with contacts identified with the sensor. The hit rate for first contacts was lower at 77%. We believe this higher error rate might arise from the difficulty in manually identifying first whisker contacts due to the reduced visibility as the stimulus bar moves into the whisker field, and the smaller degree of whisker bending we regularly see for first whisker contact. Therefore, we believe the higher error rate largely reflected observer error rather than error of the contact detector, and this was reflected in the larger rate of disagreement between human observers (80%).

Whisker trimming

A subset of mice had their whiskers ipsilateral to the stimulus either abruptly trimmed from full pad to no whiskers, or progressively trimmed from a full pad to four adjacent whiskers either in the same row (C1-C4) or arc (B2-D2), then to two adjacent whiskers either in the same row (C1-C2) or arc (B2-C2), then to one whisker (C2), and finally no whiskers. Once mice reached '8Ori'

criterion, mice were tested for two sessions prior to trimming to determine baseline performance. After each subsequent trimming procedure, mice were tested with the resulting configuration of whiskers over two sessions. For the progressive trimming group, mice were randomly assigned to the row or arc whisker conditions. When trimming from a full pad to four whiskers, mice were briefly anesthetized with 2-3% isoflurane after the second full pad session to eliminate any lingering impact of being under isoflurane. All other trimmings were done while mice were head-fixed and running on a treadmill.

Calcium imaging

Calcium imaging experiments were performed in mice expressing GCaMP6s in excitatory neurons via tetO-GCaMP6s x Camk2a-tTA or intracranial injection of AAV9 syn-GCaMP6s (titer 8e11 vg/mL) (Figures 4 and S4-9). After reaching training proficiency, mice were implanted with a cranial window on the side contralateral to stimulus presentation and following recovery they were returned to training for several days before being moved to an identical behavioral training apparatus connected to a two-photon microscope (Sutter MOM, Sutter inc.). Mice were given an additional 1-3 training days on the microscope rig to acclimate to the new environment. As two-photon microscopes provide many additional distractors to trained mice (e.g., temperature, sounds, environment) we reduced our d' criterion for inclusion to 1.0 (60% of recordings passed this threshold). Imaging fields of view were identified by manually deflecting whiskers and navigating towards areas with substantial, broad GCaMP fluorescence. Subsequent recording days were placed such that the same cells would not be recorded in separate days. All recordings were performed in L2/3 imaging three 800 x 800 µm planes, spaced 30-50µm apart, at 5.2-6.2Hz with ~100mW 920nm laser light (Coherent Chameleon) using a resonant galvo system. Images were acquired using ScanImage (Vidrio Inc.) with custom behavioral control software. Tiff files were motion corrected, cell masks were determined, and source fluorescence and OASIS(Friedrich et al., 2017) deconvolved signal data was extracted using Suite2p(Pachitariu et al., 2016). To confirm our imaging system has sufficient resolution to independently distinguish tuned neighbors, we measured the optical point spread function (PSF) of our imaging system and determined it to have a radial resolution of 0.49µm and axial resolution of 3.4 µm (Figure S4I) which is smaller than our pixel sampling, demonstrating that the optical resolution of our microscope is not a limiting factor, and supporting the notion that fluorescence from one cell is unlikely to contaminate any but the closest pixels due to the two photon excitation system itself. To quantify any cross-contamination between cells, we plotted the spatial distribution (i.e., distance to nearest neighbor) between tuned cells (Figure S4J; top) and all other cells (Figure S4J; bottom). We find that no cell pairs are closer than the optical performance of our microscope. Furthermore, we looked to see how many cells are unexpectedly close to each other, i.e., occurring closer together than a typical cell's width. We found that less than 0.25% of tuned pairs and 0.5% of any pairs of cells are closer together than the average width of a cell (determined to be 7µm radius in our data). This analysis implies that the vast

majority of our cells should have little contamination from signals coming from the cell bodies of other cells.

As GCaMP6s has slow kinetics relative to the underlying changes in spike rate(T. W. Chen et al., 2013), we focused our analysis on a period after the animal's whiskers had made contact with the object but before the animal had made a behavioral response. For each recording, we identified the imaging frame in which the animal began slowing down, which was highly correlated with the first whisker touches (see Figure S2, S3). This frame, until the end of the 'response window' (i.e., when the stimulus leaves the whisker field), is called the standard window and was used for subsequent analysis (Figure S4).

We analyzed calcium responses both with ΔF/F and OASIS deconvolved Ca^{2+} activity; both methods gave qualitatively similar results (see Figure S4) and relied on Suite2p for data extraction and calculation. For all methods, a weighted pixel mask for each cell was created based on the correlation of nearby pixels over time. Pixel masks were manually categorized as 'cells' or 'not cells' and only 'cells' were included for analysis. For ΔF/F calculation, each cell's detected fluorescence was first neuropil subtracted. The average fluorescence of an anulus (not containing another cell) of up to 350 pixels was considered neuropil. A neuropil coefficient (c) was calculated for each cell as described in(Pachitariu et al., 2016) and the final fluorescence was calculated as

$$F = F_{cell} - c * F_{neuropil}$$

F_0, the 'baseline' fluorescence, was calculated with a moving average of the 10th percentile of a 1000 frame window (approx. 3 minute); this moving average corrected for very slow drift in imaging conditions. ΔF/F is

$$(F - F_0)/F_0$$

Finally, as the absolute value of ΔF/F spans a wide range (likely due to differences in F_0), for display purposes each cell's activity was scaled via z-scoring across the time series and pre-stimulus activity was subtracted. Each cell was processed independent of all other cells; thus, this operation could not affect calculated tuning preference or statistical significance. To demonstrate how this source extraction code operates on imaging data, we take two contrasting FOVs from the same recording as examples: one FOV where we have high signal from one cell adjacent to a few lower signal cells (Figure S4C-E), and a second where we have low mean signal from many cells within close proximity of one another (Figure S4F-H). In both cases we see that the ROI masks are not contaminated by neighboring cells and allow the extraction of clear, isolated responses from each of the cells. Deconvolved calcium activity was calculated using the OASIS algorithm(Friedrich et al., 2017), implemented in Suite2p(Pachitariu et al., 2016). This estimated the time and number of spikes that led to the observed calcium fluorescence. As with ΔF/F the absolute magnitude of estimated spikes varied widely, as such each cell's response was z-scored

across time and baseline subtracted. Analysis was based on the mean Z-scored deconvolved calcium activity from the standard window unless otherwise noted.

A trial was excluded if its run speed before stimulus presentation deviated more than 2 S.D. from its mean run speed. Tuned cells were defined as cells whose evoked responses to each oriented stimulus passed an ANOVA p<0.01, and these cells were further divided by their peak response. If a cell responded more on the catch trials than to any stimulus it was categorized as a suppressed cell. Touch cells were defined as cells that were not tuned but passed an ANOVA p<0.01 to all orientations and the catch trial. In all Calcium Imaging based figures error bars denoted a 95% confidence interval. Cross-validated tuning curves were calculated from the mean deconvolved activity (unless otherwise noted) and scaled from 0 to 1. Alternating trials from each cell were assigned to a sort group or a display group and tuning curves were calculated from each group. The order of the cells was set by the tuning preference from the sort group while the tuning curve from the display group was presented. Cells were excluded from this plot if the correlation between their sort group tuning and display group tuning was < 0.5 (of the main data set 2960/3416 87% tuned cells pass this threshold). Principal component analysis (PCA) was performed on the full unrolled deconvolved calcium activity traces of every cell per experiment and subsequent responses were averaged by stimulus condition. Maps of tuning preference were presented as the projection of all three imaging planes with the outline of each detected source color coded by preferred tuning or touch responsive category. Orientation selectivity was calculated as the Euclidean Norm of the mean response to each oriented stimulus. As it is difficult to be certain what 0 activity looked like in calcium data, this response vector (v) was normalized from minimum to maximum activity. A selectivity of 1 would denote a response to only one orientation, whereas a selectivity of 0 would denote the same response to all stimuli.

$$\text{Selectivity} = 1 - \frac{\left|\sqrt{\sum v^2} - 1\right|}{\sqrt{N} - 1}$$

ROC analysis was performed as previously described (Stüttgen and Schwarz, 2008). Briefly: single trial calcium responses were separated into two groups, A and B. Thresholds spanning the entire range of values in either group were tested, and the rates at which either group was above a given threshold were plotted against each other. The area under this curve (AUC) represented the discriminability. In this analysis it was irrelevant if A was larger than B or vice versa as we reported the absolute discriminability or |AUC-0.5|. Here 0 represented identical distributions whereas the maximal value 0.5 indicated that A and B were non overlapping distributions. As this metric can be biased by low trial counts, if A or B had fewer than 10 observations then that score was excluded. The shuffle control in this section was created by randomly sampling A and B groups from all observed trials. To be even more conservative, the number of samples in A and B were matched to the fewest samples in any of the comparisons for that cell.

In trimming experiments, intrinsic imaging was first performed to identify which whisker was optimally located in the cranial window for imaging. Whiskers were then trimmed to a column of three whiskers and the experiment began as described above, including manually deflecting the remaining whiskers to find areas with large GCaMP responses. Roughly half-way through a typical recording session, the whiskers above and below the principle imaged whisker were trimmed to create the single whisker recording set. As mice were unable to perform the task with a single whisker, recordings were included only if the animal had a performance accuracy d' of 1.0 or higher on the three-whisker condition, but all trials (success and failures) were included in analyses.

Intrinsic imaging

Intrinsic optical imaging was performed through the cranial window to confirm that either the C1 and/or the C2 barrel was located within the window to guide trimming for calcium imaging experiments. Prior to intrinsic optical imaging, anesthesia was induced as described above and mice were administered 0.01mg/kg Xylazine. Anesthesia was maintained with 1% isoflurane during imaging. Images were acquired at 60Hz with a 12-bit 1M60 camera (DALSA DS-21-01M60) and microscope fitted with two 52mm camera lenses (Nikon 52) using custom-written MATLAB software. The brain was illuminated with red (630nm) LEDs. The C2 and/or C1 whisker was threaded through a wire loop connected to a Noliac piezo bender (Noliac Systems, NDR6110-100) and deflected at 20Hz for 4 seconds for 15 trials with a 6 second inter-trial interval. Mice were given 24 hours to recover.

Optogenetic stimulation *in vivo*

For optogenetic experiments light was delivered via a 400μm diameter optical fiber resting on the thinned skull over S1 or V1. Either a 470nm LED (M470F3, Thorlabs) at 8-12mW (for eGtACR1 expressing or PV-Cre::Ai32 mice) or 617nm LED (M617F2, Thorlabs) at 15-18 mW (for eNpHR3.0 expressing mice) was used. Light intensity was controlled by analog outputs to the LED driver (LEDD1B, Thorlabs) and calibrated with a photodiode and power meter (PM160T, Thorlabs). For behavioral experiments, a square light pulse was applied for 2 second intervals. To ensure photoinhibition before the first whisker contact and throughout the response window, optogenetic stimulation started 1 second prior to the stimulus reaching the target position and was sustained until the end of the response window. Optogenetic stimulation trials were randomly chosen on 33% of all trials. A masking light (blue for eGtACR1 and PV-Cre::Ai32 experiments, red for eNpHR3.0 experiments) was used to control for LED stimulation on all trials and an eye patch was positioned over the right eye of the mouse to prevent any visual cue which may have been gained through the masking light.

Histology and image acquisition

Transgenic and virally injected mice were anesthetized with 5% isoflurane and ketamine and perfused transcardially with 4% paraformaldehyde (PFA). Their brains were removed, stored overnight in 4% PFA at 4°C, and then cryoprotected for at least 24 hours in 30% sucrose buffer solution at 4°C. A sliding microtome (American Optical Company) was used to take 40μm coronal sections of S1 and/or V1. Sections were mounted on glass microscope slides using Vectashield mounting medium with DAPI to non-selectively stain cells and protect tissue from photobleaching. Sections were imaged using a confocal microscope with both a 4X and 20X air objective.

Behavioral data analysis

$$\text{Percent correct} = 100 * \left(\frac{Hit}{Hit+Miss} + \frac{CR}{CR+FA} \right)/2$$

was used during training to advance mice through each stage of training. Discriminability index (d') was used to more precisely evaluate the ability of the mice to discriminate between GO and NOGO stimulus orientations. In calculating d', Hit Rate and false alarm Rate,

$$\text{Hit Rate} = \frac{Hit}{Hit + Miss}$$

$$\text{FA Rate} = \frac{FA}{FA + CR}$$

are considered. More precisely, d' is a measure of the difference between the z-transforms of Hit rate and FA Rate:

$$d' = z(Hit\ Rate) - z(FA\ Rate)$$

The effective limit of d' is 6.93, typical values are around 2.0, and we selected 1.5 as our performance criterion for reliable discrimination. Chance levels of discriminability corresponded to d'=0. We reported overall d' values for a complete session as well as d' for pairs of GO/NOGO stimuli whose orientations were equal and opposite. For the analysis of lick probability, we quantified the proportion of trials for each stimuli where mice made a GO response. The psychometric curve of lick probability was fit with a Wichmann and Hill psychometric fit.

If a mouse failed to make GO responses for 32 consecutive trials, we assumed the mouse was sated and excluded these trials and any subsequent trials from our analysis, except during the trimming experiments. If a mouse did not reach 240 trials within a session, data from that entire session was excluded. All times reported during a trial were measured from the onset of the response window (0 seconds).

QUANTIFICATION AND STATISTICAL ANALYSIS

All statistical analyses were performed using MATLAB. The analyses performed were ANOVAs, with multiple comparisons and Wilcoxon rank sum. Unless otherwise noted, all tests were two-tailed and all plots with error bars were reported as mean ± SEM. Sample size was not predetermined using power analysis.

Movie 1. Somatosensory neurons respond to oriented stimulus, Related to Figure 4

Motion corrected and trial averaged pixel-wise $\Delta F/F$ evoked by oriented stimulus across all three planes from a single recording. Depth below the dura for each imaging plane is listed above each panel. Magenta square indicates the time that the stimulus is present, with the corresponding stimulus orientation listed above. Imaged at 6Hz, playback speed is 2x real time.

References

Ahissar, E., Assa, E., 2016. Perception as a closed-loop convergence process. Elife.

Ahissar, E., Knutsen, P.M., 2008. Object localization with whiskers. Biol. Cybern.

Andermann, M.L., Moore, C.I., 2006. A somatotopic map of vibrissa motion direction within a barrel column. Nat. Neurosci. 9, 543–551.

Anjum, F., Turni, H., Mulder, P.G.H., van der Burg, J., Brecht, M., 2006. Tactile guidance of prey capture in Etruscan shrews. Proc. Natl. Acad. Sci. 103, 16544–16549.

Arabzadeh, E., Petersen, R.S., Diamond, M.E., 2003. Encoding of whisker vibration by rat barrel cortex neurons: Implications for texture discrimination. J. Neurosci. 23, 9146–9154.

Brecht, M., Preilowski, B., Merzenich, M.M., 1997. Functional architecture of the mystacial vibrissae. Behav. Brain Res.

Brecht, M., Roth, A., Sakmann, B., 2003. Dynamic receptive fields of reconstructed pyramidal cells in layers 3 and 2 of rat somatosensory barrel cortex. J. Physiol. 553, 243–265.

Brumberg, J.C., Pinto, D.J., Simons, D.J., 1996. Spatial gradients and inhibitory summation in the rat whisker barrel system. J. Neurophysiol. 76, 130–140.

Bruno, R.M., Khatri, V., Land, P.W., Simons, D.J., 2003. Thalamocortical Angular Tuning Domains within Individual Barrels of Rat Somatosensory Cortex. J. Neurosci. 23, 9565–9574.

Chen, J.L., Carta, S., Soldado-Magraner, J., Schneider, B.L., Helmchen, F., 2013. Behaviour-dependent recruitment of long-range projection neurons in somatosensory cortex. Nature 499, 336–340.

Chen, T.W., Wardill, T.J., Sun, Y., Pulver, S.R., Renninger, S.L., Baohan, A., Schreiter, E.R., Kerr, R.A., Orger, M.B., Jayaraman, V., Looger, L.L., Svoboda, K., Kim, D.S., 2013. Ultrasensitive fluorescent proteins for imaging neuronal activity. Nature.

Curtis, J.C., Kleinfeld, D., 2009. Phase-to-rate transformations encode touch in cortical neurons of a scanning sensorimotor system. Nat. Neurosci. 12, 492–501.

Diamond, M.E., Von Heimendahl, M., Knutsen, P.M., Kleinfeld, D., Ahissar, E., 2008. "Where" and "what" in the whisker sensorimotor system. Nat. Rev. Neurosci. 9, 601–612.

DiCarlo, J.J., Johnson, K.O., 2000. Spatial and Temporal Structure of Receptive Fields in

Primate Somatosensory Area 3b: Effects of Stimulus Scanning Direction and Orientation. J. Neurosci. 20, 495–510.

Drew, P.J., Feldman, D.E., 2007. Representation of moving wavefronts of whisker deflection in rat somatosensory cortex. J. Neurophysiol. 98, 1566–1580.

Friedrich, J., Zhou, P., Paninski, L., 2017. Fast online deconvolution of calcium imaging data. PLoS Comput. Biol.

Gibson, J.J., 1962. Observations on active touch. Psychol. Rev. 69, 477–491.

Govorunova, E.G., Sineshchekov, O.A., Janz, R., Liu, X., Spudich, J.L., 2015. Natural light-gated anion channels: A family of microbial rhodopsins for advanced optogenetics. Science (80-.).

Hires, S.A., Pammer, L., Svoboda, K., Golomb, D., 2013. Tapered whiskers are required for active tactile sensation. Elife.

Hong, Y.K., Lacefield, C.O., Rodgers, C.C., Bruno, R.M., 2018. Sensation, movement and learning in the absence of barrel cortex. Nature 561, 542–546.

Hsiao, S., 2008. Central mechanisms of tactile shape perception. Curr. Opin. Neurobiol. 18, 418–424.

Hsiao, S.S., Lane, J., Fitzgerald, P., 2002. Representation of orientation in the somatosensory system. Behav. Brain Res. 135, 93–103.

Hutson, K.A., Masterton, R.B., 1986. The Sensory Contribution Cortical Barrel. October 56.

Isett, B.R., Feasel, S.H., Lane, M.A., Feldman, D.E., 2018. Slip-Based Coding of Local Shape and Texture in Mouse S1. Neuron 97, 418-433.e5.

Jacob, V., Le Cam, J., Ego-Stengel, V., Shulz, D.E., 2008. Emergent Properties of Tactile Scenes Selectively Activate Barrel Cortex Neurons. Neuron 60, 1112–1125.

Jadhav, S.P., Wolfe, J., Feldman, D.E., 2009. Sparse temporal coding of elementary tactile features during active whisker sensation. Nat. Neurosci.

Jones, L.M., Lee, S.H., Trageser, J.C., Simons, D.J., Keller, A., 2004. Precise temporal responses in whisker trigeminal neurons. J. Neurophysiol. 92, 665–668.

Kathleen Kelly, M., Carvell, G.E., Kodger, J.M., Simons, D.J., 1999. Sensory loss by selected whisker removal produces immediate disinhibition in the somatosensory cortex of behaving rats. J. Neurosci. 19, 9117–9125.

Kim, J., Erskine, A., Cheung, J.A., Hires, S.A., 2020. Behavioral and Neural Bases of Tactile Shape Discrimination Learning in Head-Fixed Mice. Neuron.

Kleinfeld, D., Delaney, K.R., 1996. Distributed representation of vibrissa movement in the upper layers of somatosensory cortex revealed with voltage-sensitive dyes. J. Comp. Neurol.

Kleinfeld, D., Deschênes, M., 2011. Neuronal basis for object location in the vibrissa scanning sensorimotor system. Neuron.

Knutsen, P.M., Ahissar, E., 2009. Orthogonal coding of object location. Trends Neurosci.

Knutsen, P.M., Biess, A., Ahissar, E., 2008. Vibrissal Kinematics in 3D: Tight Coupling of Azimuth, Elevation, and Torsion across Different Whisking Modes. Neuron.

Knutsen, P.M., Pietr, M., Ahissar, E., 2006. Haptic object localization in the vibrissal system: Behavior and performance. J. Neurosci.

Krupa, D.J., Wiest, M.C., Shuler, M.G., Laubach, M., Nicolelis, M.A.L., 2004. Layer-specific somatosensory cortical activation during active tactile discrimination. Science (80-.). 304, 1989–1992.

Kwon, S.E., Tsytsarev, V., Erzurumlu, R.S., O'Connor, D.H., 2018. Organization of orientation-specific whisker deflection responses in layer 2/3 of mouse somatosensory cortex. Neuroscience 368, 46–56.

Lavzin, M., Rapoport, S., Polsky, A., Garion, L., Schiller, J., 2012. Nonlinear dendritic processing determines angular tuning of barrel cortex neurons in vivo. Nature 490, 397–401.

Lederman, S.J., Klatzky, R.L., 1987. Lederman&Klatzky1987 Handmovements.pdf. Cogn. Psychol. 19, 342–368.

Leiser, S.C., Moxon, K.A., 2007. Responses of Trigeminal Ganglion Neurons during Natural Whisking Behaviors in the Awake Rat. Neuron 53, 117–133.

Mardinly, A.R., Oldenburg, I.A., Pégard, N.C., Sridharan, S., Lyall, E.H., Chesnov, K., Brohawn, S.G., Waller, L., Adesnik, H., 2018. Precise multimodal optical control of neural ensemble activity. Nat. Neurosci. 21, 881–893.

Minnery, B.S., Simons, D.J., 2003. Response properties of whisker-associated trigeminothalamic neurons in rat nucleus principalis. J. Neurophysiol. 89, 40–56.

O'Connor, D.H., Peron, S.P., Huber, D., Svoboda, K., 2010. Neural activity in barrel cortex underlying vibrissa-based object localization in mice. Neuron 67, 1048–1061.

Otchy, T.M., Wolff, S.B.E., Rhee, J.Y., Pehlevan, C., Kawai, R., Kempf, A., Gobes, S.M.H., Ölveczky, B.P., 2015. Acute off-target effects of neural circuit manipulations. Nature 528, 358–363.

Pachitariu, M., Stringer, C., Schröder, S., Dipoppa, M., Rossi, L.F., Carandini, M., Harris, K.D., 2016. Suite2p: beyond 10,000 neurons with standard two-photon microscopy. bioRxiv.

Perrett, D.I., Rolls, E.T., Caan, W., 1982. Visual neurones responsive to faces in the monkey temporal cortex. Exp. Brain Res.

Petersen, C.C.H., 2019. Sensorimotor processing in the rodent barrel cortex. Nat. Rev. Neurosci.

Pluta, S., Naka, A., Veit, J., Telian, G., Yao, L., Hakim, R., Taylor, D., Adesnik, H., 2015. A direct translaminar inhibitory circuit tunes cortical output. Nat. Neurosci. 18, 1631–1640.

Pluta, S.R., Lyall, E.H., Telian, G.I., Ryapolova-Webb, E., Adesnik, H., 2017. Surround Integration Organizes a Spatial Map during Active Sensation. Neuron 94, 1220-1233.e5.

Polley, D.B., Rickert, J.L., Frostig, R.D., 2005. Whisker-based discrimination of object orientation determined with a rapid training paradigm. Neurobiol. Learn. Mem. 83, 134–142.

Ramirez, A., Pnevmatikakis, E.A., Merel, J., Paninski, L., Miller, K.D., Bruno, R.M., 2014. Spatiotemporal receptive fields of barrel cortex revealed by reverse correlation of synaptic input. Nat. Neurosci.

Sachidhanandam, S., Sreenivasan, V., Kyriakatos, A., Kremer, Y., Petersen, C.C.H., 2013. Membrane potential correlates of sensory perception in mouse barrel cortex. Nat. Neurosci.

Saig, A., Gordon, G., Assa, E., Arieli, A., Ahissar, E., 2012. Motor-sensory confluence in tactile perception. J. Neurosci.

Simons, D.J., 1985. Temporal and spatial integration in the rat SI vibrissa cortex. J. Neurophysiol. 54, 615–635.

Simons, D.J., Carvell, G.E., 1989. Thalamocortical response transformation in the rat vibrissa/barrel system. J. Neurophysiol.

Slotnick, B., 2009. A SIMPLE 2-TRANSISTOR TOUCH OR LICK DETECTOR CIRCUIT. J. Exp. Anal. Behav.

Sofroniew, N.J., Vlasov, Y.A., Hires, S.A., Freeman, J., Svoboda, K., 2015. Neural coding in barrel cortex during whisker-guided locomotion. Elife 4, 1–19.

Stüttgen, M.C., Schwarz, C., 2008. Psychophysical and neurometric detection performance under

stimulus uncertainty. Nat. Neurosci.

Timofeeva, E., Lavallée, P., Arsenault, D., Deschênes, M., 2004. Synthesis of multiwhisker-receptive fields in subcortical stations of the vibrissa system. J. Neurophysiol. 91, 1510–1515.

Vilarchao, M.E., Estebanez, L., Shulz, D.E., Férézou, I., 2018. Supra-barrel Distribution of Directional Tuning for Global Motion in the Mouse Somatosensory Cortex. Cell Rep. 22, 3534–3547.

Waiblinger, C., Brugger, D., Schwarz, C., 2015. Vibrotactile discrimination in the rat whisker system is based on neuronal coding of instantaneous kinematic cues. Cereb. Cortex 25, 1093–1106.

Wekselblatt, J.B., Flister, E.D., Piscopo, D.M., Niell, C.M., 2016. Large-scale imaging of cortical dynamics during sensory perception and behavior. J. Neurophysiol.

Woolsey, T.A., Van der Loos, H., 1970. The structural organization of layer IV in the somatosensory region (S I) of mouse cerebral cortex. Brain Res.

Yang, H., Kwon, S.E., Severson, K.S., O'Connor, D.H., 2015. Origins of choice-related activity in mouse somatosensory cortex. Nat. Neurosci. 19, 127–134.

Supplementary Figures

Brown, J., Oldenburg, I.A., Telian, G.I., Griffin, S., Voges, M., Jain, V., Adesnik, H.A. Spatial Integration During Active Tactile Sensation Drives Orientation Perception. Neuron. 2021 May 19;109(10):1707-1720.e7. https://doi.org/10.1016/j.neuron.2021.03.020.

.

A

Rostral presentation

1st whisker Contact

Catch Trials

Target Position

Home Position

Motor

B

'GO' trial → 'hit' Lick → Water Reward → New Trial

'GO' trial → 'miss' No Lick → New Trial

'NOGO' trial → 'false alarm' Lick → Air Puff & Time Out → New Trial

'NOGO' trial → 'correct rejection' No Lick → New Trial

Catch trial → → New Trial

C

Start Trial | Photostimulation | End Trial

Mouse runs ~50 cm | Stimulus moves to target position 2-3s | Response Window 1s | Stimulus moves to home position 1-1.5s | Waiting Period New Orientation Selected 3-5s

1st Whisker Contact | Air Puff | Water Reward | Time Out 3-5 s

D

1Ori_auto + 💧

Anticipatory Licking > 70%? — Yes → 1Ori

No

Performance >70%? — Yes → 2Ori

No & 10% Catch

Performance >70%? — Yes → 8Ori

No & 10% Catch

d' >1.5? — Yes → Experimentation

No & 10% Catch

E

Moving Fraction Correct

Mouse 1
Mouse 2
Mouse 3
Mouse 4
Mouse 5
Mouse 6
Mouse 7
Mouse 8

Trial number

1Ori_auto | 1Ori | 2Ori | 8Ori

d'

Session Number

F

Reverse contingency

'NOGO' 0° 'GO'
+45° −45°

Lick Probability

Original
Reverse

Stim. Orientation (°)
−45 −29 −15 −7 7 15 29 45 C

131

Figure S1. Orientation discrimination task design, Related to Figure 1

A. Schematic of behavioral task. The stimulus bar is presented rostrally to the mouses right whisker field. Mice can contact the bar as it travels into the 'target position'. For catch trials, the stimulus bar is held outside the whisker field. The 'home position' is jittered on each trial (red area).

B. GO/NOGO trial structure.

C. Timeline of trial structure.

D. Block diagram of progressive training paradigm.

E. *Left:* Moving average performance over training for 8 example mice. Dashed line: 70% correct performance. *Right:* d' over each session for the corresponding mice, dashed line: 1.5 d'. Colored lines represent training stage.
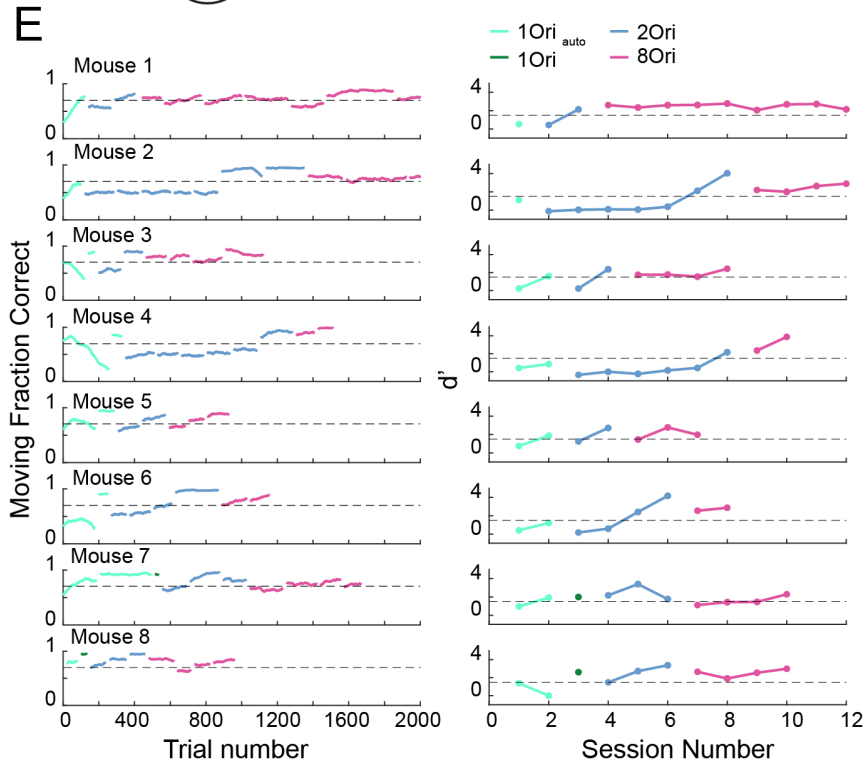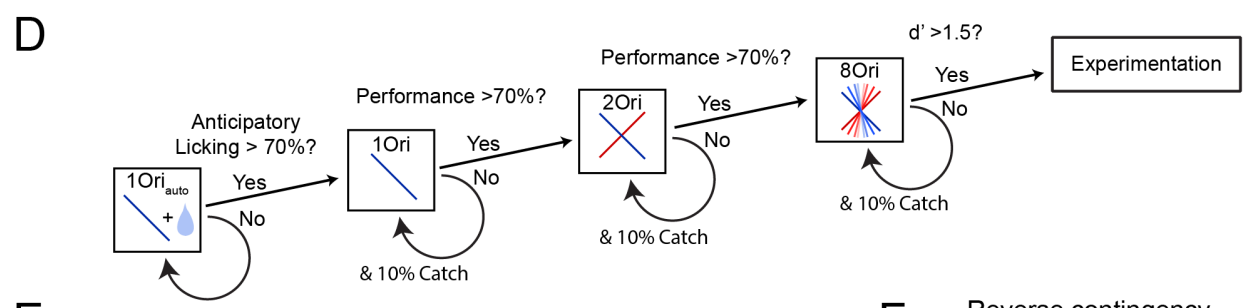
F. Performance on reverse GO/NOGO contingency with a full whisker pad (*top*: schematic, *bottom*: psychometric curve of performance (n=5 mice, averages from individual mice (gray); mean ± SEM and fit (black) and for comparison original contingency data as in Figure 1E (red)). Dashed lines represent midpoints for 0° orientation and 0.5 lick probability.

A

Photodiode

IR Light Beam

5cm

IR LED
950nm

DAC

B

Full Pad

2 Whisker

Normalized Voltage

Time (s)

Sensor identified contact
Image validated contact
Voltage threshold

C

First Contact

All Contacts

Frac. of Trials

Hit   FA   Miss

D

Piezo Freq. (Hz)

Hits

Location (cm)

Subsample of image frames
2 Whisker

-0.08s -0.07s -0.06s -0.05s -0.04s -0.03s -0.02s

-0.01s 0.00s 0.01s 0.02s 0.03s 0.04s 0.05s

E

Full Pad

2 Whisker

Stim. Orientation (°)

Time (s)

F

Full Pad

2 Whisker

Whisker contact rate (Hz)

+45° -45°

Time (s)

G

Full Pad

2 Whisker

Cumulative whisker contact No.

+45° -45°

Time (s)

H

Full Pad
All Trials

2 Whisker
All Trials

First Contact (s)

Stim. Orientation (°)

I

Success Trials

Success Trials

Latency to lick (s)

Stim. Orientation (°)

J

Success Trials

Success Trials

No. of Contact

Stim. Orientation (°)

K

All Trials

All Trials

No. of Contacts

Success
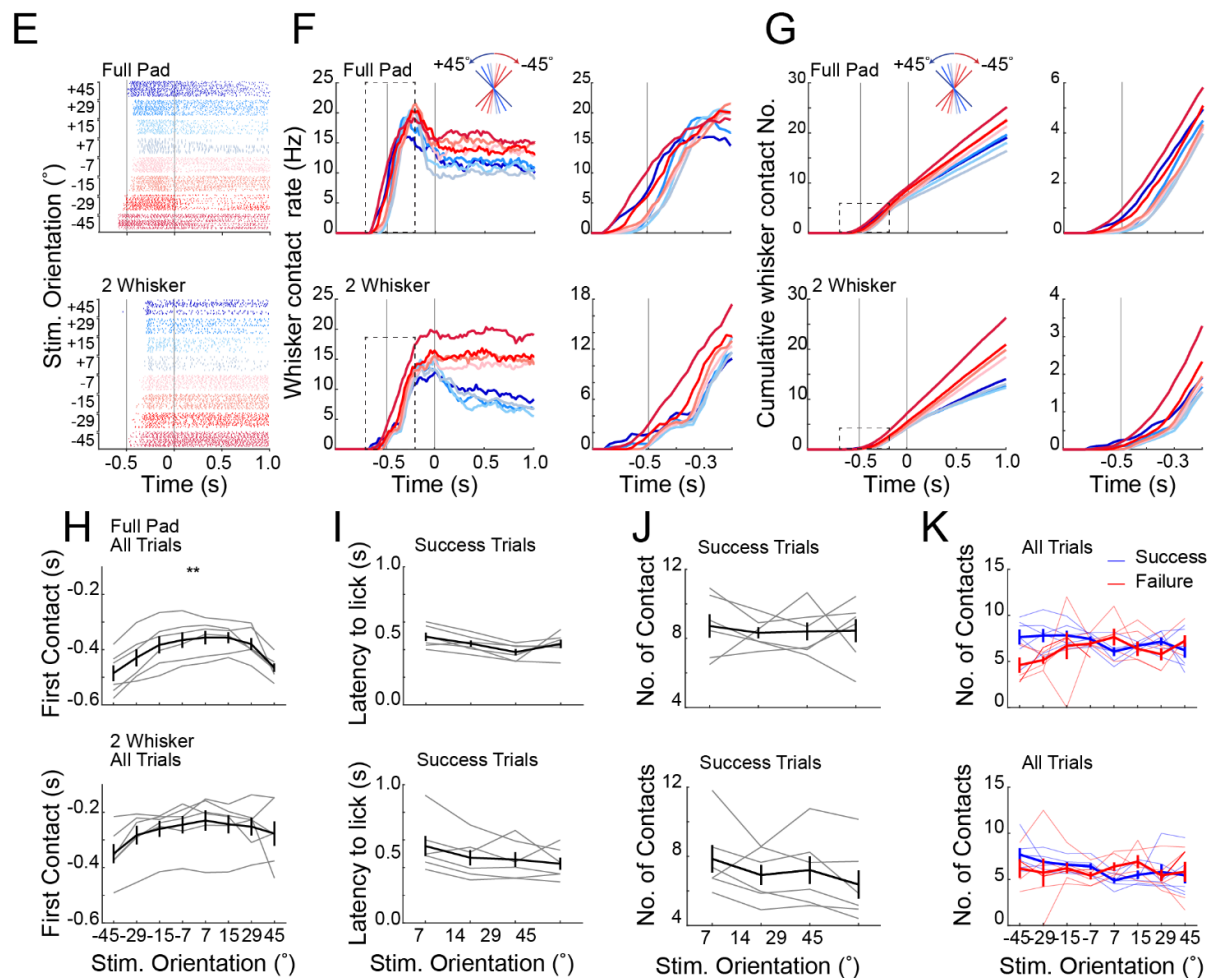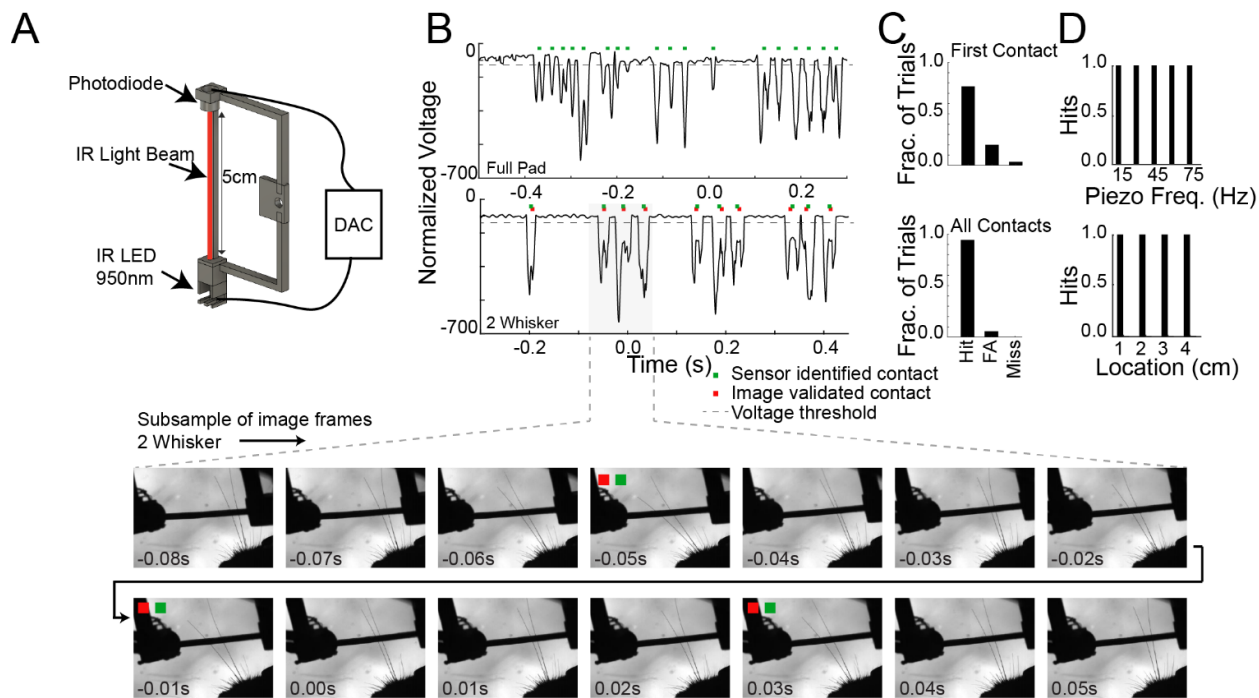Failure

Stim. Orientation (°)

133

Figure S2. Identification of whisker contacts during the task, Related to Figure 1

A. Schematic of stimulus bar with IR LED beam and photodiode for touch detection.

B. Normalized and smoothed signal from photodiode for an example trial of a mouse performing the task with full whisker pad (*top*) and two whiskers (*bottom*); Voltage deflection threshold (3 SD from baseline, grey dashed line). Photodiode detected whisker contacts (green square) and for the two-whisker trace visually identified whisker contacts (red square). *Below*: a subset of high-speed imaging frames from the two-whisker data.

C. Validation of the touch detector with simultaneous high-speed imaging for mice trimmed to two whiskers. Validation for first whisker contact (*top*) and subsequent contacts (*bottom*) (n=3 mice, 3 sessions, 30 trials for first contact, 76 trials for subsequent).

D. Whisker tethered piezo validation at different frequencies (*top*), and different contact points along the stimulus bar (*bottom*) (n= 60 repetitions at each condition).

E. Raster plot for an example mouse with full whisker pad (*top*) and two-whiskers (*bottom*) showing detected whisker contacts (colored tick marks) sorted by stimulus orientation. Gray lines indicate time points –0.5 and 0 seconds for visual guide.

F. Whisker contact rate for full pad (*top*) and two-whisker (*bottom*) sessions separated by stimulus orientation. Box represents zoomed in panel shown to the right.

G. As in F but cumulative whisker contact number over time.

H. Time of first whisker contact for all trials from full whisker pad data (*top*) and two-whisker data (*bottom*) over all stimulus orientations (n=3 mice, 6 sessions, **p<0.01, ANOVA).

I. Latency from first whisker contact to lick response for success trials for full pad data (*top*) and two-whisker data (*bottom*) (n=3 mice, 6 sessions).

J. Number of whisker contacts before lick response on success trials for full pad data (*top*) and two-whisker data (*bottom*) (n=3 mice, 6 sessions).

K. Number of whisker contacts within 0.3 seconds from first contact for all trials separated into success (blue) and failure (red) trials for full whisker data (*top*) and two-whisker data (*bottom*, individual sessions shown in lighter colors and group mean ± SEM, solid line; n=3 mice, 6 sessions).
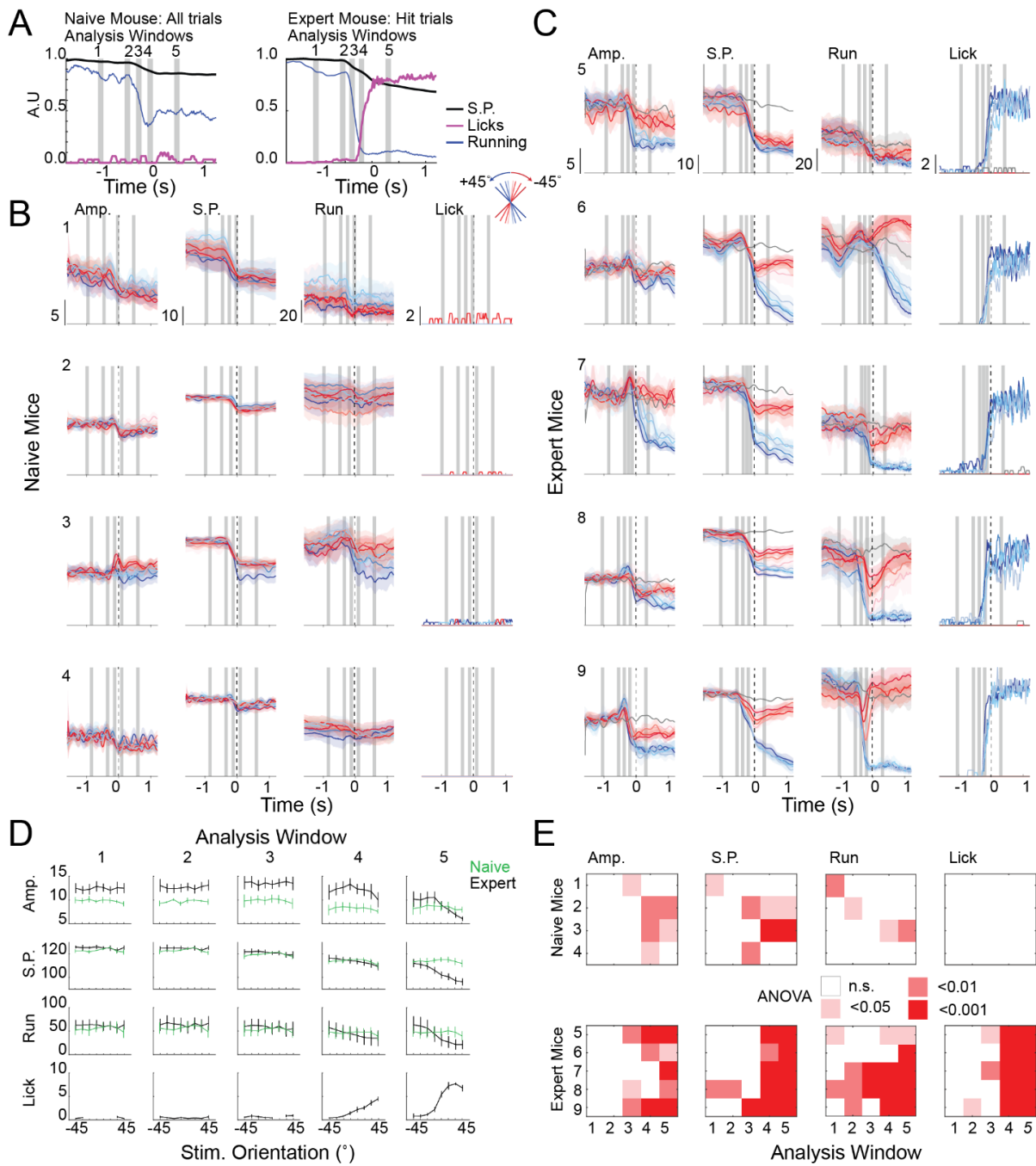
Figure S3. Learning induced changes in running, whisking, and licking behavior, Related to Figure 1

A. Example naive (*left*) and expert (*right*) mouse average run speed (blue), whisker set point (S.P.; black), lick rate (magenta) for all trials (naive mice) and hit trials (expert mice). Vertical gray lines represent analysis windows; (#1) baseline, (#2-4) start, middle and end of sampling window, (#5) response window. See methods.

B. Behavior responses from all trials for naive mice separated by stimulus orientations. Average whisker amplitude (Amp.), whisker set point (S.P.), running velocity (Run) and lick rate (Lick) ± confidence interval (n=4 mice). Individual colors represent stimulus orientation. Vertical gray lines represent each analysis window as in A. Dashed black line represents time 0 corresponding to the start of the response period.

C. As in B but success trials for expert mouse (n=5 mice).

D. Mean measurements during each analysis window across each stimulus orientation for naive (green) and expert (black) mice.

E. Statistical test of significance (ANOVA) between each orientation, for each mouse, for each analysis window and for each behavior for naive (*top*) and expert (*bottom*) mice (white, P=ns; light pink=*P<0.05, light red **P<0.01, red ***P<0.001.

A Raw Fluorescence Example

B Raw Fluorescence Each Recording

M4 FOV1   M4 FOV2   M3 FOV 1

M3 FOV2   M3 FOV3   M3 FOV4

M2 FOV1   M2 FOV2   M1 FOV1

C Mean Image   Cell Mask   Neuropil Mask

E Cell 1   Cell 2   Cell 3

D

F Mean Image   Cell Mask   Neuropil Mask

H Mean of Brightest Trial

G

I Optical PSF   Radial Distance (μm)   Axial Distance (μm)

J Distance to Nearest Tuned Neighbor (μm)   Tuned Cells

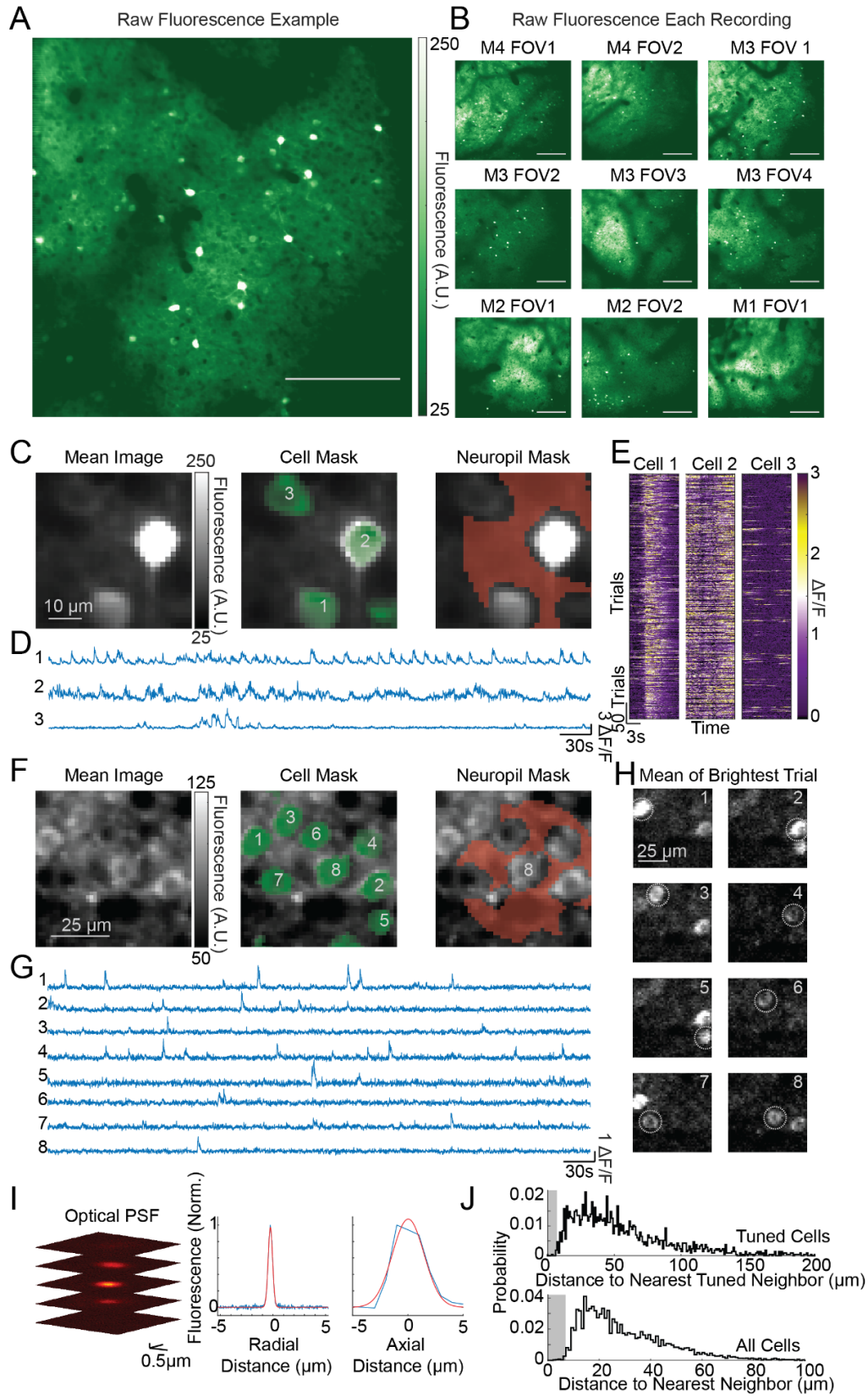Distance to Nearest Neighbor (μm)   All Cells

137

Figure S4. Imaging quality and source separation, Related to Figure 4

A. Motion corrected mean raw fluorescence image from a single imaging plane from an example mouse. Scale Bar 200µm.

B. As in A but from a single plane from each mouse (M) and session included in the analysis.

C. Motion corrected mean image of raw fluorescence (*left*), weighted pixel cell masks are overlaid on the mean image (*middle*), the region that the neuropil signal is extracted from for cell #2 (*right*).

D. Example ΔF/F traces from each cell within the FOV in C.

E. ΔF/F responses of each cell in C, aligned to the start of a trial, all trials from one recording session are presented.

F. As in C, but from a region that appeared much dimmer in the mean image.

G. As in D.

H. Average fluorescence from the trial when each cell in F is most active. White circle denotes the cell of interest.

I. Optical point spread function (PSF) of our imaging system, image of a 200nm fluorescent bead imaged at high zoom and planes spaced by 1µm (*letf*). The fluorescence profile over radial (*middle*) and axial (*right*) distance, raw data (blue) is fit with a gaussian (red). FWHM radial 0.49µm, axial 3.4µm.

J. Spatial distribution of nearest tuned (*top*) or any (*bottom*) neighboring cells. Gray area represents the average width of an ROI.

A Fluorescence (ΔF/F)

Pre Stimulus | Pre First Lick | -0.5s | 'Standard Analysis Window' | +0.5s | +1s

n=99 Tuned, 0.98% | n=343 Tuned, 3.4% | n=1,208 Tuned, 12% | n=2,150 Tuned, 21% | n=2,823 Tuned, 28% | n=3,202 Tuned, 32%

Stim Orientation (°)

Normalized Response

Response Window

Run Change | First Lick | Reward Delivery

Licking
Mean Fluorescence
Running
Mean Decon. Ca²⁺ Activity

Standard Analysis Window

B Deconvolved Calcium Activity

n=69 Tuned, 0.68% | n=1,165 Tuned, 11% | n=2,342 Tuned, 23% | n=2,960 Tuned, 29% | n=3,234 Tuned, 32% | n=3,282 Tuned, 32%

Stim Orientation (°)

Normalized Response

-45° | 7°
-29° | 15°
-15° | 29°
-7° | 45°
| Unresponsive
| Untuned
| Suppressed

C Three Planes Projected

100μm

D Naïve Mice; Deconvolved Calcium Activity

Pre Stimulus | Pre Acceleration | -0.5s | 'Standard Analysis Window' | +0.5s | +1s

n=8 Tuned, 0.3% | n=315 Tuned, 14% | n=276 Tuned, 12% | n=421 Tuned, 19% | n=501 Tuned, 23% | n=538 Tuned, 24%
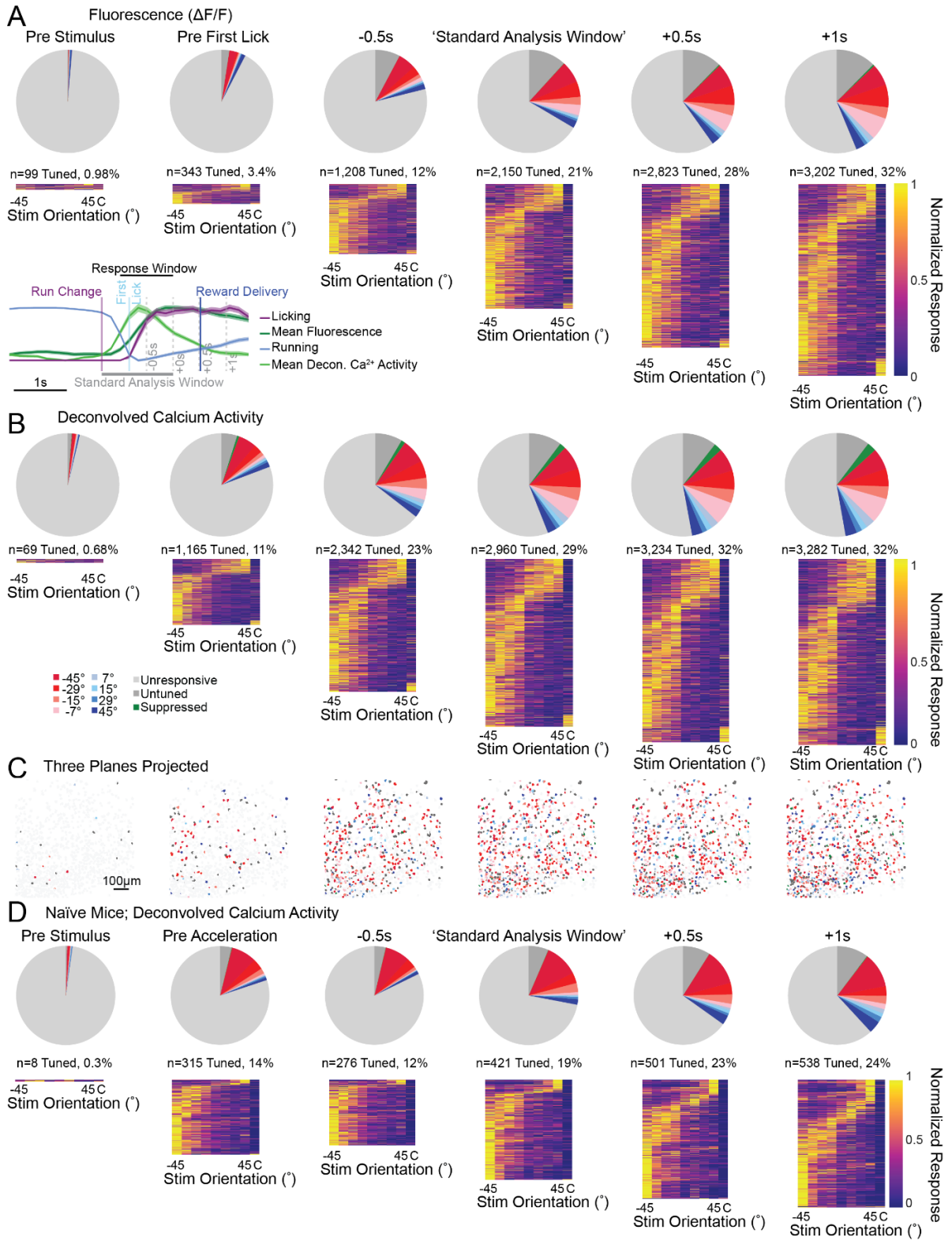
Stim Orientation (°)

Normalized Response

139

Figure S5. Establishing the window for calcium response analysis, Related to Figure 4

A. *Top:* The proportion of touch responsive or tuned cell for each analysis window (see Methods). The color (blue to red) indicates preferred orientation of neurons, (dark gray) untuned neurons, (green) suppressed neurons, and (light gray) unresponsive neurons as in Figure 4 (n=4 mice, 9 recordings, 10,140 cells). *Bottom*: The cross-validated tuning curves for all tuned neurons for each analysis window. Tuning curves are normalized and sorted by the preferred stimulus of half the data that is not shown. *Inset:* Trace of a representative mouse's run speed (all trial types, blue), lick rate (Hit trials, purple), mean calcium fluorescence (mean z-scored ΔF/F, dark green), or deconvolved calcium response (mean z-scored deconvolved calcium activity, light green). Standard analysis window (gray bar), run deviation frame, aka the estimated time of first contact (purple), response window (black line), beginning of the lick response (in hit trials, light blue), time of reward delivery (dark blue).

B. As in (A) but analyzed from deconvolved calcium activity data.

C. Stimulus preference maps of all neurons recorded in a single recording session as a function of the analysis window; 3 imaging planes are superimposed. Significantly tuned cells are color coded by their preferred orientation (red to blue), untuned but touch-responsive cells (dark gray), and unresponsive cells (light gray).

D. As in (A) but analyzed from untrained, naive (n=2 mice, 3 recordings, 2,200 cells). The 'pre-lick' period is now a window that ends when the mouse begins to accelerate after stimulus presentation.
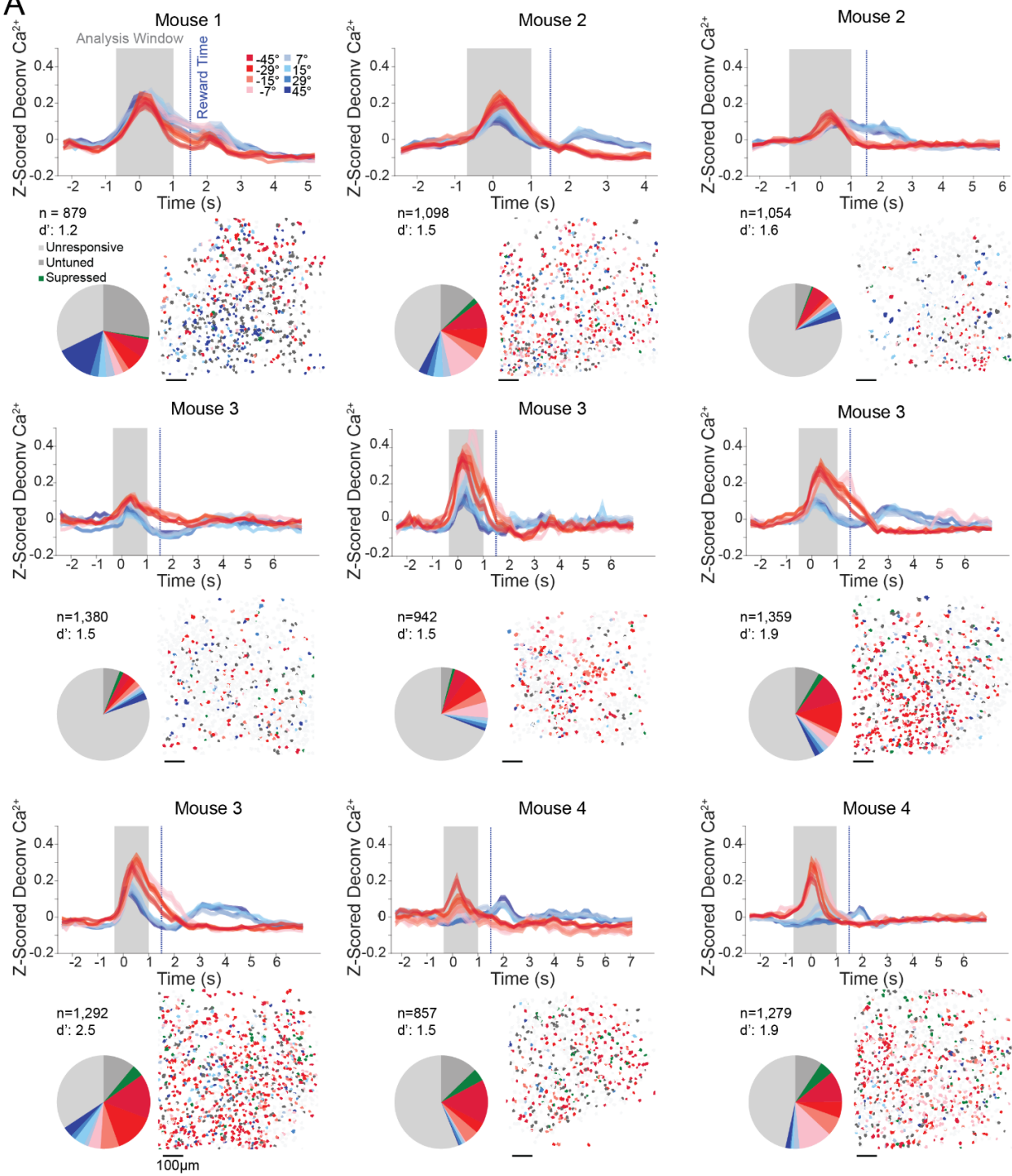
A

Mouse 1

Mouse 2

Mouse 2

Mouse 3

Mouse 3

Mouse 3

Mouse 3

Mouse 4

Mouse 4

Figure S6. Calcium responses from each field of view, Related to Figure 4

A. For each recording, *top,* mean (±95% confidence interval) population deconvolved calcium activity for each presented orientation (see inset). Gray window: the analysis window used see Figure S5). Blue dotted line: the time of reward delivery. Inset: the number of detected neurons, and d' recorded during this session. *Bottom left*: Pie chart showing the relative percent of neurons that were unresponsive, untuned, suppressed, or tuned as in Figure 4C. *Bottom right*: stimulus preference map of all neurons recorded in a single recording session; 3 imaging planes are superimposed as in Figure 4F (Scalebar 100µm). The example data in Figure 4 comes from Mouse 1.
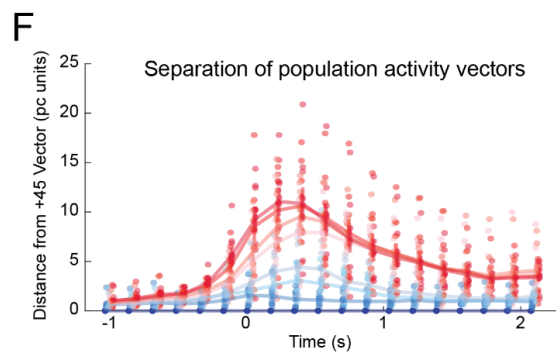
A

Sort Half of Data   Display Half of Data

Normalized Response

Stim Orientation (°)

Count

Inclusion Threshold

Tuning Curve Correlation

B

Tuned Cells
(aka p<0.01 and cross validated correlation >0.5)
Non-tuned Cells

Mean Evoked ΔF/F in Respnse Window

ANOVA P Value of Tuning

Note: 33 cells with P Value <1e-50 omited

C

Max Observed ΔF/F

Mean Evoked ΔF/F in Respnse Window

Example Cells from Figure 4B
Example Cells from Figure S4F

Overall Mean Observed ΔF/F

Mean Evoked ΔF/F in Respnse Window

D

All Detected Cells
(Same as in Fig S5 B)

Cells With Max
Observed ΔF/F > 1

Cells With Max
Observed ΔF/F > 2

Cells With Max
Observed ΔF/F > 5

Cells With Max
Observed ΔF/F > 10

n = 10140   n = 9973   n = 7755   n = 2699   n = 754

-45°
-29°
-15°
-7°
7°
15°
29°
45°
Unresponsive
Untuned
Suppressed

E

Selectivity

p<1e-99

p<1e-99

p<0.05

p<1e-43

p<1e-99

p<0.001

Full Pad   Random   Shuffled   Three Whiskers   One Whisker   Shuffled

F

Separation of population activity vectors
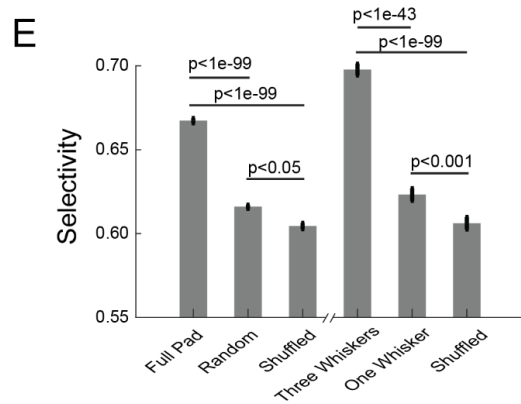
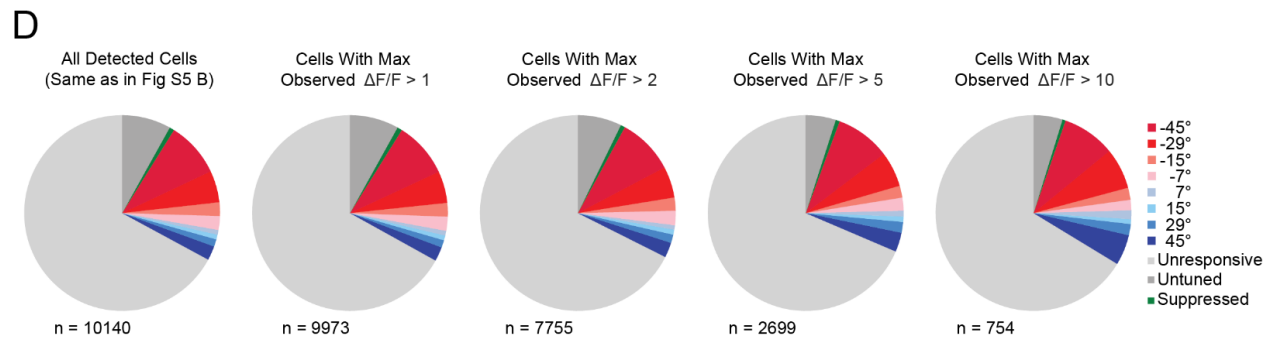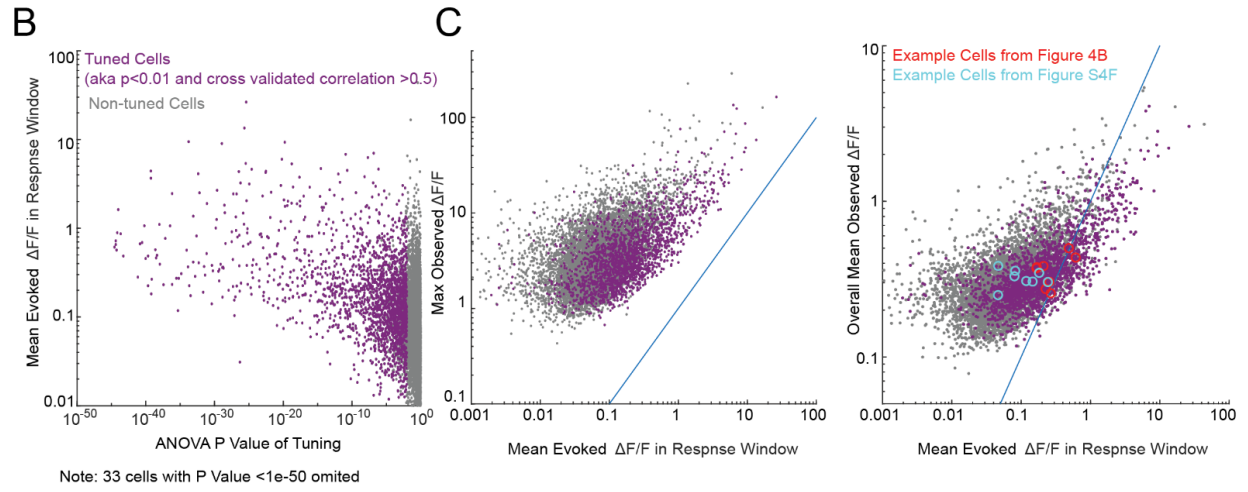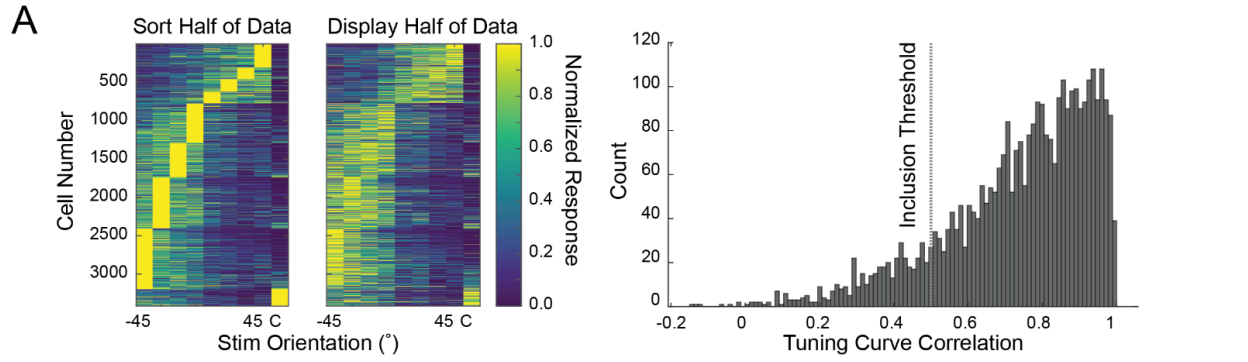Distance from +45 Vector (pc units)

Time (s)

143

Figure S7. Population metrics of calcium imaging data, Related to Figure 4

A. Explanation of cross-validated tuning curves. *Left*: data was split in half and assigned to a sort half (*left*) or a display half (*right*). Tuning curves from cells determined to be tuned by the complete dataset (ANOVA <0.01 on all trial types excluding catch) were calculated for each half and sorted based on the response in the sort half. *Right*: histogram of the correlation between the tuning curves of each cell determined by the sorted half or the displayed half of the data. Only tuning curves from the displayed half that passed the inclusion threshold correlation of 0.5 are displayed in cross validated tuning plots. 2960/3416 (87%) tuned cells (defined as ANOVA <0.01 between orientations) passed this threshold in the standard analysis (Figure 4D).

B. Mean evoked $\Delta F/F$ during response window and corresponding ANOVA P value for all cells. Color coded by tuned (purple) and non-tuned (gray). Note: tuning requires both a low P value, and a high cross-validation correlation.

C. (*Left*) Maximum $\Delta F/F$ observed at any point during the recording session and mean $\Delta F/F$ in the response window for all cells, separated by tuned (purple) and non-tuned (gray). (*Right*) Overall mean $\Delta F/F$ response during entire recording vs the mean $\Delta F/F$ recorded during the analysis window. Example cells from Figure 4B (red) and S4F (blue) are circled.

D. Pie chart showing relative fractions of tuning for all detected cells (*left*) and with increasing restrictive criteria of $\Delta F/F$, i.e. if we only include higher signal cells how does our data change.

E. Selectivity index computed for all detected neurons from normal experiments (mean ± SEM) compared to similar metrics created by random values or shuffled data, and from neurons from the trimming experiments. P values are rank sum comparisons between populations.

F. Euclidean distance of population activity across the first 3 principal components measured in each frame as the distance from the +45° vector to each of the other orientations. Faint dots denote each recording's average, solid line denotes mean ± SEM.
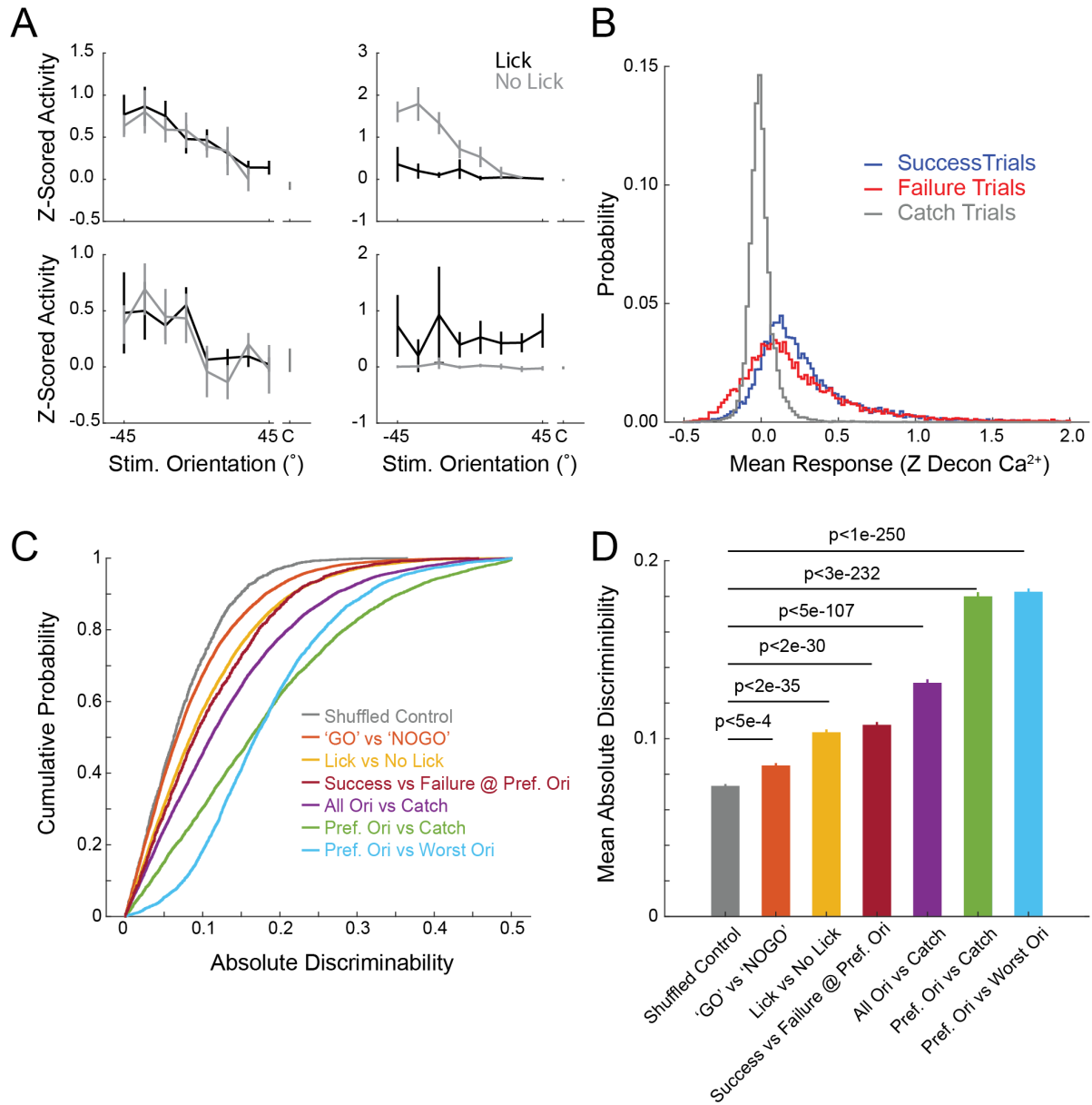
Figure S8. Modulation of neural activity by behavioral responses, Related to Figure 4

A. Tuning curve of 4 example neurons separated between lick and no lick trials (mean ± confidence interval).

B. Histogram of responses to preferred orientation during success (blue) and failure (red) trials, and the corresponding cells' responses during catch trials (gray). Only cells with at least one failure trial in the preferred condition were included (n=8,558 cells).

C. Cumulative probability plots of the discriminability calculated from the response of each neuron comparing different conditions. Analysis was restricted to the four most vertical angles (±15°, ±7°), comparisons with fewer than 10 responses in each category were excluded. If a comparison involved the preferred orientation of a cell, that orientation was derived from the full 8 orientation set, but only cells with a preference in the middle 4 orientations were used. Shuffled data matches the trial counts of the fewest trials of any of the comparisons (shuffle n=1687, GO v NOGO n=10,140, lick v no lick n=10,140, success v failure (at preferred orientation) n=1,687, all orientations v catch n=9198, preferred orientation v catch n=4,131, preferred orientation v worst orientation n=4,606 cells).

D. The mean ± SEM of the discriminability values displayed in C, and the P value (rank sum test) of the difference between this distribution and the shuffled control.
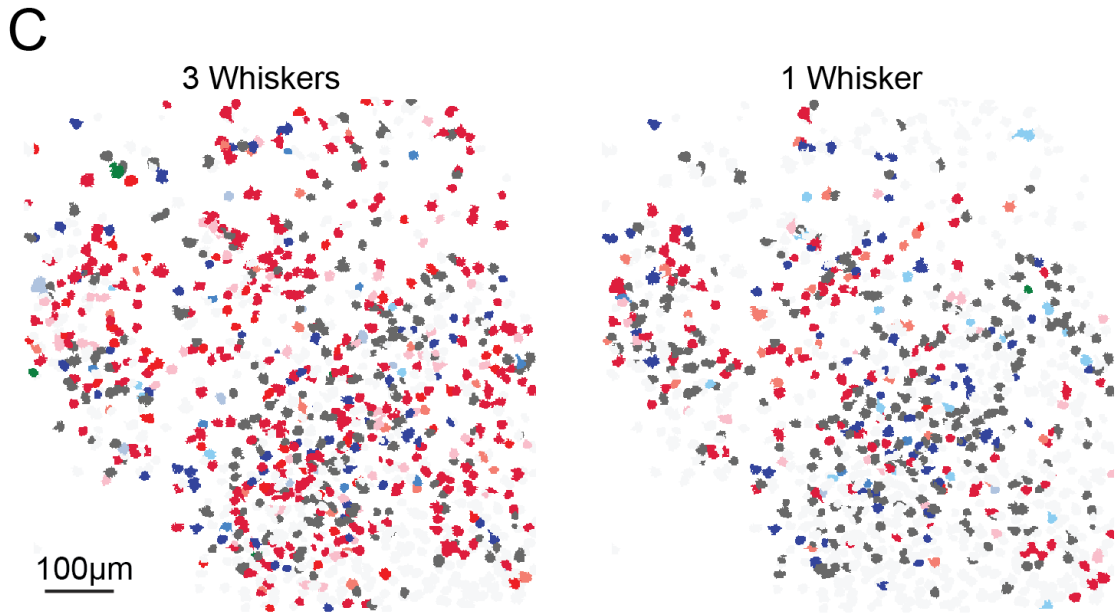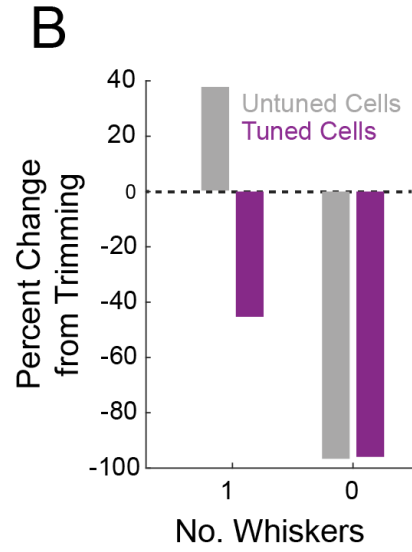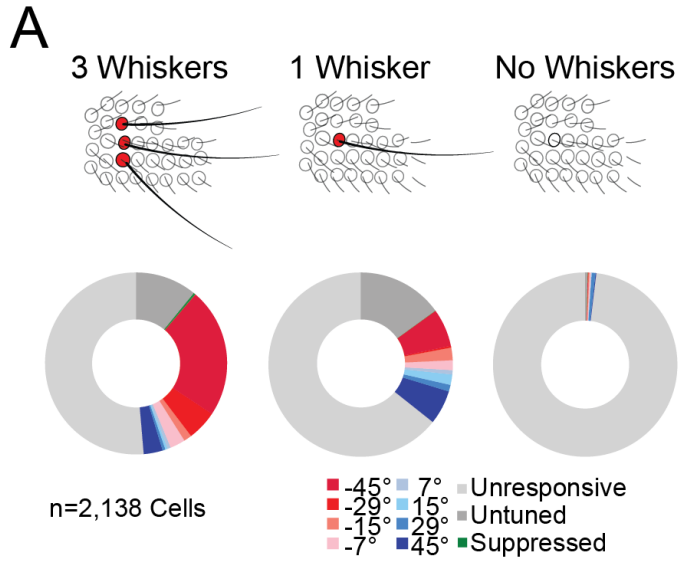
A

3 Whiskers   1 Whisker   No Whiskers

n=2,138 Cells

-45° 7°   Unresponsive
-29° 15° Untuned
-15° 29° Suppressed
-7°   45°

B

Untuned Cells
Tuned Cells

C

3 Whiskers   1 Whisker

100μm

Figure S9. Whisker trimming reduces the number of orientation-tuned cells, Related to Figure 4

A. *Top*: schematic of the trimming experiment. *Bottom*: Fraction of neurons that were significantly tuned or untuned but touch responsive in the three-whisker, one-whisker, or no whisker condition (n= 2 mice, 2,138 cells).

B. Relative change in the number of cells that could be classified as touch responsive but untuned ('untuned', gray) or significantly tuned to any orientation ('tuned cells', magenta) for the one and no whisker conditions relative to the three-whisker condition. Maps of the locations of the recorded neurons (three planes superimposed) colored according to their preferred stimuli for example mouse, with three (*left*) or one (*right*) whisker remaining.

C.

Chapter 5: The multifunctional nature of motor cortex

Foreword

This is my primary thesis project. This work began when I was a technician just before starting grad school. As soon as I heard sensory driven firing rates in whisker motor cortex (vM1) I was hooked. I became determined to identify what those units were encoding and figure out why vM1 had such detailed sensory responses. Silencing vS1 did not abolish sensory activity in vM1, leaving me and a couple other scientists in disbelief. vS1 was thought to be the major driver of vM1 sensory activity. Instead I found that vS1's role is to modulate vM1's gain, increasing vM1's sensory signal from its baseline firing rate. I wanted a more quantitative way of measuring how much sensory information was present and how it was affected by silencing. During my second lab rotation I adapted a neural decoder to use spike data instead of LFP data to address my question (Agarwal et al., 2014). I felt like a champ on the night I got the decoder to work. In retrospect, it's not very complicated but back then it was all new to me. The decoder allowed me to directly quantify and compare how much sensory information was present in vS1's and vM1's neural code. vS1 neurons carried more stimulus information, but vM1 encoded a lot more than expected, performing roughly 20% worse than vS1 and was never near chance. Silencing either region revealed that vM1 did lose information with vS1 silencing and, to my surprise, silencing vM1 reduced vS1's information. This was incredible because there were no directional changes to vS1's firing rates, the decoder found an effect that would have otherwise gone unnoticed. Finally, using a demanding whisker dependent task I found that vM1 does impact whisker movements but only if it requires adaptive whisking. Further we found that vM1 is critical for our discrimination task likely as a sensory processing region but possibly as a higher order brain region responsible for response inhibition. There are a few things I would still like to know: 1.) Does the PoM drive vM1 sensory activity? 2.) What is vM1 sensory information used for? It would be great if we could silence only the sensory neurons, and 3.) What are vM1's other roles? It is a true multirole cortical region.

Citation

Telian, G.I., Adesnik, H.A. The multifunctional nature of motor cortex. (in preparation)

Summary

The mouse whisker system is a great model to study how sensorimotor cortices encode sensory information and how that information influences motor output. Recently the lines between sensory and motor have become blurred, both can drive whisker motion and encode whisker sensory input (Ahrens & Kleinfeld, 2004; Petrof et al., 2015; Smith & Alloway, 2013). Here we probe both the sensory and motor regions simultaneously. Using extracellular recordings,

optogenetic silencing, and high-speed whisker tracking we find that vibrissae primary somatosensory cortex (vS1) and vibrissae motor cortex (vM1) robustly encode tactile stimulation from the same stimulus (Clack et al., 2012; Madisen et al., 2012). We compare the differences in their firing rates and infer what information is encoded in their populations. vM1's responses are similarly driven as vS1's but have fewer sensory evoked positions per unit. Cortical silencing revealed that vM1 activity is gain modulated by vS1 but not driven by it. Firing rates in vS1 are not modulated in a clear direction during vM1 silencing. However, a neural decoder found silencing either vS1 or vM1 decreased sensory information in the non-silenced region. Whisker motion is not affected by cortical silencing, unless mice are trained on a demanding whisker discrimination GO-NOGO task. vS1 is necessary for this task but does not impact whisker movements, acting solely in a sensory processing capacity. vM1 is also necessary for the task, particularly on NOGO trials, but vM1 also impacts whisker movement and causes mice to lick earlier. These data depict vM1 acting as a sensory region that may also act as a higher cognitive area. For the first time, we explore vM1's role as a sensory cortex, finding that vS1 gain modulates vM1, context determines how vM1 modulates whisking, and vM1 acts as a general multirole cortical region.

Introduction

The cortex has been studied across a wide range of animals due to its conserved architecture of layers and columns. Identifying cortical regions and their analog in other species has typically looked for similarities in anatomical architectonics, body movement with electrical stimulation, neural activity elicited by bodily stimulation, and more recently genomics. Names were prescribed to regions by gross characteristics such as motor cortex, because electrical stimulation most easily elicited body movement, or sensory cortex because a particular body part elicited neural activity when stimulated. As technology advances and stimulation and recording techniques become more precise the strict functional definitions of cortex are becoming blurred, especially when comparing cortical areas across species. There is evidence that shows that a cortical region in a monkey may be absolutely necessary for movement but in a mouse the whole of motor cortex can be removed and the mouse will remain mobile and exhibit minor deficits (Ueno & Yamashita, 2011).

Cortical regions in lower species, such as mice, may take on more functions then their names let on. Studies are now finding neural activity that appear out of scope for a particular region of cortex, such as visual representations found in motor cortex (S. Zhang & Dan, 2011). Or decision tuned units in Whisker Somatosensory cortex (McGuire et al., 2016). The mouse whisker somatosensory system is one such system, exhibiting atypical functions in certain brain regions. Multiple studies have confirmed that Barrel Cortex can elicit whisker movements independently from vM1 (Auffret et al., 2017; Matyas & Petersen, 2010). Other studies have shown that

150

whisker motor cortex has a mix of non-motor functions (Lopes et al., 2016) and some motor functions that appear contradictory to each other (Christian Laut Ebbesen, Doron, Lenschow, & Brecht, 2017; Sreenivasan et al., 2016). This presents a well-known system to study cortices capable of multifunctionality. Discovering the full functionality of cortex will not only shed light on the system of study but may also provide evidence highlighting the differences in cortical function across species.

In the mouse whisker system sensory activity is present in vibrissae Motor cortex (vM1) but little is known about it. It coincides with feedforward connections from the sensory cortex and is presumed that vibrissae primary Somatosensory cortex (vS1) drives sensory activity in vM1 but that has not been directly tested. In the second part of the sensorimotor loop vM1 is thought to take the sensory information from vS1 and us it to update the whisker motor program, but this has not been tested as well. Additionally, vM1's sensory responses have not been well classified and their tuning characteristics are not known.

Studying the sensory responses in vM1 may help us understand what type of neural transformations occur from a sensory region to a motor region. Quantifying how sensory information is encoded in vM1 can illuminate what information a motor region deems necessary for it to carry out its job. Studying vM1's sensory responses will produce a more complete picture of the whisker sensorimotor loop and will help us understand cortical areas that don't abide by their functional labels.

Here, we will directly characterize vM1 sensory activity and compare it to vS1's representation of the same stimulus. We will use a neural decoder to quantify the relative amount if information present in each regions' population. Then we will directly test whether vS1 drives vM1's sensory activity and determine if vM1 feedback projections to vS1 modulate vS1's sensory representations. During the silencing experiments we will also quantify its impact on decoding performance. Lastly, we will test whether vM1 and vS1 are necessary for whisker movements in two different contexts, one where mice have no task and the stimulus has no behavioral relevance, and then a demanding whisker discrimination task with behavioral relevant stimuli. This study will directly characterize vM1 sensory activity and explore how vM1 contributes to whisking and any other non-motor functions.

We found that vM1 may act as a higher order brain area as well as a sensorimotor area. During the spatial tuning experiment we found that vM1 units are driven by fewer stimulus positions than vS1 and their mean sensory evoked rates were weaker and less widely distributed than vS1. However, on a trial by trial basis vM1 units are more variable indicated by a greater Fano Factor. Decoding using vS1 data produced more accurate predictions, while using vM1 data resulted in less accurate representations than vS1 but overall very good performance. Cortical silencing revealed that vS1 does not drive vM1 sensory activity as previously thought but it is responsible

for modulating vM1's gain, increasing the distance of sensory driven firing rates from their own baseline firing rate. Without vS1 vM1 RS units broaden and both RS and FS units firing rates decrease. Silencing vM1 did not affect vS1 units' tuning and had seemingly little effect on the population's mean firing rates. Decoding found that silencing negatively impacted prediction power for both vM1 and vS1, suggesting that vM1 did affect vS1 but did not affect the entire population in the same way. Silencing vM1 and vS1 did not affect whisking. During a whisker dependent task both vS1 and vM1 were required for high performance, silencing either resulted in an increase in false alarm rates at NOGO positions. However, vS1 did not affect whisker movements, it acted solely as a sensory area, while vM1 impacted whisking and caused mice to responded earlier. Interestingly vM1 only impacted whisking in trained mice. Because vM1 caused mice to lick earlier we believe it plays a role in response inhibition, acting in some capacity as a higher cortical area. In line with other studies vM1 exhibits multirole capability in addition to whisker motor control.

Results

Rapid whisker contacts drives robust sensory responses in both vS1 and vM1

We performed preliminary hand mapping experiments in vM1 and found its sensory responses were more difficult to detect online requiring more whiskers be deflected than the responses in vibrissae somatosensory cortex. In order to investigate vM1's sensory activity we needed a method that could drive consistent sensory activity from multiple whiskers. The spatial tunning experiment, previously used in vS1 experiments, causes multiple whiskers to rapidly contact the stimulus making it a good choice for this study (S. Pluta et al., 2015; S. R. Pluta, Lyall, Telian, Ryapolova-Webb, & Adesnik, 2017). Transgenic mice, expressing Channelrhodopsin (ChR2) in parvalbumin inhibitory cells (Ai32-PV-CRE), were used in all experiments. We used these transgenic mice to silence either vS1 or vM1 by activating inhibitory neurons as this is a common and reliable method used for robust cortical silencing (Guo et al., 2014; Madisen et al., 2012).

The experiment was designed to drive strong and consistent sensory activity in both vS1 and vM1. Briefly, a headplated mouse is placed on a rotary treadmill. A vertical stimulus pole moves to either one of eight randomly selected linear positions, within reach of the mouse's whiskers, or to one control position out of reach of the whiskers (Figure 1B). The mouse's whiskers make multiple contacts against the vertical pole driving sensory activity. Each trial is randomly assigned as either a no silencing, vS1 silencing, or vM1 silencing trial, with silencing occurring during the one second analysis window (See trial structure in Figure 1B). We only analyzed running trials in order to ensure consistent sensory drive throughout the experiment as whisker motion becomes stereotyped while running quickly above a certain run speed (Sofroniew, Cohen, Lee, & Svoboda, 2014).

During the experiment, high density 32-channel silicon electrodes were lowered into vS1 and vM1. Optical fibers were placed near the electrodes enabling optogenetic silencing of recorded neural activity (Figure 1A). Recording neural activity simultaneously is a powerful technique when used in interconnected brain regions. It provides the opportunity to observe neural transformations as information flows between connected brain areas. Combining simultaneous recordings with optogenetic silencing and decoding analyses allows us to pick apart how much a cortical region contributes to another's representations. This allowed us to directly compare vS1's and vM1's activity to the same stimulus.
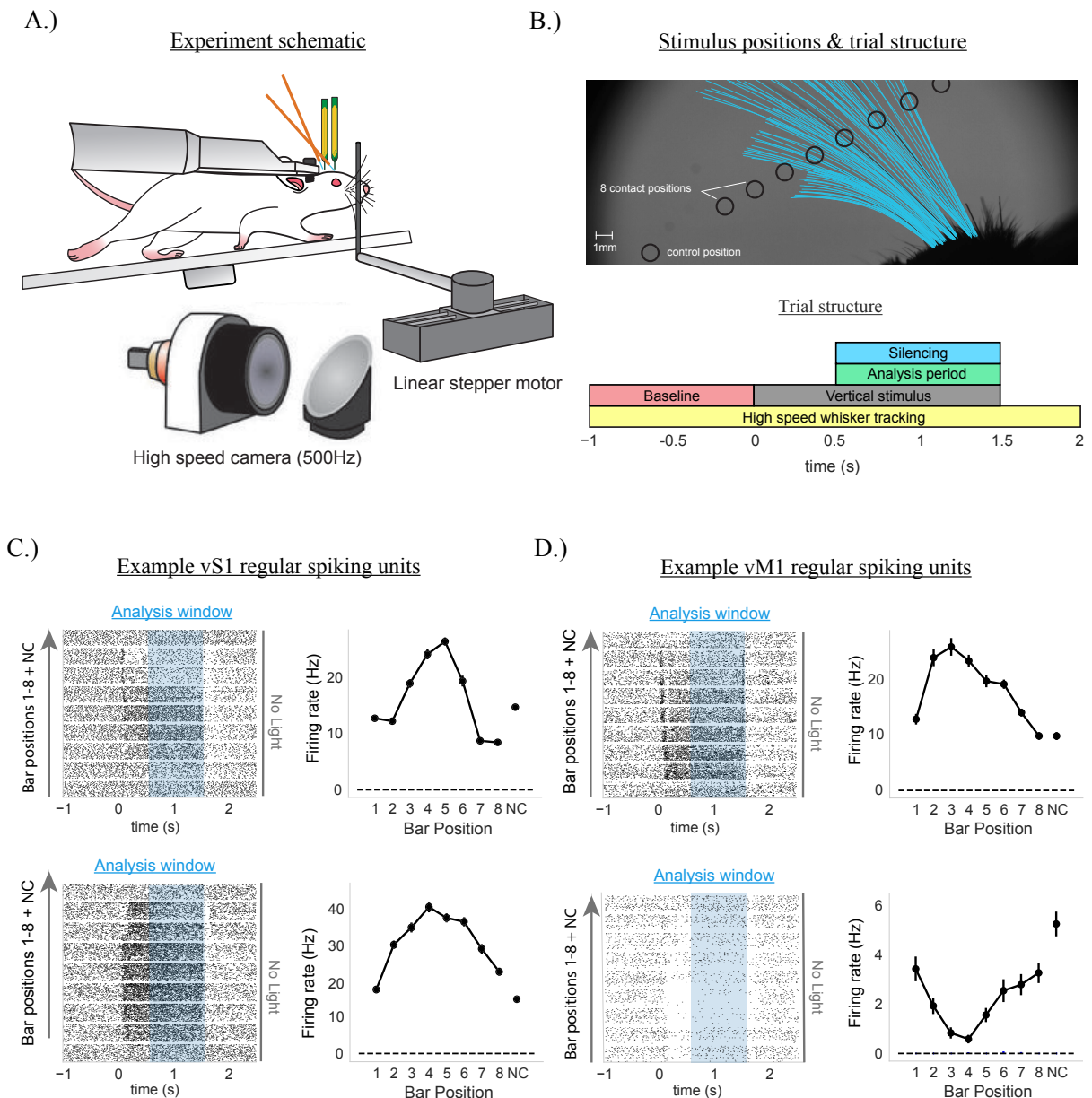
Figure 1. Spatial tuning experimental setup. A.) Experiment setup, a headplated mouse is fixed above the circular running wheel, two fiber coupled blue LEDs and two 32-channel electrodes are place over/in vS1 and vM1, a linear stepper motor moves the vertical pole stimulus in to one of eight contact positions or one control no-contact position, a high speed camera records whisker movement at 500Hz. B.) Image from high speed camera, black circles represent stimulus positions, blue traces indicate whisker positions over the course of a single whisk cycle. C.) Regular spiking vS1 units, top: example single unit, raster plot depicting trials from all positions and mean tuning curve, bottom: second example unit same layout as above. D.) Regular spiking vM1 example units, top: example unit that is sensory driven at many positions, bottom: example unit that is suppressed by stimulus contact.

Sensory driven activity was easily identifiable during experiments. It was audible through the electrophysiology recording speakers as well as easily visible is the recording traces. Only

experiments that had stable firing rates and low external noise were included in our analysis. Single units were isolated and categorized as either regular spiking (RS) or fast spiking (FS) units. Only sensory driven units were analyzed and presented here. We recorded a total of 126 units in vM1 and 131 units in vS1. The number of statistically significant sensory driven units in vM1 was much lower than that of vS1, with 86 driven units in vM1 and 119 driven units in vS1 [vM1 68.5% RS and 66.8% FS, vS1 82.0% RS and 97.3% FS units, see Figure 2B]. There are fewer sensory responsive units in vM1 relative to vS1, this may be because vM1 is a more diverse or general cortical region. A multitude of variables have previously been found encoded in vM1 neurons (Huber et al., 2012). We find it surprising that vM1 contains so many sensory driven units in a non-sensory cortical region.

Regular spiking units in vS1 were typical of our previous experiments (S. Pluta et al., 2015; S. R. Pluta et al., 2017). Sensory responses were clear and principal whiskers could be identified by hand mapping if necessary. They exhibited stable high firing rates while in contact with the stimulus pole. Two example sensory driven vS1 units are presented with their associated raster plots for all stimulus positions and tuning curves in (Figure 1c). The first unit depicted is an vS1 RS unit that encodes stimulus position via an increase and decrease in firing rate, relative to baseline. The second unit is strongly driven by the stimulus at all but one position with a Gaussian-like receptive field

We had initially hypothesized that vM1 sensory units would be weakly driven and difficult to identify due to our preliminary experiments. This would not be unexpected as the PoM region of the thalamus, with its multiwhisker representations, projects directly to vM1 (Casas-Torremocha, Clascá, & Núñez, 2017; Papale & Hooks, 2017). However, we found that vM1 firing rates were clear, well above their spontaneous baseline rates, and had tuning curves similar to vS1. Two example vM1 units are shown with their associated raster plots for all stimulus positions and tuning curves (Figure 1D). The sensory responses, after the object moves into position, are stable and consistent throughout the experiment. The first vM1 unit is a typical unit with strong and consistent sensory drive at multiple positions. The second unit is suppressed entirely by touch, making it a much less common unit, it is presented here to demonstrate that vM1 units can encode stimulus information via suppression of activity. It is more common to see individual vM1 units represent different positions with the majority driven above baseline and about 30% with suppressed activity (Figure 2C).

vM1 sensory responses are weaker and more variable than vS1 for the same stimulus

After confirming the quality of all experiments and grossly characterizing sensory driven activity we moved to compare vM1's and vS1's populations. Understanding the similarities and differences between two connected populations may shed light on the type of neural transformations that can occur between them. Somatosensory cortex has detailed sensory

information, if vM1 has less detailed representations for the same stimulus then vS1 may be responsible for transforming its detailed representation of sensory space into a simplified, broad picture for vM1. A transformation like this could imply that vM1 only needs a general picture of the tactile environment to properly carry out its role. A broad picture of the environment may be sufficient to guide slow-timescale whisker movements, such as setpoint and amplitude. The detail of a surface and the precise representations of each barrel column is likely unnecessary for guiding slow broad movements. Such detail may take up valuable computational power for little benefit.

Another case may be differences in units' Fano Factor per region. A region containing units with a high Fano Factor may suggest that precise representations are less important for that regions function. Differences in Fano Factors or other measures of spike variation may represent different levels of noise tolerance per region.

We wanted to understand the basic properties of the two sensory driven populations in order to begin searching for possible neural transformations. Fano Factors were computed for the no contact control position, to estimate baseline spontaneous activity, and for the most strongly driven position for each unit. Each unit had a preferred position, defined as the position with the greatest change in firing rate by the sensory stimulus. We were not expecting any differences between the baseline conditions but we did expect vM1 units to have greater Fano Factors during sensory drive, as converging inputs from the Barrel cortex and the PoM region of the thalamus are broadly tuned and could make spiking more variable.

During control trials the baseline firing rates of vM1 RS units had Fano Factors significantly larger than vS1 RS units at baseline firing rates. The same vM1 RS units had significantly larger Fano Factors at baseline than vS1 RS units during sensory drive while both populations were not significantly different during sensory drive (Figures 2A) [vM1 vs vS1 baseline, rank-sums p-val = 1.647 e-05, RS vM1 vs vS1 driven rank-sums p-val = 0.077, RS vM1 baseline vs vS1 driven rank-sums p-val = 0.0283]. Fast spiking units were not significantly different between vM1 and vS1 in both the control and sensory driven conditions [FS vM1vs vS1 baseline rank-sums p-val = 0.399, FS driven rank-sums p-val = 0.960]. Within regions there were no significant changes in RS Fano Factors during control and driven conditions [RS vM1 baseline vs driven p-val = 0.32, RS vS1 baseline vs driven p-val = 0.068], however there was a significant change within vS1 FS units, increasing from baseline conditions [FS vM1 baseline vs driven, Wilcoxon p-val = 0.376, FS vS1 baseline vs driven Wilcoxon p-val < 0.01].

In summary, vS1 FS units Fano Factors increase when driven. vS1 RS units were not different when sensory driven. The major difference between regions is vM1 units have relatively stable Fano Factors during baseline and sensory drive. Perhaps vM1 does not require the same

precision as vS1 or vM1 may be more noise tolerant or it is simply the result of broad inputs to vM1.

After determining the variability of the sensory responses we explored if the evoked firing rates and the number of sensory driven positions were different. First, we identified all sensory driven units, then we noted which stimulus positions evoked a sensory response. We compared the number of sensory driven positions per unit. This method estimates the rough size of a units' receptive field. We found that both vM1 RS and FS units had significantly fewer sensory driven positions to their vS1 counterparts (Figure 2B) [vM1 RS mean ± sem: 3.92 ± 0.24, vS1 RS mean ± sem, 4.90 ± 0.27, rank-sums p-val < 0.01, vM1 FS mean: 3.95 ± 0.47, vS1 mean: 5.66 ± 0.27, rank-sums p-val < 0.005]. Somatosensory units were driven by many positions as have previously been reported (S. Pluta et al., 2015; S. R. Pluta et al., 2017). Regular spiking vM1 units skewed towards fewer sensory driven positions per unit while vS1 skewed towards many sensory driven positions overall. We hypothesized that vM1 units would have a wide receptive field due to the broad sensory inputs converging on vM1 from vS1 and the PoM but that is not the case. The limited number of sensory driven positions may serve as a broad representation of space where many whiskers are making contact. A neuron may integrate inputs across many whiskers and only fire if a set number of whiskers make contact in its receptive field. If units are distributed heterogeneously then vM1 as a whole would be broadly tuned.

Now that we knew the shape of the receptive fields we moved on to measure their magnitude. While vM1 units encode fewer driven positions than we expected it was important to determine how stimuli were encoded at each position. We did this by computing the evoked firing rate for all units at all driven positions. Evoked rates were calculated by taking the firing rate during the stimulus period and subtracting off the firing rate, in an equivalent time window, during the baseline period prior to object movement. We found that while there was a lot of overlap between vM1 and vS1 evoked firing rates there were two distinct differences (Figure 2C). First, vM1 RS units had significantly lower evoked firing rates than vS1 RS units second, vM1 units' mean evoked firing rates were more tightly distributed with few units exceeding 20Hz [vM1 RS mean ± s.e.m: 4.19 ± 0.41 (Hz), vS1 RS 8.28 ± 0.48 (Hz), rank-sums p-val = 1.327e-07, Leven test of variance p-val = 8.132e-05]. Evoked rates from vS1 RS units covered a much wider range of firing rates. Similarly, FS units in vM1 had lower firing rates in a much narrower band than vS1 FS units. [vM1 FS 16.64 ± 1.40 (Hz), vS1 FS 27.22 ± 1.83, rank-sums p-val < 0.01, Levene p-val < 0.001]. This shows that vM1 units represent the same stimulus with lower and tightly bound evoked firing rates. This suggests that vM1 can accurately represent a mean variable over a longer timescale, while its single trial accuracy is less important as revealed by the Fano Factor analysis. This fits the hypothesis that vM1 cares about slow timescale variables and that a general representation of space is sufficient for vM1's role.

We performed the same analysis mentioned above, replacing evoked rates with mean absolute firing rates. The overall shape of the distribution was similar to the evoked rates. However, the differences between the means of the distributions were not as striking as those with evoked rates. There was a small and significant difference between vM1's and vS1's mean firing rates [vM1 RS 14.805 ± 0.07, vS1 20.401 ± 0.97, RS rank-rums p-val < 0.05, vM1 FS 16.64 ± 1.4, vS1 FS 27.22 ± 1.83, rank-sums p-val < 0.01]. There was also a large and significant difference between the variance of vM1units, being more tightly bound that vS1 units [RS Levene p-val =1.367e-09, FS Leven p-val < 0.01]. Both RS and FS units have lower mean firing rates than those in vS1. However, vS1 has a skewed distribution with most of its mass overlapping with vM1 mean firing rates. The long tail indicates one of the clearest differences between vS1 and vM1, the vS1 population has a sparse but influential number of strongly driven positions. Overall the majority of vM1 sensory tuned neurons overlap with vS1's absolute mean firing rates.

After determining vM1's responses were lower in both firing rate and dispersion we wanted to understand how strongly the units encoded stimuli relative to their spontaneous activity. The spontaneous firing rate of a neuron can influence its "signal-to-noise" ratio, making it easier or harder to read. If two units have the same evoked rate, say 10Hz, but one unit's baseline firing rate is 11Hz while the other unit's firing rate is 101Hz then the signal in the former will be much easier to identify, a full order of magnitude easier to identify. Thus if the vM1 population is made up of units with a variety of spontaneous rates, and similar evoked rates, then reading from the population will become more difficult with the number of high firing rate neurons present. Taking the absolute firing rate from each sensory driven position we then divided each with its baseline firing rate (Figure 2D). Similar to our previous results, vM1 had a smaller firing rate to baseline firing rate ratio. The shape of each distribution was similar in shape to their respective evoked and absolute firing rate distributions. The units with the greatest ratios were those from vS1. Sensory driven units in vM1 are limited to a smaller range of firing rates and respond to fewer stimuli.

We next wanted to classify vM1's tuning to better understand how the population encodes the spatial environment. We hypothesized that vM1 would have broadly tuned units similar to a flattened Gaussian curve, likely due to vM1's broad sensory input making it difficult to represent many positions clearly. We found that many vM1 units were irregular in shape and not the Gaussian shape we expected. Because we wanted to include all data, and not limit ourself to Gaussian shaped tuning curves, we opted for selectivity, a custom non-parametric statistic developed in the lab. We found that the mean selectivity between vM1 and vS1, for both RS and FS units, were not different [vM1 RS selectivity 0.38 ± 0.017, vS1 RS selectivity 0.42 ± 0.027, rank-sums p-val = 0.488, vM1 FS selectivity 0.33 ± 0.023, vS1 FS selectivity 0.41 ± 0.015, rank-sums p-val < 0.05]. Despite vM1 having fewer driven positions per unit and lower firing rates it contains a similar distribution of tuned units as vS1 (Figure 2F). It is likely that the lower number of driven positions is what gives vM1 its diverse tuning. If only a few positions are driven than

units with low firing rates can have high selectivity, especially if the mean firing rates don't vary like in vM1. Both vM1 and vS1 regions contain units whose tuning properties cover the same broad to slightly selective tuning space.
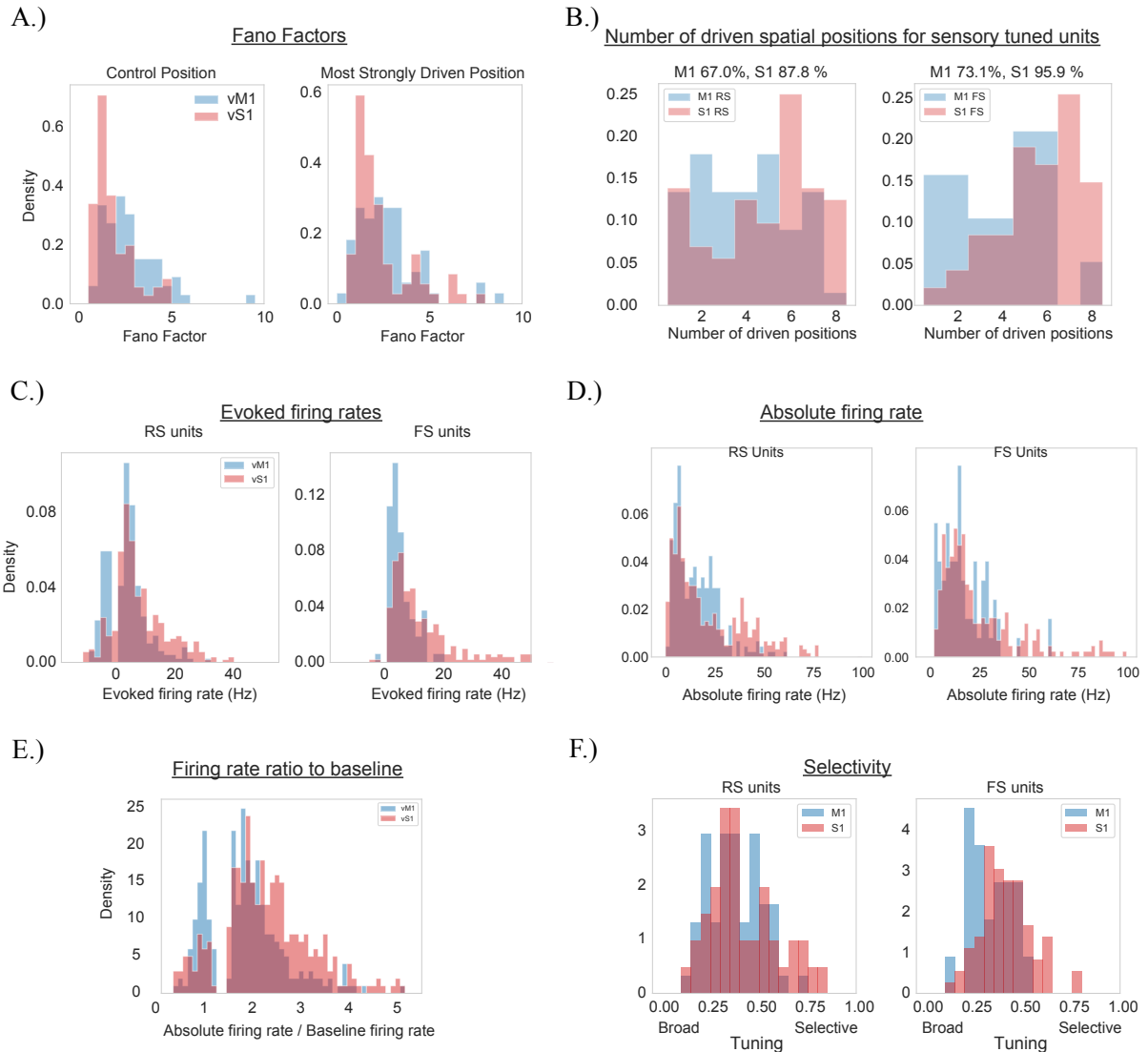

Figure 2. Firing rate analysis of all vM1 and vS1 sensory driven units. A.) Comparison of vM1 and vS1 Fano Factors for baseline/spontaneous activity (left) and for units' most driven contact position (right). B.) percentage of sensory driven units RS (left) FS (right) and distributions of the number of sensory driven bar positions per unit measuring the shape of units' receptive field. C.) evoked firing rates (firing rate during stimulus period – baseline period) for all driven positions. D.) absolute firing rates for all driven positions. E.) ratio of absolute driven firing rate to baseline spontaneous activity. F.) selectivity, classifying units tuning width ranging from broadly tuned (0) to sharply tuned/highly selective (1).

Silencing vS1 does not abolish sensory activity in vM1, while silencing vM1 has no discernable impact on vS1 firing rates

After observing the strong sensory drive in vM1 we wanted to test how the vS1 and vM1 connections impacted neural coding. We hypothesized that vS1 drove the strong sensory activity in vM1 while vM1 modulates vS1 to refine its neural tuning. There are direct cortico-cortico projections between vS1 and vM1. The feedforward connections of vS1 are thought to drive vital sensory information to vM1, which is then used to update the motor program. Many studies have shown that sensory evoked activity in vS1 is closely followed by vM1 activity but none have directly tested this. vM1 feedback projections to vS1 may modulate neural activity in order to finely tune sensory information. Previous studies have found that layer 2/3 cells in vM1 encode a variety of information including task variables, stimulus identity, and whisking kinematics (Huber et al., 2012; Petreanu et al., 2012). vM1 feedback may serve to provide vS1 with contextual information it can then integrate with sensory activity to provide a more refined sensory representation. These two reciprocally connected cortical regions have the ability to finely tune the sensorimotor loop. We wanted to understand if either region is necessary for sensory representations and, if so, what aspect of the information does it affect.

In order to determine whether vS1 and vM1 contribute to each other's sensory representations we needed to reliably silence the cortex. We used transgenic mice that express channelrhodopsin (ChR2) in parvalbumin positive (PV) inhibitory cells. This mouse line was created by crossing an LSL-ChR2-eYFP ('Ai32') mouse with a PV-Cre mouse. The cross produces mice whose cortical inhibitory cells can be activated with light, resulting in the effective silencing of all other cells within its vicinity.
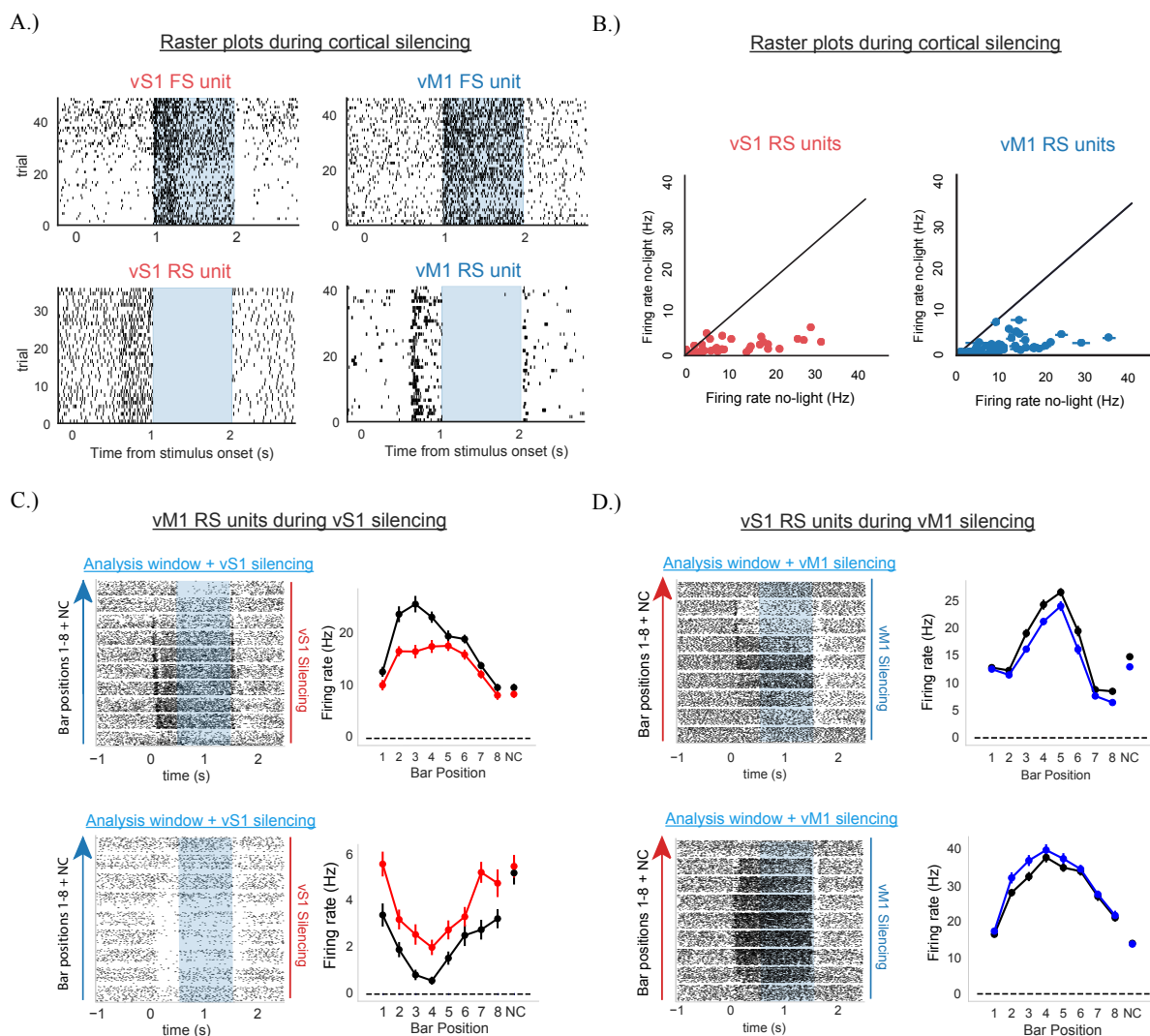
Figure 3. Activating PV+ inhibitory cells effectively silences cortex. A.) Optogenetically driven PV+ cells (top) from both vS1(left) and vM1(right) effectively silence RS units(bottom) from vS1 and vM1. B.) RS units' firing rates during silencing vs no-light conditions. C.) same vM1 units as in Figure 1D, vS1 silencing decreases the gain of vM1's sensory response bring both driven and suppressed units closer to baseline. D.) same vS1 units as in Figure 1C, vM1 silencing has a small effect on these units but is not consistent across units and doesn't impact all vS1 units.

Two example PV units are presented in Figure 3A, a fiber coupled blue LED is activated during the analysis window of the stimulus period from one to two seconds, causing an immediate increase in their firing rates. During the same light on window two exemplar RS units are depicted with the majority of their sensory driven spikes abolished. The entire RS population from both vM1 and vS1 are presented (Figure 3B), silencing reduced their largest sensory driven firing rates, ensuring that we have effectively silenced each region.

After verifying we could effectively silence vS1 and vM1 we then proceeded to test how silencing affected their sensory representations. We hypothesized that there would be a complete abolishment of sensory activity in vM1. While vM1 is known to receive sensory inputs from other regions, such as the PoM region of the thalamus and secondary cortex (vS2), it is thought that the strongest contributor is vS1. Previous studies, using voltage sensitive dye imaging, found that vM1 activity immediately follows vS1's response to whisker deflections, bolstering the idea that vS1 is the main contributor to sensory vM1. It was less clear how silencing vM1 would affect vS1. If vM1's role is to refine sensory responses or provide context to vS1 we did not expect any changes with our current experiment as mice were not tasked with identifying or discriminating sensory stimuli.

First we wanted to understand if units were always under the influence of the other region or if they only contributed when the system was under sensory drive. We first looked for any changes in the baseline spontaneous firing rates during silencing. There was no effect on spontaneous activity in either vM1 and vS1 (Figure 4A). Any observed changes with silencing were limited to driven units.

We silenced either vS1 or vM1 at random during the stimulus interval, after the object had come to a complete stop in the whisking field. The most striking effect of vS1 silencing was that it did not abolish sensory activity in vM1. On a single unit level it was clear that silencing was having an effect on vM1 but it was far from its baseline rate (Figure 3C-D). Individual tuning curves had reduced evoked rates and appeared slightly more broadly tuned. Looking at the whole population it was clear that vS1 was modulating RS and FS units; significantly reducing their mean firing rates [Wilcoxon-signed rank vM1 RS units p-val = 5.234e-07, Wilcoxon-signed rank vM1 FS units p-val = 9.548e-13]. During vS1 silencing vM1 units were modulated towards their baseline firing rates (Figure 4B). The vast majority of vM1 RS units, 70% of the driven population, increase their firing rate by stimulus contact, vS1 silencing decreased their firing rates. For the remaining 30% of vM1 RS units, those that are suppressed by stimulus contact, vS1 silencing did not decrease their firing rate, instead it increased their firing rates towards baseline. Silencing vS1 shows that during normal operation it can boost vM1's gain, giving vS1 the ability to modulate vM1's sensory signal, perhaps using its control to emphasize relevant sensory features.
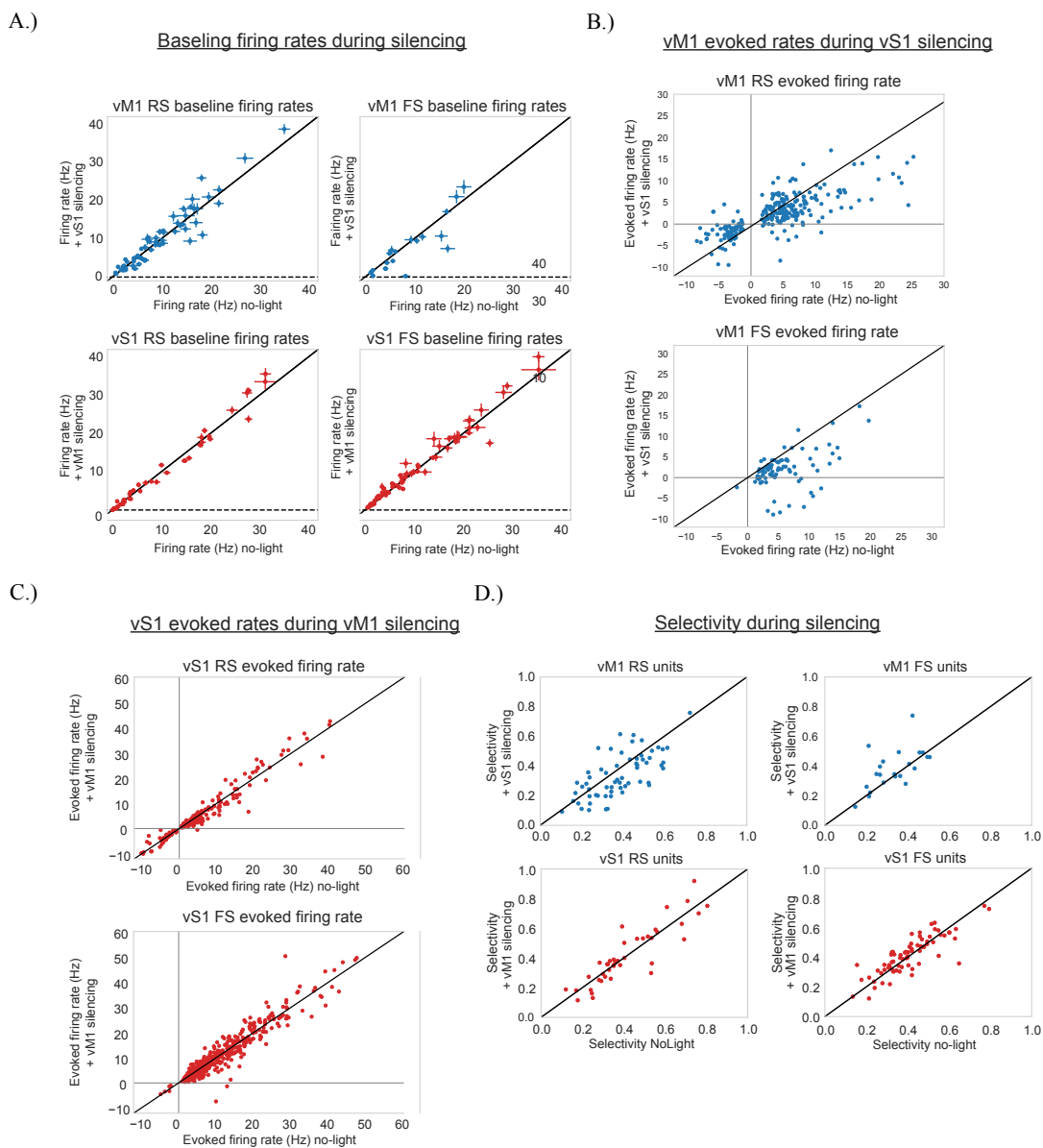
Figure 4. Effects of cortical silencing on sensory representations. A.) baseline/spontaneous firing rates, top: vM1 RS(left) and FS(right) baseline firing rates during vS1 silencing, bottom: vS1 RS(left) and FS(right) baseline firing rates during vM1 silencing, B.) vM1 evoked rates during vS1 silencing, vS1 modulates the gain of both vM1 RS and FS units. C.) vS1 evoked firing rates during vM1 silencing RS(top) and FS(bottom), vM1 does not modulate vS1 firing rates in a single direction, RS(top) and FS(bottom). D.) selectivity/tuning width during silencing, vM1 RS units broadend by vS1 silencing (top left).

The feedback projections from vM1 had little to no effect on vS1 tuning. There was no significant change across the vS1 population [vS1 RS units p-val = 0.069, vS1 FS units p-val 0.359]. However, there were many individual vS1 units that were significantly modulated by vM1 silencing, see Figure 3D. The affect was minimal and not a consistent directional effect, observing tuning curves that were either suppressed or driven during vM1 silencing.

After identifying the effect of silencing on each driven position we then wanted to understand how it impacted units' tuning. Silencing vS1 affected the firing rates of both RS and FS units, however only vM1 RS units' tuning changed, decreasing their selectivity and becoming more broadly tuned [vM1 RS Wilcoxon-signed rank p-val < 0.005, vS1 RS p-val = 0.891, vM1 FS p-val = 0.148, vS1 FS p-val 0.207]. This suggests that vS1 is responsible for modulating vM1 sensory activity in order to sharpen tuning. Silencing vM1 did not affect vS1 tuning in either the RS or FS populations. Here vM1 does not actively contribute to vS1's tuning. Since vM1's feedback pathway has been shown to modulate vS1 activity in the past, this results suggests that vM1 feedback is dependent on the environmental context of the mouse, perhaps dependent on goals and level of sensory detail required.

Neural decoding quantifies how much sensory information is present in vM1 and vS1 populations

The initial mean firing rate analyses allowed us to quantify the spiking activity of both vM1 and vS1 in response to a tactile stimuli. While it is interesting on its own, it is difficult to decipher how much information is present. Considering the observed differences between vM1 and vS1 it is difficult to tell whether those differences are meaningful. While traditional analysis methods can tell us whether two means are from different distributions or if two distributions are different, it cannot determine what impact those differences have on the underlying neural code. In order to determine how impactful these differences were we used a neural decoder to estimate how well each population represented the spatial location of the stimulus. We pooled FS units with RS units initially in order to approximate how a whole population carries information before moving on to different cell types.

A neural decoder is a part of a class of analyses commonly referred to as "optimal observers." These methods can determine how well a set of data can represent a variable of interest. We chose to adapt an optimal linear estimator (OLE), a neural decoding technique previously used in the hippocampal literature to predict the spatial position of rats via their recorded local field potentials (Agarwal et al., 2014). It is important to note that this model is not attempting to model what the brain is actually doing. Instead, it will attempt to map the input neural data to a target, the presented stimulus identity. If there is a linear combination of weights that, when multiplied by a vector of firing rates, can map single trial data to the target, the decoder will find it. This decoder estimates how much information is present in a rate code. Using the set of weights determined by the decoder we can test whether the predicted output of the decoder matches the actual value (Figure 5A). We compute percent correct classified (PCC) or the percentage of single trials that were correctly predicted during a single decoder run. This process is repeated, randomly sampling the same dataset, to estimate the range of information present in the data provided. This allows us to better estimate how well the sensory environment is mapped in a population of neurons.

Using data from a single experiment we found that the decoder made reasonable predictions for both vS1 and vM1 data. Prediction from vS1 data outperformed vM1 by 20%. However, vM1

164

still performed very well decoding 40% PCC, far from chance levels of 12.5%. Confusion matrices produced from vM1 decoding indicated that mistakes were reasonable, predicting neighboring positions for the actual position, rarely predicted distant positions. This is likely due to vM1's lower firing rates and greater single trial variability as seen in its Fano Factor distributions as both will make distinct stimuli blur together. We shuffled stimulus labels to verify that the decoder was not inherently biased, then retrained the decoder, and assessed its predictions. The PCC distributions for both shuffled vS1 and vM1 data were at chance levels centering at 12.5%. We repeated this analysis for other experiments and found that the predictive power depended heavily on the sample collected, making it difficult to make general inferences. To compensate for this all experiments were pooled, creating an artificial large population, to get a more accurate approximation of vM1 and vS1 populations.

Utilizing the entire dataset allows us to estimate the predictive power of each region as a function of population size or cell type. Using shuffled populations of different sizes can estimate the amount of information present per neuron as well as estimate how much information is added as the population grows. Here we randomly sampled n units from a population size of N. On each decoder run n units are randomly selected from N, the data is used for decoding, performance metrics (PCC) are calculated and recorded, and the process continues for x number of runs in order to get a good estimate for that subsampled population size. This process is repeated for the entire N units in the population. It is important to note that as the subsampled population n approaches the size of the total recorded population N the true width of the distribution artificially gets smaller. This is because individual units will get selected more frequency until $n == N$ units are present in the subsampled dataset. This is why the standard deviation decreases with the number of units present in the decoder.

At low subsampled population sizes vM1 and vS1 have similar predictive power. vM1 and vS1 were indeterminable with populations consisting of less than five units and remained overlapped by one standard deviation for eight units. Every additional unit from vS1 increases predictive power rapidly, quickly outperforming vM1's predictive power per unit (Figure 5C). Decoding with the mid-range number of units (20-40 units) is when the difference between regions begins to stabilize. At 20 units vS1's predictive power was 20% better than vM1 with a mean accuracy of 65% while vM1's accuracy is 45%. In order for vM1 to achieve the same predictive power that vS1 has with 20 units vM1 would require 40 units to achieve 65%. Interestingly, that is the same point where vM1's predictive power plateaus, 40 units, any additional units from this dataset make no further progress in predictive power. Around 45 units vS1 begins to plateau at 80% PCC and finally reaches a maximum at 85%. Both regions performed very well when compared to chance. Single units, even a poorly tuned ones, were able to provide some stimulus information. No single unit ever hit chance levels of 1/8 or 12.5%.

Optogenetic silencing decreases both vM1 and vS1 decoding performance

We expected silencing vS1 to decrease the predictive power of vM1 data and silencing vM1 to have no effect on vS1's predictive power. A decoder was trained on datasets composed of mean firing rates from one region while the other region was silenced. We did not use the weights found previously in the no-light trials. We wanted to determine if any stimulus information was present instead of determining whether information was encoded in the same way as the no-light condition.

First, decoders were trained with all units from a region to test if silencing produced an observable effect. Silencing vS1 decreased decoding performance using vM1 data. The change in PCC was 5% and accompanied by a noticeable difference in no-light and vS1-silencing confusion matrices (Figure 5B). Decoding with vS1 data during vM1 silencing resulted in an unexpected small decrease in performance. Because vS1 firing rates were unaffected by vM1 silencing we were dubious of this result. We repeated the decoding process multiple times to estimate the range in performance within each region's population. The PCC distributions can be seen in Figure 5B. Silencing vS1 noticeably decreases vM1's predictive power as shown by the shift in vM1's PCC distribution. However, vM1 silencing caused a small negative shift in vS1's predictive performance. To investigate this further we repeated the subsampling analysis for silenced trials in order to determine if the decrease in vS1 predictive power was constant across all population sizes.

The performance between vM1 no-light and vS1-silencing conditions started to clearly diverge as the number of units in the decoding population increased. At ten units the no-light PCC curve for vM1 was one standard deviation away from the silencing groups standard deviation. The maximum decrease in performance was a 15% reduction from the no-light condition (Figure 5D). Earlier firing rate analyses found that vM1 firing rates decrease with vS1 silencing, however it unclear how these changes affected the underlying sensory representations. Using a decoder is advantageous because we can use it to quantify how changes in firing rate affect the amount of stimulus information present in the population. All together vS1 silencing reduced vM1's mean firing rates causing a decrease of predictive power of 10-15% with a 60 unit dataset. This suggests that under normal conditions vS1 drastically improves vM1's accuracy, providing it with high fidelity information about the tactile environment.

Interested in determining if vM1's feedback influences vS1 we repeated the same analyses above with vS1 data during vM1 silencing. The firing rates of vS1's population were not significantly different during vM1 silencing. However, on a single unit level many units' did have significant changes to their tuning curves or to a few positions. Those small changes were not consistent or directional across the entire population. It is difficult to determine whether multidirectional changes are meaningful but analyses like decoding and machine learning may be able to find

relationships from seemingly random changes in firing rates. Interestingly, vS1's decoding performance dropped during vM1 silencing (Figure 5D). The maximum predictive performance of vS1 units with no-light was 85%, silencing vM1 caused that value to drop down to 75%. We found that silencing had no effect on vS1 populations with less than 20 units. After 20 units the performance trace diverges from its normal no-light trajectory. Comparing both vM1 and vS1 performance with a 60 unit population we found a comparable decrease in PCC curves during silencing.
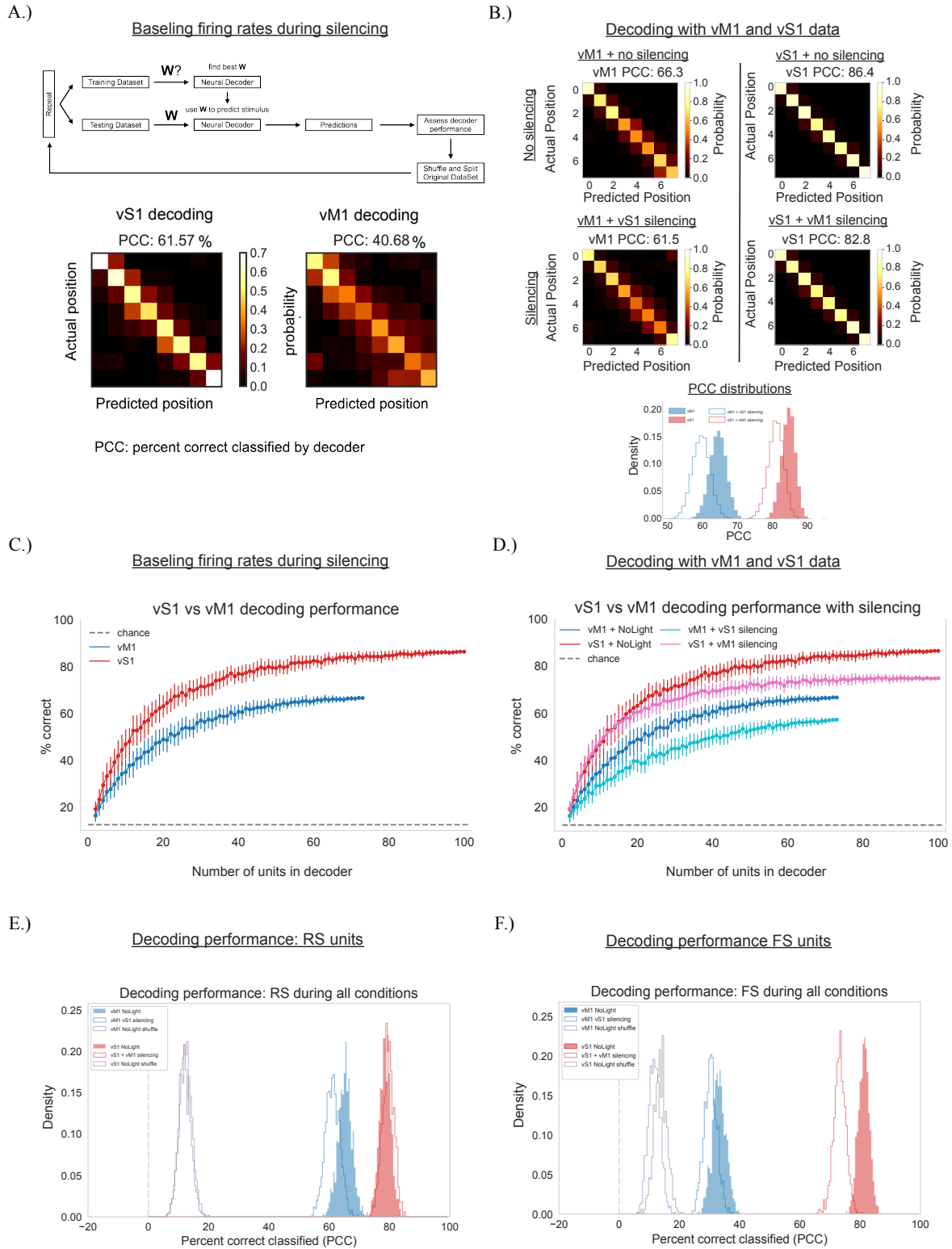
Figure 5. Decoding quantifies how well vM1 and vS1 represent sensory information. A.) decoding schematic (top), the repeat section is used to estimate PCC distributions, (bottom) decoding using single experiment data, confusion matrices summarize the probability the decoder predicts a stimulus position when given data from a

particular position. B.) Decoding with all experiments, (top) confusion matrices summarize decoder performance for vM1 and vS1 data, (middle) decoding performance during silencing, vS1 silencing decreases vM1 maximum performance by ~5%, vM1 silencing slightly decreases vS1's maximum performance, (bottom) distribution of PCC from multiple decoding runs. C.) vM1 vs vS1 decoding performance vs size of population, subsamples of units are randomly selected. The variance decreases with number of units as the same units get selected more frequently. D.) same as in C during silencing, vM1 performance decreases with vS1 silencing for all sample sizes, vS1 decreases performance with vM1 silencing for samples greater than 20. E.) RS units decoding performance during no-light, silencing, and shuffled conditions. F.) FS units decoding performance

After discovering that vM1 silencing decreases vS1's sensory representations we sought to identify what was causing it. We began by splitting data by cell-type looking for differences between RS and FS units. Regular spiking units in vS1 had high predictive power allowing the decoder to predict stimulus positions at 80% PCC. vM1 RS units also contained a high level of stimulus information, predicting up do 65% PCC. However, it was only vM1 units that were negatively affected by silencing, decreasing performance by 5-10%. vS1 RS units had absolutely no change in PCC during vM1 silencing. This suggests that vM1 feedback projections do not impact vS1 RS units, at least in this context. As a control we took both vM1 and vS1 data, shuffled them, and attempted to decode (Figure 5E). We found that both datasets were at chance levels ensuring that the decoding system is not biased internally.

Fast spiking vM1 units had moderate predictive power centered at 35%. These units, similar to their RS counterparts, also decreased their performance during vS1 silencing. The decrease was slightly less than that observed with RS units, decreasing by 5%. Unlike vM1, vS1 FS units had a huge amount of predictive power, just slightly outperforming vS1 RS units with a PCC of 80%. It is interesting to note how much stimulus information is present in FS units' firing rates. Typically FS units are less tuned than RS units (Naka, 2018; S. Pluta et al., 2015). Not only were FS units well-tuned but those in vS1 were affected by vM1 silencing with a decrease in predictive power of 7-10%. The mechanism is unclear at this point but this was the first significant affect vM1 silencing had on vS1.

Cortical silencing does not impair whisker motion

Silencing had a clear impact on firing rates as well as the amount of sensory information present in vM1, and to a much lesser extent, vS1. But we did not know if silencing had impacted whisker motion. Both motor cortex and sensory cortex have the ability to drive whisking. Motor cortex, defined and long known as the region that drives whisker motion when electrically stimulated, is thought to play a crucial role guiding whisker movements. Recent studies have found that somatosensory cortex can also drive whisker motion. When stimulated vS1 can rapidly retract whiskers independently of vM1. This means that vS1 and vM1 may work as a push-pull system, both directing whisker movements while simultaneously processing incoming sensory information. Combined with the robust sensory representations in motor cortex this further blurs

the functional lines that separate distinct cortical areas. We set out to determine whether vM1 was necessary for whisking and determine if vS1 contributes to whisker control. We hypothesized that vM1 would be necessary for whisker motion, if not for the cycle-by-cycle commands, then for slow timescale variables such as setpoint. Quantifying how silencing impacted whisking would also determine if the changes in firing rates were due to changes in whisking or from solely neural computations.

To test if vM1 or vS1 contribute to whisker motion we used a high speed camera to image the rapidly moving whiskers throughout individual trials. Our analysis focused on whisking setpoint and the dominant whisking frequency. For each variable differences were calculated between no-light and silencing conditions. Silencing vM1 did not abolish whisking, strikingly mice continued to run with no obvious changes in whisker motion. The most likely variable to be affected by vM1 silencing is setpoint, the sector of space that the whiskers are currently sweeping. We found no differences in set-point, during the no contact control position, when mice freely whisk or while mice whisk against the vertical poll stimulus. We expected vM1 to adjust setpoint in order to make optimal contact with the stimulus at its various positions. Instead, mice whisked the same way for all trials (Figure 6A). We then looked for changes in whisk frequency, we computed the dominant whisking frequency during no-light and silencing conditions and found no significant difference in whisk frequency during vM1 silencing (Figure 6A). Silencing vS1 did not affect setpoint or whisk frequency either.
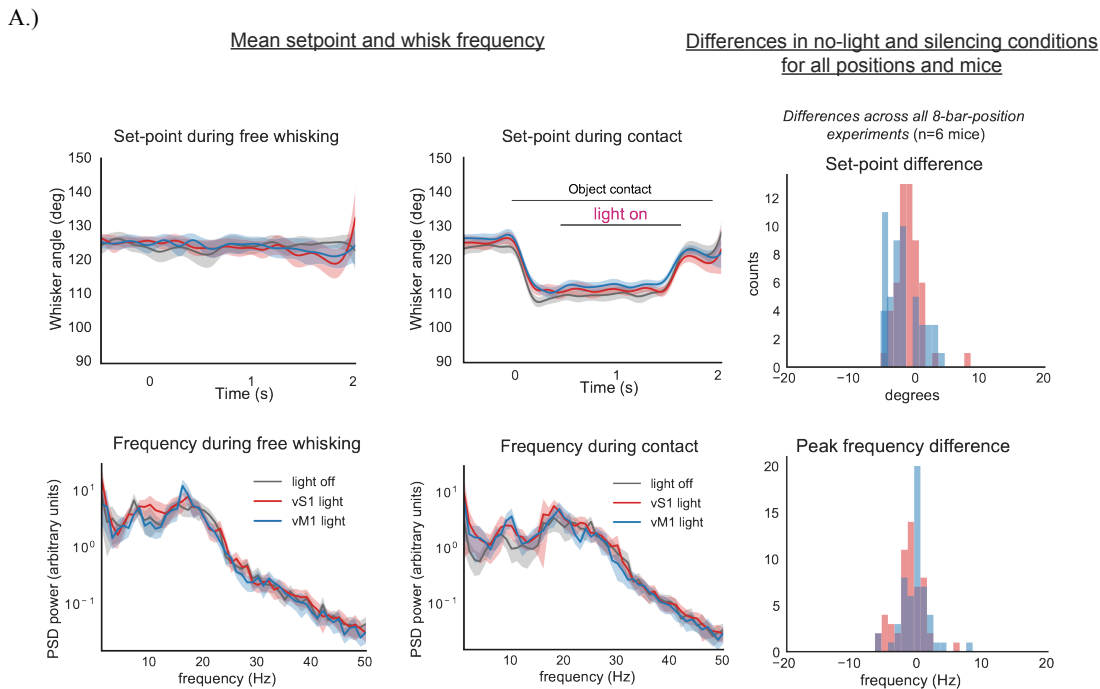
A.)

Figure 6. Silencing effects on whisking. A.) (top row) setpoint during free whisking/control position, setpoint at

contact position, distribution of mean setpoint differences (silencing vs no-light) with no significant effect. (bottom row) whisking frequency distributions for free whisking/control position, contact positions, and distribution of peak frequency differences (silencing vs no-light) with no significant effect.

Altogether, there was no evidence of even the slightest change in whisking. The incoming sensory information from vS1 to vM1 was not required to update the motor program in this context. The vM1 silencing results were the most unexpected, as whisker motor cortex is thought to drive or modulate whisker movements, guiding whiskers to sweep a sector of space. Because silencing had no impact on whisker movements we are assured that all differences in neural activity are due to changes in the underlying neural processes instead of disrupted sensory input.

vM1 and vS1 are required for a whisker dependent discrimination task.

The whisker motor program was unaffected by silencing. All previous evidence suggests that vM1 is responsible for whisker movements, with decades of evidence demonstrating that vM1 can drive whisker movement and that is encodes whisking kinematic variables. However, the neural encoding of whisker motion is correlative, it is unknown if the encoded motor variables actually contribute to motion or other processes. Stimulation experiments demonstrate vM1 has the capacity to drive whisking but it does not demonstrate that it is necessary for all types of whisker movement.

Projections from vM1 and vS1 terminate in brainstem motor nuclei. The vM1 projection terminates in the Reticular formation, a region that can produce rhythmic whisker protractions independently of vM1. While vS1 terminates on the Spinal Trigeminal nucleus, which synapses directly on the whisker pad retraction muscles. The anatomy suggests that while both vM1 and vS1 can elicit movement they most likely modulate the brainstem structures that control the cycle-by-cycle whisker commands.

Anatomy and stimulation studies show that vS1 and vM1 can modulate whisking but it is unclear when they naturally do this. We wanted to find a context where they actively modulate whisking, here we focus primarily on vM1's role. We hypothesized that cortex would modulate the whisker program if mice were in a demanding tactile environment. A place where they needed to extract detailed tactile information or perform a behaviorally relevant tactile task that demands precise whisking. Mice can control their whiskers in intricate ways, they can asymmetrically whisk, remain a constant distance from a wall using only whisker tips, and "foveate" focusing on a small region of space measuring gap distances or platform details. It is likely that these types of whisking strategies are dependent on vM1. In our eight-position pole experiment mice do not have to modulate their whisking, there is no goal or task, the sensory information is not behaviorally relevant to them. We wanted to find a context that would require cortical modulation of whisker motion.

In order to test this hypothesis, we used a whisker GO-NOGO discrimination task developed in the lab (Brown et al., 2021). Here, a bar is presented to the center of a mouse's whisking field. The bar is then rotated to one of eight angular positions, four adjacent angles are associated as "GO" trials and the others associated as "NOGO" trials (Figure 7B). Water restricted mice are trained to lick during GO trials for a water reward, licks during NOGO trials receive an air puff and a brief timeout (Figure 7A).

We expected that trained mice would need to use adaptive whisking strategies to determine if the stimulus was in a GO or NOGO angle. As the angle differences between GO and NOGO angles decrease more precise whisking would be required. We suspected that vM1 would play a crucial role for the most difficult angles, modulating whisker movements to get precise information. Alternatively, the positions with the greatest angular distance would not require adaptive whisking, expecting mice to use a simpler detection strategy. Early in training we wanted to determine if changing the experimental design and apparatus was enough to engage vM1. Silencing vM1 in mice that were completely naïve or had just begun training did not affect whisker movements. Assuring us that the lack of change in whisking was not unique to our setup.

After mice became fully trained we assessed the impact of both vS1 and vM1 silencing. Silencing vS1 drastically reduced task performance, our results conferred with previous vS1 silencing results on this task (Brown et al., 2021). Silencing caused a drastic increase in false alarm rates for NOGO trials, while GO positions were largely unaffected (Figure 7D). Additionally, whisker motion was unaffected by vS1 silencing with setpoint and whisk frequency PSD overlapping with their respective no-light condition traces (Figure 8D). In this context, vS1 acts primarily as a sensory area, playing no role in modulating the outgoing whisking strategy.

Fully trained mice depend heavily on vM1 for successful task performance. We observed a significant decrease in task performance during vM1 silencing. Similar to vS1 silencing, vM1 silencing negatively impacted NOGO trials, dramatically increasing false alarm rates. Differing from vS1, vM1 silencing had a minor effect on GO trials, decreasing licking for correct responses. The decrease in performance on silenced GO trials was variable across mice. Four example psychometric curves from four mice depicts the strong impact of vM1 silencing (Figure 7C).
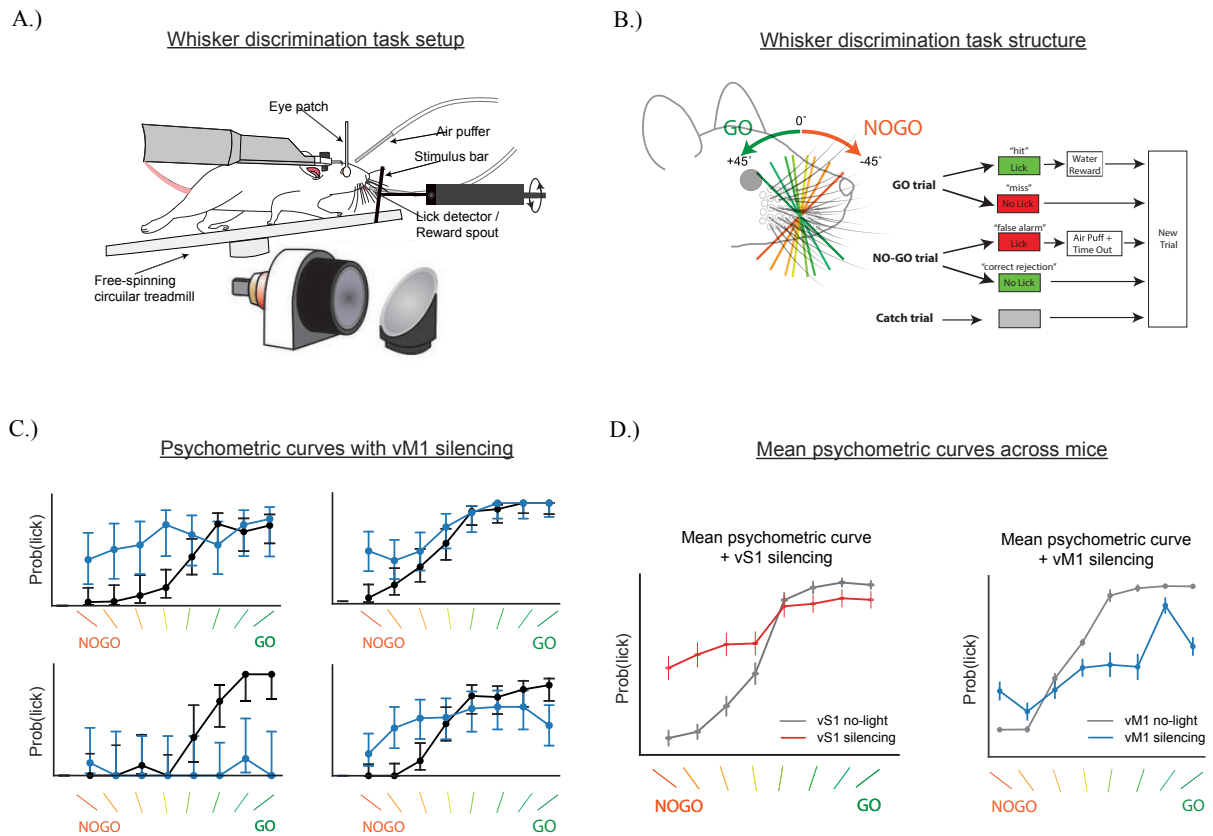
Figure 7. vM1 plays a key role in a whisker dependent discrimination task. A.) Experimental setup, the vertical pole is replaced with a rotating pole, rotated to one of eight angles. B.) GO vs NOGO positions and behavior task schematic. C.) psychometric curves from four mice, vM1 silencing decreases mouse performance impacting NOGO positions more than GO positions. D.) mean psychometric curves across mice comparing vS1 silencing (left) and vM1 silencing (right), vS1 impacts primarily NOGO positions and vM1 impacts both NOGO and GO.

Silencing vM1 during a behaviorally relevant task disrupts proper whisker motion. Silencing began at the onset of stimulus movement and ended after the decision period, remaining illuminated for two seconds (Figure 8A, blue bar: silencing period, grey bar: decision window). Whisking was affected at the onset of light, instead of at object contact as we had hypothesized. The set-point immediately retracted and was consistent across all mice tested (Figure 8C). The change was substantial, especially when compared to whisking data from previous experiments. The whiskers continued retracting until the stimulus came to rest. There was also a substantial change in the whisking frequency, the peak frequency shifted to a lower frequency during silencing (Figure 8C). Silencing vS1 did not have any effect on setpoint or whisk frequency (Figure 8D). Neither of these effects were observed when silencing untrained mice. This suggests that vM1's effect on whisking is context dependent and may change specific parameters depending on the tactile environment.
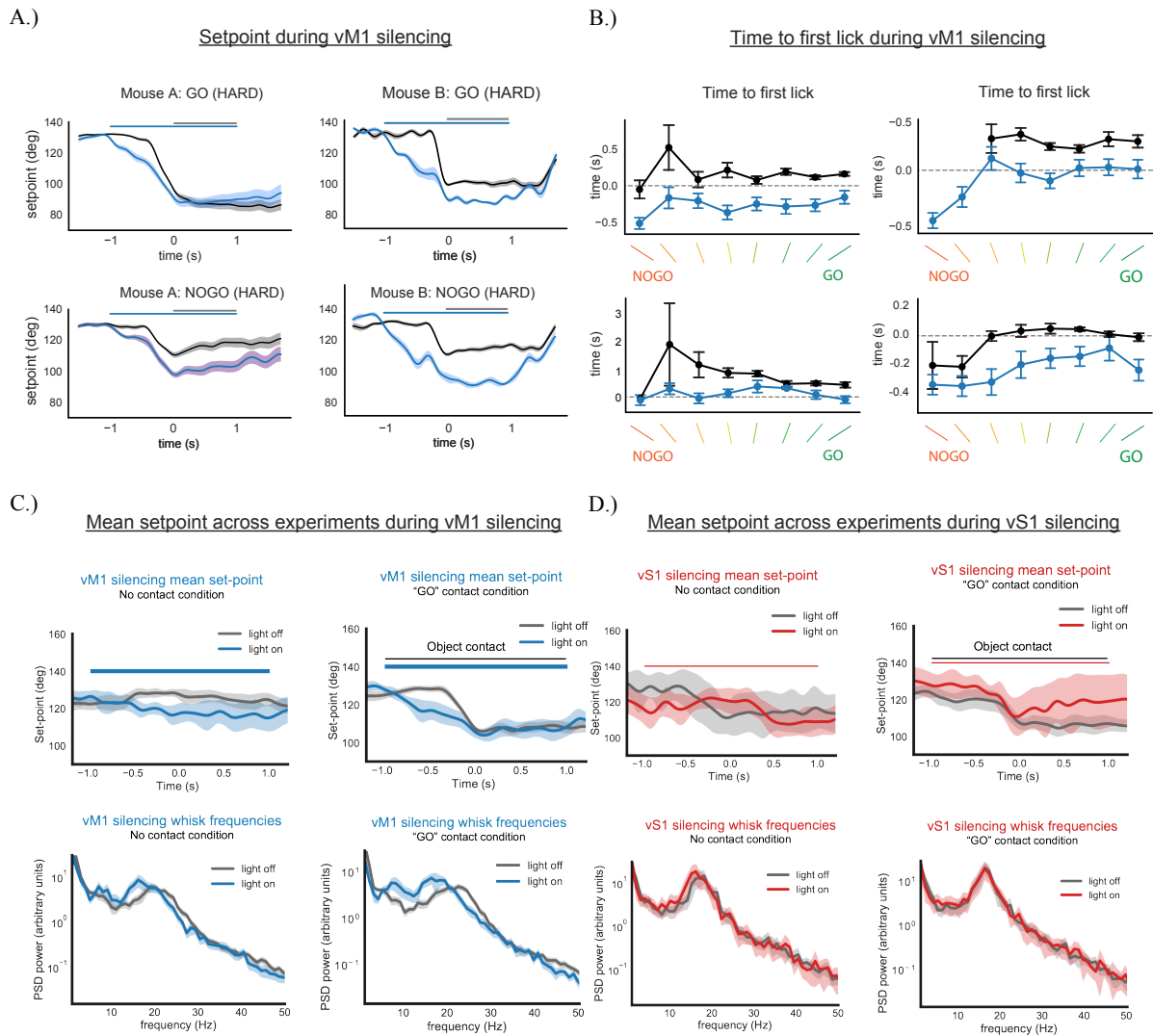
Figure 8. Silencing vM1 disrupts whisking and lick onset. A.) silencing vM1 in trained mice decreases setpoint in GO and NOGO positions regardless of difficulty. B.) silencing vM1 increases lick onset causing licks to occur prior to the stimulus comes to a stop. C.) mean setpoint across mice for not contact and contact trials, vM1 silencing reduces setpoint at light onset and shifts the whisk frequency distribution. D.) same as in C. mean setpoint and whisk frequency of trained mice during vS1 silencing, vS1 does not impact whisking during this task.

Lastly, and most unexpectedly, vM1 silencing caused an earlier onset of licking. Licking occurred prior to or immediately when the stimulus came to a stop. During non-light conditions licking occurred after the stimulus stops (Figure 8B). It appears that vM1 may play an important role withholding licks or more generally contribute to impulse control, a function that is usually carried out by higher cortical areas.

Somatosensory cortex is essential for the discrimination task but only as a sensory processing area. Silencing vS1 caused as increase in false alarm rates at the NOGO positions but did not

cause changes in whisking or other behavioral variables. Surprisingly, vM1 also impacted performance similarly to vS1 but not in the way we had hypothesized. During vM1 silencing mice licked more during NOGO positions, similar to vS1. However, vM1 silencing also impacted GO positions, decreasing licking on GO trials to a minor extent. The greatest differences from vS1 were the decrease in whisker kinematics, setpoint and whisk frequency, as well as lick onset. Only trained mice were affected by vM1 silencing, naïve mice were completely unaffected just as the mice in the earlier non-task experiment. It is important to note that our silencing paradigm likely silenced regions outside of vM1. The transgenic mouse line used here expresses ChR2 in all PV cortical cells, any light outside of vM1 would silence neighboring regions. The only likely region that could have caused this behavior is the ALM, it has been shown to affected licking direction in 2AFC tasks. However, the ALM has not been shown to impact whisking as shown here. Regardless of whether it was vM1 or not the effect of silencing did require learning to become apparent, as the same silencing technique was used in the 8-pole-position experiment and on naïve mice with no impact on whisking.

Silencing vM1 caused a consistent retraction of setpoint at the onset of light and continued until the stimulus came to a stop, this effect was observed on all trial types, including GO trials. Therefore, it is unlikely that changes in performance be attributed to changes in whisker motion, as mice were able to perform well on GO trials despite the changes in whisking. Additionally, silencing vM1 impacted lick onset causing mice to lick earlier for NOGO positions. Given the other smaller effects on licking it appears that vM1 is more than just a sensory and motor region. If the changes in performance are not due to changes in whisking then perhaps vM1 plays a more general role, acting as a sensory cortex. It is possible that vM1 may act as a higher order brain region, given its impact on response inhibition, but this requires more study.

Discussion

Our study has shown, for the first time, how vibrissae motor cortex encodes sensory information which is modulated but not driven by vS1 and identified a context where vM1 is critical for behavioral performance, whisker modulation, and lick responses. Here we explored vM1's multifunctional capability behaving as a sensory, motor, and possibly higher cognitive region. vM1 sensory activity is gain modulated by vS1 instead of being driven by vS1 as previously thought, vM1 is not necessary for whisking unless mice are in a context that demands precise sensory information, and lastly vM1 is necessary for a whisker discrimination task impacting both behavioral performance, whisker movements, and lick onset demonstrating vM1's broad capabilities. These data demonstrate that vM1 is more than just a motor cortex, acting as a general multifunctional cortical region. This expands on previous work exploring vM1's various functions and the idea it is a higher cognitive area. We believe that cortical regions in lower order animals can be more generalized than their higher order counterparts, performing a multitude of functions that would require multiple dedicated cortical regions in higher order species (C.L. Ebbesen & Brecht, 2017; Lopes et al., 2016; Petersen, 2014; Sreenivasan et al., 2016).

Sensory activity in vM1 is robust and consistent over long timescales. Driven units had little variation in their mean firing rates across many trials. However, on a trial-by-trial short-timescale level they had greater neural variability than vS1 units (higher Fano Factor), suggesting that short-timescale representations aren't necessary for vM1's role. Precise firing rates may not be necessary for the control of slow varying whisker kinematics such as setpoint and amplitude. Alternatively, if vM1 is a generalized multifunctional cortical area it may only need a general picture of the environment. In this case it may modulate other areas, such as motor regions in the brain stem, to perform a certain task acting more as a director than an actor.

Individual vM1 units respond to fewer stimulus positions than vS1 and respond with lower evoked firing rates. Given these differences it is interesting that both vM1 and vS1 have a similar distribution of broad to sharply tuned units, covering the majority of the tuning space. Non-parametric selectivity was not different between the two regions. This suggests that vM1 receives information from the entire whisker space but it is encoded at a much lower resolution than vS1's map.

Silencing vS1 decreased vM1's sensory responses. This was surprising because vS1 is thought to drive the sensory responses in vM1. The sensory drive to vM1 is likely from the PoM region of the thalamus. The PoM is a multiwhisker sensory thalamic nuclei which projects heavily to vM1. Because PoM sensory responses are not as precise as vS1's, this may provide vM1 with a broad sensory drive, providing an overview of the sensory space, which vS1 then gain modulates to

increase fidelity. It would be interesting to see if vS1 modulates units with specific sensory information, essentially boosting the signal of relevant stimuli.

vM1 silencing has little effect on vS1 firing rates. The firing rates in vS1 did not experience a directional shift in neural activity. On a single unit level some vS1 units were significantly modulated by vM1 silencing but the changes were not consistent across units. It is difficult to interpret this on a population level because it appears as noise. While the overall change in the population response may look like noise, this "scrambled" data may impact the underlying neural representations, thus causing a decrease in decoding performance. Considering the diversity of neural activity via the complexity of cortical circuits, the population response may not have to change in a singular direction in order to indicate a different representation. Methods like decoding are useful because they have a chance to determine a relationship that may be overlooked with more traditional analyses. We used a neural decoder to quantify the relative differences in sensory information between vM1 and vS1

Decoding allowed us to quantify how much sensory information was present in the vM1 and vS1 populations, finding that vS1 consistently had more information than vM1 peaking at 85% correct. Decoders using vM1 data performed well, reaching above 60% correct with sample population size of 40 units. During vS1 silencing vM1 decoding power decreased for all sample sizes, as we expected from the observed gain modulation. Surprisingly, vS1 performance also decreased during vM1 silencing. This was completely unexpected as vM1 had failed to cause a directional change in vS1 firing rates. We believe that the decoder was able to find underlying structure in vS1's data suggesting that the small changes observed in some vS1 units was enough to disrupt normal sensory representations. This indicates that vM1 feedback projections contribute to vS1's sensory representations even in the absence of a demanding task. Methods like this are incredibly powerful. While the decoder used here is simple compared to other analysis techniques, it can still contribute valuable information, finding relationships that may have been missed.

Silencing vM1 did not impact whisking during the spatial tuning task. Whisking was not abolished or affected in any way during vM1 and vS1 silencing. Both cortical regions have the ability to impact movement but they are not required in this context. The spatial tuning task is not a true task, mice do not have to extract precise sensory information, the pole positions are not associated with a behaviorally relevant reward, giving the mouse no reason to use adaptive whisking strategies. We used a tactile discrimination task to test whether a demanding tactile environment would require vM1 modulation.

In the whisker discrimination task vM1 played a crucial role impacting both performance, whisker movements, and lick response. Silencing vM1 produced similar psychometric curves to vS1 silencing. However, vM1 changed whisking while vS1 did not. We found that vM1

177

silencing caused the whiskers to retract their setpoint at the onset of light and caused them to decreased their whisk frequency. We were surprised that setpoint changed at the onset of light as we expected adaptive whisking to occur at stimulus contact. Extending the whiskers forward in expectation of the stimulus must be under vM1's active control. We believe that the changes in whisking were not responsible for the decrease in task performance. Light affected all positions, including GO positions, which mice were able to perform as usual. Additionally, silencing caused mice to lick earlier than normal. Taken together it appears that vM1 may play a role in response inhibition or in the early stages of decision making perhaps acting as a sensory accumulator. Alternatively, disrupting vM1's sensory representations may have been responsible for the mistakes. It is important to note that our silencing methods effect an area larger than vM1, which is a very small target with not clearly defined borders. We searched the literature and did not find other brain regions near vM1 that could produce the effects we observed. The ALM, which is anterior to vM1, does modulate directional licking (Chen, Li, Daie, & Svoboda, 2017), biasing mice to one side or the other during a 2AFC. However, they have not reported changes in whisking as seen here. We cannot be sure that vM1 is responsible for the behavioral effects, however it is important to note that the same silencing technique was used during the two different experiments. Whisking was only affected in trained mice, if vM1 is not responsible than one of its neighbors is.

Here we have quantified sensory tuning in vM1 for the first time while simultaneously measuring vS1's responses to the same stimulus. We found that vM1's responses are lower and driven by fewer stimulus positions than vS1. Overall, vM1 has a good representation of the sensory space but it is less detailed than vS1. We also found that vS1 is not the source of vM1's sensory representations as previously thought. Instead vS1 plays a critical role modulating the gain of vM1 sensory units. Under normal conditions vS1 increases the sensory signal away from the unit's baseline activity. vM1 silencing does not change vS1 firing rates in a directional way, decoding revealed that vM1 still impacted vS1 sensory activity decreasing prediction performance. vM1 also decreased its activity during vS1 silencing as expected due to the loss of sensory gain provided by vS1. Neither region is necessary for whisking, remaining unchanged during the spatial tuning experiment. Both vS1 and vM1 are required for a whisker discrimination task, vS1 does not impact whisking, but vM1 is responsible for behavioral performance, adaptive whisking, and response inhibition. Our study provides further evidence of vM1's many functions, future studies may gone on to find additional non-motor possibly higher order functions

Methods

Experimental apparatus

The experimental apparatus is the same used in our previous publications. Briefly, a grounded Faraday cage is mounted to an air table to encase all recording equipment. All behavioral, electrophysiological, and optogenetic equipment were grounded to the air table. Mice are headplated and positioned comfortably on the rotary treadmill. Because mouse run speed is correlated with stereotyped whisking, we take advantage of this relationship to ensure consistent sensory drive into the system only running mice are used. A vertical pole, connected to a linear stepper motor, is placed in one of eight positions within the space swept out by the whiskers and one control position where the mouse cannot make contact. Four micromanipulators were placed around the running wheel enabling the optical fibers and the NeuroNexus recording electrodes to be precisely placed above the cortex and within it respectively. Thorlabs 473nm LEDs attached to 400um optical fibers are fixed to two micromanipulators allowing us to place the fibers above the skull for optogenetic silencing. The other two micromanipulators each held a NeuroNexus high density 32-channel electrode (A1x32-Poly2 probe) with two columns of sixteen electrode contacts. Finally, below the wheel sits a mirror and a high speed video camera used to image whisker motion and its interactions with the stimulus bar.

Recording equipment

The experimental setup was controlled via custom software written in MATLAB, data acquisition, such as electrophysiology, stimulus type, run speed, and other key experimental variables where collected using SpikeGadgets recording equipment. The entire experiment would be recorded simultaneously and later broken up into trials offline. The high speed camera used for whisker tracking used proprietary software from NorPix and a custom built computer in order to acquire 500fps streamed directly to its RAID0 system. Due to computational limitations of the high speed camera's computer, videos were recorded on a per trial basis. Camera acquisition was triggered by a TTL pulse sent from the experiment control computer to ensure precise trial alignment. A pool of 1xPBS was made on the skull of the mouse during experiments, we used this to ground our electrodes.

Optogenetic silencing

Two blue 473nm LEDs were connected to 400um fiber optic cables and placed above vS1 and vM1 during each experiment. The fibers were crisscrossed to prevent light from affecting the non-silenced brain region. The fiber tips were submerged in the 1x PBS pool used for grounding our electrodes.

Whisker imaging, automated tracking, and variables of interest.

A high-speed camera (Basler acA2000-340km) was placed below the running wheel; whiskers were imaged from below using a telecentric lens (Edmund Optics NT58-257) and a mirror angled at approximately 45 degrees. Some mice and experimental setups required slight adjustments to the mirror angle to properly view the whiskers and object interaction. Whiskers were backlit from above using high-powered diffused infrared LEDs (CMVision-IR200). High-speed videos were acquired with a framegrabber (Silicon Software) at 500 frames per second with a 100-μs exposure and were synchronized with behavioral data via external triggers. Whisker tracking was performed offline using Whisk (Janelia Farms, Howard Hughes Medical Institute), which returned whisker angles and positions for every frame. Tracking data was further processed and analyzed using custom MATLAB scripts written to extract set-point, amplitude, phase, and frequency. Briefly, set-point was calculated as the average of the upper and lower peak envelope of the angle signal, amplitude was the difference of the upper and lower peak envelope, phase was the Hilbert transform of the signal, and frequency was the number of complete whisk cycles for a given unit of time.

Mice used

Ai32-PV-Cre mice with a BL6 background were used for all experiments. Mice were allowed to acclimate to headfixation, the noises of the stepper motor and lab space, as well as the periodic whisker contacts with the stimulus bar for 2-3 days prior to each experiment. If a mouse refused to run consistently or it dramatically flinched or reduced its run speed to the stimulus then it would not be used in an

Identifying recording sites

Our initial awake and headfixed experiments sought to identify coordinates for consistent electrode insertion to record sensory activity. Using sets of coordinates taken from the literature and manually deflecting whiskers to identify spiking activity, we found that a small region near +1.5mm bregma and +1.0mm lateral to the central suture allowed us to consistently find whisker sensory responses

Preparations taken before each experiment

Mice were prepared for experiments shortly before being placed on the rig. Using 1.5% isoflurane small craniotomies were placed above the C2 barrel in vS1 (-1.5mm bregma, +3.5mm to central suture) and above vM1 (+1.5mm bregma, +1.0mm to central suture). The craniotomies were kept hydrated using sterile 1x PBS and remained saturated for the duration of the experiment. Immediately after completing the craniotomies the mice were moved to the experimental rig and headfixed on the rotary treadmill. Two NeuroNexus A1x32-Poly2 probes

were lowered until the top most electrodes had visible spiking activity, typically 850um below the cortical surface of vS1 and vM1. Once the probes were settled in the brain two 400um fibers, connected to a 473nm blue Thorlabs LED, where placed adjacent to each probe. The light was briefly turned on to ensure optogenetic silencing was working as expected. The light levels were lowered to ensure that no-light from the vS1 fiber crossed to vM1 and vice versa.

Spike sorting and data preprocessing

All data was preprocessed in MATLAB. High speed video recordings were collected with a framegrabber. All other experimental data was saved to a SpikeGadgets recording file. Using command line tools from SpikeGadgets we were able to extract both the raw recorded signal from each electrode contact as well as low passed filtered local field potentials (LFPs). This data was then pre-processed with custom MATLAB code, which reorganized the raw data and added necessary parameter files required by the spike sorter KlustaKwik2 version 3.0.9. After the automated sorting completed we did the final manual curation with the Klusta the included GUI, clusters where manually labeled as single unit, multiunit, or noise.

Data such as mouse run-speed, whisker kinematics, and LFPs were extracted from the rec file and reorganized by custom MATLAB code. These data were then combined with the spike sorting data into an hdf5 file. Each experiment, and all associated data, were represented in individual hdf5 file for ease of use and for convenient sharing. All data analysis and figures were conducted with custom Python 2.7 code.

Classifying units

Using custom Python 2.7 code single units were categorized as either regular spiking (RS) or fast spiking (FS) units based on their waveform shape using a Gaussian Mixture Model clustering method. Unites were further classified as sensory driven or non-sensory driven by comparing all contact positions the control no-contact stimulus using a Kruskal-Wallis one-way test of variance with Dunn's test for multiple corrections. Alternatively, unit's evoked rates were tested against their baseline rates (Wilcoxon rank-sums corrected for multiple comparisons). Only sensory driven units were analyzed and presented here.

Measuring tuning

Selectivity is a tuning measurement that I developed in the lab that does not assume a particular shape. It considers how many positions are sensory driven and weighs them with their firing rate relative to the firing rates of other positions. If a unit has many driven positions but their firing rates are not well separated the selectivity metric will be broad, a value closer to zero. Selectivity

ranges from zero to one, where zero corresponds to a unit that has the same firing rate for all positions and a unit driven by a single position will have a selectivity value of 1.

The spatial selectivity was calculated from the normed vector of the peak normalized spatial tuning curves using raw spike rates as previously published (Pluta et al. 2017). This value was then divided by square root of *n* dimensions - 1 to restrict its range from 0 to 1. Larger values signify higher spatial selectivity (higher sharpness and lower broadness).

$$Spatial\ Selectivity\ =\ 1 - \left(\frac{\frac{||x||}{\max(x)} - 1}{\sqrt{n} - 1} \right)$$

Neural decoding

We adapted an optimal linear estimator (OLE), a neural decoding technique previously used in the hippocampal literature, to predict the spatial position of a rat via recorded local field potentials (Agarwal et al., 2014). The decoder seeks a set of weights that, when multiplied by firing rates, maps the neural input to the identity of the presented stimulus. The neural decoder was trained and tested using standard machine learning practices. We opted for k-fold cross-validation using five folds per run, typically ten folds is the standard but we had to use fewer folds due to the smaller datasets produced by electrophysiology experiments. On average we had 30 accepted trials per stimulus condition. The decoder was trained on a training dataset, a 70% split of the total data, and then tested on a test dataset, the remaining 30% of the total data, that it had not seen before. Datasets were randomly sampled from the original dataset before every training and testing run. During testing we measured how often the decoder predicted the correct stimulus positions. We then ran this process 500 times to get a distribution of performance metrics, which allowed us to see how accurate the decoder could be from a single dataset. We repeated this process for datasets with different numbers of units to approximate how predictive power changes with population size.

Chapter 6: Discussion

The role of vibrissae motor cortex is still unclear. What is clear is that vM1 does more than just motor, exhibiting clear multifunctionality, contributing to whisker movements, accurately representing sensory space, and playing a crucial role during a demanding sensory task. However, what vM1 actually does to impact performance is a question for another study. There are three possibilities: 1.) vM1 acts solely as a sensory area similar to vS1, silencing then disrupts sensory representations and downstream regions can no longer determine the true stimulus. 2.) Disrupted whisking causes a decrease in task performance. This is possible as other, more difficult to observe, kinematic variables may have changed unnoticed. 3.) vM1 acts as a higher order brain region responsible for response inhibition or sensory accumulation. This is the most intriguing prospect, a motor cortex with a range of functionality, from basic sensory processing, to adaptive whisking, and possibly complex behavioral strategies. In this case licking was primarily affected at NOGO positions, where licking must be withheld, and was normal for GO stimuli. This suggests that the action associated with the stimulus is more difficult depending on what the stimulus is. It is interesting that both vS1 and vM1 silencing increased false alarm rates at NOGO positions, the key difference is vS1 did not impact lick response onset. This is an exciting line of questioning that I hope we can answer soon.

The major caveat of this experiment is we do not know precisely what we were silencing. vM1 is a small cortical area, making it difficult to target specifically with one photon fibers and mice expressing ChR2 in all cortical PV inhibitory interneurons. Viral injections would be more precise but it would be difficult to determine if the injection was placed in the correct spot. Something that could not be verified until the mouse is sac'ed. Even then histological analysis would be vague as vM1 has no prominent landmarks denoting its boundaries. We searched the literature for neighboring cortical regions to vM1 that could cause the observed behavioral changes. The only likely candidate is the ALM, which has been shown to bias licking direction in 2AFC tasks. However, none of those studies report changes in whisking making it seem unlikely. Regardless, the same silencing technique was used for both experiments but only trained mice exhibited behavioral changes, suggesting that whatever region is impacted it requires learning.

The purpose of vM1 sensory responses is still unclear. This study quantified vM1 sensory driven units, finding that they are similarly tuned to vS1 units in tuning curve shape. They differ from vS1 with lower driven firing rates and less variable mean firing rates. These two differences likely contribute to the lower decoding performance from the vM1 population. Now that we have a general sense of vM1 tuning the larger, more interesting question remains, what does vM1 do with it? What processes depend on it? Does it come from the PoM, if so does the PoM modulate what sensory information vM1 receives?

Silencing vM1 did not significantly modulate vS1 activity in the traditional sense. The mean and variance did not shift, because standard statistical tests look for directional shifts of point estimates other "scrambled" changes are not considered significant. On a single unit level some vS1 units were affected by vM1 silencing, typically exhibiting small changes across their tuning curve but usually only a affecting a few positions. None of these changes occurred in the same direction. While seemingly random changes appear insignificant to us and our typical statistical tests there may be underlying structure present. The brain is complex and rarely follows intuition, now that modern recording tools can record large datasets consisting of hundreds to thousands of units, it seems unlikely that large populations would be affected in the same way (Durstewitz & Balauguer-Ballester, 2010). Consider a multirole cortical region consisting of neurons tuned to a disparate number of variables, here directional changes are unlikely, but there may be more complex relationships within the population.

Neural data is highly multidimensional, changes observed with just two dimensions is a small fraction of the entire picture (Stringer, Pachitariu, Steinmetz, Carandini, & Harris, 2019). That's why I believe modern analysis techniques adapted from machine learning and data science can be valuable and relatively easy to implement tools. There are many complicated tools available but I believe that simple tools can still provide a significantly deeper look into the data. Code libraries exist with analyses already coded, and due to the popularity of machine learning in the past decade and a half, many of the libraries are easy to use. Simple methods like dimensionality reduction using principal component analysis (PCA) and regression techniques can provide a better grasp of high dimensional data (Burkowski, n.d.; Hearst, Dumais, Osuna, Platt, & Schölkopf, 1998; Olshausen, 2012). In this study we implemented a linear neural decoder. The heart of it is a regression used to find the weights that map firing rates to stimulus identity. With the addition of a few equations to transform the data it becomes an effective neural decoder. It not only provides valuable insights but also opens the door to methods that can be intimidating for many.

Modern, yet simple analysis methods can provide deeper intuition as well as identify functionality that would otherwise be missed with traditional methods. In short time these analysis methods may become necessary as recorded datasets continue to increase in size and complexity.

The data presented here supports the hypothesis that functional cortical areas in mice, a lower order species, can be multifunctional regions not limited to their functional definitions. The multirole capability likely increases as the species get simpler. If this is true it raises a number or questions. Such as, when does cortical localization become advantageous, is every cortex capable of being localized or dispersed, is there an advantage to generalist cortical areas. It will be interesting to discover the hidden capabilities of "localized" cortical regions in the near future.

Bibliography

Agarwal, G., Stevenson, I. H., Berényi, A., Mizuseki, K., Buzsáki, G., & Sommer, F. T. (2014). Spatially distributed local fields in the hippocampus encode rat position. *Science (New York, N.Y.)*, *344*(6184), 626–630. https://doi.org/10.1126/science.1250444

Ahrens, K. F., & Kleinfeld, D. (2004). Current flow in vibrissa motor cortex can phase-lock with exploratory rhythmic whisking in rat. *Journal of Neurophysiology*, *92*(3), 1700–1707. https://doi.org/10.1152/jn.00404.2004

Auffret, M., Ravano, V. L., Rossi, G. M. C., Hankov, N., Petersen, M. F. A., & Petersen, C. C. H. (2017). Optogenetic stimulation of cortex to map evoked whisker movements in awake head-restrained mice. *Neuroscience*, 1–15. https://doi.org/10.1016/j.neuroscience.2017.04.004

Berg, R. W., & Kleinfeld, D. (2003). Rhythmic whisking by rat: retraction as well as protraction of the vibrissae is under active muscular control. *Journal of Neurophysiology*, *89*(1), 104–117. https://doi.org/10.1152/jn.00600.2002

Brecht, M., Schneider, M., Sakmann, B., & Margrie, T. W. (2008). Whisker movements evoked by stimulation of single pyramidal cells in rat motor cortex. *Nature*, *427*(6976), 704–710. https://doi.org/10.1038/nature02266

Brown, J., Oldenburg, I. A., Telian, G. I., Griffin, S., Voges, M., Jain, V., & Adesnik, H. (2021). Spatial integration during active tactile sensation drives orientation perception. *Neuron*, *109*(10), 1707-1720.e7. https://doi.org/10.1016/j.neuron.2021.03.020

Burkowski, F. (n.d.). PCA Tutorial.

Casas-Torremocha, D., Clascá, F., & Núñez, Á. (2017). Posterior Thalamic Nucleus Modulation of Tactile Stimuli Processing in Rat Motor and Primary Somatosensory Cortices. *Frontiers in Neural Circuits*, *11*(September), 1–19. https://doi.org/10.3389/fncir.2017.00069

Chen, T. W., Li, N., Daie, K., & Svoboda, K. (2017). A Map of Anticipatory Activity in Mouse Motor Cortex. *Neuron*, *94*(4), 866-879.e4. https://doi.org/10.1016/j.neuron.2017.05.005

Clack, N. G., O'Connor, D. H., Huber, D., Petreanu, L., Hires, A., Peron, S., … Myers, E. W. (2012). Automated tracking of whiskers in videos of head fixed rodents. *PLoS Computational Biology*, *8*(7), e1002591. https://doi.org/10.1371/journal.pcbi.1002591

Curtis, J. C., & Kleinfeld, D. (2009). Phase-to-rate transformations encode touch in cortical neurons of a scanning sensorimotor system. *Nat Neurosci*, *12*(4), 492–501. https://doi.org/10.1038/nn.2283

de Vries, S. E. J., Lecoq, J. A., Buice, M. A., Groblewski, P. A., Ocker, G. K., Oliver, M., … Koch, C. (2020). A large-scale standardized physiological survey reveals functional

organization of the mouse visual cortex. *Nature Neuroscience*, *23*(1), 138–151. https://doi.org/10.1038/s41593-019-0550-9

Diamond, M. E., von Heimendahl, M., Knutsen, P. M., Kleinfeld, D., & Ahissar, E. (2008). "Where" and "what" in the whisker sensorimotor system. *Nature Reviews. Neuroscience*, *9*(8), 601–612. https://doi.org/10.1038/nrn2411

Donoghue, J. P., & Wise, S. P. (1982). The motor cortex of the rat: Cytoarchitecture and microstimulation mapping. *Journal of Comparative Neurology*, *212*(1), 76–88. https://doi.org/10.1002/cne.902120106

Durstewitz, D., & Balauguer-Ballester, E. (2010). Statistical Approaches for Reconstructing Neuro-Cognitive Dynamics from High-Dimensional Neural Recordings. *E-Neuroforum*, *1*, 89–98. https://doi.org/10.1007/s13295-010-0011-0

Ebbesen, C.L., & Brecht, M. (2017). Motor cortex - To act or not to act? *Nature Neuroscience Reviews*, *in press*(11), 694–705. https://doi.org/10.1038/nrn.2017.119

Ebbesen, Christian Laut, Doron, G., Lenschow, C., & Brecht, M. (2017). Vibrissa motor cortex activity suppresses contralateral whisking behavior. *Nature Neuroscience*, *20*(1), 82–89. https://doi.org/10.1038/nn.4437

Elie, J. E., & Theunissen, F. E. (2015). Meaning in the avian auditory cortex: neural representation of communication calls. *European Journal of Neuroscience*, *41*(5), 546–567. https://doi.org/10.1111/ejn.12812

Farkas, T., Kis, Z., Toldi, J., & Wolff, J. R. (1999). Activation of the primary motor cortex by somatosensory stimulation in adult rats is mediated mainly by associational connections from the somatosensory cortex. *Neuroscience*, *90*(2), 353–361. https://doi.org/10.1016/S0306-4522(98)00451-5

Feldmeyer, D., Brecht, M., Helmchen, F., Petersen, C. C. H., Poulet, J. F. a, Staiger, J. F., … Schwarz, C. (2013). Barrel cortex function. *Progress in Neurobiology*, *103*, 3–27. https://doi.org/10.1016/j.pneurobio.2012.11.002

Finger, S. (2010). Chapter 10: the birth of localization theory. *Handbook of Clinical Neurology*, *95*, 117–128. https://doi.org/10.1016/S0072-9752(08)02110-6

Gioanni, Y., & Lamarche, M. (1985). A reappraisal of rat motor cortex organization by intracortical microstimulation. *Brain Research*, *344*(1), 49–61. https://doi.org/10.1016/0006-8993(85)91188-6

Guo, Z. V, Li, N., Huber, D., Ophir, E., Gutnisky, D., Ting, J. T., … Svoboda, K. (2014). Flow of cortical activity underlying a tactile decision in mice. *Neuron*, *81*(1), 179–194. https://doi.org/10.1016/j.neuron.2013.10.020

Hall, Robert; Lindholm, E. (1974). Organization Of Motor and Somatosensory Neocortex in the Albino Rat. *Brain Research*, *66*, 23–38.

Hearst, M. a., Dumais, S. T., Osuna, E., Platt, J., & Schölkopf, B. (1998). Support vector machines. *IEEE Intelligent Systems and Their Applications*, *13*, 18–28. https://doi.org/10.1109/5254.708428

Helmchen, F., Gilad, A., & Chen, J. L. (2018). Neocortical dynamics during whisker-based sensory discrimination in head-restrained mice. *Neuroscience*, *368*, 57–69. https://doi.org/10.1016/j.neuroscience.2017.09.003

Hill, D. N., Curtis, J. C., Moore, J. D., & Kleinfeld, D. (2011). Primary motor cortex reports efferent control of vibrissa motion on multiple timescales. *Neuron*, *72*(2), 344–356. https://doi.org/10.1016/j.neuron.2011.09.020

Huber, D., Gutnisky, D. a., Peron, S., O'Connor, D. H., Wiegert, J. S., Tian, L., … Svoboda, K. (2012). Multiple dynamic representations in the motor cortex during sensorimotor learning. *Nature*, *484*(7395), 473–478. https://doi.org/10.1038/nature11039

Kajikawa, Y., & Schroeder, C. E. (2011). How local is the local field potential? *Neuron*, *72*(5), 847–858. https://doi.org/10.1016/j.neuron.2011.09.029

Kleinfeld, D., Ahissar, E., & Diamond, M. E. (2006). Active sensation: insights from the rodent vibrissa sensorimotor system. *Current Opinion in Neurobiology*, *16*(4), 435–444. https://doi.org/10.1016/j.conb.2006.06.009

Kleinfeld, D., Berg, R. W., & O'Connor, S. M. (1999). Anatomical loops and their electrical dynamics in relation to whisking by rat. *Somatosensory and Motor Research*, *16*(2), 69–88. https://doi.org/10.1080/08990229970528

Kleinfeld, D., & Deschnes, M. (2011). Neuronal basis for object location in the vibrissa scanning sensorimotor system. *Neuron*, *72*(3), 455–468. https://doi.org/10.1016/j.neuron.2011.10.009

Koralek, K. A., Jensen, K. F., & Killackey, H. P. (1988). Evidence for two complementary patterns of thalamic input to the rat somatosensory cortex. *Brain Research*, *463*(2), 346–351. https://doi.org/10.1016/0006-8993(88)90408-8

Lanzio, V., West, M., Koshelev, A., Telian, G., Micheletti, P., Lambert, R., … Cabrini, S. (2018). High-density electrical and optical probes for neural readout and light focusing in deep brain tissue. *Journal of Micro/ Nanolithography, MEMS, and MOEMS*, *17*(02), 1. https://doi.org/10.1117/1.JMM.17.2.025503

Li, C.-X., & Waters, R. S. (1991). Organization of the Mouse Motor Cortex Studied by Retrograde Tracing and Intracortical Microstimulation (ICMS) Mapping. *Candian Journal of Neurologial Science*, *18*, 28–38.

Lopes, G., Nogueira, J., Paton, J. J., & Kampff, A. R. (2016). A robust role for motor cortex. *BioRxiv*, 058917. https://doi.org/10.1101/058917

Mackay, D. J. C. (2003). *Information Theory , Inference , and Learning Algorithms*.

Madisen, L., Mao, T., Koch, H., Zhuo, J., Berenyi, A., Fujisawa, S., … Zeng, H. (2012). A

toolbox of Cre-dependent optogenetic transgenic mice for light-induced activation and silencing. *Nature Neuroscience*, *15*(5), 793–802. https://doi.org/10.1038/nn.3078

Matyas, F., & Petersen, C. C. H. H. (2010). Motor Control by Sensory Cortex Ferenc. *Science*, *330*(November), 1240–1244.

McGuire, L. M., Telian, G., Laboy-Juárez, K. J., Miyashita, T., Lee, D. J., Smith, K. A., & Feldman, D. E. (2016). Short Time-Scale Sensory Coding in S1 during Discrimination of Whisker Vibrotactile Sequences. *PLOS Biology*, *14*(8), e1002549. https://doi.org/10.1371/journal.pbio.1002549

Mitzdorf, U. (1985). Current source-density method and application in cat cerebral cortex: investigation of evoked potentials and EEG phenomena. *Physiological Reviews*, *65*(1), 37–100.

Miyashita, E., Keller, A., & Asanuma, H. (1994). Input-output organization of the rat vibrissal motor cortex. *Experimental Brain Research*, *99*(2), 223–232. https://doi.org/10.1007/BF00239589

Naka, A. S. (2018). Inhibitory pathways in the neocortical microcircuit.

Neafsey, E. J., Bold, E. L., Haas, G., Hurley-Gius, K. M., Quirk, G., Sievert, C. F., & Terreberry, R. R. (1986). The organization of the rat motor cortex: A microstimulation mapping study. *Brain Research Reviews*, *11*(1), 77–96. https://doi.org/10.1016/0165-0173(86)90011-1

Ni, J., & Chen, J. L. (2017). Long-range cortical dynamics: a perspective from the mouse sensorimotor whisker system. *European Journal of Neuroscience*, *46*(8), 2315–2324. https://doi.org/10.1111/ejn.13698

Olshausen, B. A. (2012). Linear Hebbian learning and PCA, 1–8.

Papale, A. E., & Hooks, B. M. (2017). Circuit changes in motor cortex during motor skill learning. *Neuroscience*, *368*, 283–297. https://doi.org/10.1016/j.neuroscience.2017.09.010

Petersen, C. C. H. (2014). Cortical Control of Whisker Movement. *Annual Review of Neuroscience*, (May), 183–203. https://doi.org/10.1146/annurev-neuro-062012-170344

Petreanu, L., Gutnisky, D. a., Huber, D., Xu, N., O'Connor, D. H., Tian, L., … Svoboda, K. (2012). Activity in motor–sensory projections reveals distributed coding in somatosensation. *Nature*, *489*(7415), 299–303. https://doi.org/10.1038/nature11321

Petrof, I., Viaene, A. N., & Sherman, S. M. (2015). Properties of the primary somatosensory cortex projection to the primary motor cortex in the mouse. *Journal of Neurophysiology*, *113*(7), 2400–2407. https://doi.org/10.1152/jn.00949.2014

Pluta, S., Naka, A., Veit, J., Telian, G., Yao, L., Hakim, R., … Figure, S. (2015). A direct translaminar inhibitory circuit tunes cortical output. *Nature Neuroscience*, *18*(11), 1–11. https://doi.org/10.1038/nn.4123

Pluta, S. R., Lyall, E. H., Telian, G. I., Ryapolova-Webb, E., & Adesnik, H. (2017). Surround Integration Organizes a Spatial Map during Active Sensation. *Neuron*, *94*(6), 1220-1233.e5. https://doi.org/10.1016/j.neuron.2017.04.026

Sanderson, K. J., Welker, W., & Shambes, G. M. (1984). Reevaluation of motor cortex and of sensorimotor overlap in cerebral cortex of albino rats. *Brain Research*, *292*(2), 251–260. https://doi.org/10.1016/0006-8993(84)90761-3

Shin, H. C., & Chapin, J. K. (1990). Mapping the effects of motor cortex stimulation on somatosensory relay neurons in the rat thalamus: Direct responses and afferent modulation. *Somatosensory & Motor Research*, *7*(4), 421–434. https://doi.org/10.3109/08990229009144717

Smith, J. B., & Alloway, K. D. (2013). Rat whisker motor cortex is subdivided into sensory-input and motor-output areas. *Frontiers in Neural Circuits*, *7*(January), 4. https://doi.org/10.3389/fncir.2013.00004

Sofroniew, N. J., Cohen, J. D., Lee, a. K., & Svoboda, K. (2014). Natural Whisker-Guided Behavior by Head-Fixed Mice in Tactile Virtual Reality. *Journal of Neuroscience*, *34*(29), 9537–9550. https://doi.org/10.1523/JNEUROSCI.0712-14.2014

Sreenivasan, V., Esmaeili, V., Kiritani, T., Galan, K., Crochet, S., & Petersen, C. C. H. (2016). Movement Initiation Signals in Mouse Whisker Motor Cortex. *Neuron*, *92*(6), 1368–1382. https://doi.org/10.1016/j.neuron.2016.12.001

Stringer, C., Pachitariu, M., Steinmetz, N., Carandini, M., & Harris, K. D. (2019). High-dimensional geometry of population responses in visual cortex. *Nature*, *571*(7765), 361–365. https://doi.org/10.1038/s41586-019-1346-5

Ueno, M., & Yamashita, T. (2011). Kinematic analyses reveal impaired locomotion following injury of the motor cortex in mice. *Experimental Neurology*, *230*(2), 280–290. https://doi.org/10.1016/j.expneurol.2011.05.006

Victor, J. D., & Purpura, K. P. (2007). Metric-space analysis of spike trains: theory, algorithms and application, (768508551). https://doi.org/10.1088/0954-898X/8/2/003

Zhang, K., Ginzburg, I., Mcnaughton, B. L., Sejnowski, T. J., Hartley, T., Lever, C., … Naughton, B. L. M. C. (2014). Interpreting Neuronal Population Activity by Reconstruction : Unified Framework With Application to Hippocampal Place Cells Interpreting Neuronal Population Activity by Reconstruction : Unified Framework With Application to Hippocampal Place Cells, 1017–1044.

Zhang, S., & Dan, Y. (2011). Long-range and local circuits for top-down modulation ofvisual cortex processing, *88*(2011), 169–173.